

Towards a More Controllable Sensorised Soft Gripper - A Data-driven Approach

by

Khaled Elgeneidy

A Doctoral Thesis

Submitted in partial fulfilment of the requirements for the award of
Doctor of Philosophy of Loughborough University

August 2018

EPSRC Centre for Innovative Manufacturing in Intelligent Automation

Wolfson School of Mechanical and Manufacturing Engineering

© by Khaled Elgeneidy 2018

ACKNOWLEDGEMENTS

First and foremost, all thanks are due to God for providing me with the strength and patience to overcome the challenges I faced throughout my PhD journey and for blessing me with the amazing family and friends who were always supporting me. It was indeed a challenging yet very rewarding experience that I am grateful to have completed.

I'm grateful to my supervisor **Dr Niels Lohse** for his continuous guidance and support throughout my PhD. I would like to thank him not only for being a professional critique of my work, but also for being a great supporter that cared for my personal wellbeing. I will always look up to him as an inspiring academic to learn from.

I would like to also thank my supervisor **Prof. Michael Jackson** for giving me the opportunity to pursue my PhD as part of the "*EPSRC Centre for Innovative Manufacturing in Intelligent Automation*" and providing me with the resources and motivation to complete my research.

I am glad and honoured to have been part of the **Intelligent Automation family** and the wider **Loughborough community**. I would like to express my sincere gratitude to fellow researchers, technicians and administration staff for their generous support that aided the completion of my PhD. I am thankful to all my amazing **friends** for their constant motivation and inspiration.

I am eternally indebted to my parents, for being the amazing parents they are. I am grateful to my mother **Ghada Mansour** for her endless love and continuous care despite the physical distance between us. Your constant motivation helped me complete this thesis. I am thankful to my father **Ahmed Elgeneidy** for inspiring and supporting me to peruse my PhD. To all my **family members**, I thank you for your prayers and your continuous encouragement.

With heartfelt gratitude, I dedicate this thesis to you to my beloved wife **Ranya Elsawah**, who happily made incredible sacrifices to join me during my PhD journey and support me with her endless love and care. It is only fitting for this thesis to be submitted in August, in memory of our fourth year as a happily married couple, wishing us many more years of joy and success.

Finally, I was delighted to have been blessed with my lovely daughter **Jayan Elgeneidy** as I embarked on writing my thesis. I would like her to know that despite the challenges of being a new parent at this critical time, she was the best gift I ever had! I wish you all the happiness and success in your life, and I hope that one day you will enjoy reading your father's thesis.

ABSTRACT

Robotic grippers have been constantly improving over the years to become more dextrous and adaptable in handling difficult objects with variations in their shape or uncertainty in their positioning. A challenge that remains difficult until now is the ability to handle delicate objects that can be easily considered as defective due to their interaction with the gripper, such as the case for food products or finely machined parts. An interesting emerging approach to tackle this challenge is to rethink the origin of the problem, which is the fact that all conventional grippers are made of hard and rigid components that can easily damage objects during grasping if not precisely controlled based on reliable sensory feedback. Hence, creating gripper fingers from soft materials makes them inherently safe and relaxes the need for sophisticated sensing and complex control. However, several open research challenges exist that are hindering the full utilisation of soft robotic components. In the context of soft grippers, relying primarily on the soft nature of the fingers to passively and gently adapt to its targets although highly desirable, consequently means that no sensory feedback is available to have better control over the grasping process or confirm its success.

In this research, a low-cost soft gripper was developed based on the ribbed pneumatic bending actuators with embedded bend sensing, in order to investigate the potential for sensor-guided control of soft gripper fingers. A purely data-driven approach is proposed that utilises basic sensory feedback to accurately estimate and control the bending of individual soft gripper fingers using simple empirical models that do not require any material characterisation or precise physical models. First, an experiment was designed to study the effect of varying the internal channel dimensions of soft finger samples with the same outer size, on their bending and force responses at variable input pressures. The results of this experiment provided useful design guidelines that can be followed to maximise the bending and force capabilities of the soft fingers and identified the best performing design of those tested. The experiment also illustrated how the soft finger's behaviour is governed by its designed morphology, which is consistent for fixed input conditions. The second step was to embed the soft fingers with resistive flex sensors, which change in resistance during bending without hindering the desired compliance. Additionally, onboard pressure sensors were used to measure the actual internal pressure developed inside the finger during actuation. Linear regression and artificial neural networks (ANN) are two common data-driven techniques that were implemented in this research. Both were fed with training data consisting of the flex and

pressure measurements acquired by testing a soft finger sample at different pressure levels and orientations, with the corresponding synchronised bending angle measured using a vision system. The developed models were successfully validated using new data acquired at untrained conditions, with the ANN providing more accurate bending estimations at the expense of heavier computation. Lastly, a PID controller was developed which utilises the simple empirical model to estimate the current bending angle, calculates the error from a target value, and outputs a duty cycle value for the PWM signal regulating the supplied pressure. The controller was successful in controlling the modelled sensorised soft finger to accurately follow stepped and sinusoidal reference signals.

Moreover, the combined multi-sensory feedback from the complete soft gripper was analysed to investigate the possibility of distinguishing between the free-bending and contact states, as well as differentiating between objects of different sizes. The main interest here was to evaluate if useful inferences can be made using the raw data from the flex and pressure sensors without having to model the real bending response of each soft finger individually. An experiment was conducted which involved grasping a set of objects of variable sizes and weights and collecting the resulting sensory feedback. The results of the experiment provided a clear relationship between the grasped object size and the averaged final flex sensor readings from opposing fingers supplied with the same pressure input. The results also showed the possibility of achieving contact detection by simply monitoring the current flex sensor's response during grasping and comparing it to the known free-bending response. A clear deviation can be witnessed at the occurrence of contact depending on the object size, which can be then used to stop the actuation. Furthermore, an interesting observation from this experiment was witnessed when monitoring the flex sensor's response during grasping against the measured internal pressure. Two distinct response curves were identified which reflects whether the object was grasped at the fingertips (precision) or encapsulated within the gripper (power), providing additional useful feedback about the grasp using simple sensory feedback.

The last contribution of this research was the investigation of additive manufacturing as an alternative fabrication method to the manual multi-stage soft lithography technique. Automating the fabrication of soft grippers is not only desired for its speed and ease of use, but more importantly to improve the output consistency so that an empirical model derived for a specific actuator design can be potentially used for different samples with minimal need for updating. Functional soft finger based on the pleated morphology and flexible strain

sensors were successfully 3D printed using a standard material extrusion-based printer after tuning the print parameters. The bending and force responses of the unit were experimentally characterised, and fatigue tests conducted to evaluate consistency. The printed soft finger was able to operate at higher pressures and hence generated larger contact forces while maintaining the desired compliance. Combining two of those units results in a two-fingered soft gripper that can be easily customised and directly printed in a single stage. The proposed data-driven modelling approach was successfully implemented using the printed finger as an additional validation to demonstrate the flexibility of using this approach with different actuator morphologies and materials. The outcomes of this investigation provided design guidelines and print settings recommended to successfully print air-tight soft fingers and highly flexible strain sensors.

Finally, the results of this research deliver a simple purely data-driven approach for modelling and controlling soft grippers that are not limited to a specific morphology or material, as well as an automated process for fabricating those with better consistency. The key requirement is to generate relatively small datasets from simple, inexpensive sensors during the systematic experimental testing, as demonstrated in this research with the moulded and 3D printed soft gripper fingers. Ultimately, with innovations in additive manufacturing technologies enabling more difficult geometries and wider choices of flexible materials to be printed, combined with advanced machine learning algorithms processing larger grasping datasets, more dextrous sensorised soft grippers can be reliably printed to safely manipulate delicate targets in various real-life applications.

PUBLICATIONS

The following are the publications arising from the research work presented in this thesis:

1. **K. Elgeneidy**, N. Lohse, and M. Jackson, "*Experimental Analysis of the Bending Response of Soft Gripper Fingers*," in *Volume 5B: 40th Mechanisms and Robotics Conference*, 2016, vol. 5B–2016, p. V05BT07A064.
2. **K. Elgeneidy et al.**, "Data-Driven Bending Angle Prediction of Soft Pneumatic Actuators with Embedded Flex Sensors" in *IFAC-PapersOnLine*, 2016, vol. 49, no. 21, pp. 513–520.
3. **K. Elgeneidy**, N. Lohse, and M. Jackson, "*Bending angle prediction and control of soft pneumatic actuators with embedded flex sensors – A data-driven approach*," *Mechatronics*, vol. 50, pp. 234–247, Oct. 2018.
4. **K. Elgeneidy**, G. Neumann, M. Jackson, and N. Lohse, "Directly Printable Flexible Strain Sensors for Bending and Contact Feedback of Soft Actuators," *Front. Robot. AI*, vol. 5, no. February, pp. 1–14, 2018.
5. **K. Elgeneidy**, G. Neumann, S. Pearson, M. Jackson, and N. Lohse, "*Contact Detection and Size Estimation Using a Modular Soft Gripper with Embedded Flex Sensors*", 2018 IEEE/RSJ International Conference on Intelligent Robots and Systems (IROS 2018), Accepted.

TABLE OF CONTENTS

ACKNOWLEDGEMENTS	II
ABSTRACT	III
PUBLICATIONS	VI
TABLE OF CONTENTS	VII
LIST OF FIGURES	X
LIST OF TABLES	1
CHAPTER 1: INTRODUCTION	2
1. 1. Highlights on the Evolution of Robotic Grippers	2
1. 2. Research Motivation	7
1. 3. Aim and Objectives	9
1. 4. Research Scope	10
CHAPTER 2: Literature Review	11
2. 1. The Rise of Soft Robotics	11
2. 2. Innovative Soft Actuation Methods for Grasping	13
2.2.1. Fluidic Actuation	14
2.2.1. Passive Underactuation	17
2.2.2. Granular Jamming	18
2.2.3. Shape-Memory Alloys (SMAs)	19
2.2.4. Electroactive Polymers (EAPs)	21
2.2.5. Controlled Adhesion	23
2. 3. Morphologies of Pneumatic Bending Actuators	25
2. 4. Fabrication of Pneumatic Elastomer based Grippers	28
2.4.1. A Practical Guideline for Soft Lithography Approach	29
2.4.2. The Potential of Additive Manufacturing	32
2.4.3. 3D Printing of Soft Materials	34
2. 5. Embedded Sensing for Soft Actuator Control	36
2.5.1. Conductive silicone rubbers	36
2.5.2. Conductive liquid metals	37
2.5.3. Commercial Flexible Sensors	38
2. 6. Identified Knowledge Gaps	40
CHAPTER 3: Research Methodology	42
3. 1. Research Questions	43
3. 2. Proposed Approach	47
3.2.1. Inherently Safe Soft Grippers for Handling of Delicate Objects	47
3.2.2. Pneumatic Bending Actuators as Soft Gripper Fingers	48

3.2.3.	Bio-inspired Control	49
3.2.4.	Data-driven Modelling and Control.....	51
3.3.	Research Objectives:	54
CHAPTER 4: Experimental Analysis of Soft Fingers		55
4.1.	Introduction:	55
4.2.	Design of Experiment	56
4.3.	Experimental Setup and Procedure	59
4.3.1.	Pneumatic Control Board	59
4.3.2.	Bending Angle Measurement via Image Processing	61
4.4.	Results and Discussions.....	63
4.4.1.	Evaluating Consistency.....	63
4.4.2.	Analysis of the Free-Bending Response	70
4.4.3.	Radial Expansion.....	73
4.4.4.	Internal Pressure Response.....	74
4.4.5.	Analysis of the Resultant Contact Forces	76
4.5.	Conclusions and Perspective	79
CHAPTER 5: Data-driven Modelling and Control of Soft Fingers		82
5.1.	Introduction	82
5.2.	Embedding Flex sensors	83
5.3.	Experimental Testing.....	84
5.3.1.	Pressure Control Using High-Speed Valve Switching	85
5.3.2.	Embedded Flex Sensor Characterisation.....	87
5.4.	Data-Driven Modelling of the Free Bending Response	89
5.4.1.	Regression Analysis	91
5.4.2.	Artificial Neural Networks	94
5.5.	Closed loop PID control of soft finger bending	96
5.6.	Conclusion	101
CHAPTER 6: A Modular Soft Gripper for Sensor-guided Grasp Feedback		103
6.1.	Soft gripper porotype development	104
6.1.1.	Entirely soft silicone rubber grippers	104
6.1.2.	Modular two-fingered soft gripper	105
6.1.3.	Reconfigurable Multi-fingered soft gripper with embedded flex sensing	107
6.2.	Design of experiment	108
6.3.	Results	110
6.3.1.	Size estimation	110
6.3.2.	Weight estimation.....	111
6.3.3.	Contact Detection	113
6.3.4.	Grasp type Identification.....	114

6. 4.	Discussion.....	116
6. 5.	Conclusions	118
CHAPTER 7: Direct Printing of Soft Fingers with Integrated Strain Sensing		121
7. 1.	Fused Filament Fabrication of soft fingers.....	122
7.1.1.	FFF Printing Hardware.....	122
7.1.2.	Design Guidelines.....	123
7.1.3.	Flexible filament printing settings	126
7.1.4.	Repeatability Analysis	128
7.1.5.	Fatigue Analysis.....	130
7. 2.	Dual-extrusion 3D Printing of Flexible Strain Sensors.....	133
7.2.1.	Design Concept.....	134
7.2.2.	Dual-extrusion printing settings.....	135
7. 3.	Integrated Strain Sensing in Printed Actuators.....	138
7.4.1.	Direct printing in a sideways configuration.....	138
7.4.2.	Direct printing in an upright configuration	139
7.4.3.	Two-stage printing and welding.....	140
7. 4.	Printed Sensor Acquisition and Characterisation.....	141
7. 5.	Characterisation of Bending Response	144
7.5.1.	Empirical modelling	145
7.5.2.	Validation Tests	147
7. 6.	Contact Force Analysis	148
7. 7.	Discussion and conclusion.....	151
CHAPTER 8: Conclusions.....		153
8. 1.	Research Overview.....	153
8. 2.	Research Contributions.....	155
8.2.1.	<i>Vision-aided experimental characterisation of soft bending actuators</i>	<i>155</i>
8.2.2.	<i>Accurate data-driven modelling and control for sensorised soft fingers</i>	<i>157</i>
8.2.3.	<i>Contact detection and size estimation for a modular soft gripper</i>	<i>158</i>
8.2.4.	<i>Automated fabrication of soft actuators and sensors via FFF printing.....</i>	<i>160</i>
8. 3.	Future work and applications.....	162
REFERENCES.....		165
APPENDICES.....		176
Appendix (A) – Arduino Code for Pneumatic Control Board		176
Appendix (B) – Halcon Image Processing Code		180
Appendix (C) – Additional Experimental Results		185
Appendix (D) – Datasheets for Sensors and Components.....		189
Appendix (E) – Soft Finger Design.....		194
Appendix (F) – Materials Specifications for FFF.....		195

LIST OF FIGURES

Figure 1: Examples of common industrial grippers	2
Figure 2: Examples of commercial anthropomorphic grippers.....	3
Figure 3: Examples of popular underactuated grippers (a) Pisa Hand (b) Robotiq Gripper (c)Velo Gripper	4
Figure 4: Examples of commercial soft grippers	5
Figure 5: Summary of the evolution of robotic grippers.....	6
Figure 6: Desired properties of a soft gripper.....	8
Figure 7: Opposing research directions in developing compliant grippers.....	8
Figure 8: The scope of this project within the framework of typical pick and place scenario	10
Figure 9: Classification of Robots with increasing Degrees of Freedom	11
Figure 10: Examples of the diverse soft robotic applications..	13
Figure 11: A classification of soft actuation technologies for soft grippers.....	14
Figure 12: Examples of the use of artificial muscles (contracting PAM [30], Shadow Dextrous hand).....	15
Figure 13: Examples for soft fluidic actuators].	16
Figure 14: Examples of underactuated grippers. (a) Festo's FinRay gripper, (b) SDM hand.	18
Figure 15: Examples of jamming grippers. (a) The Universal Gripper [50] (b) JamHand [53]	19
Figure 16: Actuation of a meshworm soft robot [57] and soft octopus arm [58] using SMA	21
Figure 17: Examples applications for DEAs in: (a) delicate grasping [72], and (b) underwater robots [73].	22
Figure 18: Soft grippers combining electroadhesion with (a) DEAs [79], and (b) pneumatic actuation [80].	24
Figure 19: Examples applications for Geckoadhesion in (a) climbing [83], and (b) grasping [85].	25
Figure 20: An illustration for the cylindrical morphology showing (A) neutral and (B) actuated states [21].	26
Figure 21: An illustration for the ribbed morphology showing (A) neutral and (B) actuated states [21].	26
Figure 22: An illustration for the pleated morphology showing (A) neutral and (B) actuated states [21].	27
Figure 23: CAD model and the 3D printed soft gripper main mould	29
Figure 24: Mixing and degassing the Eco-Flex material.....	30
Figure 25: demoulding the cured material from the 3D printed mould	30
Figure 26: Fabricating a basic soft gripper prototype	31
Figure 27: Early examples of utilising 3D printing with soft robotics [96][97][98].	33
Figure 28: 3D printing of conductive material into the silicone rubber matrix [120]	37
Figure 29: Multi-layered conductive channels for measuring pressure and strain [125]	38
Figure 30: bending a sample flex sensor	39
Figure 31: Illustration of the desired traits from using a soft gripper	47
Figure 32: The bio-inspired analogy between the proposed control paradigm of soft grippers and octopus.....	50
Figure 33: Flowchart outlining the proposed control architecture.....	53
Figure 34: a cross-sectional illustration comparing the three different internal channel designs achieved by varying R while fixing outer dimensions and the number of chambers.....	56
Figure 35: Summary of the studied factors and responses in the designed experiment	57

Figure 36: Fabricating a batch of soft finger samples with variable channel patterns	59
Figure 37: Schematic diagram of the control board design by the soft robotics toolkit.....	60
Figure 38: Experimental setup showing the pneumatic control board components	61
Figure 39: Visualisation of the output from the image processing program tracking trajectory and segmenting cross-sectional area of the deforming actuator	62
Figure 40: Experiment setup for bending analysis (left) and force analysis (right)	63
Figure 41: overlaid image frames showing a soft finger deforming at 12 and 16 Psi input pressures.....	64
Figure 42: Highlighting variance in final bending angle due to fabrication for each finger design	65
Figure 43: Pressure response at different actuation pressures	66
Figure 44: Trajectory response at variable actuation pressure inputs	66
Figure 45: bending angle response at different actuation pressures	67
Figure 46: Cross-sectional areas at different actuation pressures	68
Figure 47: Pressure response for different actuation duration.....	68
Figure 48: Trajectory response at different actuation durations.....	69
Figure 49: Cross-sectional area response under different actuation durations.....	69
Figure 50: bending angle response at different actuation durations	70
Figure 51: Comparing the trajectory path of all fingers	71
Figure 52: comparing the maximum bending angle of all fingers at variable pressures.....	72
Figure 53: Effect of the ratio and number of chambers on the maximum bending angle.....	72
Figure 54: Effect of the chamber width on the maximum bending angle at variable supply pressures.....	73
Figure 55: Comparison of change in the cross-sectional area among all fingers	74
Figure 56: The effect of the Ratio and the number of chambers on the cross-sectional area.....	74
Figure 57: Comparing the internal pressure response of all fingers	75
Figure 58: The effect of the ratio and number of channels on the internal pressure response	76
Figure 59: Comparing the maximum resultant forces measured	77
Figure 60 Effect of the ratio and number of chambers on the resultant contact forces	77
Figure 61: Bending angle response when making contact at different locations.....	78
Figure 62: Maximum resultant force when making contact at different locations.....	78
Figure 63: Soft Pneumatic actuator sample embedded with a flex sensor	84
Figure 64: Experimental setup for testing soft actuators embedded with a flex sensor	85
Figure 65: A schematic for the pneumatic circuit controlling the actuation	86
Figure 66: Damping of oscillations in internal pressure measurements using a pneumatic tank and resistance .	87
Figure 67: Flex sensor response against the internal pressure at variable durations.....	88
Figure 68: Flex sensor response against the internal pressure at variable pressures.....	88
Figure 69: Flex sensor response against the internal pressure at variable orientations.	89
Figure 70: Sample of the feedback from the flex sensor, pressure sensor, and bending angle when bending the actuator twice at a 0° orientation	91
Figure 71: Sample of the test results comparing the prediction accuracy of the three regression models.....	94
Figure 72: ANN training results	95
Figure 73: Comparing error residuals of regression models and trained ANN	96
Figure 74: Schematic diagram of the controller architecture.....	97

Figure 75: Sample data for the internal pressure response to the change in the duty cycle of the PWM signal ..	99
Figure 76: Bending angle response to a stepped and sinusoidal reference signals	100
Figure 77: Grasping a cube and a complex 3D printed object using a simple soft gripper.....	105
Figure 78: Soft gripper prototype with the 3D printed body and interchangeable fingers	106
Figure 79: Grasping tests of components with different weights and delicacy	107
Figure 80: A reconfigurable soft gripper prototype consisting of four sensorised soft finger modules.....	108
Figure 81: Sample images for grasping tests showing the soft gripper successfully grasping a 25.4mm sphere, light bulb, and a cuboid block.....	110
Figure 82: Final readings from embedded flex sensors against the grasped object size	111
Figure 83: Final readings from embedded flex sensors against the grasped object weight.....	112
Figure 84: Comparing the effect of object weight on the final flex sensor reading for both the 50.8 and 25.4 mm spheres	112
Figure 85: Comparing the flex sensor responses for contact and free-bending scenarios	113
Figure 86: Flex sensor response against the measured internal pressure during actuation	115
Figure 87: Flex sensor response against the measured internal pressure with responses from test objects	115
Figure 88: TAZ 5 3D printer and the Flexytruder unit	122
Figure 89: A cross-sectional view of the pleated morphology of the printed soft finger	123
Figure 90: Comparing the increase in the length of the chambers' top profile using different geometries	124
Figure 91: Printing of a soft gripper finger sample in sideways configuration.....	126
Figure 92: slicing results from Cura software showing one continuous contour for the printer to follow	127
Figure 93: The variation in the absolute trajectory response between repetitions for one sample	129
Figure 88: The variation in the relative trajectory response between the five tested samples	129
Figure 95: Comparing the deviation in the retracted and actuated positions after 1000 actuations	130
Figure 96: The bending angle measurements	131
Figure 97: The image processing output for tracking the tip trajectory after 500 cycles	132
Figure 98: The design of the printed strain sensor (dimensions in mm) with the flexible NinjaFlex body (grey) and embedded conductive PLA tracks (black).	135
Figure 99: Printing the flexible strain sensor with embedded conductive tracks.	136
Figure 100: Initial tests showing a change in sensor's resistance upon bending	138
Figure 101: Printing a complete sensorised gripper finger in sideways orientation.....	139
Figure 102: Printing a complete sensorised soft finger in an upright orientation	139
Figure 103: comparing the measured resistance of the conductive tracks in flat and bent orientations	140
Figure 104: Welding the printed bending actuator and strain sensor together to create a sensorised actuator. (a) Individual actuator and sensor after printing, (b) soldering iron used to weld along the raised step of the sensor, (c) sensorised actuator after welding.	140
Figure 105: Wiring of the printed strain sensor using conductive threads glued to the exposed terminals.....	141
Figure 106: Schematic design of the printed sensor acquisition circuit.....	142
Figure 107: Acquisition circuit simulation at different amplification gains	143
Figure 108: Sample voltage output (after analogue to digital conversion) from the acquisition circuit when repeatedly bending the printed sensor.....	144
Figure 109: Printed strain sensor response against the internal pressure	145

<i>Figure 110: Image processing program tracking the bending trajectory of a tested printed soft finger sample</i>	<i>146</i>
<i>Figure 111: Sensory readings for deriving the empirical model</i>	<i>146</i>
<i>Figure 112: Comparing the prediction accuracy of derived empirical models.....</i>	<i>147</i>
<i>Figure 113: Results of the validation tests.....</i>	<i>148</i>
<i>Figure 114: Resultant contact force response for varying input pressure values</i>	<i>149</i>
<i>Figure 115: Embedded flex sensor response against input pressures during contact state</i>	<i>149</i>
<i>Figure 116: Comparing the free bending response of the embedded sensor to that when making contact.....</i>	<i>150</i>

LIST OF TABLES

<i>Table 1: Comparing the benefits and limitations of the three classes of soft bending actuators</i>	<i>28</i>
<i>Table 2: Comparing the properties of commercial soft printable and moldable materials</i>	<i>35</i>
<i>Table 3: Values of the studied design parameters for the soft fingers set</i>	<i>58</i>
<i>Table 4: Comparison of the regression statistics for the three derived models</i>	<i>93</i>
<i>Table 5: Error statistics for testing the trained ANN</i>	<i>95</i>
<i>Table 6: Summary of the properties of the test objects</i>	<i>109</i>
<i>Table 7: Summary of print settings for sideways configuration</i>	<i>128</i>
<i>Table 8: Summary of print settings for upright configuration in dual-extrusion mode.....</i>	<i>137</i>
<i>Table 9: Goodness of fit for the derived empirical model.....</i>	<i>147</i>

CHAPTER 1: INTRODUCTION

1. 1. Highlights on the Evolution of Robotic Grippers

Grippers mounted on industrial manipulators have been used for decades to manipulate objects on production lines with remarkable speed and repeatability. The vast majority of these industrial grippers are simple parallel-jaw grippers or task-oriented grippers that are designed to achieve a particular operation accurately (Figure 1) [1]. Despite the fact that such grippers are fast, accurate and reliable in structured industrial environments, they are actually inflexible and cannot adapt to variability hindering their utilisation in unstructured environments. The lack of flexibility and adaptation of these industrial grippers limited their success to high volume production processes, in which the same exact task needs to be repeated exactly for thousands of times. While complex tasks in unstructured environments that involve some variability or uncertainty are left for human operators to handle. Furthermore, as the cost labour increases by time and skilled labour become scarce; the need for flexible and adaptable grippers that can manipulate various objects is becoming increasingly desired [1]. Therefore, there is a need for more flexible grippers that are capable of performing a wide variety of tasks on different parts, while adapting to unpredicted variations arising in the process as a human operator would naturally do.

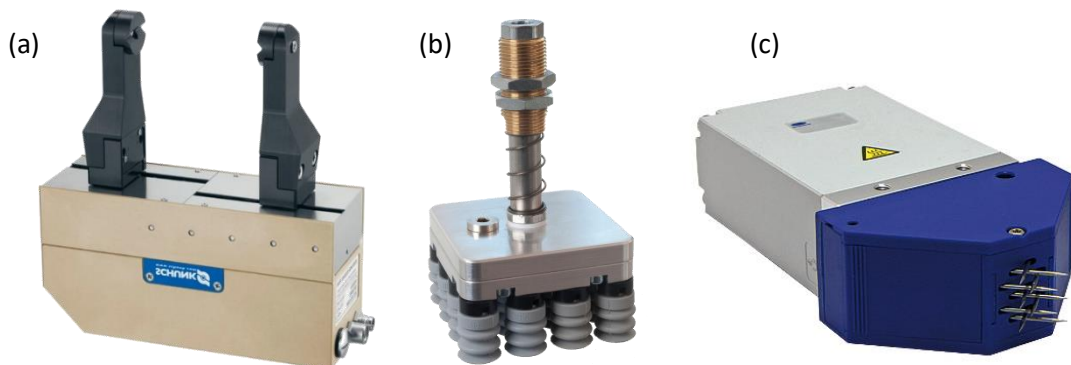


Figure 1: Examples of common industrial grippers
(a) Mechanical Parallel-jaw gripper¹ (b) Vacuum suction gripper² (c) Needle gripper³

¹ SCHUNK parallel-jaw gripper: https://schunk.com/gb_en/gripping-systems/category/gripping-systems/schunk-grippers/parallel-gripper/

² Vacuum grippers: https://www.fipa.com/en_US/products/2357872-vacuum-grippers/

³ Needle gripper: <https://www.schmalz.com/en/vacuum-technology-for-automation/vacuumcomponents/special-grippers/needle-grippers/>

Over the past decades, Researchers have been inspired by the superior capabilities of the human hand to develop flexible dextrous grippers that mimic the shape and performance of the human hand (Figure 2). The aim was to develop anthropomorphic (hand-like) grippers that can manipulate different complex objects and adapt to unexpected variations in the grasping process. This motivated the development of numerous sophisticated grippers that are able to perform various complex manipulations effectively [2]. However, these complex and bulky grippers are usually limited to research labs with hardly any presence in the manufacturing industry [3]. This is mainly because reliable performance in achieving dextrous manipulations requires sophisticated sensors, many actuators, and complex control, which all contribute to the high cost of these grippers. Hence, despite the tremendous research efforts made in developing novel anthropomorphic grippers, the vast majority remained unappealing for the industry to adopt into their production processes. Instead, manual workers remained responsible for handling complex processes with high degrees of variability, while standard mechanical grippers were preferred for simple processes with high production rates.



Figure 2: Examples of commercial anthropomorphic grippers.

(a) Shadow Hand⁴, (b) SCHUNK Hand⁵, (c) DLR Hand.⁶

After recognising the need for grippers that can adapt to variability and uncertainty while being simple and inexpensive to remain attractive for industry, the new concepts adopting a minimalistic design approach gained more attention. Researchers reconsidered the approach of mimicking the full capabilities and structure of the human hand and focused on achieving the key abilities required with the simplest possible designs. Underactuation was considered

⁴ Shadow dextrous hand: <https://www.shadowrobot.com/products/dexterous-hand/>

⁵ SCHUNK SVH 5-finger hand: https://schunk.com/gb_en/gripping-systems/highlights/svh/

⁶ DLR hand: <https://www.dlr.de/rm/en/desktopdefault.aspx/tabid-11671/#gallery/28631>

as a different approach towards designing grippers that are flexible but not as complex as the sophisticated anthropomorphic grippers (Figure 3). The concept of the underactuated gripper is to design creative mechanical structures with fewer actuators than its degrees of freedom [3]. Hence, using fewer actuators not only has the benefit of simplifying the control of the grasping process, but also reduced the overall size and weight of the gripper. In addition, underactuated grippers mostly rely on the passive compliance of their compliant mechanical design to conform to the grasped object, avoiding the need for expensive sensors that were previously used in complex grippers adopting the active compliance approach [4]. In other words, intelligence became actually embedded within the mechanical design of the gripper to reduce the complexity of sensing and burden in software programming. However, the reduced sensing capabilities together with the increased compliance of underactuated grippers have the risk of decreasing the robustness and reliability of their grasp. Nevertheless, the pursuit for novel flexible grippers continued to grow, seeking to accomplish notable compliance and adaptation to uncertainties with even simpler and cheaper designs.

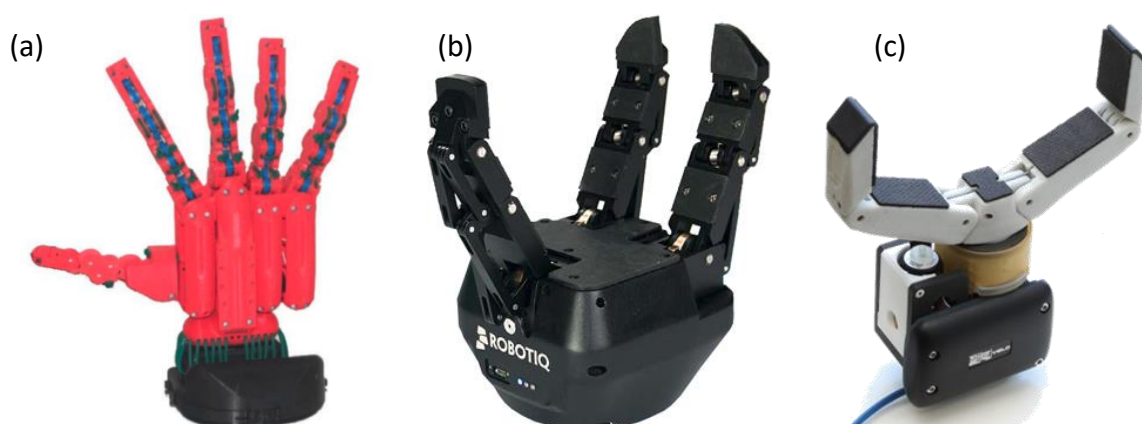


Figure 3: Examples of popular underactuated grippers
(a) Pisa Hand⁷ (b) Robotiq Gripper⁸ (c) Velo Gripper⁹

Furthermore, in an attempt to even further reduce the complexity of the grippers and enhance their compliance to adapt to a wider range of objects, researchers were inspired by the softness of the human hand to develop what is referred to as “soft grippers” (Figure 4). As the name implies, these grippers are made entirely or partially of soft materials that are highly deformable, enabling surface adaptation with minimal contact forces [5]. In fact, soft grippers are also classified as being underactuated since very few actuators are driving many degrees

⁷ Pisa Hand: <http://www.handcorpus.org/?p=1321>

⁸ Robotiq 3-finger gripper: <https://robotiq.com/products/3-finger-adaptive-robot-gripper>

⁹ Velo gripper: <http://www.willowgarage.com/velo2g>

of freedom. Such high compliance not only improves the grasp by increasing the contact area, but also the contact forces can be evenly distributed over a larger area. Hence, soft grippers have the added benefit of handling objects that are delicate in nature safely, and even provide safe human-robot interactions. Thus, recently researchers have been developing novel concepts for highly flexible soft grippers with the simplest possible designs and hardware requirements to keep their cost minimum. However, although many of these grippers are showing great potential for manipulating a wide variety of objects using simple designs and manufacturing procedures, the limited control over the accuracy and reliability of grasping indicates that further research is still needed to meet the robustness and reliability standards of the manufacturing industry. The jamming gripper from Empire Robotics (Figure 4) is an example on how challenging it is to achieve successful commercialisation, even with such an innovative gripper concept that demonstrated remarkable capabilities that surpass traditional grippers in many aspects. Challenges in achieving the required reliability and durability for industry standards forced the company to eventually close its doors. Soft Robotics Inc. on the other hand, it is probably the only company specialising in soft grippers that managed to successfully commercialise its innovative soft pneumatic gripper based on the team's pioneering research at Harvard's Whitesides Research Group. Both grippers demonstrated how an entirely passive solution relying solely on material softness could achieve remarkable compliance that surpasses that of conventional rigid grippers. However, the lack of sensing capability limits their application to standard pick and place tasks since no grasp quality feedback or control can be achieved.

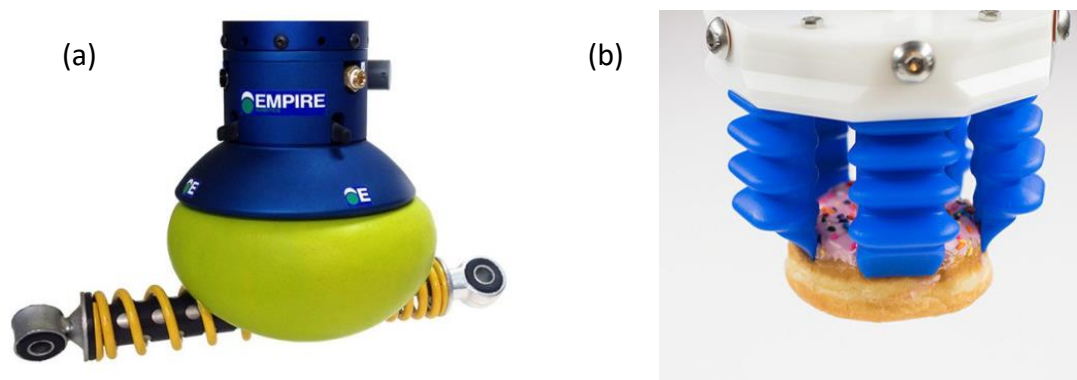


Figure 4: Examples of commercial soft grippers

(a) Soft Jamming Gripper by Empire Robotics.¹⁰ (b) Soft pneumatic gripper by soft robotics Inc.¹¹

¹⁰ Empire Robotics: <http://empirerobotics.com/>

¹¹ Soft Robotics Inc.: <https://www.softroboticsinc.com/>

In conclusion, it is clear that researchers have gradually diverted from developing complex dextrous grippers that attempt to exactly replicate the structure and functionality of the human hand, to developing simpler underactuated and even soft grippers that mimic the compliance of the human hand while maintaining simpler design and manufacturing. Hence, there is an evident trend towards simplifying the hardware requirements and mechanical construction of the robotic grippers as shown in Figure 5, in an attempt towards reducing their cost, size, weight, and programming complexity. Additionally, the passive compliance through ingenious designs and adaptability to unpredicted variability, remain to be the key criterion in innovating grippers that can handle ultimately any object regardless of its material or shape. However, a typical trade-off accompanied with improved compliance and adaptation is the reduced robustness in grasping and limited control over the position of fingers. Therefore, an obvious yet challenging question motivating this research arises;

Is it possible to develop a simple yet highly compliant gripper that is capable of adapting to various complex and delicate objects, while achieving the industrial accuracy and reliability requirements?



Figure 5: Summary of the evolution of robotic grippers

1. 2. Research Motivation

This research project is motivated by the need to develop highly compliant grippers that can adapt to variations in the geometry, material, and location of objects to be grasped, as a vital step towards the automation of processes exhibiting a level of uncertainty in rather unstructured environments. Considerable research work has been previously conducted in developing compliant grippers that can manipulate objects which are complex in geometry, but the delicacy of the object to be manipulated was usually overlooked. Thus, the ability of the gripper to safely handle delicate objects without deforming their geometry or damaging their surface finish will be prioritised in this research. This is an important aspect evident in processes involving the handling of delicate targets such as crops, various food products, and even living organisms. It only comes naturally to consider making the gripper itself out of a soft material when considering handling soft objects that are prone to damage from interactions with rigid surfaces. Hence, a special interest in this research will be to introduce “softness” to the developed gripper, in order to achieve the desired high compliance, adaptation to variability, and safe interaction with the surrounding environment.

Moreover, recognising the limitations of anthropomorphic grippers outside the research lab environments, it became evident that achieving flexibility in rigid grippers through an active compliance approach results in bulky and expensive grippers that are complicated to control for delicate manipulation tasks. Hence, the approach in this research is encouraged by the rising trend in creating grippers that are simple in structure with minimal hardware and software requirements. A simple highly compliant gripper is sought, which sacrifices some of its dextrous functionality in order to reduce its cost, weight, hardware requirements, manufacturing difficulty, and even programming complexity. This approach could motivate industries to consider such grippers as a potential candidate for handling complex processes that are currently perceived as being inefficient to automate [6]. A gripper with such interesting traits (illustrated in Figure 6) can be used in countless applications; ranging from automating the handling of different complex and delicate objects on production lines while mounted on a robotic manipulator, to safely assisting people in their various daily tasks when attached to service robots operating in houses.

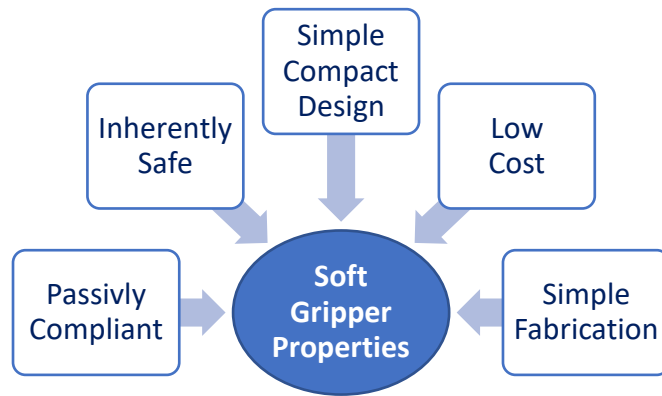


Figure 6: Desired properties of a soft gripper

In conclusion, increased flexibility in grippers is desired by industries to automate a broader range of complex handling processes in more unstructured environments, yet at the same time design simplicity with its consequent characteristics remains a requirement for grippers to be efficient in industrial applications. This need is motivating the development of a gripper that lies somewhere in the gap between sophisticated anthropomorphic grippers that are accurate but very expensive, and simpler compliant grippers that are much cheaper but not as accurate (Figure 7). In other words, there is a need for a gripper that can combine the flexibility of simple highly compliant grippers, with the accurate control that can be achieved by advanced grippers. Although adaptation to uncertainty via enhanced compliance is desired by various industries to enable automating processes with uncontrollable variability, it will not be accepted by industries if it does not demonstrate a deterministic performance that can be accurately controlled. Thus, the gripper should be flexible enough to adapt to a wide variety of objects with different geometries and materials, but at the same time can be accurately controlled to achieve stable grasps. Achieving this challenging tradeoff is motivating this research to investigate solutions that could introduce reliable sensing and control capabilities to highly compliant soft grippers as a step towards better utilisation of soft grippers in real life applications.

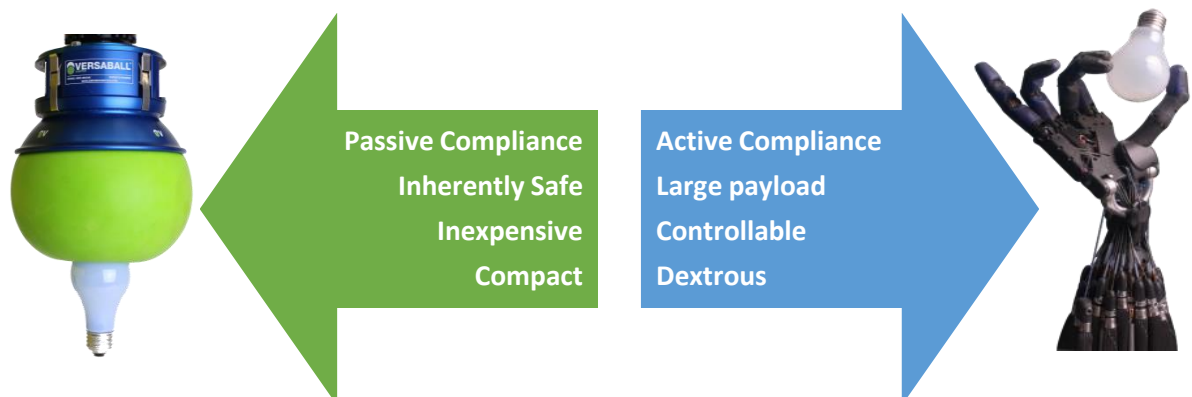


Figure 7: Opposing research directions in developing compliant grippers

1. 3. Aim and Objectives

The aim of this research is to develop a highly compliant gripper that can be controlled to safely grasp objects that are complex in geometry and delicate in nature, while minimising cost and structural complexity. Ultimately, by combining adaptation to variations, with a more controllable grasping, the proposed gripper could be eventually positioned somewhere in the gap between complex anthropomorphic grippers developed in research labs, and simpler task-oriented grippers commonly used in the industry. A soft highly compliant gripper that incorporates flexible sensors is envisioned, which provides bending feedback so that the gripper fingers can be controlled accurately. Such an approach can simplify the challenges in accurately modelling the complex behaviours of soft bodies. Hence, empirically driven models can be used as part of a high-level controller to process the multi-sensory readings infer useful grasp information for control purposes. Moreover, a simple design with embodied intelligence represented in the geometry and material properties of the gripper is sought, so as to reduce the programming complexity by transferring part of the intelligence to the morphology of the gripper. This allows the gripper to passively comply with objects of different geometries based on the interactions between the gripper morphology and the external environment. Hence, the adaptation to variations and uncertainty in objects to be handled can be achieved at the mechanical level without the need for computationally exhaustive control algorithms. To achieve this long-term aim, the following general objectives will need to be achieved:

- Conducting a literature review to identify an appropriate soft actuator concept that fulfils the requirements of the envisioned soft gripper, as well as a flexible bend sensor that can be seamlessly integrated with that actuator.
- Identifying an appropriate soft material to be utilised in producing the gripper so that it is inherently safe, in addition to practising the relevant production techniques to understand their capabilities and limitations.
- Investigate the key effects of the gripper finger morphology on its grasping performance through systematic experimentation.
- Embedding flexible sensors within the soft finger body and developing appropriate data acquisition to provide a reliable bending feedback.
- Developing a closed-loop controller that accurately estimates and controls the bending of soft fingers using the available sensory feedback.

- Developing a soft gripper prototype that combines the sensorised soft fingers in different arrangements to conduct grasping tests.
- Concluding the findings of this research and providing guidelines for realising more controllable low-cost soft grippers.

1. 4. Research Scope

Due to the multi-disciplinary nature of the robotics field in general and the soft robotics field more specifically, it will be difficult for a single researcher to tackle all the various research challenges from different backgrounds. Hence, in this research, the author will initially discuss the different research challenges, while eventually narrowing down the scope to the primary aspect of the challenge, which is controlling sensorised soft gripper fingers. Hence, this research will involve the design, production, characterisation, sensing, modelling and control of a prototype for the proposed soft gripper, as a step towards an approach for developing more controllable soft grippers. On the other hand, challenges related to the material science aspect that can potentially improve the performance of the gripper through synthesising new materials with enhanced properties, are outside the scope of this research. Instead, silicone rubber materials that are commonly used to fabricate soft robotic components will be exploited in the production of the envisioned soft gripper. This is because commercial products are available in a range of Shore hardness values and are relatively easy to prepare. Furthermore, it will be assumed that the position and orientation of the target object to be grasped can be identified using adequate 3D vision detection methods, which for a soft gripper does not need to be extremely precise. Also, it is assumed that the developed soft gripper can be in future work mounted to a robot arm so that the robot controller can be programmed to position the gripper on top of the target object. Programming a robot arm to move the gripper to a desired pose is a common task in robotics that does not involve significant research. Yet, future work can address how accelerating a soft gripper can potentially affect the grasp stability. Thus, the research will primarily focus on the grasping phase which involves controlling and monitoring the soft gripper fingers based on the integrated sensory feedback (Figure 8).

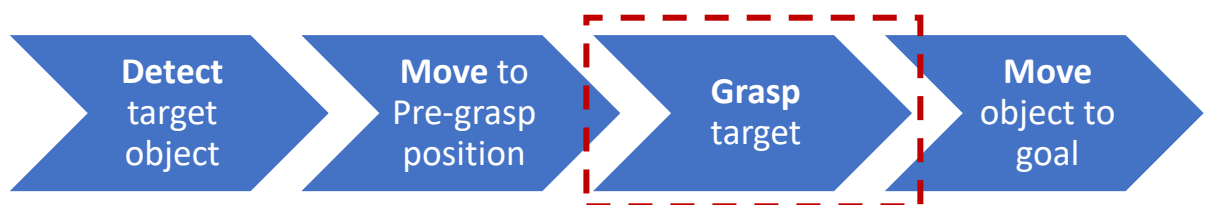


Figure 8: The scope of this project within the framework of typical pick and place scenario

CHAPTER 2: Literature Review

2. 1. The Rise of Soft Robotics

Robots have long been made of hard rigid structures with a number of flexible joints that allow mobility based on their type and configuration. The design approach has always been to minimise any vibrations and deformations in the robot structure by manufacturing it from stiff and hard materials, in order to adhere to the assumptions made in the standard kinematics and dynamics studies. Using forward kinematics engineers are able to analyse and optimise the configuration of the robot in advance and predict the exact location of the robot's end effector accurately. Similarly, inverse kinematics can be used to determine the appropriate configuration and joint angles for a robot to reach a precise target point. Hence, these highly accurate rigid robots were widely adopted in many manufacturing applications, performing specific tasks with high repeatability and precision in known structured environments. Furthermore, for such a stiff structure to achieve a flexible motion, the joints are utilised to add as many degrees of freedom as required to enable the robot to cover the working space effectively. Hence, more degrees of freedom are needed to improve the flexibility of the robot motion, allowing it to perform more versatile and complex tasks with a broader range of configurations to reach the same point in the workspace.

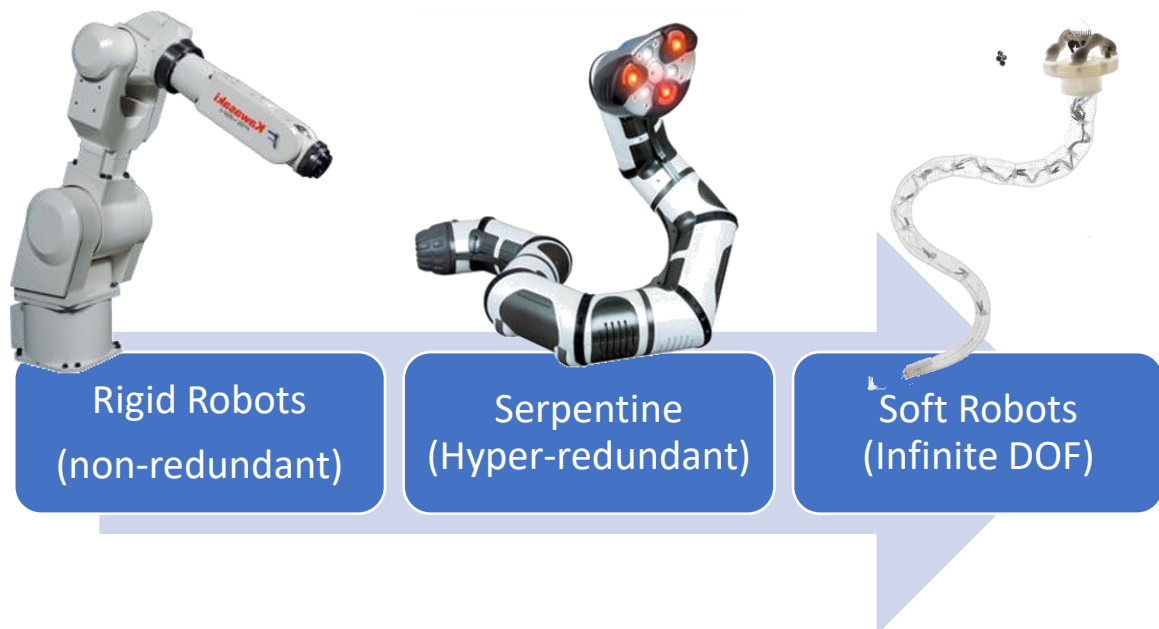


Figure 9: Classification of Robots with increasing Degrees of Freedom

The need for more flexible and dextrous robots has led to the development of the *Hyper-redundant robots*, which have a larger number of joints and hence higher degrees of freedom.

Additionally, *Serpentine* robots (commonly referred to as snake robots) can be considered as the most flexible form of hyper-redundant robots, in which the robot utilises a large number of joints to achieve snake-like locomotion that enables it to manoeuvre in confined spaces effectively [7]. More recently, a completely new class of robots has emerged, referred to as *Soft Robots*, has been attracting extensive research especially during the past five years [8]. These robots are inherently compliant due to the fact that they are made of soft materials that exhibit substantial deformations as part of their normal operation. The characteristic of large deformation in soft robotics contradicts with the foundations of conventional rigid robot design, in which deformation is considered a problem that needs to be minimised. Yet, it creates new interesting capabilities that await exploration [9][10]. The use of soft bodies that undergo continuous large deformations means a new level of flexibility in robotics, in which degrees of freedom are theoretically infinite with no singularity problems. Such exciting abilities opens up new fields of applications in unstructured environments that were rather challenging for conventional hard robots [11]. Examples of their diverse applications include: an assistive soft glove for hand rehabilitation [12], a soft robotic gripper for underwater sampling of delicate species [13], soft untethered robots for autonomous locomotion through varying surface conditions [14][15], an autonomous soft robotic fish capable of fast body motion [16], a soft anthropomorphic hand that can achieve complex grasp types [17], a soft manipulator inspired by the octopus tentacles for minimally invasive surgeries [18], and a soft octopus inspired robot for underwater locomotion and grasping [19]. Therefore, it is expected that soft robots would excel in applications that involve unstructured environments or task variations, which would benefit from their remarkable compliance and passive adaptation [20]. Grasping unknown objects that are sensitive to damage is just one example that is investigated in this research.

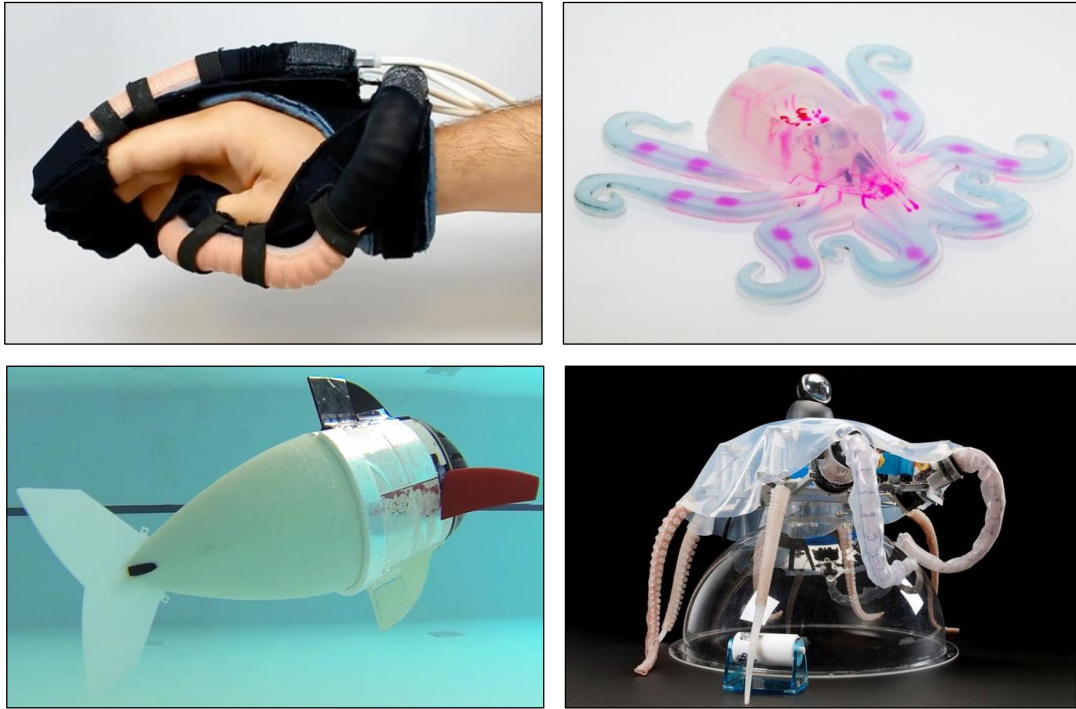


Figure 10: Examples of the diverse soft robotic applications. Soft wearable glove [12], Soft Octobot [15], Soft robotic fish [16], and octopus inspired soft robot [19].

2. 2. Innovative Soft Actuation Methods for Grasping

Conventional rigid grippers are normally actuated using electric motors, which can be found in numerous types and sizes and have been used for a very long time. Controlling motors to drive gripper finger links is now a well-established task that can be achieved with great precision in many applications from wheeled robots to industrial manipulators. However, being rigid and dense limits their integration with soft-bodied robots. Hence, researchers have been developing interesting concepts for novel actuators that are made from soft materials, so that they can be combined with soft robots without restricting their desired traits. In fact, soft actuators are not actually considered a separate component but rather an integral part of a soft robot, which can act as a limb for locomotion or a finger for grasping [21]. In the context of soft grippers, several novel soft actuation methods have been utilised to achieve adaptable grasping behaviour. Although most of those grasping technologies have gained popularity during the past few years, some of the underlying concepts have been originally proposed long ago, but became more practical to achieve recently with the advances in soft materials and their fabrication methods [22]. Despite the diversity of the various soft gripper designs, they can be generally classified according to the grasping technology as outlined in Figure 11 [23][24]. In the following sections, each grasping technology will be reviewed, outlining the benefits, limitations, and relevant soft grippers. Figure 11 shows a classification of relevant soft actuation technologies that can be utilised for soft grippers.

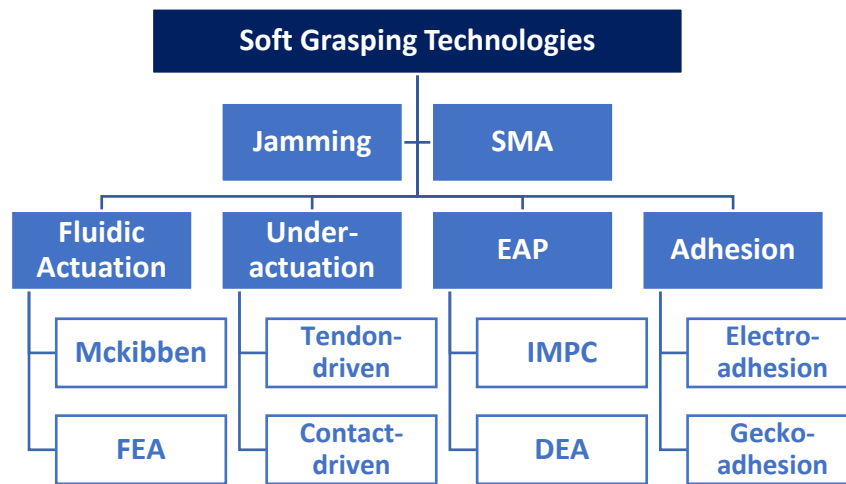


Figure 11: A classification of soft actuation technologies for soft grippers

2.2.1. Fluidic Actuation

Probably the most common soft grasping method is the use of fluidic energy to power soft actuators. Normally pneumatic actuation is the standard fluidic energy source used due to its ease of availability, although using hydraulic or other fluids are still applicable. Pneumatically powered actuators can be divided into two distinct classes; the first and the older is the artificial muscles, while the more widely adopted in soft robotics is the fluidic elastomer actuators, which have been created following different morphologies.

Pneumatic Artificial Muscles (PAMs)

The earliest method in soft actuation was inspired by the anatomy of the muscle and is commonly referred to as 'Pneumatic Artificial Muscles' (PAM). These actuators are made of an elastomeric bladder that is surrounded by stiff helical fibres as reinforcements and operated using a pressurised fluid [41]. They are also sometimes called 'Pressurised Artificial Muscles' when other pressurised fluids are used for actuation, yet mostly air is used because of its high compressibility, rapid inflation, ease of venting and availability [25]. When a muscle is pressurised, the bladder expands causing the muscle to contract as shown in (Figure 12a). Moreover, the pressurised artificial muscles have several unique advantages that encouraged engineers to research their use in prosthetic and robotic applications [26].

- High power to weight ratio in the range of 500 W/kg, which exceeds that of electric motors in the range of 100 W/kg.
- High power to volume ratio, which makes them easier to be integrated within systems when size needs to be minimised.
- The manufacturing process is relatively simple and cheap compared to conventional hard actuators, because of their simple structure and cheap components.

The most famous and developed pneumatic artificial muscle is the ‘McKibben’ muscle that was invented by Joseph McKibben in the 1950s [27]. Yet it was not until the 1980s that the McKibben muscle was commercialised to be used widely in broader applications when Bridgestone Corporation revived it under the name ‘rubbertuator’ [28]. Moreover, after nearly 10 years Bridgestone stopped their development of the McKibben muscles, but it had already spread enough that other companies continued their use and development for more applications. A famous implementation of a gripper based on the concept of the McKibben muscle is the ‘Shadow Dextrous Hand’ developed by Shadow Robot Company (Figure 12b), which uses forty air muscles to achieve remarkable dexterity of the hand. However, despite using relatively soft actuators, the hand remains rigid and is hence not classed as a soft gripper. Within the soft robotics domain, pneumatic muscles have been mostly used to create continuum arms [29], and some examples for legged robot locomotion [28]. However, implementations as a soft gripper finger are not common, which is likely due to the enhanced softness and wider morphologies realised by later fluidic elastomer actuators.

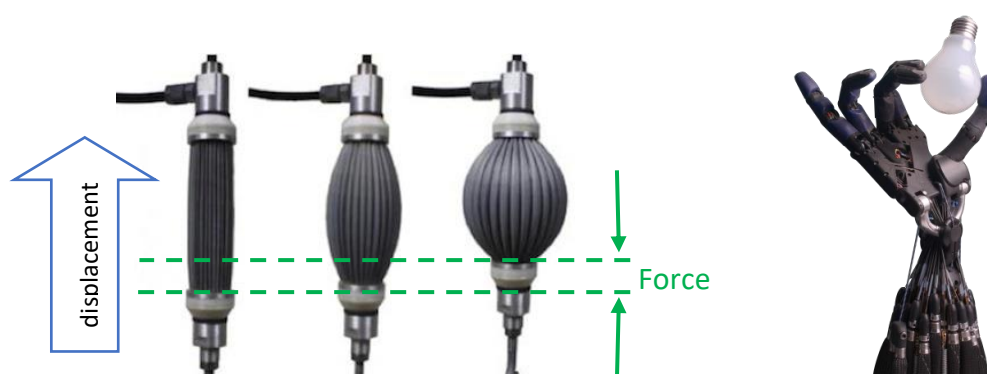


Figure 12: Examples of the use of artificial muscles (contracting PAM [30], Shadow Dextrous hand¹²)

Fluidic Elastomer Actuators (FEAs)

FEAs (also referred to as soft pneumatic actuators) are the most common actuation method for soft robots in general. The origins of the technology are old, but more recently it grew in popularity with the rise of the soft robotics field. The research by Whitesides Group at Harvard University is one of the main driving forces for spreading this soft actuation concept with their work on “PneuNets” in short for pneumatic networks [25]. PneuNets comprises of a series of air channels inside a soft material (commonly silicone rubbers), which when pressurised generates motion based on the geometry of these channels and the material that has been used to create them (Figure 13). Similar to artificial muscles, FEAs utilise pressurised air to generate motion, yet a wider range of motion types can be achieved. Hence, the unique

¹² Shadow hand: <https://www.shadowrobot.com/products/dextrous-hand/>

feature of FEAs is the ability to program their behaviour in advance through their morphology, which is defined by the material properties and designed geometry [31]. This allows the generation of different motion types depending on the design of the actuator. However, this also means that the ability to accurately predict and control the designed behaviour is more difficult to achieve during actuation [32]. Another interesting feature of FEAs is the fact that they are made from the same elastomer materials used to create soft robots, so they become in a sense a functional part of the robot body, resulting in more compact designs. This would be of special interest for this research to enable a compact gripper design. Additionally, the soft elastomers used in fabrication are highly stretchable and very light, allowing operation at low-pressure supply compared to PAMs. Although the maximum force output from FEAs is still limited compared to PAMs, they feature remarkably high power-to-weight ratio due to their extremely light weight. Scaling up FEAs and the use of external reinforcements, such as the case for the Pneuflex actuator, enhances their force generation capability [17]. The production process of FEAs is fairly simple and inexpensive since the elastomers used to make the actuator can be shaped using the now well-established soft lithography process [33]. The applications of FEAs are quite diverse; popular examples include the famous multi-gait soft robot [34], a rehabilitation glove that adapts to the human finger motion [35], and an autonomous soft robotic fish [16]. For soft grippers, FEAs have shown their promising potential to create highly compliant soft grippers that are well suited for delicate manipulation. Notable examples include; the famous simple soft gripper that passively picked up an egg [22], a miniaturised soft gripper that picked up small fish eggs [36], and a more recent soft finger for biological deep-sea sampling [13]. More recently, 3D printing technologies have opened new possibilities in manufacturing directly printable soft grippers based on similar pneumatic actuators [37].

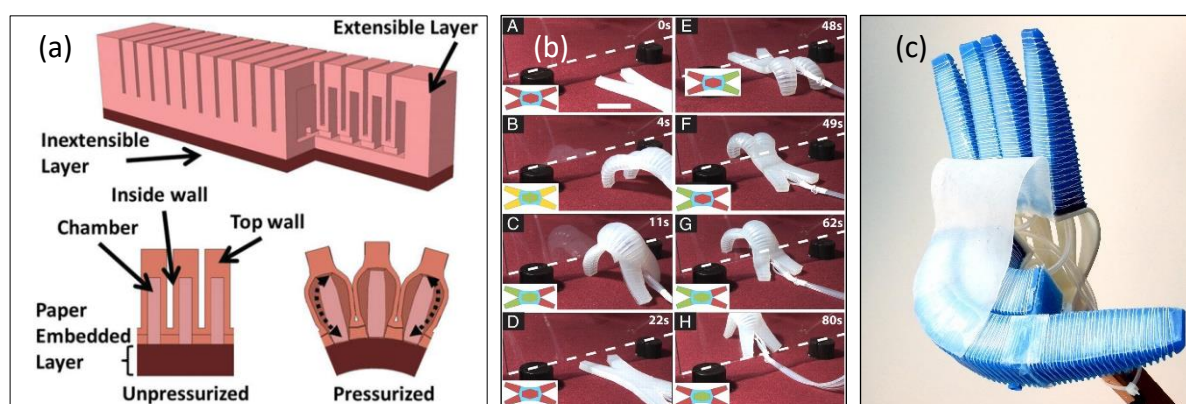


Figure 13: Examples for soft fluidic actuators: (a) PneuNet actuator [25], (b) multi-gait soft robot [34], and (c) RBO hand [17].

2.2.1. Passive Underactuation

As discussed in the previous chapter, the concept of underactuated mechanism was utilised in robotics to create passively compliant grippers [38]. This class of grippers is still made mostly from rigid links and driven by electric actuators, so they are not soft grippers per say. However, they utilise underactuation to emulate compliant behaviours that are similar to soft grippers and employ flexible elements such as tendons or flexible membrane to introduce some softness to their structure. Hence the reason for including them in this review. This class of grippers can be divided into two categories;

- The first is tendon-driven grippers, which use electric motors to pull tendons that are driving underactuated fingers.
- While the second is contact-driven grippers, in which the motors are directly driving the underactuated fingers, yet form closure is achieved passively by the fingers interaction with their targets.

I. Tendon-driven

Inspired by human fingers, tendon driven grippers attempt to mimic their compliance through the use of tendons, joints and springs. Numerous designs for tendon-driven grippers have been developed over the years, famous examples include the Pisa hand [39], the UNPI hand [40], the Valo gripper [41], and the Awiwi robot hand [42]. A common trend with tendon-driven grippers is to design the links so that they are easily reproducible through 3D printing, which results in light weight, modular, and open sourced grippers [43], [44]. A notable example of a tendon-driven partially soft gripper is the SDM hand (Figure 14) [45]. Similar to other tendon-driven grippers, it uses a linkage of underactuated fingers but also combines soft membranes as joints between the finger links for enhanced compliance. However, this remarkable gripper lacked any sensing capabilities that could improve the control over the grasping process, a limitation that was later addressed in the new version that was made possible using shape deposition manufacturing to embed a compact pressure sensor at the fingertips [46]. This version of the gripper was intended for surgical operations that would benefit from a safer soft gripper that also can provide force feedback to the user to prevent tissue damage. Still, the sensing feedback was limited to an LED that turns red when the forces at the fingertips increase above a certain threshold. In contrast to the minimalistic design approach adopted by the previous example, other attempts focused on developing anthropomorphic fingers inspired by the human finger structure [47]. An impressive work in this direction presented a highly biomimetic anthropomorphic hand that closely mimics its human counterpart by employing artificial joints, tendons, and ligaments [48]. Despite the

tremendous progress resulting in various tendon-driven grippers that are capable of manipulating a broad range of complex components, they are not the best choice when it comes to safely handling soft deformable objects as they are still made out mostly of rigid components with limited or no sensing capabilities.

II. Contact-driven

The second category of passive underactuated grippers is those that utilise the contact with their targets to achieve form closure. A remarkable example for this class is the FinRay gripper concept (Figure 14) used in the bionic handling assistant developed by Festo, which was inspired by the structure of fish scales [49]. The gripper is made from a relatively soft material developed by Festo which can be directly 3D printed to the shape of the gripper. Again, no active sensing is known to be incorporated with this gripper. The fingers are not soft enough to deform as elastomer based soft actuators, yet the ingenious design of the fingers allows to passively adapt its profile to different objects. The reduced softness may not be favoured for handling very sensitive targets, yet on the other hand, it enhances the carrying payload of the FinRay gripper when compared to most pneumatic actuators.

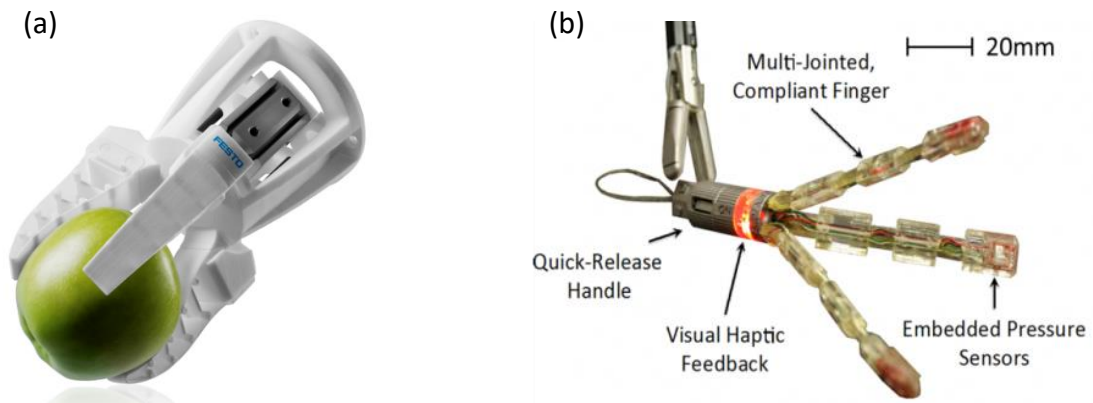


Figure 14: Examples of underactuated grippers. (a) Festo's FinRay gripper, (b) SDM hand.

2.2.2. Granular Jamming

Moreover, a novel grasping technology that inspired the robotics community was proposed by Cornell Creative Machines lab which became known as the universal jamming gripper (Figure 15) [50]. It combined the desired benefits of softness in grippers while having the ability to increase the stiffness of the gripper to maintain a stable grasp. The gripper utilises the physical phenomena in which jamming granulated material (such as coffee) will cause them to harden as one stiff body. To achieve this, a mass of granulates is enclosed in a soft

membrane which can conform to various objects; then negative pressure is applied to harden the granules around the grasped object creating a stiff gripper that can achieve stable grasps. Later on, positive pressure was also used to reverse the phenomena and allow the gripper to actually throw the grasped object towards a certain target [51]. Although the concept of the jamming gripper succeeded in grasping a wide range of objects via its controlled stiffness, grasping delicate objects might not be its area of speciality, especially as no sensing is incorporated to detect contact or monitor the forces imposed on the grasped object as the granules harden around it. Additionally, the fact that the gripper encapsulates the target in a soft membrane rather than articulated fingers means that no control can be achieved, as the grasping process is entirely passive with limited chance of achieving more sophisticated in-hand manipulation. Nevertheless, combining particle jamming with another grasping technology is a promising research direction that could result in hybrid soft gripper concepts that bring out the best of each technology. This has been already achieved with fibre-reinforced soft actuators to create a soft pneumatically actuated gripper that also uses vacuum to achieve variable stiffness capability [52]. Another example is the two-fingered hand, called JamHand, which demonstrated dextrous manipulation using minimal actuation with the support of granular jamming bags at fingertips (Figure 15) [53].

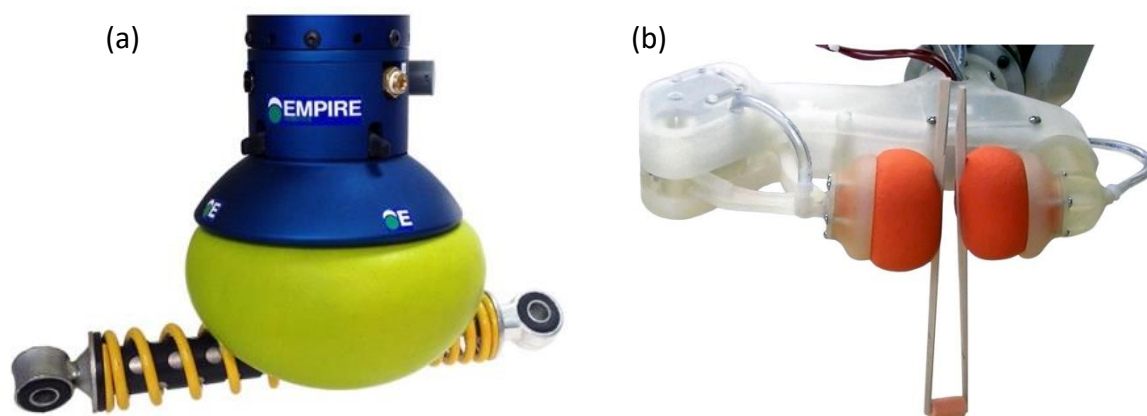


Figure 15: Examples of jamming grippers. (a) The Universal Gripper [50] (b) JamHand [53]

2.2.3. Shape-Memory Alloys (SMAs)

Shape memory alloys (SMA) have been long used as an unconventional method of actuation in different types of applications. SMA has a unique property, called the “shape memory effect”, by which it is able to recover their original shape after being deformed by heating above their phase transformation temperature (from martensite to austenite) [54]. However, at high temperatures, deformations can be fully recovered by just releasing the applied loads, a behaviour that is referred to as “superelasticity”. Knowing that the phase transformation of

SMA affects properties such as thermal conductivity, resistivity, and Young's modulus [55]. It is also known that the properties of SMA are very sensitive to the exact composition, grain size, heat treatment and loading conditions. In addition, including small quantities of additional elements to the composition of SMA would also have considerable effects on the material properties [54]. Numerous types of SMA are available with varying properties depending on all the above-mentioned conditions. The most widely used SMA material in industrial applications is the Nickel-Titanium alloy (NiTi), while Nickel-Titanium-Copper alloy (NiTiCu) is another popular SMA that is widely used in the medical field [55]. A number of advantages have motivated the use of SMA as actuators in different applications over the years; these can be summarised below [56]:

- SMA is light in weight and compact in size, with high power/weight ratios. Making them a strong alternative to conventional actuators for making compact light robots.
- The ability to work in a liquid environment without losing their mechanical properties encourages the use of SMA in underwater robots.
- The cost of SMA is relatively low compared to other traditional actuators.
- A wide variety of techniques that can be employed in the manufacturing process to produce SMA actuators in different configurations.

On the other hand, the following disadvantages of SMA have to be recognised:

- Although the required voltage supply for heating is relatively low, the efficiency in terms of power consumption is quite poor.
- Generally, the control of SMA using thermo-mechanical models for closed-loop control is actually quite complex since it is difficult to predict the behaviour of SMA with reasonable accuracy.
- The actuation speed is rather slow since SMA needs time to heat up to the required temperature for actuation to be achieved.
- Limited strains can be achieved using SMA, which means the maximum displacement that can be achieved may not be sufficient for many applications. However, techniques such as winding SMA into springs are used to increase the overall strain.

The softness, lightness, and compact size of SMA motivated their use in actuating various types of soft robots that normally do not require high actuation forces. Examples of such applications include; the ground locomotion of a meshworm soft robot (Figure 16) [57], the underwater locomotion and grasping of soft octopus arms (Figure 16) [58] [59], tunable stiffness of planar auxetic structures [60], multi-gait locomotion of a starfish soft robot [61], and in soft wearable robots [62].

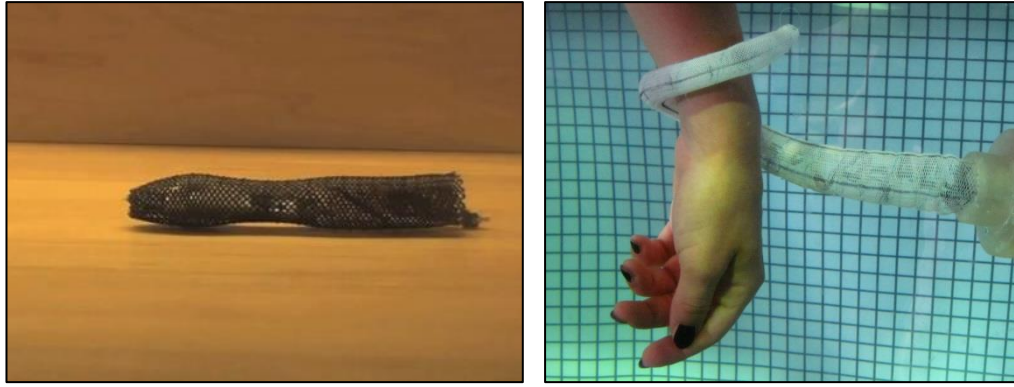


Figure 16: Actuation of a meshworm soft robot [57] and soft octopus arm [58] using SMA

2.2.4. Electroactive Polymers (EAPs)

Another soft actuation technology that can enable grasping is the use of electroactive polymers, which can reversibly deform upon electrical stimulation. Previously the interest in this class of materials has faded out gradually, but more recently with the rise of soft robotics, they are being revisited as a potential approach for producing novel artificial muscles [63]. EAPs can be divided into mainly two categories:

- i. **Dielectric Elastomer Actuators (DEAs):** An electric field is generated upon a polymer film that is sandwiched between two compliant electrodes, in order to generate coulomb forces that drive the motion of the DEA. This approach requires high voltage supply in the kV range, yet needs small currents. DEAs unique traits are; large actuation strokes, fast response, impressive efficiency and easy shaping [64].
- ii. **Ionic Polymer-Metal Composites (IPMCs):** Here the actuation mechanism involves the diffusion of ions in a fixed polymer network in response to a lower activation voltage in comparison to DEAs. However, most IMPCs can only work in aqueous media with short life cycles due to material degradation. Also, their response is slow, with low output efficiency and exhibit hysteresis [65].

For soft gripper applications, the implementations using IMPCs are rather few [66], probably due to the aforementioned limitations. Although the requirement of operating in aqueous media can be a limitation for many applications, it can be potentially exploited for applications that already operate in aqueous environments. A notable example is the development of a soft artificial cilium that replicates the motion of biological cilia via IMPCs [67]. Additionally, IMPCs were found to exhibit programmable shape memory properties, which can be furthered exploited to enhance their utilisation [68]. On the other hand, DEAs have been more successfully utilised as soft grippers. Early demonstration was achieved with what was referred to as self-organized dielectric elastomer minimum energy structures (DEMESs) [69].

Other soft gripper examples demonstrated using DEAs for handling deformable targets [70]–[72]. Additionally, biomimetic underwater robots were developed based DEAs [73]. Compared to pneumatic actuators and shape memory alloys, DEAs excel in the following aspects [74]:

- The most attractive feature of EAPs is their ability to emulate the operation of biological muscles in terms of large actuation strains, high fracture toughness, and inherited vibration damping.
- Another interesting feature that is lacking in other grasping technologies is the ability to reverse the actuation process to achieve sensing functionality in the same material.
- DEAs exhibit very fast response speeds and do not exhibit unpredictable motions, unlike the case of shape memory alloys.
- They do not require heavy hardware components when compared to compressors for pneumatic actuators. Although requiring less bulky high-voltage generates.

On the other hand, there are a number of drawbacks that limit the practical use of DEAs:

- The main drawback is the high operating voltage requirement, which includes the risk of electric discharge and the increased operating cost.
- Additionally, an improved actuation force is necessary if it would replace the more popular pneumatic actuators.
- More compliant electrodes with longer life cycles are required to enable reliable integration of this actuation technology with soft-bodied robots.
- Improved models of EAPs are necessary for accurate prediction of their behaviour.

Therefore, EAP technology is not as mature as the more established pneumatic actuation and hence require further research to allow their full utilisation. The emulation of the operation of biological muscles is probably the main driving motive to reconsider EAPs for biologically inspired soft robots, which can realise interesting concepts in soft grippers once their durability and controllability are improved.

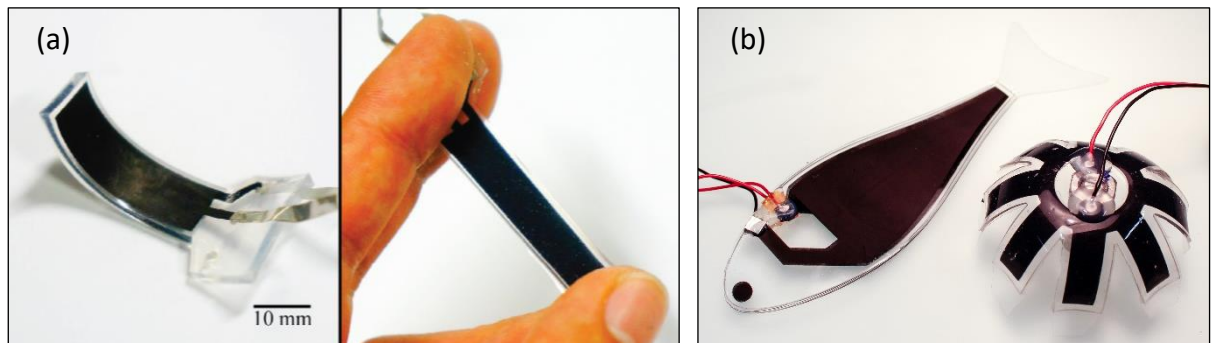


Figure 17: Examples applications for DEAs in: (a) delicate grasping [72], and (b) underwater robots [73].

2.2.5. Controlled Adhesion

This unique class of grasping technology relies on adhesive forces to gently pick various objects that could be several times the size and weight of the gripper. Since this process imposes minimal compressive forces on the target, it is well suited for handling delicate targets. However, adhesive forces are heavily dependent on having a clean contact area with its target to ensure a successful grasp, which limits their success with more complicated geometries. Mainly two adhesion modes have been successfully utilised to create remarkable soft grippers; Electroadhesion, and Geckoadhesion.

Electroadhesion

Electroadhesion exploits the electrostatic forces generated between positive and negative charges to lift objects, which has been shown to work on either smooth or rough surfaces [75]. This is achieved in electroadhesion through the application of a strong electric field to cause electrostatic induction on a conductive object and induce polarisation charges in a dielectric object. To generate strong electric fields, electroadhesive grippers require high voltage supply in the kV range, which can be considered a limiting requirement for this technology. On the other hand, electroadhesive grippers excel in handling delicate targets, such as the case of wafer handling [76] and textiles [77]. By tuning the geometry of the electrodes and insulation layer thickness, it has been demonstrated in the literature that improvements in the picking performance of electroadhesive grippers can be achieved [78]. Probably the most famous soft gripper based on electroadhesion is the one developed by Grabit Inc¹³. The fingers are made of a very thin and flexible PCBs with interdigitated electrode patterns, which generates the electroadhesive forces. The fingers are still moved externally by electric motors to move towards the object, yet the actual picking process is achieved through electroadhesion. The gripper successfully demonstrated picking different objects that may not be considered as particularly heavy, yet are still many times the weight of the fingers lifting them. On the other hand, the main challenges associated with soft grippers utilising electroadhesion are:

- The need for a high voltage supply that might not be feasible for some applications.
- The hysteresis caused by residual charges after turning off the voltage supply, which could require an active mechanism for quick detachment.
- The waiting time needed to generate maximum adhesive forces.
- The influence of surface conditions, such as dust and moisture, on the performance.

¹³ Grabit Inc.: <https://grabitinc.com/products/>

The best potential for electroadhesion seems to be realised when coupled with other grasping technologies. A notable example has been demonstrated through a versatile compact soft gripper that combined electroadhesion with a stretched dielectric elastomer actuator [79]. Another example demonstrated combining a stretchable electroadhesive pad with a soft pneumatic gripper to enable picking flexible objects off non-planar surfaces [80] (Figure 19).

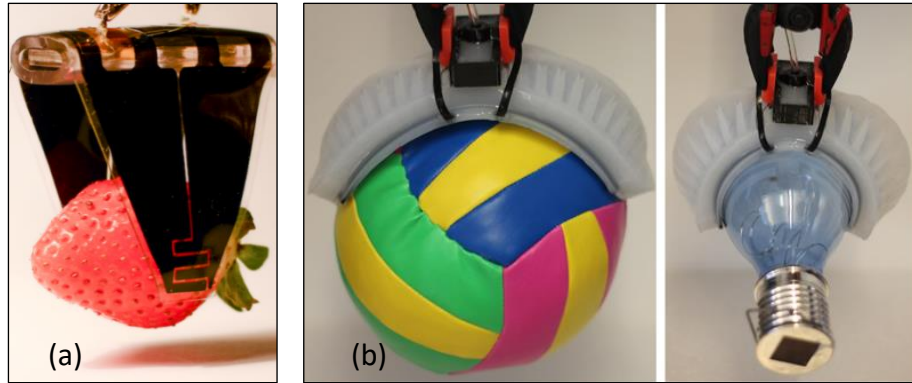


Figure 18: Soft grippers combining electroadhesion with (a) DEAs [79], and (b) pneumatic actuation [80].

Geckoadhesion

As the name implies, Geckoadhesion is inspired by Geckos which have microfibers on their feet that allow them to climb various surfaces through van der Waals forces [81]. Geckoadhesion occurs when pressing microfibers normal to their surface (pre-loading), which can work on smooth or rough surfaces, yet struggles with low surface-energy materials [82]. The more popular applications of Geckoadhesion are for wall climbing robots [83], perching mechanisms for aerial robots [84], and has been implemented with soft grippers as well. A notable example is a passive mechanism that preloads and releases microfibres which have been arranged on a flexible film substrate [85][86]. The gripper was able to pick a range of curved objects as shown in Figure 19. Probably the most impressive feature of Geckoadhesion grippers, in general, is the fact that objects that are several hundred times the gripper weight can be lifted, which is more than achieved by any other grasping technology. Furthermore, combining Geckoadhesion with other grasping technologies can again lead to novel grasping solutions. In one approach, a soft gripper made of an inflatable membrane was covered with mushroom-shaped microfibres to add Gecko inspired adhesion [87]. The gripper utilised its soft membrane to achieve a larger contact area and demonstrated picking different steel balls. Another approach was achieved with a multi-fingered gripper from liquid crystal polymer, which was integrated with a geckoadhesive pad on the fingertips [88]. The gripper utilised magnetic forces to direct the adhesion pads to the object, while using thermal actuation to

bend the fingers. Despite the versatility of Geckoadhesion, challenges remain in dealing with rougher surfaces and handling of deformable objects.

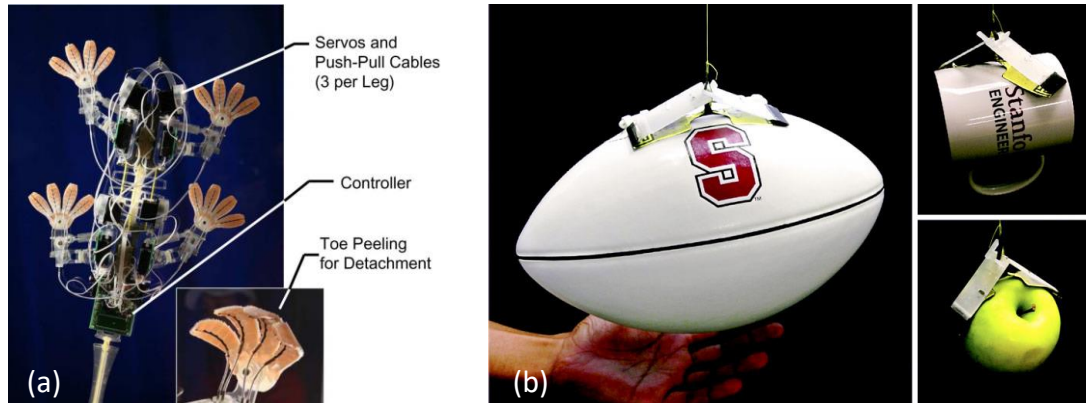


Figure 19: Examples applications for Geckoadhesion in (a) climbing [83], and (b) grasping [85].

2. 3. Morphologies of Pneumatic Bending Actuators

From the conducted comparison of different soft actuation methods for soft grippers, soft pneumatic actuators (SPAs) are the most developed and have been already used as soft grippers as reviewed. Among the key traits of SPAs is their ease of fabrication from different elastomers with varying Shore hardness depending on application needs, while being able to generate a wide range of forces and bending response depending on the chosen morphology and material. Additionally, their response is fast in grasping and releasing compared to methods that rely on heating, chemical reaction, or adhesion. Pneumatic actuators are also easy to combine with other actuation methods as shown in the previous section. Hence, SPAs are considered in this research, specifically bending actuators since they are able generate a bending motion that is analogous to that of human fingers [89]. This bending motion can be in a sense preprogrammed to achieve different trajectories by varying the morphology [32]. Additionally, the softness of bending actuators encourages safe interactions with human operators and enhances their adaptation to various complex and delicate objects. Soft bending actuators can be classified into three main categories according to their morphology. Those categories are; the pleated, cylindrical, and ribbed structure designs [21]. The first design is the cylindrical structure, which is typically composed of a soft outer layer with embedded cylindrical channels, and a stiffer central core that accommodates the transmission lines feeding those internal channels. Upon pressurisation, the channels will deform circumferentially and longitudinally based on the geometry and dimensions of their cross-sectional area. The stiffer core serves as an inextensible yet flexible constraint that directs the deformation to create only a bending motion.

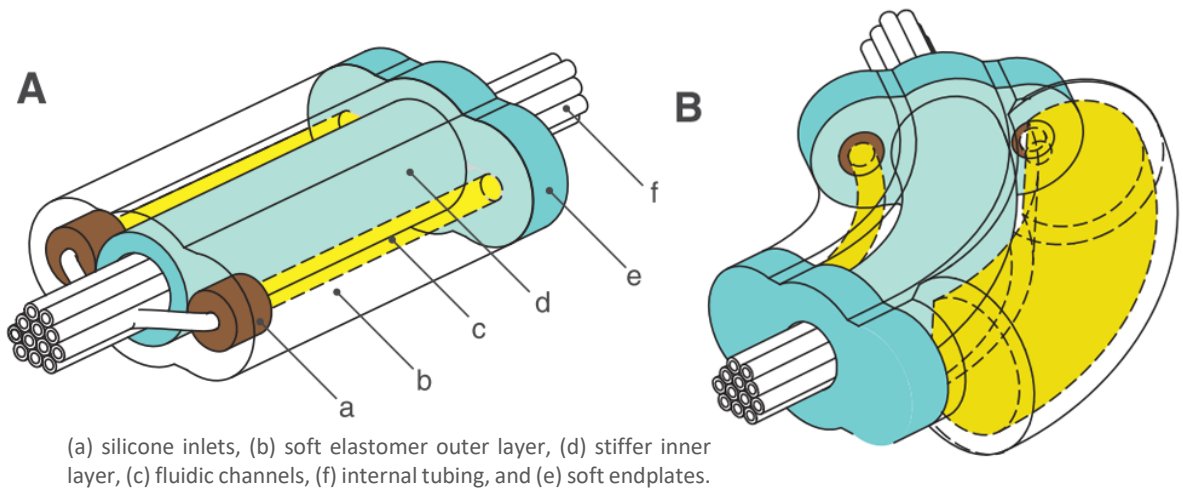


Figure 20: An illustration for the cylindrical morphology showing (A) neutral and (B) actuated states [21].

The second structural design is the ribbed segments, which is composed of two parts with an inextensible but flexible constraint layer separating those two parts. The upper part forms the majority of the bending actuator and is cast to create the geometry of fluidic channels, while the lower part is simply to seal the fluidic channel and encapsulate the strain layer in between. When the fluidic channels are pressurised, the air chambers expand pushing the ribs separating the chambers, which effectively mitigates the applied pressure. The presence of the constraint layer converts this deformation into a bending motion, as the chambers continuous to expand. The cylindrical structure of soft bending actuators is commonly used to create soft manipulators with added modifications [58], [90], due to its relatively easy production and ability to incorporate separate transmission lines within its core to separately actuate each chamber. These traits become partially useful when creating long manipulators that need to achieve more complex motions within a 3D space.

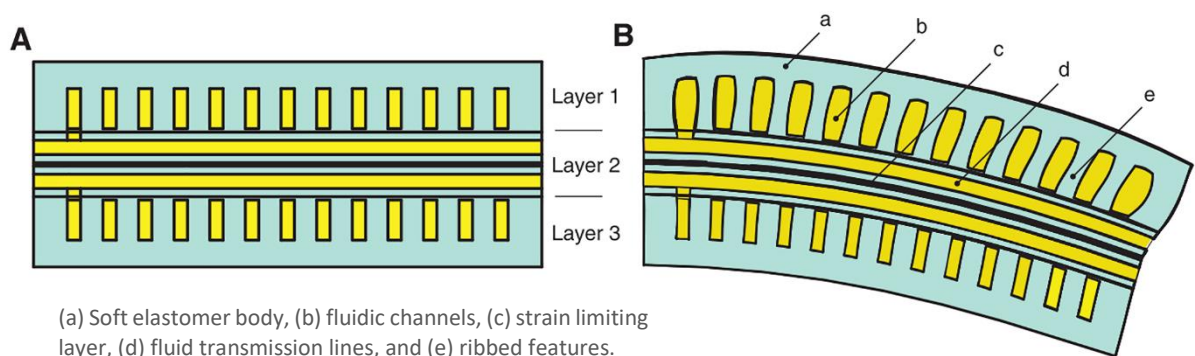


Figure 21: An illustration for the ribbed morphology showing (A) neutral and (B) actuated states [21].

Finally, the pleated structural design is based on the ribbed segments, but gaps are introduced between chambers creating discrete segments. All the chambers are still connected to each

other at the base similar to the ribbed design, so that they can all be actuated from the same inlet. The bending mechanism of the pleated design is also similar to the ribbed design, but here the chambers are not directly pushing against the same common rib separating them. Instead, each chamber is separately deforming its outer ribs until they make contact and start to push against each other. The presence of the strain limiting layer again directs the deformation to create a bending motion.

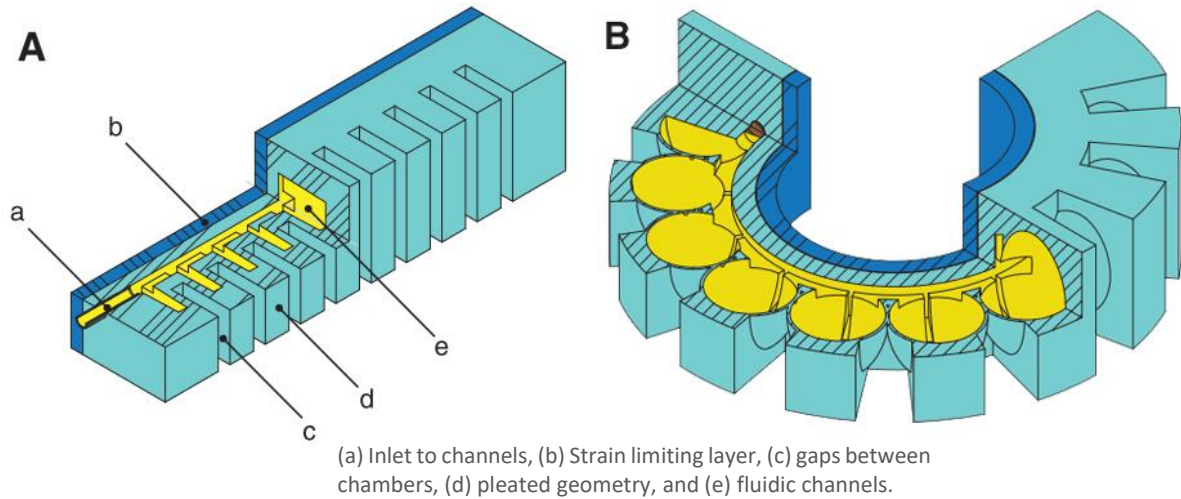


Figure 22: An illustration for the pleated morphology showing (A) neutral and (B) actuated states [21].

The useful applications of each actuator morphology are defined through its traits and limitations, which are highlighted in Table 1 and discussed here in more details. Pleated design of soft actuators excels in terms of energy efficiency and is able to achieve maximum bending angles [21]. However, the gap separation between air chambers causes increased static bending under gravity and general dynamic instability, especially when made of soft elastomers with low Shore hardness. This can be reduced by using slightly stiffer elastomers with higher Shore hardness, but will in return increase the energy requirements to achieve the same bending angle. Implementing this structure is also the hardest to produce reliably compared to the other two structures. On the other hand, the cylindrical design of soft actuators is much easier to produce and able to generally withstand higher pressures since the deformation is away from the interface between the fabricated layers [21]. However, the primary drawback associated with this design is the excessive radial deformation exhibited during bending. This not only results in a significant increase in the overall actuator volume that could cause undesired interactions with the environment, but also results in excessive circumferential strains that could shorten the life cycle of such actuators. In contrast to the pleated design, which suffers minimum strain during deformation due to the separation between chambers [21]. As for the ribbed design, the actuator is able to achieve large bending

angles with less fluid energy input and far less deformation when compared to cylindrical design [21]. Additionally, the structure is generally more stable and exhibits less deformation under its own weight compared to the ribbed design.

Table 1: Comparing the benefits and limitations of the three classes of soft bending actuators

	Main benefits	Main limitations
cylindrical	<ul style="list-style-type: none"> • Higher resilience and durability. • Can withstand higher actuating pressures. • Simplest to fabricate. • Several transmission lines can be incorporated at the core easily. 	<ul style="list-style-type: none"> • Exhibits excessive deformations and high circumferential strain. • Higher fluid energy required to achieve bending.
Pleated	<ul style="list-style-type: none"> • Capable of bending to higher curvatures at a given input pressure. • A bidirectional design is capable of exerting the highest forces. • Least strain during deformation. 	<ul style="list-style-type: none"> • Most complex to fabricate. • Requires the use of higher Shore hardness materials, which increases fluid energy requirements.
Ribbed	<ul style="list-style-type: none"> • Achieves more bending than the cylindrical design. • Soft materials with low Shore hardness can be used. • Easier to fabricate than pleated design. 	<ul style="list-style-type: none"> • Difficult to incorporate multiple transmission lines. • Prone to delamination at higher pressure supply.

2. 4. Fabrication of Pneumatic Elastomer based Grippers

Silicone rubber materials are soft and durable capable of withstanding deformations up to several times their original length, which made them a popular choice for many soft robotics applications [91]. Additionally, they can be easily shaped using simple moulding and lamination techniques. The moulds are often 3D printed from ABS or PLA filaments, as a fast and inexpensive method to fabricate them with the required features. The common process to produce soft robotics components from silicone rubbers is achieved through a multi-stage moulding process referred to as ‘soft lithography’ [33]. This involves the use of moulds to cast silicone rubber materials into the required geometry, which is then bonded together by spreading a thin layer of uncured silicone rubber [21]. Uncured silicone rubber acts as an adhesive material in this case to bond cured soft bodies together.

2.4.1. A Practical Guideline for Soft Lithography Approach

A simple soft gripper that is based on the very first soft gripper design proposed by Harvard's Wyss Institute for Biologically Inspired Engineering [22], was recreated here to demonstrate the production process and acquire a practical sense of its capabilities and limitations. The soft gripper is composed of four soft bending actuators based on the ribbed morphology and was entirely made from Ecoflex-50¹⁵. The fluidic channel pattern was imprinted using 3D printed moulds and sealed using a flat base layer made from the same material or a stiffer grade if desired. The strain limiting layer can be in the form of a sheet of cloth or paper at the base, to prevent the fingers from extending allowing only the desired bending motion. Flexible sensors can be also added as part of the strain limiting layer, in order to change in resistance as the soft finger bends, as later detailed in chapter 5. The general procedure followed in the fabrication of this soft gripper is summarised in the following steps:

- 1) **Design and Print Moulds:** The first step is to design the moulds with the negative of the internal channel geometry that needs to be imprinted on the main finger body. SolidWorks was used to design the moulds, which were printed from ABS filament using a standard 3D printer that achieves the desired printing accuracy (Figure 23).

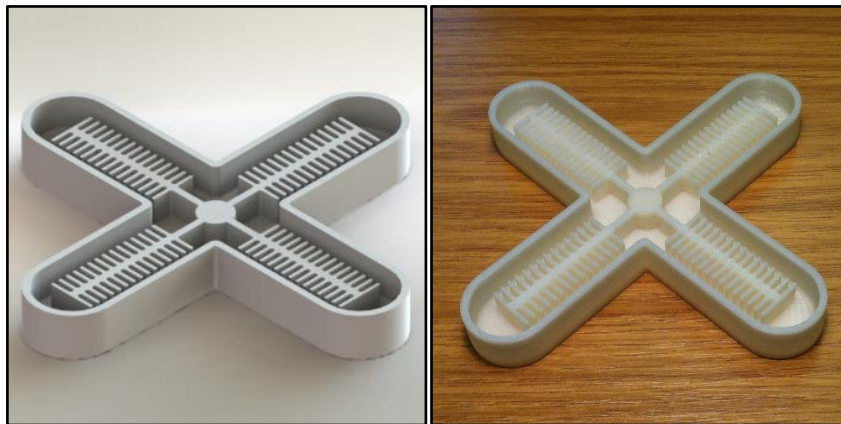


Figure 23: CAD model and the 3D printed soft gripper main mould

1. **Mixing and Degassing:** EcoFlex-50 is prepared by equal volumes from each of the provided bottles into a plastic cup and stirred for about 2 minutes to mix the required amount of material. At this stage, lots of air bubbles get trapped in this viscous mixture and hence is placed in a vacuum chamber set at -900 mbar pressure, for around 3 minutes until all air bubbles can be seen to escape the material (Figure 24).

¹⁵ **Ecoflex material:** http://www.smooth-on.com/Silicon-Rubber-an/c2_1115_1130/index.html



Figure 24: Mixing and degassing the Eco-Flex material

2. **Moulding:** The degassed mixture is then slowly poured into the 3D printed moulds at an angle to reduce the chances of creating air bubbles. Further degassing might be required at this stage if excessive air bubbles get trapped. The filled mould is left to cure for at least 6 hours at room temperature, or can alternatively be placed in a heated oven at 60°C for about 30 minutes to speed up the curing process. However, accelerating the curing process encourages air bubbles to be trapped as the material becomes more viscous before air bubbles can escape the surface. After curing is complete, the moulded parts can be carefully peeled from the mould as illustrated the figure below. Knowing that moulds that have been 3D printed at a finer layer height would have a smoother surface finish that makes the demoulding process easier.



Figure 25: demoulding the cured material from the 3D printed mould

3. **Strain Limiting Layer:** the main body of the soft finger and the flat sealing layer can be bonded together by spreading a thin layer (around 1 mm) of mixed Eco-Flex material on the sealing layer, and carefully placing and aligning the main body on top. Care must be taken during placement to avoid clogging the internal channels with the uncured bonding material. A strain limiting layer is necessary to prevent the soft actuator from extending allowing only the desired bending motion. This is achieved by simply placing a piece of paper when bonding the actuator parts together.

4. **Pneumatic Connection:** the last step is to connect a tube to the internal channels of the soft gripper to supply the pressurised air through a needle. The tube can be bonded directly to the soft finger body as well, yet using a needle eases the switching between soft finger samples during testing. Figure 26 shows the simple soft gripper prototype successfully grasping different objects relying solely on its passive compliance.



Figure 26: Fabricating a basic soft gripper prototype

The described fabrication procedure can be followed to create different designs of soft robotic components, as long as the design can be divided into planar parts and it is feasible to 3D print the required moulds to imprint its geometric features. Further modifications can be made to this process such as the addition of external braiding for stiffening the soft fingers [92] or the use of a retractable-pin or lost-wax core to create different internal features [21]. Yet the underlying principles of the described moulding process remains similar. Moreover, when conducting preliminary grasping tests using this simple soft gripper the actuation pressure and duration were estimated based on learned experience. Both the pressure and duration of actuation, decide the volumetric flow rate of air pumped inside the soft fingers and hence determine the amount of bending achieved. Supplying excessive flow rate results in excessive bending of the soft fingers, which causes the fingers to flip and lose contact with the grasped object. On the other hand, supplying insufficient flow rate results in limited bending that might not be sufficient for the soft fingers to firmly grasp the object and hence slippage might occur. Therefore, it is evident that an understanding of the bending response of such soft fingers is essential to be able to predict the resulting bending angle according to the set input conditions, which is investigated in Chapter 4. This also highlights the need for sensory feedback to detect contact with the object and prevent excessive or insufficient fluidic energy supply as further discussed in Chapter 5.

2.4.2. The Potential of Additive Manufacturing

The conventional soft lithography method for fabricating soft grippers made of silicone rubber materials is limited in terms of scalability, repeatability, and accuracy. This is mainly due to the manual multi-stage nature that is prone to variation and requires waiting for curing. Additionally, the moulding process is limited to creating mostly 2.5D shapes with a consistent cross-section. Adding internal or more complex features is also difficult. The retraction pin casting method was proposed to overcome this limitation, yet only simple internal geometries can be created limited by the shape of the pin [16]. Lost wax casting is another alternative method that can create more complex internal channels, but the multi-stage nature of the process makes it time-consuming and requires replacing of the internal core each time [30]. Thus, recent attention has been directed towards the potential for additive manufacturing of functional soft robotic components with more complex morphologies. This has been discussed in recent review papers that were published towards the end of this project [93]–[95]. According to the ISO/ASTM 52900 International Standard, the definitions of additive manufacturing processes that are relevant to soft material printing include:

- Material extrusion, in which material filament is dispensed through a hot nozzle to create the desired part layer by layer. Fused Filament Fabrication (FFF) is a popular material extrusion process, since it requires relatively inexpensive printer hardware compared to other 3D printing technologies.
- Material jetting, in which droplets of the build material are selectively deposited on the build surface from a moving nozzle. This is the case for Polyjet printers which simultaneously deposit and cure a photopolymer resin. The technology also enables multi-material and multi-colour prints, but commercial polyjet printers are significantly more expensive than FFF printers.
- Vat photopolymerization, which involves curing a vat of liquid photopolymer resin layer by layer through a light-activated polymerization process. Stereolithography is a Vat Photopolymerization process that uses an ultraviolet laser beam to selectively solidify layers of a photopolymer resin into the desired geometry.

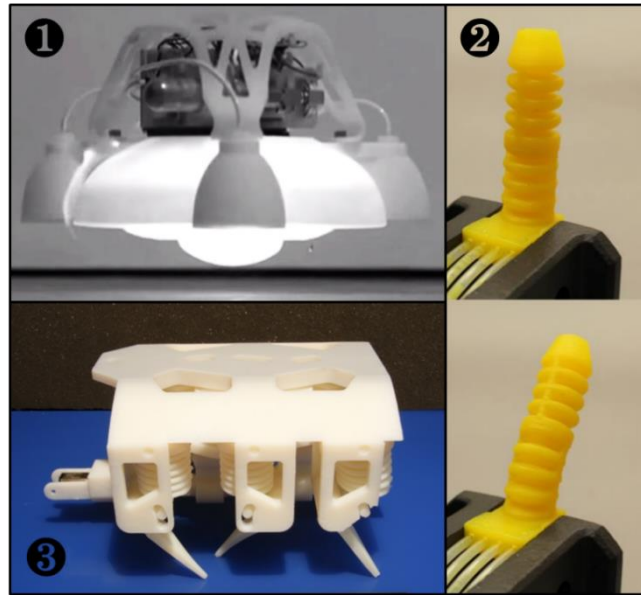


Figure 27: Early examples of utilising 3D printing with soft robotics [96][97][98].

One of the earliest attempts directed at 3D printing for soft robotics, was demonstrated by 3D printing a functionally graded combustion driven jumping robot using an advanced multi-material polyjet printer (Connex500, Stratasys)[96] (Figure 27-1). Another early attempt also demonstrated printing a complete hydraulically actuated hexapod robot including the fluids sealed inside the actuators using the same 3D printing technology [98] (Figure 27 -2). Later, a soft gripper based on fluidic actuators was 3D printed using the same technology for picking up delicate objects [99]. Interesting work on 3D printing a variety of soft tactile sensors has been successfully demonstrated using multi-material polyjet printers to enable printing the complete sensor including the soft membrane [100]. Although the multi-material polyjet printers used in those examples can create impressive parts with a range of material hardness, creating internal structures is challenging since they must be filled with support materials that are difficult to extract without damaging the printed parts. In addition, the mechanical properties of the printed materials suffer from poor durability and tear resistance that greatly limits the life cycle of printed actuators. Moreover, custom 3D printing processes were developed to print soft actuators, which include: a digital mask projection stereolithographic capable of printing soft antagonistic actuators with better mechanical properties [97] (Figure 27 -3), a low-cost planar printer setup for printing bending actuators (pouch motors) [101], and digital light processing based 3D printing for stretchable elastomers [102]. Those custom 3D printing setups provide more affordable solutions that are customised to produce good results for specific actuator designs. However, being a customised printing process makes it more difficult to replicate by others with and limits the material choices available when

compared to the commercial multi-material 3D printers. A more recent approach is to utilise the well-established and easily accessible Fused Filament Fabrication (FFF) technology as faster and more consistent alternative to the conventional manual fabrication, while being more affordable with better mechanical properties compared to advanced polyjet printers. Recently, the potential of utilising FFF was investigated for 3D printing high-force bending actuators as soft grippers [37]. Another recent and relevant work involved a soft gripper 3D printed using FFF and a haptic glove attached with flex sensors for telemanipulation applications [103]. It can be therefore concluded that 3D printing technology, especially FFF, has the potential of revolutionising the fabrication of soft robotics components, to achieve more sophisticated and reliable results compared to manual approaches. Combining this with the potential for 3D printing soft sensors opens a completely new realm of possible applications for soft actuators that can be directly 3D printed with the required embedded sensing [104].

2.4.3. 3D Printing of Soft Materials

New flexible material filaments are now commercially available to print using common FFF printers. Those material filaments are formulated from thermoplastic polyurethane (TPU) that enable flexible printed parts that are also strong and durable. Many TPU filaments have been developed by different companies over the past few years, but at the time of conducting this review, the most flexible option was NinjaFlex material from NinjaTek (datasheet in Appendix (F) – Materials . Table 2 summarises the material properties of popular flexible material filaments for FFF, in comparison to commercially available silicone rubbers commonly used for moulding soft actuators. The table also includes the corresponding material properties of the Tango black material, which has been previously used with advanced polyjet 3D printers as discussed in the previous section. The comparison highlights the superiority of low Shore hardness grades of common silicone rubber materials, such as Ecoflex-30, in terms of material softness and elongation. However, the manual multi-stage fabrication process associated with silicone rubber remains a limitation. 3D printing of silicone rubbers is hence, becoming increasingly desired especially with the rise of soft robotics. This is motivating researchers (and companies like Wacker group) to invest into new technologies to reliably 3D print silicone rubbers into complex shapes [105][15]. On the other hand, polyjet 3D printing is a more mature additive manufacturing technology with commercial printers available that can 3D print complex multi-material objects. However, looking at Table 2, it can be observed that although materials that are as soft as 28A Shore hardness are available, their elasticity, tensile

and shear strength is still limited compared to silicone rubbers. This limits their functionality due to early material fatigue when used for intensive applications involving repeated high strains [106]. Additionally, the shelf-life of photopolymers in general is known to degrade under prolonged ultraviolet (UV) light exposure, heat, and humidity, which limits the reliability of parts printed from those materials [107]. Hence, this motivated the consideration of new commercially available flexible materials that can be 3D printed using the well-established FFF process. Not only is the 3D printer hardware significantly cheaper than polyjet printers, but also allows printing of flexible materials such as Ninjaflex that has significantly better elongation at break and tensile strength than Tango Black. This comes at the expense of higher Shore hardness, but still soft enough for many soft robotic applications. Therefore, among the well-established technologies for 3D printing flexible materials, FFF can offer a low-cost alternative to challenges with the manual fabrication of soft robotic components. Alternative solutions can become available in the near future with the ongoing development of new 3D printing technologies to reliably 3D print silicone rubbers, as well as the release of new flexible materials for polyjet printers that offer enhanced mechanical properties.

Table 2: Comparing the properties of commercial soft printable and moldable materials

	3D Printing					Soft Lithography		
	FFF Flexible Filaments			PolyJet Flexible materials		Silicone Rubbers		
	TPU Ultimaker	Cheetah	Ninjaflex	Tango Black	Tango Black Plus	Dragonskin-30	Elastosil M4601	Ecoflex-30
Shore hardness	95A	95A	85A	60-62A	26-28A	30A	28A	30A
Elongation at break	580%	580%	660%	45-55%	170-220%	364%	700%	900%
Tensile strength	39 MPa	39 Mpa	26 Mpa	1.8-2.4 MPa	0.8-1.5 MPa	3.45 Mpa	6.5 Mpa	1.38 Mpa
Tear strength	--	--	--	3-5 Kg/cm	2-4 Kg/cm	19.2 Kg/cm	30.56 Kg/cm	6.78 Kg/cm
Specific gravity	1.22	1.22 g/cc	1.19 g/cc	1.14-1.15 g/cc	1.12-1.13 g/cc	1.08 g/cc	1.13 g/cc	1.07 g/cc

2. 5. Embedded Sensing for Soft Actuator Control

Soft robots currently rely on the embedded intelligence of their morphology to passively adapt to task variations and processes uncertainties. However, sensor-guided control would be necessary for applications that require a deterministic performance that can be reliably monitored and controlled. Hence, incorporating sensing capabilities into soft robots is the first step to achieve accurate closed-loop control. Due to the fact that soft robots are made of soft and highly deformable materials, the sensors to be embedded need to exhibit similar flexibility to avoid hindering the desired compliance. Hence, there is a need for a new class of soft electronics, which can stretch and deform as necessary, so that complete circuits can be embedded or attached to soft robots easily without affecting their behaviour [108]. Thus, researchers have been developing novel solutions for flexible and stretchable electronics over the past years for the seamless integration of sensors into soft-bodied actuators [109]. In fact, the research into soft sensing solutions has been mainly driven by the wearable sensors domain, which also requires sensors that can be safely attached to human skin as outlined in a recent review [110]. Applications for wearable sensors range from medical screening and diagnostics to motion tracking of limbs for assistive devices [111][112][113][114]. The general approach in soft sensors is to embed a conductive extendable material in a designed layout within the soft body, then measure a physical property (usually resistance) of this material that changes with the deformation of the body [115]. Hence, this physical property can be then related to the actuator response that needs to be sensed. Hence, the performance of those sensors mainly depends on the properties of the conductive sensing material, and the modality of the sensor is determined through the geometric design of the conductive tracks. It has been identified from the literature review that the main soft sensing approaches that could be smoothly integrated with soft actuators to measure and control their response can be classified into three categories based on their flexible conductive material:

2.5.1. Conductive silicone rubbers

The first approach to create flexible and stretchable sensors that can be seamlessly embedded into soft-bodied actuator is to mix conductive additives to the same silicone rubber materials used to create the soft actuators [116]. One way of achieving this is through mixing different forms of carbon additives with silicone rubbers to create stretchable soft sensors that can be easily moulded [117][118]. A characterisation of the relation between the electrical resistance of this composite material to the applied pressure has been successfully achieved [119]. In addition, an interesting manufacturing process was developed in which carbon grease is

injected through a syringe needle into the soft matrix using a 3D printing process, to create various patterns of carbon within the soft material [120]. Also, the processes are potentially scalable through a customised 3D printing process injecting carbon grease into a silicone rubber reservoir as shown in Figure 28 [120]. The material was successfully utilised in creating embedded soft strain sensors within the body of a two-fingered soft gripper to relate the deformation of the fingers to the actuated linear displacement [121]. Also, it was demonstrated to detect grasped objects and recognise their different sizes using an adaptive neuro-fuzzy controller [122]. The main challenge with conductive silicone rubber sensors is the difficulty in producing sensors with consistent electrical properties, since repeated deformation may affect the spread and orientation of carbon particles within the soft material. This also introduces noise and hysteresis errors in the readings. Also, stable electrical connections are difficult to achieve and can introduce additional fluctuations in the readings.

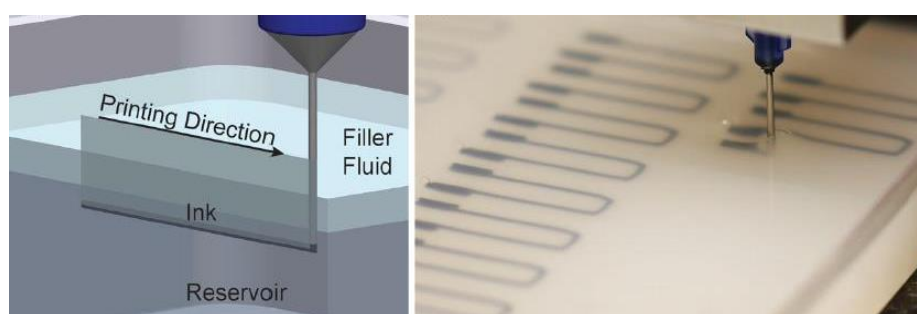


Figure 28: 3D printing of conductive material into the silicone rubber matrix [120]

2.5.2. Conductive liquid metals

Recognising the limitations with carbon filled silicone rubbers, a more popular soft sensing approach was achieved by filling patterns of micro-channels imprinted within an elastomer body with a conductive liquid metal material called Eutectic Gallium-Indium (EGaIn). EGaIn is highly conductive and has unique rheological properties that allow it to readily flow into channels of micro scale when a certain amount of pressure is applied [123]. Thus, simple moulding techniques can be used to create channels of different cross-sectional areas and patterns within a soft body, then EGaIn can be injected to fill these channels as a flowing liquid, which solidifies into an elastic material once the applied pressure is removed. Hence, different physical parameters can be measured. Moreover, it has been demonstrated that different physical parameters can be successfully measured using a novel soft sensing concept depending on the designed geometry and orientation of the conductive channels [123]. Notable previous work has demonstrated the use of this sensing approach to measure parameters such as: Multi-axis forces [124], strain [125], shear [89], Elongation [126], curvature [127], and pressure [128]. It was also demonstrated that by stacking layers of EGaIn

sensors, additional sensing modality could be combined together, such as the multi-modal strain and curvature sensor shown in Figure 29 [129]. Despite the promising multi-modal sensing capability of EGaln based soft sensors and the ease of bonding to silicone rubber bodies, they have not yet been sufficiently utilised and evaluated for grasp feedback applications. Notable recent examples demonstrating relevant sensor-based control of soft actuators include: position and force control of soft bending actuators using feed-forward models in conjunction with a PID controller [130], controlling the bending of soft beams actuated by an antagonistic pair of SMAs [131], detecting the presence of an object grasped using a simple soft gripper [132], and flex and twist feedback for braided pneumatic actuators [133].

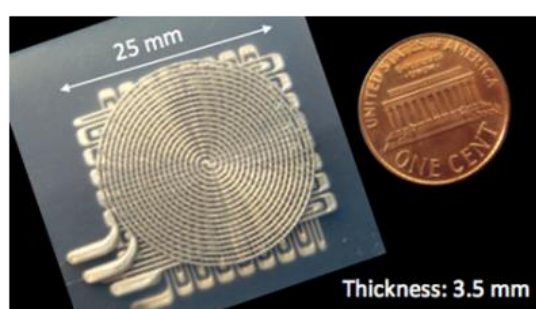


Figure 29: Multi-layered conductive channels for measuring pressure and strain [125]

On the other hand, the process of creating the embedded micro-channels and injecting conductive liquid metal is a manual, multi-stage process that requires skill and experience to achieve a consistently reliable output. Automating this fabrication process using 3D printing is an open challenge that can enable mass production of scalable and customisable sensors, as highlighted in a recent review [134]. Although usually needed in small quantities, the conductive EGaln material is still very expensive and requires special care in handling as it is corrosive. The strain feedback from this approach was reported to be mostly linear and highly repeatable, yet still suffered from some hysteresis at higher strain rates due to wiring and the time taken for EGaln material to refill the deformed micro-channels [125]. Improved sensory feedback with reduced hysteresis was achieved using a hybrid method combining two liquid conductors: an ionic solution and channels of EGaln material [89].

2.5.3. Commercial Flexible Sensors

Another approach for embedding strain sensing capability into soft actuators is the use of existing sensing components that are thin and flexible enough to avoid interfering with the actuator's functionality. This can be achieved using off-the-shelf conductive fabrics, as shown by embedding pieces of conductive lycra (Electrolycra) in soft arms for spatial configuration

reconstruction [135], and as a sensor for tactile sensing [136], as well as embedding electro-conductive yarn in a soft manipulator for bending elongation feedback [137]. Optical fibres have been also used as macrobend stretch sensors for pose sensing in soft continuum robot arms [138]. Another attractive commercially available option is resistive flex sensors that are made of thin and flexible films, which change its resistance upon bending [139]. Relevant work demonstrated utilising the feedback from flex sensors embedded into soft actuators to achieve: haptic identification of grasped objects using a trained algorithm [140], controlling the shape of soft fingers actuated using antagonistic shape memory alloys [141], and a recently published paper demonstrating closed-loop control for cylindrical soft actuators [142].

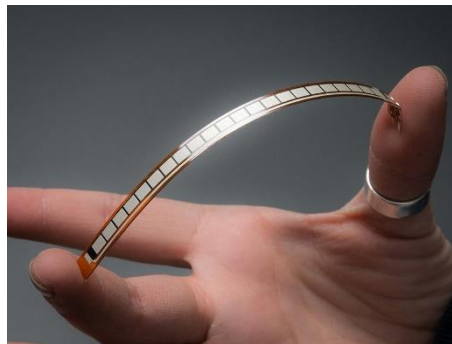


Figure 30: bending a sample flex sensor

The main advantage of using commercially available flexible sensory elements such as the flex sensors compared to using conductive silicone rubber or EGaIn filled silicone rubbers lies mainly in their ease of availability at a relatively low budget. They are also flexible enough to maintain the soft actuator's compliance when embedded inside it. Flex sensors specifically are unique for their lightness, compactness, and robustness [139]. They also come with ready terminals that facilitate stable wiring without introducing significant noise to the readings, which is a challenge for elastomer-based sensors. However, the sensitivity of different samples is not identical, which means that each has to be individually calibrated to be used. Also, since they come in specific sizes, then the actuator has to be designed around the sensor's dimensions. Hence, it would be interesting to devise a method for fabricating similar resistive sensors that offer better customisation and consistency of the samples.

2. 6. Identified Knowledge Gaps

After reviewing the novel soft actuator and soft sensor concepts that have emerged from the developing soft robotics research area, it is clear how promising soft gripper concepts can be developed utilising those technologies to achieve remarkable capabilities that are rather challenging for conventional rigid grippers. However, soft robotics research is still in its early stages, with lots of research challenges that need to be investigated to enable full utilisation of its products. Based on the findings of the conducted literature review, the following knowledge gaps have been identified, which are relevant to soft grippers and the broader soft robotics research area as well.

- **Enhancing the payload of soft grippers**

As previously discussed, the use of soft materials enhances compliance but consequently reduces the payload of soft grippers required to lift and maintain a stable grasp over denser objects. One approach to tackle this challenge is through a combination of soft and stiffer materials were incorporated within the structure of the gripper to achieve the difficult optimisation between softness and stiffness based on the intended application, similar to what has been achieved in the SDM hand [45]. Alternatively, following the footsteps of the universal jamming gripper, a promising approach is through incorporating variable stiffness into soft grippers so that the gripper can be soft during grasping when compliance is needed, and more rigid after grasping when a stable grasp is required [143]. In fact, alternative novel approaches for achieving controlled stiffening are being proposed, which has been compared in a recent review [144].

- **The need for generalised design guidelines and supporting software**

Due to the fact that the basic principles of soft grippers defy the foundations of traditional hard grippers with rigid links, conventional methods commonly used in modelling, design, manufacture, sensing, and control of traditional hard linked grippers are no longer applicable for soft grippers. A lot of the work developed in the soft robotics area during the past few years, before conducting this review, relied on experimental investigations to come up with application-specific solutions that are not easily transferable. Hence, there is a need for a standardised design guidelines and supporting software tools that take into consideration this new paradigm in development of soft grippers, to systematically guide the development of soft robots in general according to the application needs [29].

- **Simplifying accurate modelling of complex behaviours**

The soft hyperelastic materials commonly used to produce soft grippers exhibit non-linear deformations that are difficult to model accurately, especially when combining different materials and operating at a wide strain range [145]. Simplified modelling techniques and reliable simulation tools are essential to fully utilise the capabilities of soft grippers [146]. Those will aid the process of designing soft grippers based on their simulated response, rather than through experimental trial and error that does not always lead to optimised solutions. Deriving precise models through analytical and finite element methods have proven to be a challenging, case-specific process, which motivates the consideration of alternative data-driven approaches. With the advances in machine learning techniques and the new perspective from morphological computation regarding material non-linearity as a computation source, an overlap between the two fields can yield exciting solutions that learn and exploit the complex behaviour of soft actuators through intelligent algorithms.

- **Sensor-enabled feedback control and grasp feedback**

Despite the desired traits of passive compliance, it is clear that embedded sensing would be essential to provide useful grasp feedback and enhanced controllability for a more reliable soft gripper performance. Since soft grippers are made of soft and highly deformable materials, the sensors to be integrated need to share the same properties as well to ensure smooth integration. The advances in flexible and stretchable sensors have provided novel soft sensors as reviewed here, yet their utilisation in soft grippers is still not fully realised [147]. A methodology for deciding the appropriate type, quantity, location, and orientation of those soft sensors is also lacking. Limited research has been directed towards the closed-loop control of sensorised soft actuators, despite the promising abilities to have a controllable soft gripper. Yet with advances in soft sensor fabrication and efficient modelling techniques, accurate control can be made possible that can be potentially extended to different soft gripper designs.

In summary, the rising area of soft robotics in general and soft gripper specifically is full of research opportunities that need to be investigated before their capabilities can be realised. In this research, the focus would be mainly on the last identified knowledge gap related to the sensor-enabled control of soft grippers. The following chapter will discuss more details about the specific research questions that will be tackled in this research.

CHAPTER 3:

Research Methodology

It is clear from the literature review that considerable research has been directed towards developing flexible robotic grippers that are capable of handling a wide range of objects and adapting to uncertainties arising during grasping operations. Although many of those grippers are showing promising performance in manipulating complex objects, they are still mainly limited to applications within research lab environments. A key reason behind this is the fact that accurate performance that can meet industrial standards usually comes at an undesired high price and bulky structure, which hinders the feasibility of such grippers in real industrial applications. These challenges motivate the consideration of soft grippers as an alternative approach in achieving highly compliant grippers that are able to handle objects that are both complex and delicate, while being more compact in structure and much cheaper to produce compared to traditional rigid grippers. The utilisation of soft and highly elastic elastomers, allows soft grippers to passively conform to complex geometries through the interaction between the target object and the gripper morphology. This passive compliance raises the need for expensive sensing and sophisticated grasp controllers, which reduces the cost and size of soft grippers. Additionally, being soft in nature not only allows the grasping of delicate objects safely, but also encourages safe human-robot interactions. On the other hand, the limited feedback and control over the gripper performance are still hindering the full utilisation of soft grippers in real industrial applications. Despite being a highly desired trait in soft grippers, the enhanced passive compliance has its undesired limitations. The lack of sensing means that no feedback is available regarding the grasp quality or success. Furthermore, the highly non-linear nature of the soft elastomers used to create soft grippers makes accurate prediction and control of their behaviour a very challenging task. This limits the applications of soft grippers in more complex tasks that require a highly reliable and deterministic performance. Thus, it would be interesting to research the possible approaches for accurately modelling and controlling highly compliant soft grippers that can reliably and safely handle various complex and delicate objects, with the aim of taking a step towards extending their utilisation in automating more difficult handling tasks in less structured environments.

3. 1. Research Questions

The aim of this research is to develop a feedback controlled soft gripper that combines the benefits of the passive compliance realised through the embodied intelligence of the soft gripper's morphology, and improved controllability by embedding flexible sensors for grasping feedback. A purely data-driven approach is proposed in this research to derive simple empirical models that can be utilised by a high-level controller to accurately position the soft fingers towards their target based on the resulting sensory feedback. On the other hand, the grasping mechanism is delegated to the morphology of the gripper body as the soft fingers interact and adapt to targets of varying shapes and delicacy. Ultimately, the results of this work will demonstrate a new methodology for developing controllable soft grippers, following a purely data-driven approach that can be applied to different soft actuators without any complex mathematical modelling, as long as reliable feedback from flexible sensors can be generated. To achieve this, the following research questions have been identified to be addressed in this research:

1. Is there a clear and consistent relationship for the free-bending response of soft bending actuators that can be described by simple empirical models?

In a soft robotics context, the control is largely delegated to the morphology of the soft body, which is determined through its geometry and material properties. Hence, the bending response of a soft gripper finger can be in a sense preprogrammed via the design of the internal fluidic channels and selection of the material used in creating the finger. Since material science is outside the scope of this project, commercially available elastomers that are widely used in the soft robotics fields will be utilised to create the soft gripper fingers studied here. Hence, the first objective of this research will be to evaluate the consistency of the free-bending response of an appropriate soft finger morphology at different input conditions through systematic experimentation. The nature and consistency of the relationship between the input pressure and resulting bending will determine the feasibility of the proposed data-driven approach and the methods required to accurately capture this relationship for reliable control. An experimental setup would be required that allows consistent testing of soft fingers at controlled input pressures and durations, while automatically imaging and processing the resulting bending behaviour for analysis. Several design variations for the selected actuator morphology will be generated and tested in this experiment to confirm the consistency of the results. This will allow studying the effect of varying the dimensions of the internal fluidic channels on the maximum bending and force

capabilities for a given input pressure so that the best performing design can be identified. Furthermore, the experiment will also provide practical insights into the limitations of the manual fabrication process and recommended operating pressure to be used in the following stages. Having this clear understanding of the consistency of the bending response and key design parameters affecting it will not only facilitate the design process of soft grippers, but also paves the way for accurately controlling their response.

2. How accurate can the bending of soft fingers be modelled and controlled when following a purely data-driven approach utilising feedback from embedded flexible sensors?

The recent attempts in developing soft grippers have mostly relied on their soft nature of the gripper to achieve passive compliance without the need for sophisticated sensory feedback or online control [148]. However, the conducted literature review identified modelling and controlling soft robotic actuators as a critical research challenge that still requires further research, in order to realise more reliable soft robots that can be utilised in real-life application [149]. Conventional model-based control that is commonly used with traditional rigid robots becomes too complex when trying to account for the highly non-linear behaviour of hyper-elastic soft bodies. This results in computationally expensive models that are not best suited for real-time control, while being constrained to the exact geometry and material that have been modelled. A purely data-driven approach is proposed in this research that utilises experimental data from testing soft fingers with embedded flexible sensors to attempt to capture their bending behaviour, while implicitly accounting for sources of variations that are otherwise difficult to model mathematically. Such a data-driven approach lifts the need for complex analytical or numerical modelling approaches, which are difficult to derive accurately considering the highly non-linear nature of soft fingers, especially when considering material combinations or added reinforcements. Yet, this would require embedding the soft fingers with flexible sensing capability, to provide positional and grasp feedback, and aid sensor-guided control operations. Several novel flexible and soft sensors have been proposed over the past few years, which can be potentially integrated with soft-bodied robots [120][124]. From the literature review, resistive flex sensors have been identified as a potential sensing solution that is flexible to bend, inexpensive, and commercially available. Yet, the quality and repeatability of its sensory feedback will have to be systematically evaluated at different operating conditions when embedded within a soft finger. Afterwards, empirical models can be derived using common data-driven modelling techniques, in order to quantify their prediction accuracy as an evaluation of the proposed data-driven modelling approach.

Furthermore, the soft gripper controller will follow biologically-inspired control architecture, in which a simple high level controller can achieve more sophisticated behaviours by utilising the embodied intelligence of its morphology [59]. The high-level closed-loop controller will process generated sensory feedback through the data-driven models, in order to estimate and control the free-bending of the individual soft gripper fingers. While the soft gripper body will passively conform to target objects upon contact, elevating the need for precise grasp planning. The controller will have to regulate the pressure supply to the soft fingers based on the error between the estimated and target bending angles, which can be achieved using low-cost hardware via high speed valve switching [35]. The performance of such a controller will also be evaluated by measuring how accurate a modelled soft actuator with embedded sensing can follow a target reference signal.

3. Can the simple feedback from sensorised soft gripper fingers be further utilised to enable contact detection and additional grasp feedback?

The lack of sensory feedback in soft robotic components limits their reliability for autonomous applications. More specifically, for an entirely passive soft gripper, not only is no feedback available to detect when contact is made with the target object, but also no information can be inferred regarding the properties of the grasped object. Hence, the embedding of flexible sensors in soft gripper fingers can enable a more deterministic grasping performance following a sensor-guided control approach. However, the requirement of having a highly flexible sensor that does not hinder the desired compliance and the challenges in interfacing multiple sensors through soft materials limits the choices of feasible sensors to integrate. Thus, it would be interesting to investigate if the same sensory feedback from embedded flex sensors can be further utilised to provide additional grasp feedback. Contact detection would be essential to allow the controller to switch from estimating free-bending angles based on the derived empirical models, to potentially monitoring the grasp quality. Additional inferences about the grasped object can be then made to confirm if it falls within the expected size or weight of the intended target. Despite the fact that making grippers from soft materials with low Shore hardness results in inherently safe fingers are less likely to damage delicate targets, it could be still desirable to have some rough qualitative measure for contact force for even safer and more reliable performance. The force feedback can in this case guide the controller to stop the supply pressure if it exceeds a set threshold.

4. Can 3D printing technology be utilised to aid the automation of the manual fabrication process of soft grippers for a faster and more consistent output?

Another challenge limiting the applications of soft robotics is the highly manual nature of its multi-stage fabrication process, which introduces sources of variation due to human error at different stages of the production. This could affect the dimensions as well as the material properties of the products. Hence, the uncertainty in the output limits the efforts in deriving generic models that can maintain their prediction accuracy across different samples made from the same material and following the same design. As discussed in the literature, a growing interest now is to investigate the utilisation of 3D printing technologies to fabricate soft robotic component more efficiently with a faster and more consistent output that is less dependent on human skills [91]. In this research, the well-established material extrusion-based printing will be investigated as an alternative fabrication process that requires relatively inexpensive printer hardware and commercially available flexible material filaments. It is hypothesized that by tuning the printing parameters, successful fabrication of functional air-tight soft gripper fingers can be achieved. Systematic experimentation will be necessary to evaluate the reliability of the printed actuators and characterise their bending and force responses. Additionally, it would be interesting to investigate the possibility of printing flexible strain sensors that can be easily integrated to the printed actuators, so that directly printable and customisable sensorised soft gripper can be realised. The sensors also will be characterised in order to evaluate their capabilities and limitations as part of a soft gripper finger, in comparison to the commercially available flex sensors. Moreover, this additional work will provide an opportunity to further test the adopted data-driven modelling approach with soft grippers following a different morphology and made from a different material. Accurately modelling the bending response of printed actuators will be an additional confirmation of the potential of the proposed data-driven approach in modelling a wide range of soft robotics components as long as adequate sensory feedback can be generated.

In summary, the underpinning research hypothesis can be stated as follows:

Purely data-driven models utilising simple feedback from embedded flexible sensors can be derived to accurately estimate and control the bending of soft gripper fingers for sensor-guided grasping operations.

3. 2. Proposed Approach

3.2.1. Inherently Safe Soft Grippers for Handling of Delicate Objects

When considering the challenge of handling delicate objects that can be easily damaged by hard contact, it makes sense to consider making the gripper itself from a soft material that ensures soft contact. Hence, the proposed robotic gripper should be not only soft enough to safely handle objects of a delicate nature, but also highly compliant to conform to their complex geometry. Additionally, the complexity of the gripper should be minimised to reduce its cost, weight, size, and manufacturing difficulty, in order to improve its chances of being utilised in industrial applications. This is important since, as highlighted in the literature review, previous attempts in developing dextrous grippers with active compliance relying on sophisticated sensors and bulky actuators have resulted in complex and expensive grippers that were unattractive for industries to utilise [150]. Therefore, such requirements motivated the consideration of the increasing research trend in soft deformable robots, as a promising approach for developing adaptable grippers that are made of soft inexpensive and highly deformable materials [20]. A soft gripper with deformable fingers is expected to exhibit sufficient compliance to conform to objects of various geometries while maintaining gentle distributed interactions with delicate targets. In addition, the soft material used in producing soft grippers is actually light in weight, inexpensive, and can be easily shaped. All these are desirable traits that satisfy the design requirements of the proposed gripper discussed in Chapter 1 so that it can safely handle delicate objects, as illustrated in Figure 31.

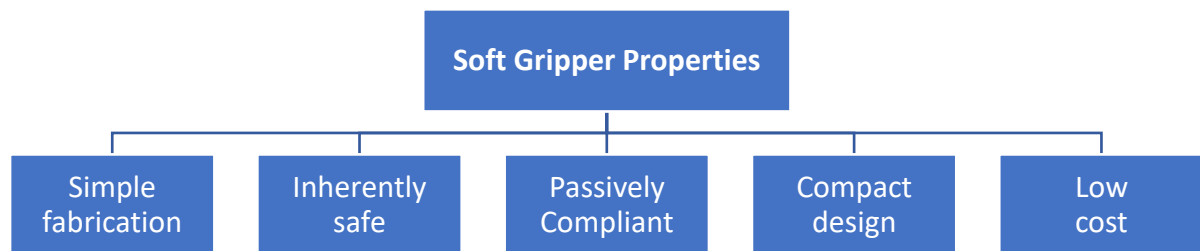


Figure 31: Illustration of the desired traits from using a soft gripper

On the other hand, the improving the accuracy of the soft gripper involves a major research challenge that is drawing the attention of researchers in the soft robotics field. Modelling and simulating the behaviour of highly deformable soft materials has proven to be a very complex non-linear task, which is difficult to achieve with the acceptable accuracy necessary to predict and optimise the motion of the gripper fingers. The task becomes even more challenging when considering gripper fingers that are made of more than one material with different stiffness,

while attempting to make contact with different unknown objects at any location along the fingers. In a typical grasping scenario, the non-linear deformation of each gripper finger is not only determined by the applied actuation force, but is also affected by the weight and shape of the grasped object, which might not be known in advance. Hence, model-based control of the highly non-linear deformation of a soft gripper is clearly a difficult approach for accurate and reliable control of the gripper fingers, which would hinder the desired versatility and adaptability of the gripper as a full understanding of all external factors becomes necessary.

3.2.2. Pneumatic Bending Actuators as Soft Gripper Fingers

Similar to human fingers, the primary motion required for a gripper finger is bending towards the inside of the gripper body to achieve grasping, in addition to limited lateral motion that could allow changing of the grasping mode based on the target object [151]. Hence, the desired gripper fingers need to exhibit a bending mechanism analogous to hand grasping, while maintaining simple hardware and software requirements that limited the usability of previous attempts to exactly copy the design of human hands. Based on the conducted literature review, soft pneumatic actuators provide an excellent candidate to achieve this and have been repeatedly adopted as a soft finger for highly compliant soft grippers [61][152]. The fact that they can be fabricated from highly flexible materials with low Shore hardness enables naturally safe interactions with delicate targets, which is a crucial requirement for the intended application here. The main challenge associated with this class of soft gripper fingers, is the difficulty in accurate prediction and control of their behaviour, due to the non-linear nature of the elastomer materials used to create them. This challenge has been attracting researchers to study the behaviour of soft actuators in general, in an attempt to understand the effects of underlying design factors contributing to their response [153][154]. However, a full understanding of the effects of various design parameters on the response of soft bending actuators is still work in progress, with no complete design guidelines to customise soft bending fingers based on the intended application.

Furthermore, when comparing the different soft actuator morphologies in the literature review, it was revealed that the ribbed morphology would be preferred when considering low Shore hardness silicone rubbers, due to its reasonable fluidic energy requirement, improved structural stability, and minimal radial deformation. The pleated morphology can also be another alternative to adopt as a soft finger since it shares similar traits, but with improved actuation efficiency at the expense of reduced dynamic stability. Although it can be argued that the ribbed design is actually more efficient since softer materials can be used to create it,

which would require a lower operating pressure range. Additionally, the separation of internal chambers in the pleated design with gaps does improve the actuation efficiency as less material will be deformed, yet it limits the number of chambers that can be created for a given length of the actuator. Hence, larger actuators will need to be designed to achieve a specific bending range, which consequently would consume higher fluidic energy supply. Nevertheless, both the pleated and ribbed designs have been already utilised by several researchers in attempts to create simple soft fingers that are able to bend in a way analogous to that of a human finger [12], [140], [141]. In this research work, the optimal morphology will be chosen based on the chosen material for fabrication and research needs as later explained in chapters 4 and 7. Nevertheless, the adoption of the emerging soft actuator concepts allows relying on their passive compliance and inherently safe interactions to solve the risk of damaging delicate targets during grasping. However, this opens other challenges with regards sensing and control which are the key research challenges to be addressed in this research.

3.2.3. Bio-inspired Control

The response of soft fingers based on soft actuators is mainly governed by two aspects; the first is the morphology of the actuator itself, while the second is the fluidic energy source in the form of the input actuation pressure. The morphology is defined not only by the properties of the material used to create the soft actuator, but also the design of the internal fluidic channels. Together, the material properties and actuator geometry define how the actuator responds to external stimuli whether it is the pneumatic supply for actuation or the interaction with an object. Those, however, are predefined design parameters that cannot be varied during operation, so they have to be defined prior to the fabrication of the actuator based on the intended application. Thus, in order to control the behaviour of a soft actuator during operation, the primary controllable variable for online control is the supplied actuation pressure energising the grasping mechanism.

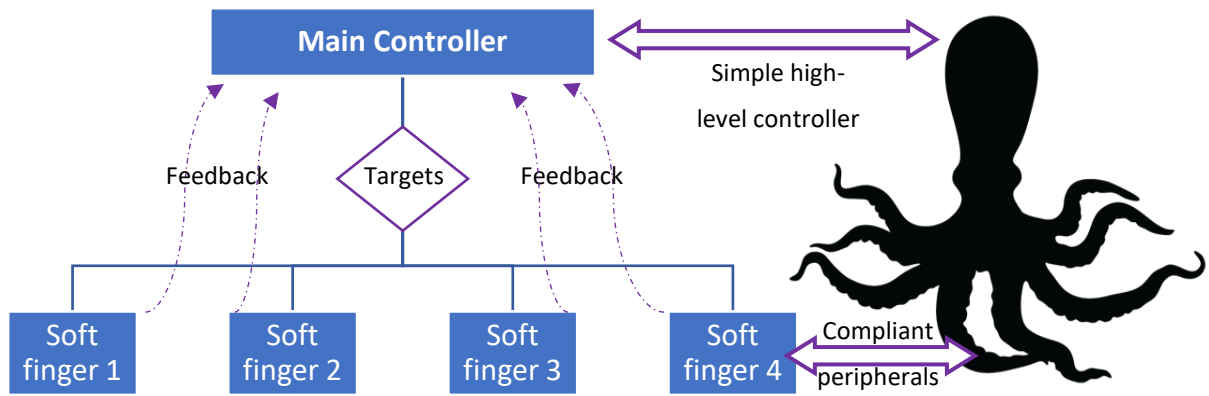


Figure 32: The bio-inspired analogy between the proposed control paradigm of soft grippers and octopus

Inspired by nature, it has been observed that soft-bodied creatures rely on the geometry and material properties of their bodies to interact and adapt to the surrounding uncertain environment. Hence, an interesting research direction now is looking at what is referred to as ‘Morphological computation’, in which the control of a soft body is partially delegated to its morphology to passively respond to external stimuli from the environment [31]. Such an approach reduces the complexity of the control algorithms since part of the control is achieved passively through the embodied intelligence of the morphology. In this way, the traditional separation between mechanics and control no longer exists, but rather the soft robot can exploit the morphology of its body to inherently accomplish some of the control tasks as it interacts with the surroundings. In a sense, the control process can be looked to as being decentralised, in which low-level control is achieved through morphological computation, while the main controller focuses on higher level control in terms of planning, decision making, and learning. This new control paradigm resembles how living creatures interact in real life with the highly unstructured and uncertain environments in nature (Figure 32). Previous research on the octopus revealed how it could utilise the morphology of its tentacles to achieve skilful underwater locomotion and grasping, despite their relatively limited processing power and simple nervous system [155]. However, the methodology for implementing this innovative approach in controlling various soft robots, in general, is still a work in progress, which is investigated in this research work in the context of controllable soft grippers. Therefore, this novel control paradigm will be adopted in this research, in an attempt to develop a more controllable soft gripper that utilises its morphology to gently and passively adapt to its targets, while processing the embedded sensory feedback using a high-level controller to infer more information about the grasp state and grasped object properties. The control architecture is hence divided into two main levels as follows:

- I. **Morphological Computation:** The low-level control of the grasping mechanism is delegated to the physical morphology of the soft gripper. The embodied intelligence of the gripper morphology will be responsible for achieving the desired passive compliance, which allows the gripper to gently conform to delicate objects of different shapes as it interacts with their profile. Hence, having an understanding of how key design parameters affect the bending and force responses of the soft gripper fingers is important and will be addressed in chapter 4.
- II. **Main Controller:** The high-level controller responsible for monitoring and processing the readings from embedded sensors in real-time, to accurately estimate the position of each gripper finger and control them accordingly to reach a target position. Additionally. The controller should combine the multi-sensory feedback from all the sensorised soft fingers to attempt to infer more information about the grasp state and the grasped target's properties. An example would be detecting contact with the target and estimating its size after grasping, which can only be achieved when fusing the multi-sensory feedback from opposing soft fingers, rather than processing the feedback from individual sensors separately. The potential for this will be evaluated in Chapter 6. The additional grasp feedback can allow the controller to take corrective actions, if needed, such as ending the actuation to avoid excessive contact or compensate for the loss of pressure to maintain a stable grasp.

3.2.4. Data-driven Modelling and Control

Modelling and controlling the complex bending response exhibited by the non-linear elastomer materials commonly used to fabricate soft actuators, has proven to be a challenging task facing the soft robotics community [156]. Most of the modelling work for soft actuators was directed for continuum arms [157], as well as for other locomoting soft robots such as snake [158], fish [16], and the famous octopus robot tentacles [159]. Yet, limited work has been accomplished in the context of soft gripper specifically. Modelling the response of soft bending actuators specifically can be achieved in three main approaches; experimental characterisation [32], finite element modelling [160][161], and explicit analytical modelling [162][163]. Notable recent work compared the results from the three approaches (analytical, finite element method, and experimental) for the case of fibre-reinforced bending actuators with a single chamber [164]. It was shown that with reasonable assumptions the analytical modelling processes could be simplified to provide adequate results that are in-line with

experimental data. However, the resulting analytical model is computationally demanding since it has to be solved numerically. The finite element model was also successful in predicting the actuator bending, yet with less accuracy than the analytical model. For both analytical and finite element modelling, the resulting model is specific to the studied morphology with the chosen materials, dimensions, and assumptions. Additionally, both approaches require an accurate material model and relevant coefficients that can capture the nonlinear behaviour of the hyperelastic materials used. This becomes even more complicated if the soft actuators are made of combinations of different materials, or when trying to fully account for the effects of external reinforcements or embedded components. Furthermore, there is always the uncertainty associated with the manual fabrication of soft actuators, which could induce variations in the geometry or material properties that are difficult to account for in theoretical models [165].

Those challenges motivated the consideration of a purely-data driven approach based on experimental data that implicitly accounts for the effects of uncontrollable variations, without the need for precise physical or material models. It is hypothesized that by generating sufficient data from experiments conducted under different input conditions, a simple empirical model can be derived to accurately estimate the bending angle based on multi-modal sensory feedback. In this case, the model essentially provides the input to output mapping for control purposes, rather than attempting to model the physical deformation of the soft body. Assuming that the soft gripper fingers are able to a large extent maintain a consistent trajectory path for a given input pressure supply, then the empirical model can be potentially utilised to accurately control the soft fingers at variable input conditions. This would require systematic experimentation to collect sufficient data at different operating conditions. A closed-loop controller can be developed in this case to regulate the supply pressure based on the sensory feedback processed through the derived empirical models, in order to control the positioning of a soft finger within its bending plane. Hence, if accurate measurements can be made for the current bending angle of a sensorised soft actuator, then any deviation from the previously modelled free-bending trajectory path can be assumed to be caused by contacting the target object. Consequently, when a soft finger is prevented from further bending due to external contact with an object, then most of the input fluidic energy actuating the finger will be mitigated to the contact areas to generate contact forces. Thus, it is hypothesised that a correlation can be made between the deviation from predicted fingertip position and the imposed contact forces on the object. This would be an interesting approach in making a qualitative inference regarding the grasping strength, which would be particularly

beneficial for the handling of delicate objects. Having theoretically infinite degrees of freedom depending on the morphology and contact state of the soft fingers, is desirable as a form of embodied intelligence that enables passive adaptation to interactions. However, with limited sensory feedback it becomes challenging to infer the current state of the soft finger. Hence, it would be interesting as well to study how the limited sensory feedback available from opposing soft fingers can be combined and processed to make new inferences regarding the contact state and grasped object properties, which is currently difficult to achieve for soft grippers. Figure 33 outlines the overall control architecture envisioned for the proposed data-driven approach.

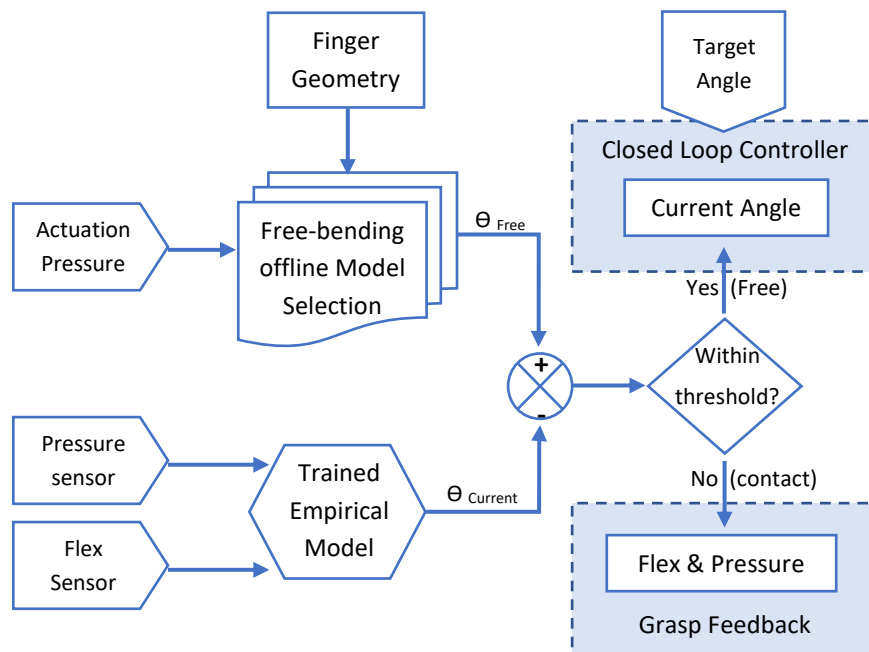


Figure 33: Flowchart outlining the proposed control architecture

3. 3. Research Objectives:

The objectives of this research can be summarised as follows:

- Develop a test rig that enables systematic experimental testing and characterisation of soft gripper fingers under controlled input conditions.
- Evaluate the consistency and quality of the experimental data of testing soft fingers with variable morphology and input conditions as an early verification of the feasibility of the proposed data-driven approach.
- Investigate the effect of key design parameters defining the morphology of the soft fingers, to better understand the role of the finger morphology (low-level control) and identify the best performing design to be adopted in the subsequent work.
- Identify a suitable sensing option that is flexible enough to be seamlessly embedded into soft fingers without hindering their desired compliance.
- Characterise the response of the embedded sensor at different input conditions.
- Evaluate the potential of modelling the free-bending response of individual soft actuators using appropriate data-driven methods and compare their prediction accuracy.
- Develop a closed-loop controller that utilises feedback from the embedded sensor and the derived empirical models to control the bending of soft fingers. Evaluate the accuracy of controlling the bending when following a given reference signal.
- Design and fabricate a soft gripper with embedded sensors for delicate grasping.
- Investigate the possibility of detecting contact with a grasped object and inferring additional grasp feedback using the available sensory feedback.
- Investigate the potential of 3D printing technologies as an alternative fabrication process.
- Investigate the possibility of directly printing flexible sensors as a customisable alternative to commercially available options. Characterise their response and limitations.
- Apply the same data-driven approach to model the response of printable soft actuators with integrated sensors as an additional verification to the proposed data-driven approach.

CHAPTER 4:

Experimental Analysis of Soft Fingers

Addressed Research Question: *Is there a clear and consistent free-bending response for soft bending actuators that can be described by simple empirical models?*

Chapter Objectives:

- Construct an experimental setup for controlled testing of soft actuator samples.
- Develop an image processing program to record the bending response.
- Evaluate the consistency of the bending response at different pressure inputs.
- Identify the best performing design to adopt in the following work.

Generated Publication: K. Elgeneidy, N. Lohse, and M. Jackson, “*Experimental Analysis of the Bending Response of Soft Gripper Fingers*,” in Volume 5B: 40th Mechanisms and Robotics Conference, 2016, vol. 5B–2016, p. V05BT07A064.

4. 1. Introduction:

The literature review showed a growing interest in creating highly compliant grippers that utilise soft pneumatic actuators as soft fingers. Due to the non-linear nature of hyperelastic materials used in fabricating soft actuators, conventional design and modelling techniques are no longer applicable. This gave rise to a new paradigm in designing soft actuators in which their morphology, expressed by the geometric and material properties, can be exploited as a computation mean to achieve more complex interactions. This challenge has been attracting research into analysing different soft actuator morphologies, in an attempt to devise a more systematic design approach that allows defining the desired responses according to the application needs. However, a full understanding of the effects of various design parameters on the overall response of different soft actuators is still a work in progress. The primary aim of this chapter was to assess the consistency of the bending response of soft bending actuators following the ribbed morphology to evaluate the feasibility of adopting the proposed data-driven approach. This also involved studying the relationship between the input pressure and output bending to determine the appropriate data-driven modelling techniques that can be implemented in the next stages. Samples with variations in the design of their internal fluidic channels were tested to confirm that the results are not restricted to a specific design. This provided an opportunity to analyse the effect of changing the internal channel morphology on the bending and force responses so that the best performing soft finger design can be identified and adopted in the following stages. This work serves as a step towards establishing

a structured guideline for designing and testing soft bending actuators for enhanced bending and force generation. Paving the way for the data-driven modelling and control work based on the outcomes of this chapter.

4. 2. Design of Experiment

An experiment was designed to test soft fingers samples, which are based on the ribbed bending actuator morphology, with different internal channel dimensions. The experiment was divided into two stages; the first stage focused on analysing the free-bending response of the soft finger samples, while the second stage focused on the force analysis during contact with an obstacle along their bending trajectory. The experiment aimed to evaluate the bending consistency of the tested samples at different pressures and durations, as well as characterising how the bending and force responses are influenced by the variations in the dimensions of the internal channels. Figure 34 shows a cross-section through the typical geometry of the ribbed actuator morphology. The key design parameters defining the internal channels are hence:

- w : the individual air chamber width,
- h : height of an individual air chamber,
- t : the thickness of the wall between consecutive chambers,
- n : the total number of chambers.

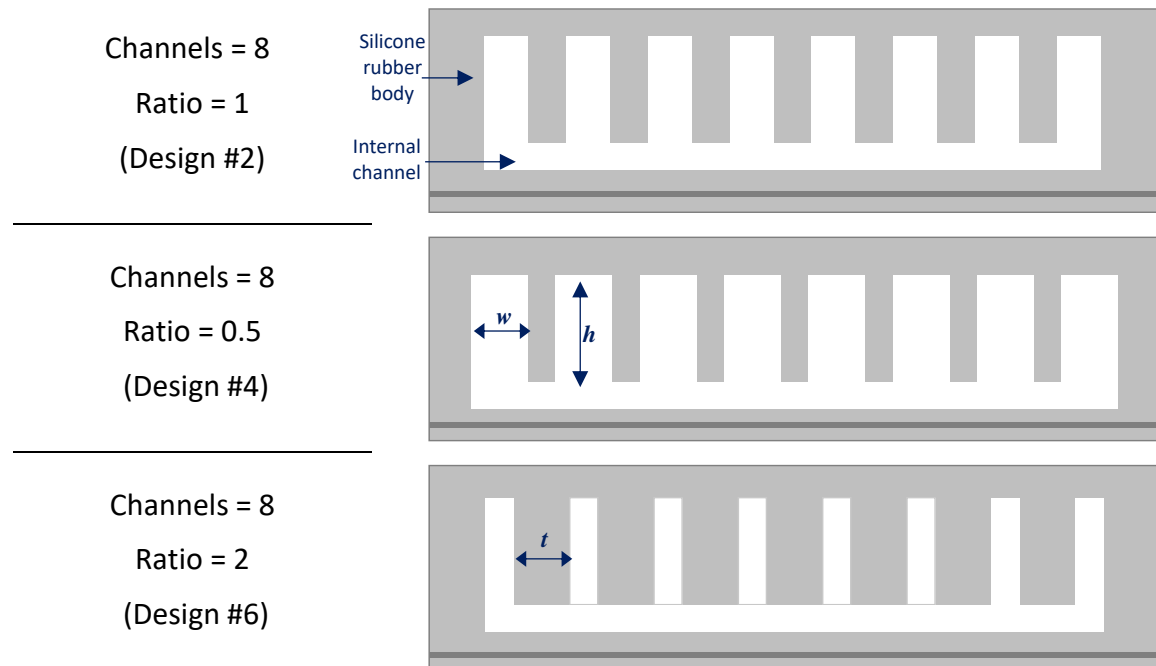


Figure 34: a cross-sectional illustration comparing the three different internal channel designs achieved by varying R while fixing outer dimensions and the number of chambers

The chamber height was not included in this experiment since it has been already investigated in previous work, which showed that further increase to chamber height would only increase the actuator's size and weight with no clear benefit to performance [25]. Also, the outer dimensions of all finger samples were fixed to allow a systematic comparison that focuses solely on the effect of the internal channel geometry driving the bending mechanism. Hence, all soft finger samples were designed to be 20 mm in width and 10 mm in height, which is similar to the size of soft actuator tested in previous work [25], with a shorter length of 70 mm since the intended application is different and a lower Shore hardness material is used here.

Furthermore, a dimensionless design parameters R was defined, which is the ratio between the chamber width w and wall thickness t . By testing R and n at combinations of different values, practical values of w and t can be consequently derived since the outer dimensions of the actuator are fixed. Hence, w and t are essentially dependent parameters defined by the chosen values of R and n . According to this, a factorial experiment design was adopted since the key design parameters of interest (R and n) can be defined at discrete levels, while t and w are dependent factors that are calculated accordingly. Hence, a particular interest in this experiment is to investigate how the defined design parameter R can be utilised to improve the performance of the soft fingers, which for the knowledge of the author has not been studied in any previous research. A summary of the studied factors and responses for the design of the experiment is illustrated in Figure 35.

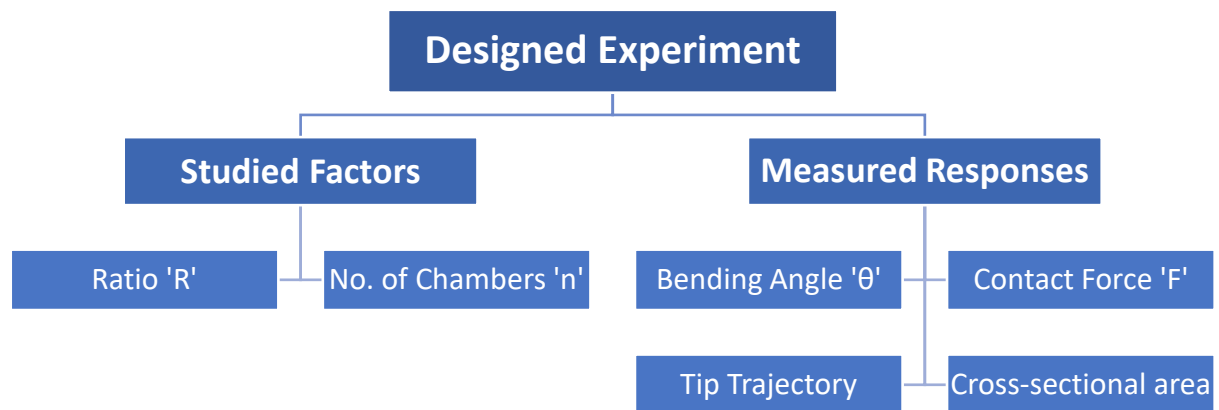


Figure 35: Summary of the studied factors and responses in the designed experiment

A set of soft fingers were designed with the same outer dimensions while changing only dimensions of the internal fluidic channels based on combinations of different values of R and n as outlined in Table 3. A total of six finger designs were generated covering three levels of R of 0.5, 1, and 2, which corresponds to a wall thickness that is half, equal to, or double the chamber width respectively. While n was tested at two levels resembling high (16 chambers)

and low (8 chambers). The high value is similar to previous work [25] and was defined based on the maximum number of chambers that can be fitted within the fixed actuator length, while resulting in wall thickness values of a minimum 1 mm. The low value was chosen to be half of that value, which keeps the maximum wall thickness to 4 mm. The finger set was designed to result in a practical range of values for the wall thickness and chamber width (between 1-4mm) that is commonly used when fabricating this kind of soft actuators [21]. Since the outer dimensions of all fingers are held constant as previously mentioned, fingers with the same ratio level will have the same total volume of internal chambers being pressurised. Hence, the primary difference between fingers at the same ratio level is that the same volume is divided into a large (16) or small (8) number of chambers by adjusting the values of wall thickness and chamber width accordingly.

Table 3: Values of the studied design parameters for the soft fingers set

Finger Design Number	Studied Design Parameters		Dependant Design Parameters	
	Ratio w/t (R)	No. of Chambers (n)	Wall Thickness (t) in mm	Chamber Width (w) in mm
1	1	16	1.5	1.5
2	1	8	3	3
3	0.5	16	1	2
4	0.5	8	2	4
5	2	16	2	1
6	2	8	4	2

The required moulds to fabricate the required soft fingers were designed on SolidWorks using a design table, so that soft finger designs with different internal channel dimensions can be automatically generated according to the values of the design parameters input in the design table. This provides a quick and systematic way of generating design variations of the internal channels for fingers of the same size. Details of the mould design is attached in Appendix (E) – Soft Finger Design . All the designed moulds were 3D printed as commonly done in previous work to facilitate fast and inexpensive fabrication of custom moulds. An extrusion-based 3D printer with a 0.5 mm nozzle was used to print the required moulds. Dimensions of the printed moulds was measured to verify accuracy and were found to fall within the range of +/- 0.15 mm. These moulds were then used to cast EcoFlex-50 silicone rubber material to create the soft finger parts and bond them together using the previously introduced soft lithography technique. The result is a set of identical looking soft fingers from the outside, yet the internal channels are different as seen in Figure 36.



Figure 36: Fabricating a batch of soft finger samples with variable channel patterns

The samples were experimentally tested in order to measure the intended bending and force responses and relate how the studied factors affect them. The bending response of the soft fingers being investigated in this experiment can be quantified primarily by measuring the maximum bending angle θ , and tracking the trajectory path of the fingertip as it deforms during actuation. Additionally, measuring the cross-sectional area of the soft finger during actuation provides a quantified evaluation of the undesired radial expansion that can hinder the grasping process as the fingers become bulkier. These responses were measured for each tested soft finger sample, actuated repeatedly at different pressure values and actuation durations. Furthermore, in the second phase of the experimentation, the maximum resultant forces imposed by a soft finger when making contact with an object along its path, is also measured to study how it is related to the studied internal channel design parameters. Knowing the maximum contact forces generated by a soft finger during grasping is important as it reflects the maximum payload capability of a soft gripper.

4. 3. Experimental Setup and Procedure

4.3.1. Pneumatic Control Board

A pneumatic control board was built based on the design provided on the soft robotics toolkit¹⁶ (shown in Figure 37), to allow controlling the pneumatic supply to the tested soft finger samples. The supply valve is controlled via the Arduino board, which can be programmed to set the required actuation duration and pressure (code provided in Appendix (A) – Arduino Code for Pneumatic Control Board). The pressure supply to the system originates from pneumatic lines, similar to those available in industrial setting. This fixed supply pressure is then regulated by an Arduino board via a pulse width modulation (PWM) signal that controls the opening and closing of high-speed switching solenoid valves. By changing the duty cycle

¹⁶ <https://softroboticstoolkit.com/book/control-board>

of the PWM signal using on-board potentiometers, the effective internal pressure reaching the soft fingers can be changed during operation. This provides a low-cost alternative to industrial pressure regulators, which were not available for this project. Pressure sensors at the outlet of the valves are used to measure the actual pressure passing through the pneumatic lines in real-time before it reaches the target soft actuators. Additionally, onboard pressure sensors (Honeywell-ASDXAVX100PGAA5) measure the actual internal pressure passing through the pneumatic lines at a rate of 100 Hz before reaching the tested soft actuators. Datasheet for the sensor and the calibration function provided in Appendix (D) – Datasheets

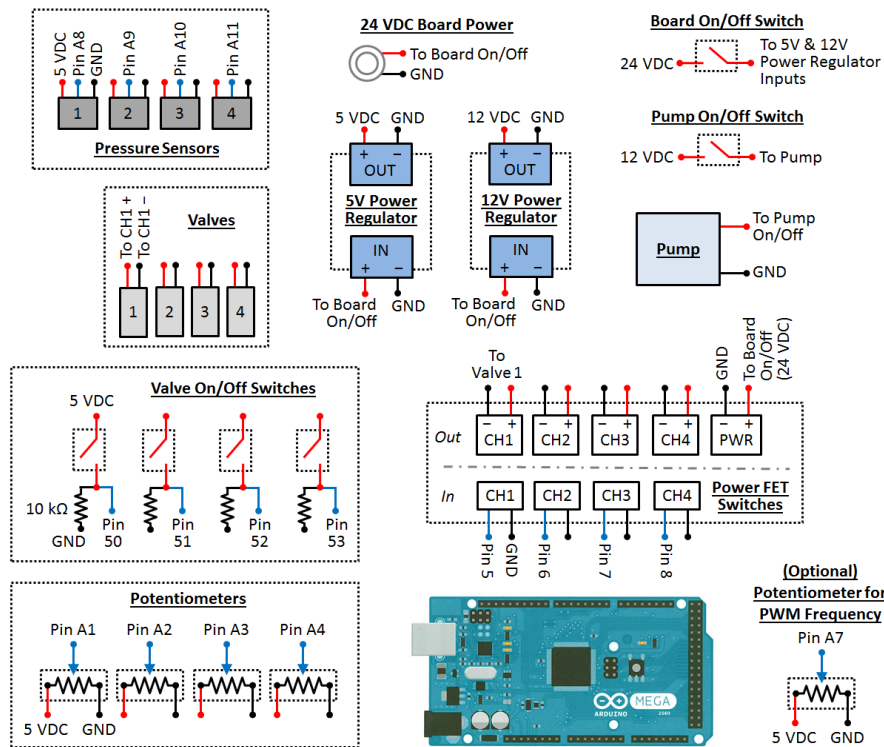


Figure 37: Schematic diagram of the control board design by the soft robotics toolkit

The board consists of the following components, which are displayed in Figure 38.

- **Solenoid valves** (SMC-VQ110U-5M, Valve 3-Way, NC, 24DC, High Flow) fixed on a manifold, to direct the flow of compressed air.
- **Pressure sensor** (Honeywell-ASDXAVX100PGAA5 sensor, 100 PSI GAUGE 5V) connected at the output tubes, through connectors, to measure the actual pressure inside.
- **Arduino Mega** as a programmable microcontroller, to control the actuation duration through set timers, and supply the PWM signal required for pressure control.
- **Power MOSFETs** to enable the switching of solenoid valves according to the PWM signal supplied by the Arduino board.

- **Rotary potentiometers** in order to change the supplied pressure passing in the channels, by changing the duty cycle of the PWM signal.
- **Power regulators** to step down the voltage supplied to the Arduino board and the pressure sensor from 24V to 5V.
- In addition to other supplementary components such as: breadboard, tubes, connectors and power jacks.

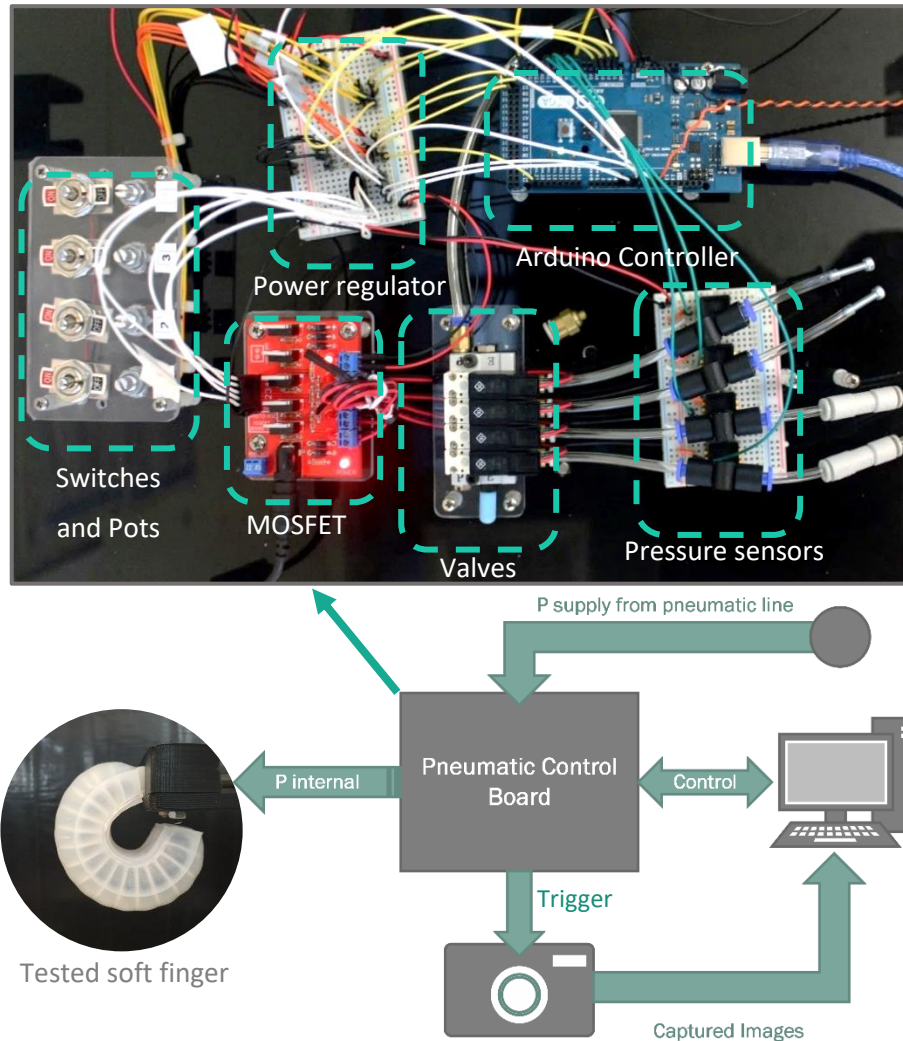


Figure 38: Experimental setup showing the pneumatic control board components

4.3.2. Bending Angle Measurement via Image Processing

The tested soft finger samples are attached to a frame using a 3D printed fixture to ensure they all fixed in the same location throughout testing. The printed fixture guides a 1.8 mm diameter needle to puncture the base of the tested soft finger, to supply pressurised air to its internal channels. Fixing the inlet needle diameter to be used with all tested fingers ensures a consistent flow rate of pressurised air, which can only be varied by changing the pneumatic supply pressure. A high-speed camera (MAKO G-223) mounted at the opposing end of the frame captures image frames at 130 Fps, to record the deformation of the tested soft fingers

throughout the actuation. The fast frame rate is required to allow capturing a sufficient number of images within short actuation durations. Calibration for the intrinsic and extrinsic camera parameters was conducted following a standard calibration routine implemented in Halcon library using a checkerboard pattern, to allow measurements in real-world coordinates. The calibration mean error was 0.01 mm at a focal length of 17.5 mm. During a typical actuation test, the camera is externally triggered via the Arduino microcontroller to ensure that the sensory readings and captured image frames can be synchronised.

An image processing program (Appendix (B) – Halcon Image Processing Code) was developed using Halcon library¹⁸ to process the acquired image frames in order to: (a) automatically identify the actuator body, (b) record the trajectory of the detected actuator tip, (c) calculates the bending angle, and (d) radial expansion of the tested soft fingers at each image frame. The program segments the deforming soft finger body using automatic thresholding aided by a dark background. A successfully segmented body is highlighted in red by the image processing program as shown in Figure 39. Contours defining the circumference of the segmented blob representing the actuator body are then extracted, and the position of the tip is calculated within each image frame for trajectory tracking. Afterwards, the bending angle θ can be calculated with respect to the axis passing through the base of the soft actuator, as illustrated in the sample output shown in Figure 39. All necessary data about the bending response are hence automatically calculated for each test.

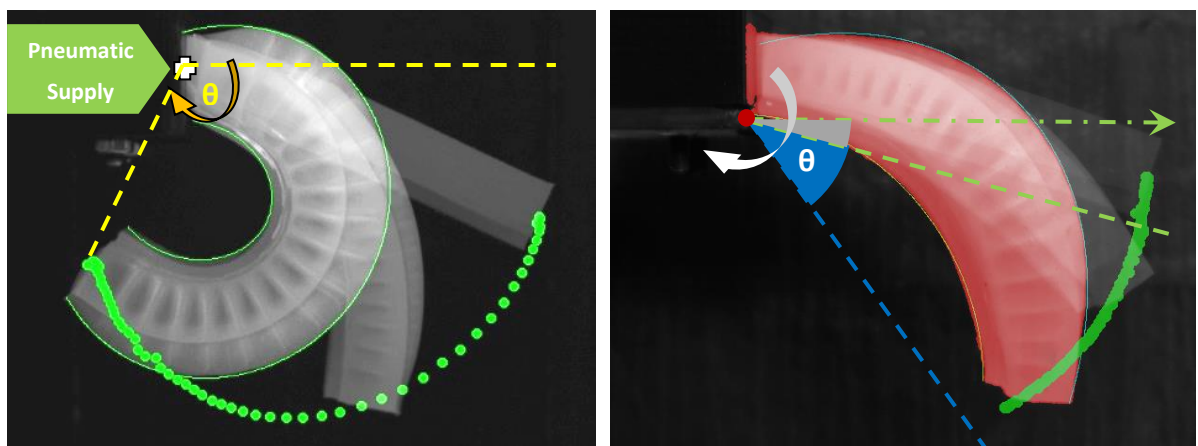


Figure 39: Visualisation of the output from the image processing program tracking trajectory and segmenting cross-sectional area of the deforming actuator

Furthermore, for the force analysis experiment, the same setup was used with the addition of a sensitive force torque sensor (Schunk Mini45) mounted on the frame with a 3D printed post

¹⁸ <http://www.mvtec.com/products/halcon/>

on top to measure the generated contact forces upon contact as shown in Figure 40. This assembly was fixed on the frame at a location along the trajectory path of the soft finger to ensure contact will be made upon actuation, which will consequently generate forces to be measured by the sensor. The location of the force post was fixed throughout the test for a fair comparison between fingers.

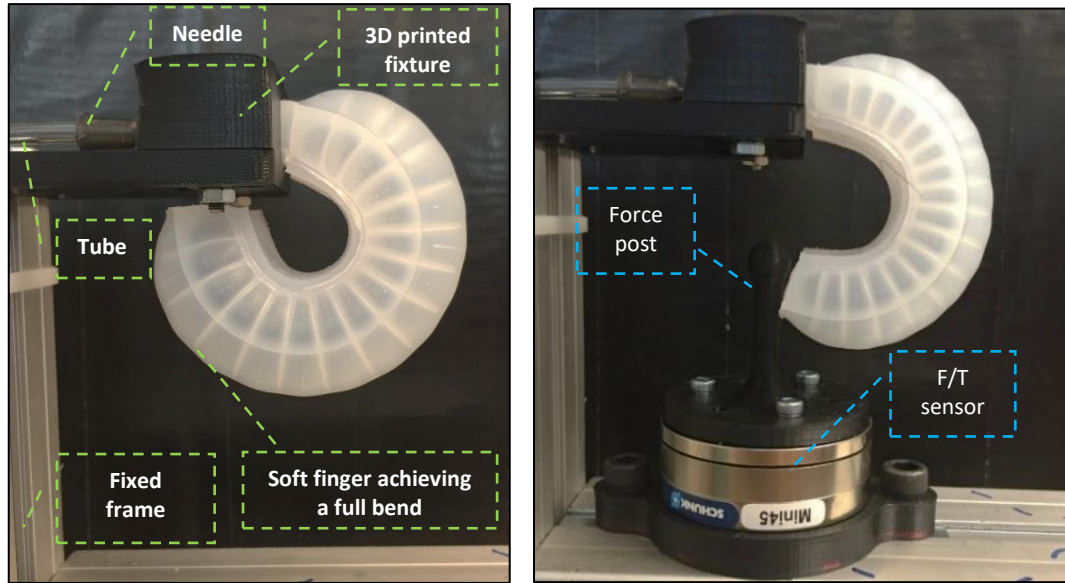


Figure 40: Experiment setup for bending analysis (left) and force analysis (right)

4. 4. Results and Discussions

This section presents the outcomes of the experiments conducted for the bending and force analysis of the fabricated set of soft fingers. First, preliminary tests were conducted on individual soft fingers, in order to verify the repeatability of their response at variable actuation pressures and durations. This would also give an insight about the feasibility of effectively controlling soft fingers by varying the supplied pressure. Afterwards, further tests were conducted, in which the set of soft fingers were all tested at the same input conditions recommended from the preliminary results, so that their performance can be compared and the best performing soft finger design identified. Furthermore, the second stage of the experiments involved the analysis of the contact forces imposed by each soft finger in the fabricated set, in order to identify the soft finger design that can maximise the grasping forces at a given pneumatic supply pressure.

4.4.1. Evaluating Consistency

The first stage of the experimental testing focused on verifying the repeatability of the bending response of soft fingers, by testing individual soft fingers at variable pressure inputs and actuation durations. Sample of the results is presented here, showing the trajectory path,

bending angle, cross-sectional area and pressure response, of soft finger design number 2, when tested repeatedly at variable input pressures and durations. The results showing the bending responses for the remainder of finger designs are included in Appendix (C) – Additional Experimental Results. The first section of the consistency evaluation tests the soft finger repeatedly at variable pressure inputs of 10, 12, 14, 16 and 18 Psi, for the same fixed duration. The actuation time was set at 400 ms, which was heuristically chosen to allow enough time for sufficient bending at low pressures, while not exceeding maximum bending (hitting the base) at the highest pressure input. The second section of the consistency evaluation shows the same responses when testing the soft finger again at a fixed pressure input of 10 Psi, while varying the actuation duration from 200 ms to 500 ms at 100 ms increments. The minimum pressure value was chosen for this test to have a wider range of feasible actuation durations. Figure 41 shows sample image frames captured by the high-speed camera while testing the soft finger under two of the tested input pressure values, to highlight the bending mechanism.

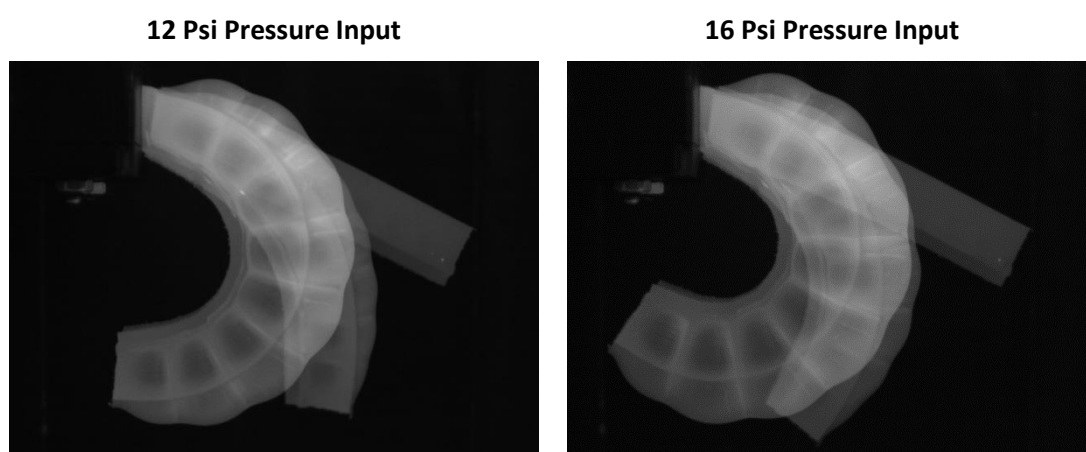


Figure 41: overlaid image frames showing a soft finger deforming at 12 and 16 Psi input pressures

Due to the manual nature of the fabrication process, small variations can exist between samples of the same finger design. To minimise this undesired variance when comparing different finger designs, all tested fingers are fabricated as one batch from the same silicone rubber mix to ensure consistent material properties across. Nevertheless, the manual moulding process might introduce additional random variation due to human error, which depends on human skill and experience with the fabrication process. Hence, many samples were fabricated before this evaluation as a training on fabricating soft actuators, to avoid problems such as trapped air bubbles and misalignment as discussed in section 2.4.1. Figure 42 compares the mean final bending angle achieved by all six finger designs when tested using a supply pressure of 10 Psi. The error bars represent the variation between three samples for each finger design, which

can be seen to be limited compared to the differences between finger designs. Hence, it can be assumed that the studied design parameters have a significant effect on the final bending angle that clearly exceeds the variation between samples of the same design. The effects of each of those design parameters are investigated later in section 4.4.2.

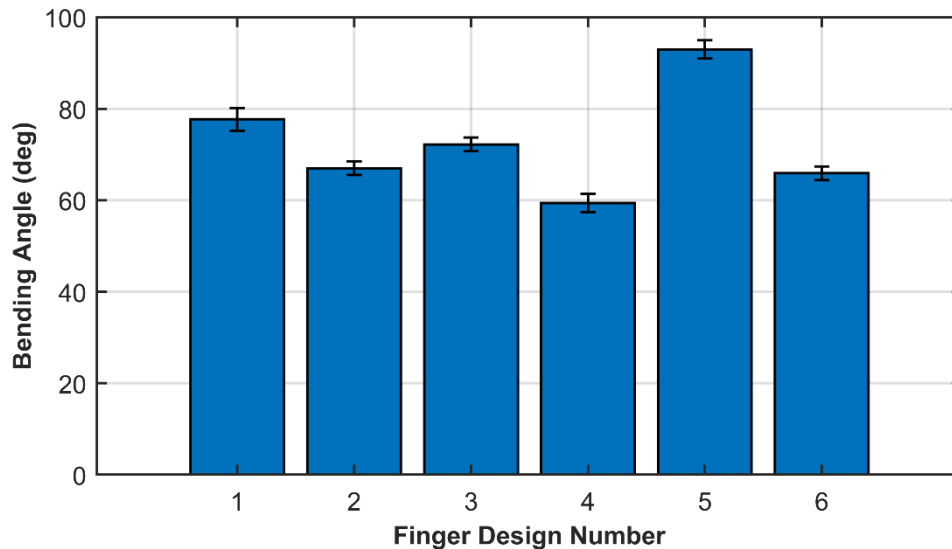


Figure 42: Highlighting variance in final bending angle due to fabrication for each finger design

I. Variable Actuation Pressures

All soft fingers were repeatedly tested at input pressures ranging from 10 to 18 Psi at 2 Psi increments. The pressure sensors on the pneumatic control board measured the actual pressure developing inside the soft fingers, following the calibration function provided in the datasheet and implemented in the Arduino code. The pressure response for an individual soft finger is presented in Figure 43. As to be expected, higher pressure supply results in a higher measured internal pressure. However, the maximum value of the pressure developed inside the soft finger channels was always lower than the supplied input pressure. This is mainly due to the highly flexible nature of the silicone rubber materials used in fabrication, which causes the soft finger body to easily deform and the internal channels to continue to expand. In addition to the pressure drops along the pneumatic tubes supplying the soft finger. Thus, the measured internal pressure will be less than the supplied pressure, especially for short actuation duration, since the pneumatic supply originates from a high-flow pneumatic line designed for industrial applications. It can be also observed in Figure 43 that oscillations in the response are more evident at higher input pressures. Additionally, the mechanical switching of the supply valve seems to introduce an initial spike in the measured pressure response, yet the flow quickly stabilises, and the readings then become smoother. A pneumatic reservoir can be added to the pneumatic circuit if needed to dampen out spikes.

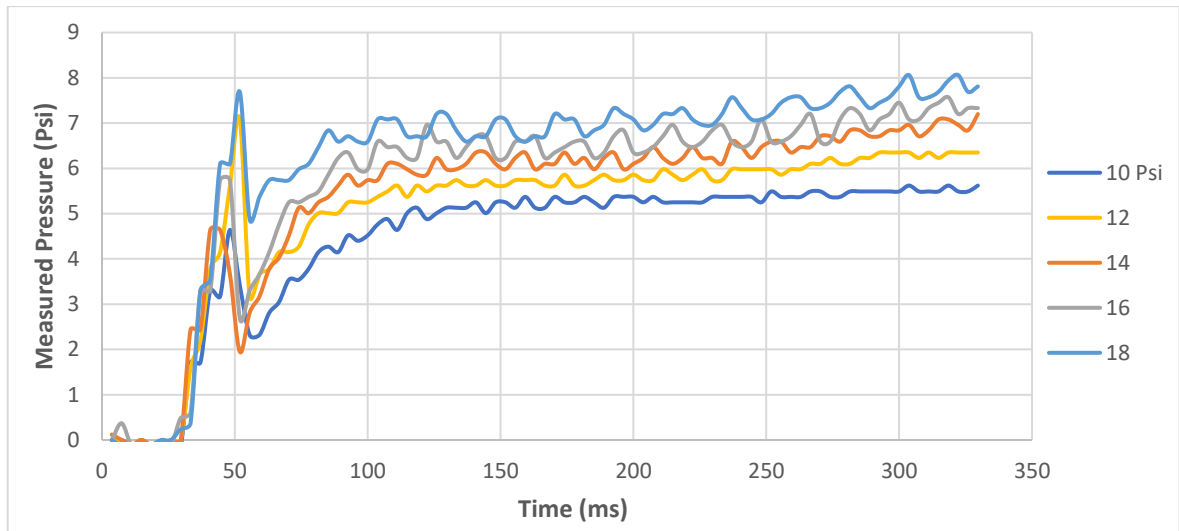


Figure 43: Pressure response at different actuation pressures

The soft finger maintained its trajectory profile as seen in Figure 44, when actuated at the tested range of pressure inputs ranging from 10 Psi to 18 Psi, reaching further along the trajectory profile when at higher pressure supplies. Again, some limited oscillations can be witnessed in the trajectory path, which is more significant at higher pressure inputs when the dynamic effects of the nonlinear nature of the silicone rubber material become more evident. The higher input of actuation pressure forces the soft finger to deform at higher acceleration, which does not allow the material enough time to stabilise with the expansion in the internal channels. However, this test shows that actuating the soft fingers at pressure inputs of less than 12 Psi results in a smoother trajectory with less oscillations.

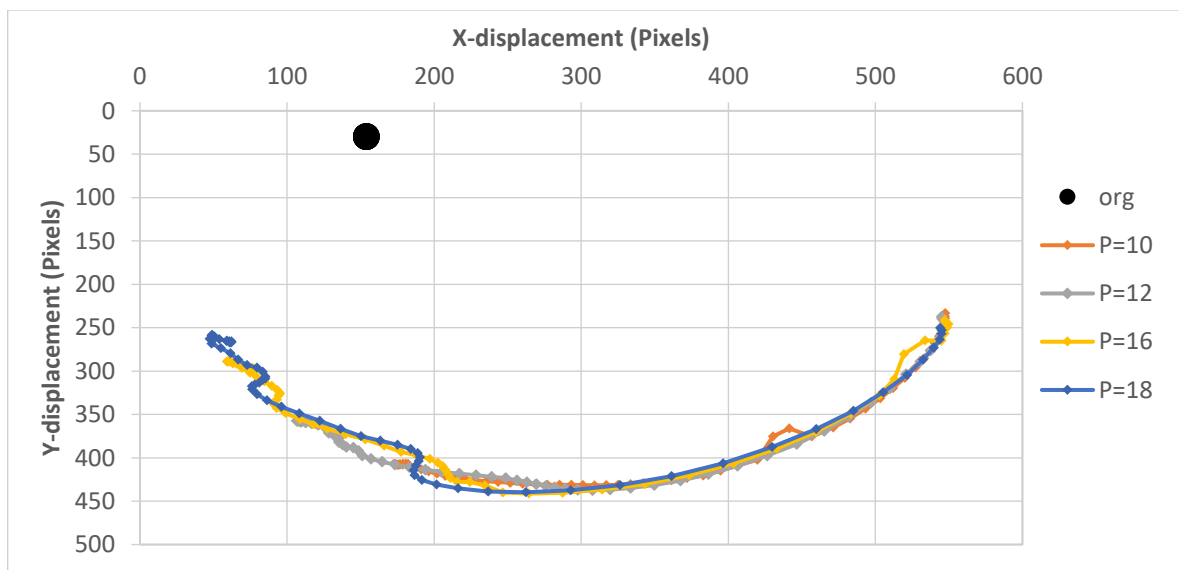


Figure 44: Trajectory response at variable actuation pressure inputs

In Figure 45, the bending angle response of the tested soft finger at different actuation pressure input is presented. The oscillations occurring at higher pressure inputs become much clearer in this plot. As to be expected, the maximum bending angle reached by the soft finger consistently increases with the increase in supplied input pressure. However, this comes at the expense of response smoothness that can be a problem when it comes to controlling the bending angle of soft fingers. Hence, in the following sections, the pressure supply will be set at a value of 10 Psi, which is provided the most linear and stable response shown.

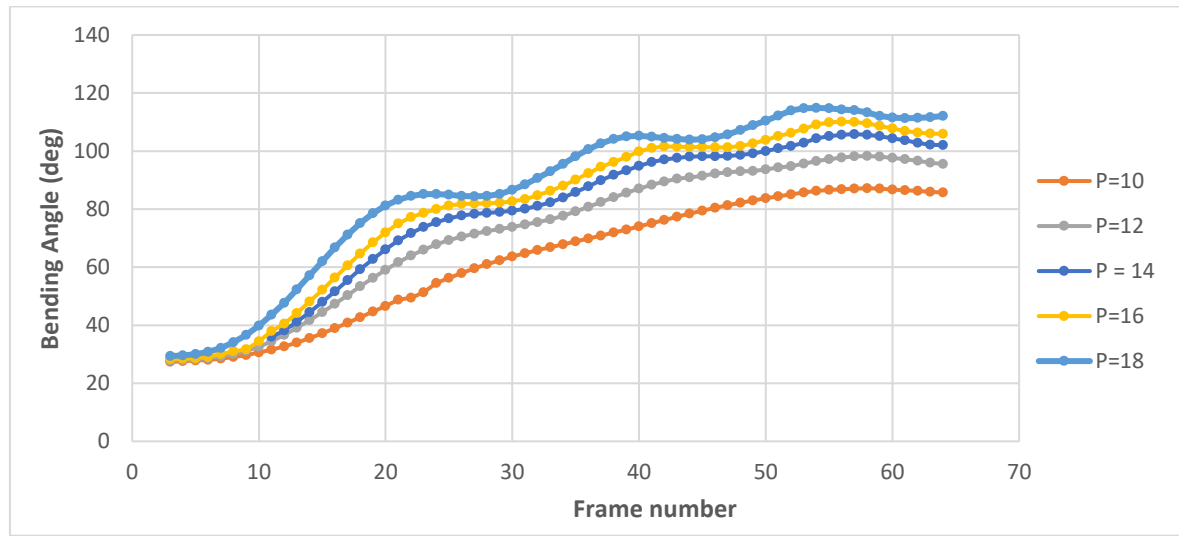


Figure 45: bending angle response at different actuation pressures

Furthermore, looking at the cross-sectional area of the soft finger measured using the vision system during actuation at the tested pressure levels, it is clear that consistent response is seen in Figure 46, which increases with the increase of supplied pressure as expected. Measuring the cross-sectional area is an indicator of how much energy is wasted in the undesired radial deformation of a soft finger, which would be a useful parameter to compare the designed set of soft fingers tested in this experiment.

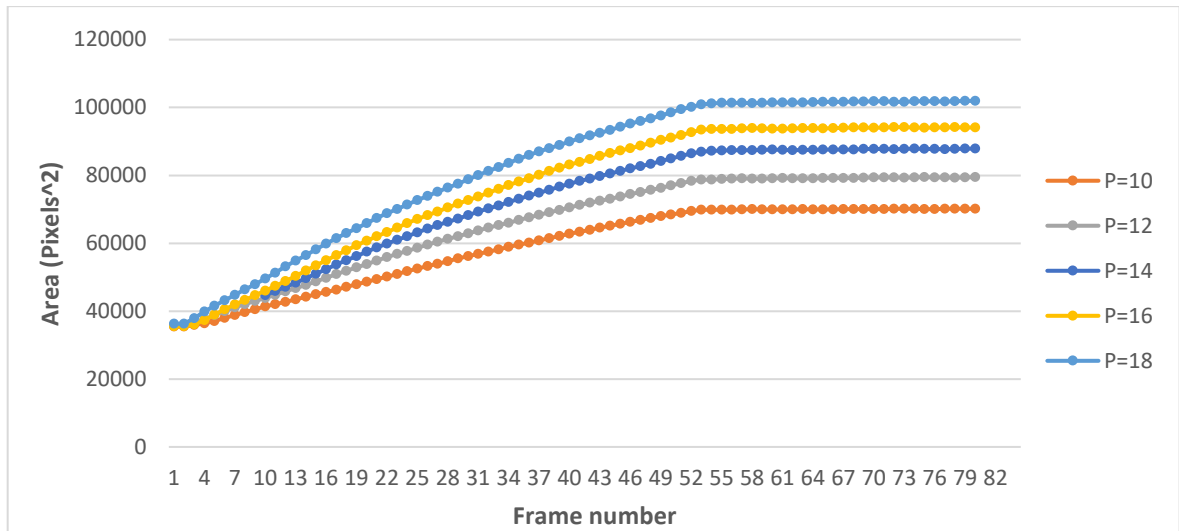


Figure 46: Cross-sectional areas at different actuation pressures

II. Variable actuation durations

The same tests were again repeated for the same soft finger design, but this time for different actuation durations while fixing the step pressure input at 10 Psi, which is the value that resulted in the most linear response without significant oscillations. A consistent pressure response was recorded using the pressure sensor as the finger was tested for variable durations from 200 ms to 500 ms. In all the tests, the response was the same as seen in Figure 47, settling at a maximum measured pressure value of about 4.8 Psi. This plot shows that the pressure response is repeatable at a given pressure input, with the potential of utilising this data later for controlling the position of soft fingers.

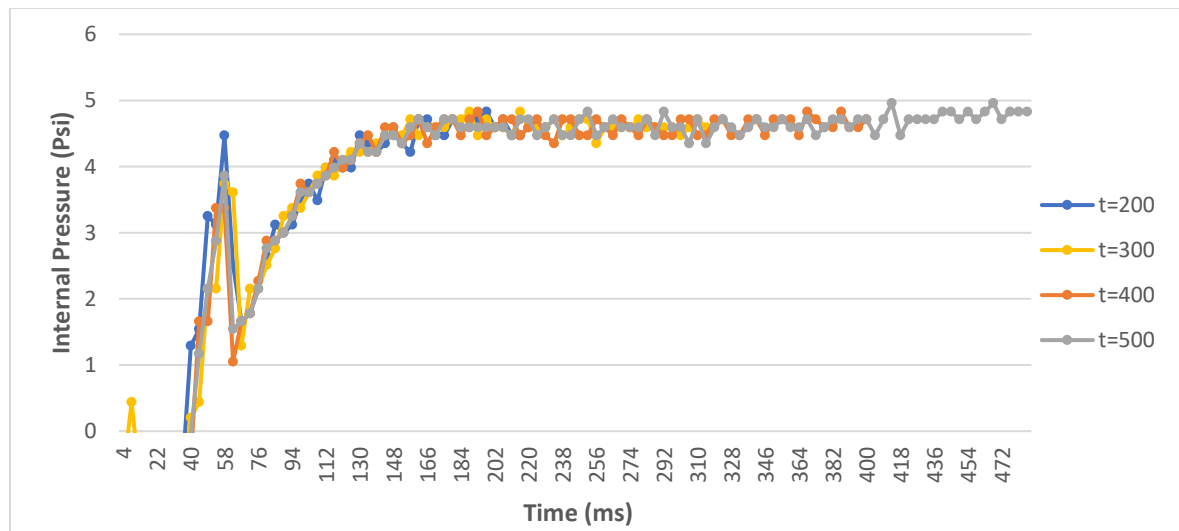


Figure 47: Pressure response for different actuation duration

Additionally, Figure 48 shows consistency in the trajectory path as the soft finger was tested at the variable actuation durations. This again confirms that the trajectory profile of the soft

finger is repeatable for a given pressure input, reaching further along this unique path as the actuation duration is increased. It can also be noticed that the response is stable without any significant oscillations since the input pressure was held at a low value of 10 Psi as recommended in the previous tests.

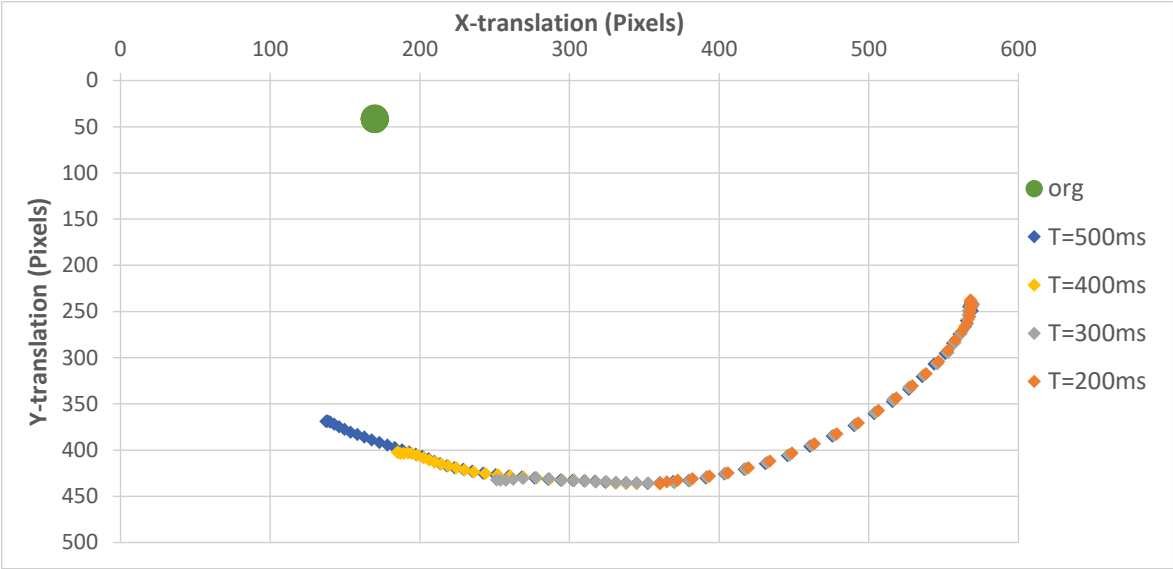


Figure 48: Trajectory response at different actuation durations

Figure 49 further confirms the consistency of the results, as the same profile for cross-sectional area response is seen, reaching higher values due to further expansions at longer actuation durations.

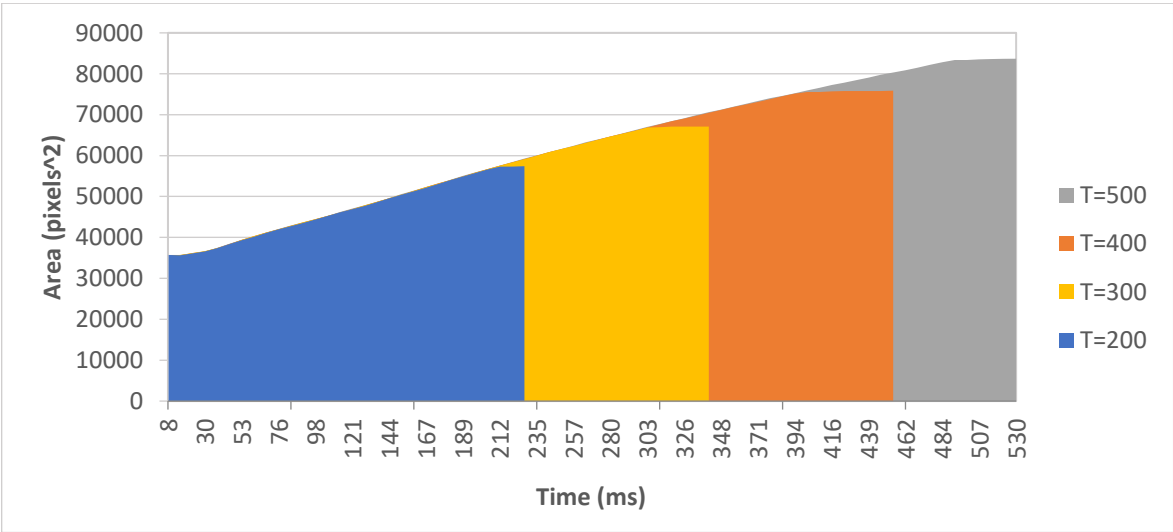


Figure 49: Cross-sectional area response under different actuation durations

Finally, the bending angle response of the soft finger at the tested actuation durations is shown in Figure 50. Again, a consistent response can be seen, which is extended as the duration increases. Additionally, the response is mostly linear and hence can be approximated

by a simple linear model, which simplifies the subsequent modelling and control work. The repeatability of the resulting bending angle encourages the control of the soft finger position through simple models that describe the response of each soft finger at a given actuation pressure. Knowing this simple model means the soft finger can be stopped at a specific point along its known trajectory to achieve the desired bending angle.

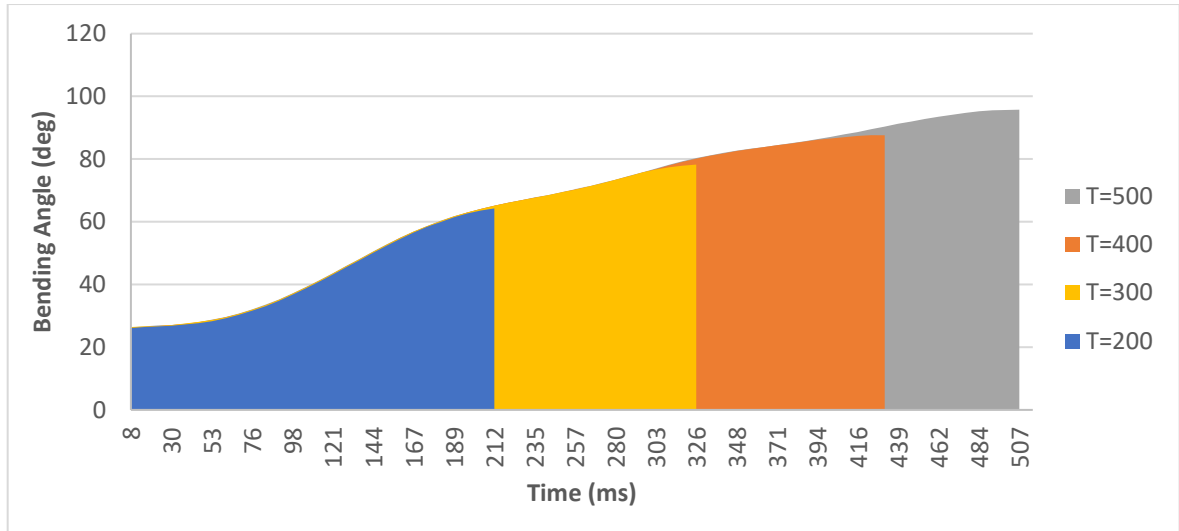


Figure 50: bending angle response at different actuation durations

Analysis of the Free-Bending Response

After confirming the repeatability of the bending response of soft fingers at different pressures and actuation durations, the experimental investigation continues by comparing the performance of the set of soft fingers samples at a fixed actuation duration of 400 ms and pressure supply of 10 Psi, as recommended by the previous tests.

Trajectory Path

The first measurable response that describes the bending behaviour of the tested soft fingers is the trajectory path followed by the fingertip within its bending plane. Figure 51 compares the trajectory paths of the six tested soft fingers by plotting the calibrated X and Y coordinates of their fingertips acquired from the image processing program. Examination of the results shows that fingers with smaller chamber width can travel further away, with finger5 achieving the longest translation since it has the smallest chamber width of only 1 mm. Finger4, on the other hand, achieved the least translation among the tested samples since it was designed with the largest chamber width of 4mm. It can also be observed that all fingers, despite the differences in their internal channel geometry, follow the same path initially and later start to deviate until stopping at different positions within the bending plane. This indicates that the effect of varying the design parameters investigated here is not significant in the beginning,

but become more evident later in their trajectory. It is hypothesised that due to the nonlinear deformation of the silicone rubber material, the initial phase of the bending trajectory is mainly governed by the chamber height as the top material layer above the internal channels deform. Hence, since all fingers have the same chamber height, they initially follow the same path. As the pressure in the chambers builds up, the stretched top layer material hinders radial deformation, directing more pressure towards the internal walls. This causes later a unique path for each soft finger according to dimensions of its internal chambers.

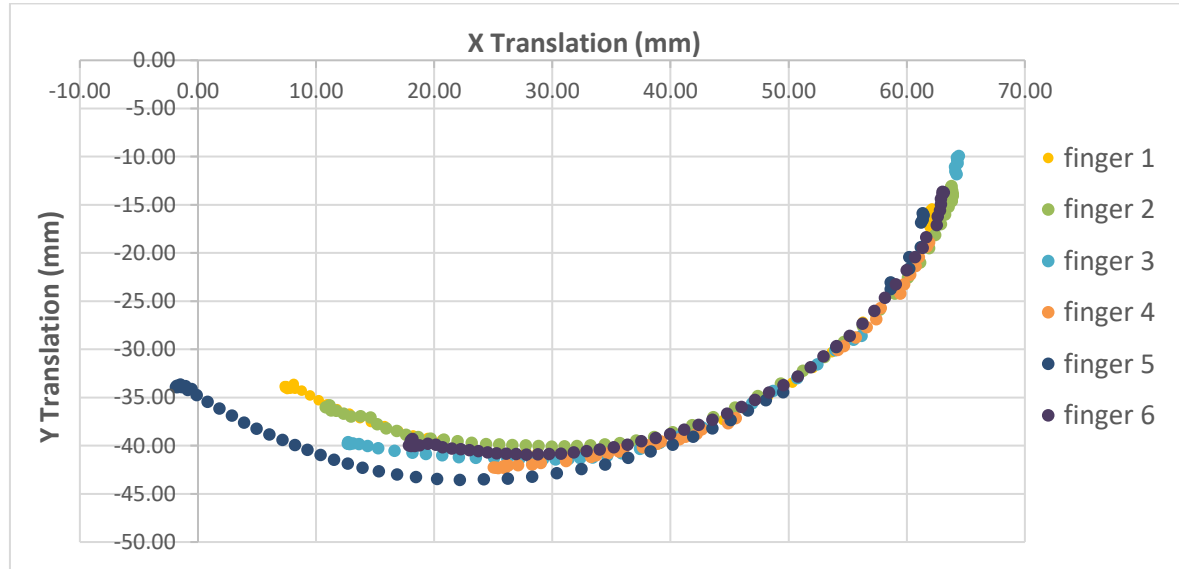


Figure 51: Comparing the trajectory path of all fingers

Maximum Bending Angle

The second response measured using the vision system is the maximum possible bending angle. Figure 52 shows the bending angle response achieved by each finger under the same input conditions. The graph shows how a simple and consistent relationship exists between the supply pressure and the maximum bending for all tested fingers. This important graph can be used not only to size an appropriate compressor based on the maximum bending desired, but also it can be used as a feed-forward model to predict how much bending is expected based on the supply pressure. It also confirms the efficiency of finger 5 in achieving more bending for the same pressure.

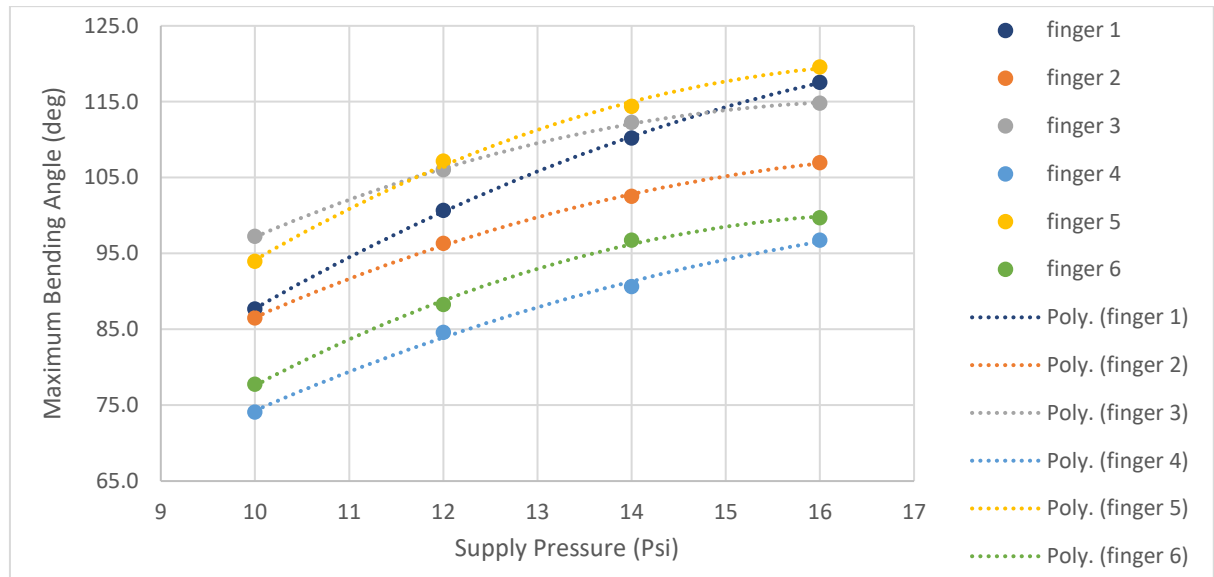


Figure 52: comparing the maximum bending angle of all fingers at variable pressures

In Figure 53, the ratio between the wall thickness and chamber length is plotted against the maximum bending angle achieved by each soft finger sample. The graphs show that increasing the number of chambers generally enhances the maximum bending angle, which becomes more substantial when $R=2$. This important observation means that by designing the internal channels of a soft finger following a ratio of 2 rather the commonly adopted ratio of 1, higher bending angles can be achieved using the same fluidic energy supply. However, the effect is only significant when having a larger number of internal chambers. Hence, further tests will be necessary to derive a more generic relationship that can describe this relationship outside the tested values.

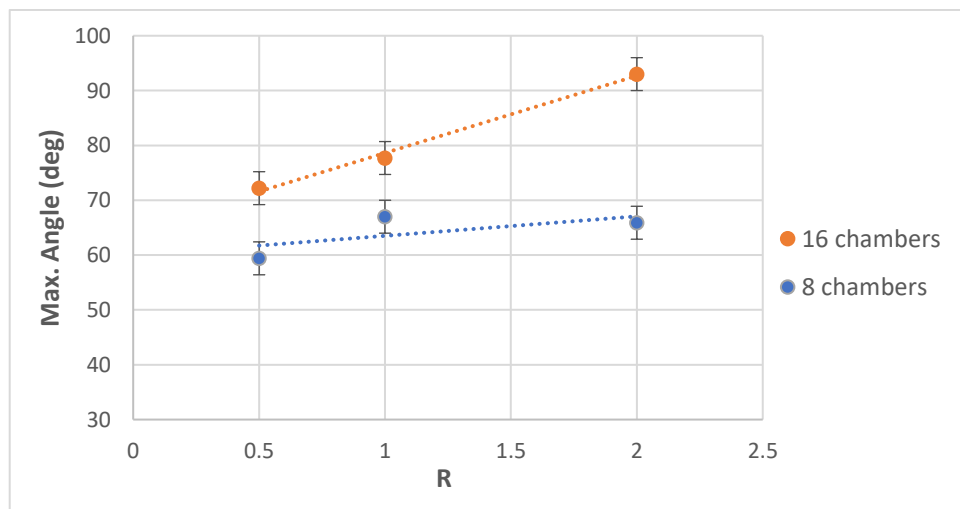


Figure 53: Effect of the ratio and number of chambers on the maximum bending angle

On the other hand, Figure 54 illustrates the significance of the chamber width on the maximum bending angle achieved by each finger. The relationship was consistent across the

different supply pressure values and highlights the need for designing the internal channel with the minimum possible chamber width. However, this would be limited by the fabrication capability and hence would benefit from further enhancement through tuning of the other design parameters.

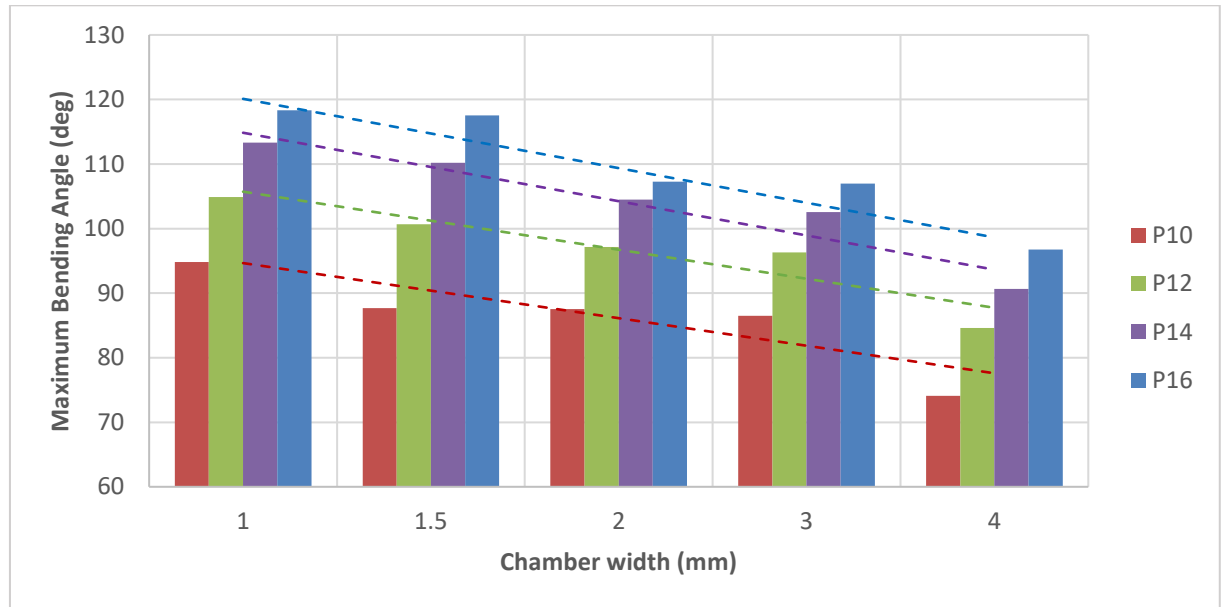


Figure 54: Effect of the chamber width on the maximum bending angle at variable supply pressures

4.4.3. Radial Expansion

Looking at the change in cross-sectional area for each finger during its actuation, it can be seen in Figure 55 that fingers with $R = 2$ are consistently showing the least expansion in the cross-sectional area. This means that fingers designed with internal dimensions following this ratio should be expected to waste minimum energy in undesired radial deformation and transmit more of the supplied fluid energy in bending and applying forces upon contact. Such characteristic would be desired when using these soft fingers in grasping applications so that the finger remains compact and the radial expansion does not hinder the grasping process.

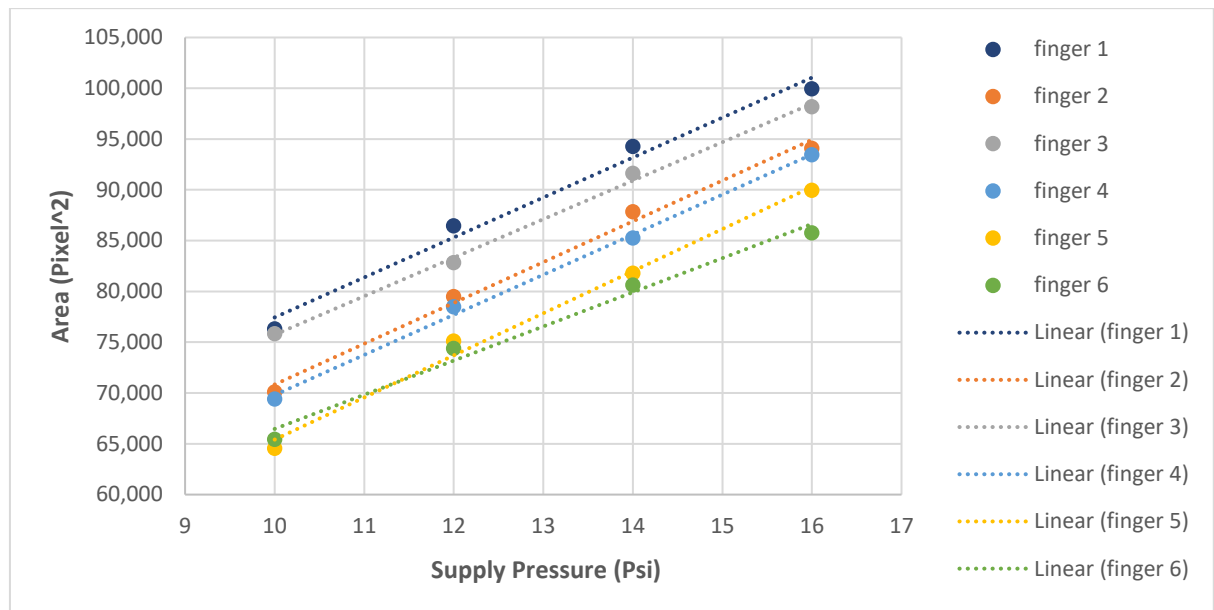


Figure 55: Comparison of change in the cross-sectional area among all fingers

The effects of R and n are further highlighted in Figure 56. It can be observed that generally having more channels causes an increase in the undesired radial expansion. However, this can be minimised when maintaining $R=2$, to benefit from the enhanced bending desired. This finding emphasises the value of studying the effect of R on this experiment.

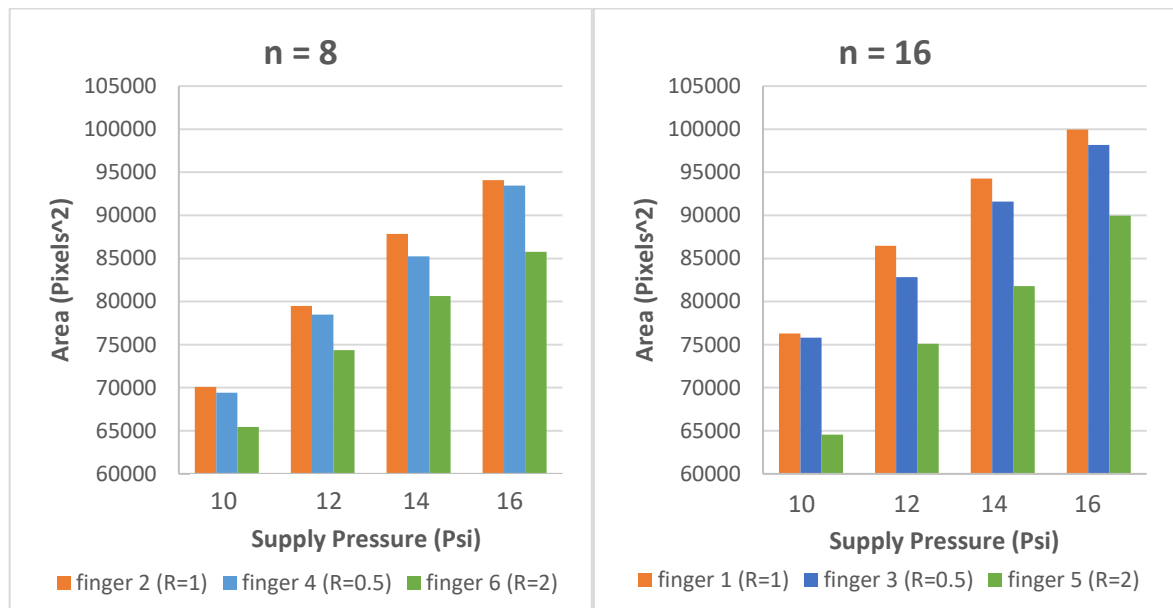


Figure 56: The effect of the Ratio and the number of chambers on the cross-sectional area

4.4.4. Internal Pressure Response

Figure 57 compares the pressure response of all fingers when actuated by the same step signal of 10 Psi. It can be observed that the highest internal pressure response was achieved by fingers 5 and 6. Although fingers 5 and 6 exhibit a very similar pressure response, they have

different internal channel design. The only common parameter is the ratio, which also accounts for the total volume of the internal channels since the outer dimensions of all fingers are fixed. Fingers 5 and 6 have a total volume that is smaller than the remaining fingers, which is why the pressure response was considerably higher. Having a higher pressure response by minimising the total volume of air channels inside a soft finger, would encourage larger deformations and hence further bending. However, the results of this experiment showed that finger 5 was able to achieve more bending than finger 6, although both of them had the same pressure response. This is believed to be due to the same total volume being divided into twice the number of chambers of finger 6 with each chamber width being half that of finger 6.

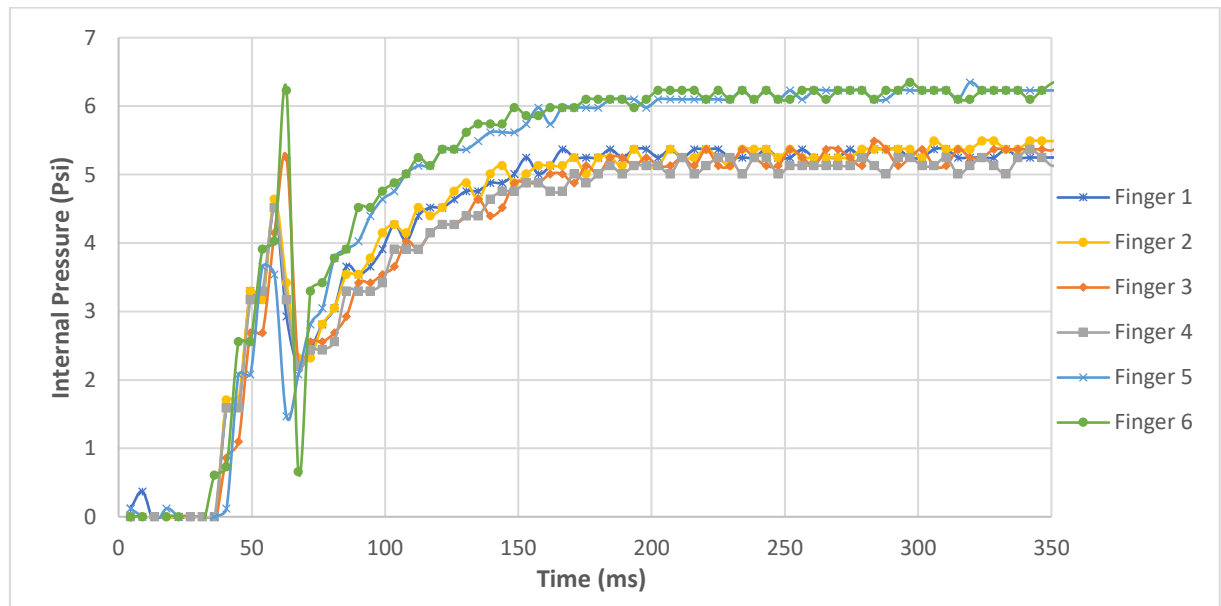


Figure 57: Comparing the internal pressure response of all fingers

To better visualise the effect of the R and n on the internal pressure response, Figure 58 compares the maximum internal pressure measured for each soft finger at each of the supplied pressure inputs. It is clear how fingers with $R=2$ are able to reach higher internal pressures compared to those having the same number of chambers. Yet, the effect of the number of chambers on the internal pressure response is not very significant.

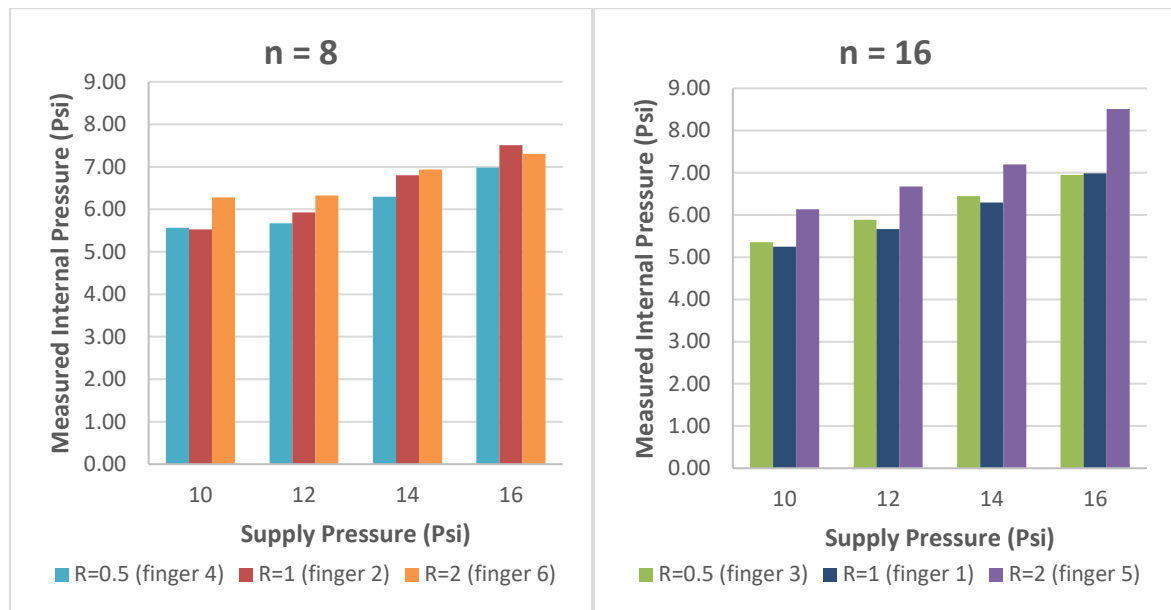


Figure 58: The effect of the ratio and number of channels on the internal pressure response

4.4.5. Analysis of the Resultant Contact Forces

Moreover, the second phase of the experimentation was concerned with measuring the maximum resultant force imposed by each of the tested soft fingers, when making contact with a force post attached to a sensitive force/torque sensor (Schunk Mini45). This would be useful to identify finger designs that are able to provide a more stable grasp especially when lifting heavier objects. The tests were performed at different pressure levels, with multiple repetitions to verify acquired force readings. Looking at Figure 59, the maximum force applied by a soft finger among the tested set is finger 5, while the least is finger 4. It can be noticed that fingers are arranged in ascending order of air chamber width, with finger 5 at the top with the smallest width of 1 mm, while finger 4 being at the bottom with a width of 4 mm. This signifies that the width of the air chamber determines how much force a soft finger can impose on an object for a given pressure and actuation duration. The minimum chamber width value is limited to 1 mm due to the limitations of the current fabrication process, and hence R becomes an additional parameter to tune for further increase in the maximum forces. As to be expected, increasing the pressure will result in higher forces imposed regardless of the finger design, but rather the morphology of the finger decides the rate at which the imposed forces can be increased for a given increase in applied pressure.

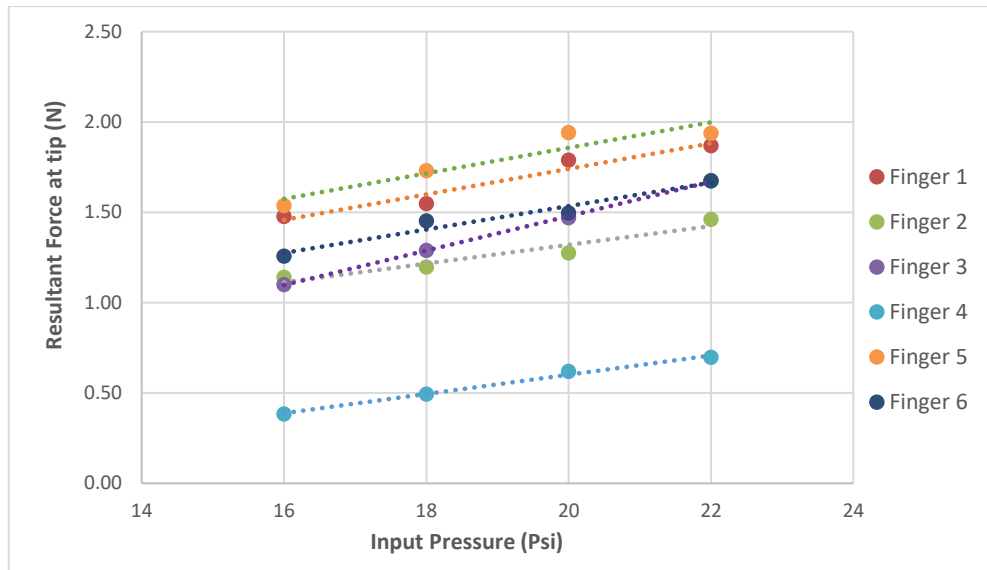


Figure 59: Comparing the maximum resultant forces measured

Figure 60 further illustrates these observations by plotting the ratio against maximum force imposed at a different number of chambers. It is clear that a larger number of chambers and higher R values both contribute to higher contact forces, which explains the superiority of finger 5 in comparison to the remaining fingers. It is important to note that the values of the forces shown here were recorded after some bending of the tested soft fingers, and hence are not necessarily the maximum possible forces to be generated by the fingers. The value of the measured forces largely depends on the type and position of the target object, as well as the location of the contact point along the finger's length.

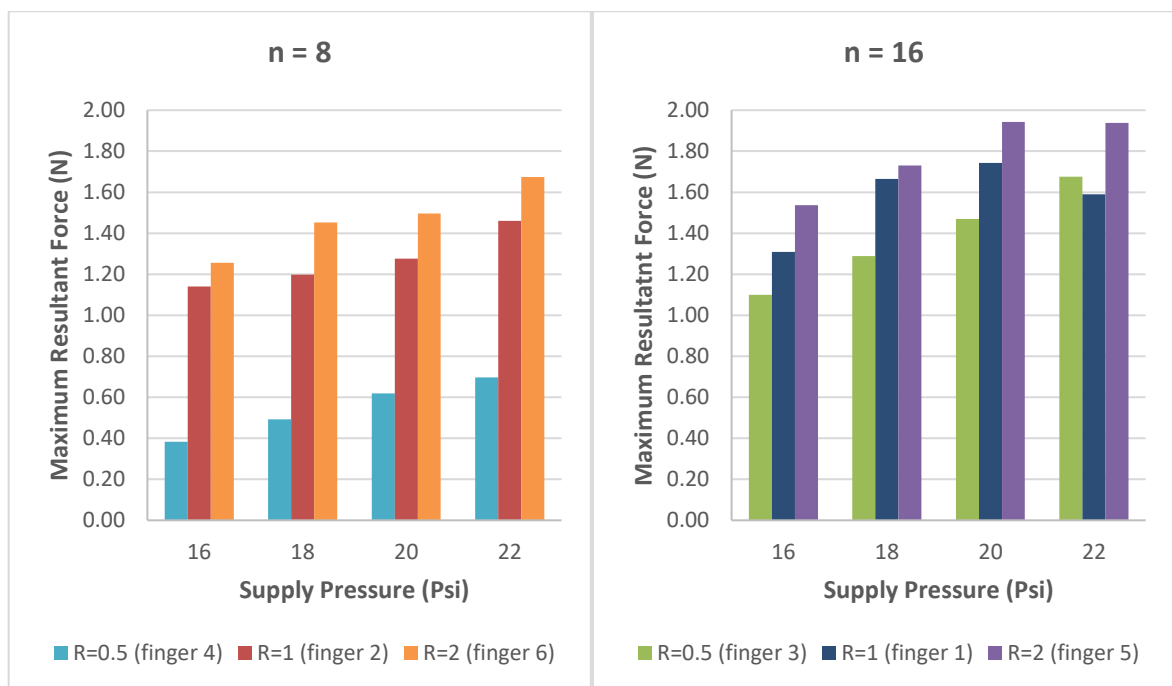


Figure 60 Effect of the ratio and number of chambers on the resultant contact forces

Moreover, to highlight how the force measurement is largely dependent on the contact scenario, an additional experiment was carried out to measure the maximum resultant forces imposed by soft finger upon touching the force post at different locations along its path. Figure 61 shows how a consistent bending is witnessed for each test, but a different final value is reached in due to making contact with the force post at different locations. The corresponding resultant contact forces generated for each case is plotted in Figure 62, which shows how placing the force post at different locations along the trajectory of a sample soft finger results in different maximum contact force for the same input pressure. This is because some of the fluidic energy is directed towards deforming the soft finger further along its trajectory, so less energy will be directed to generate forces upon contact. This observation highlights the impact of the initial position of the soft finger with respect to a target object for grasping applications.

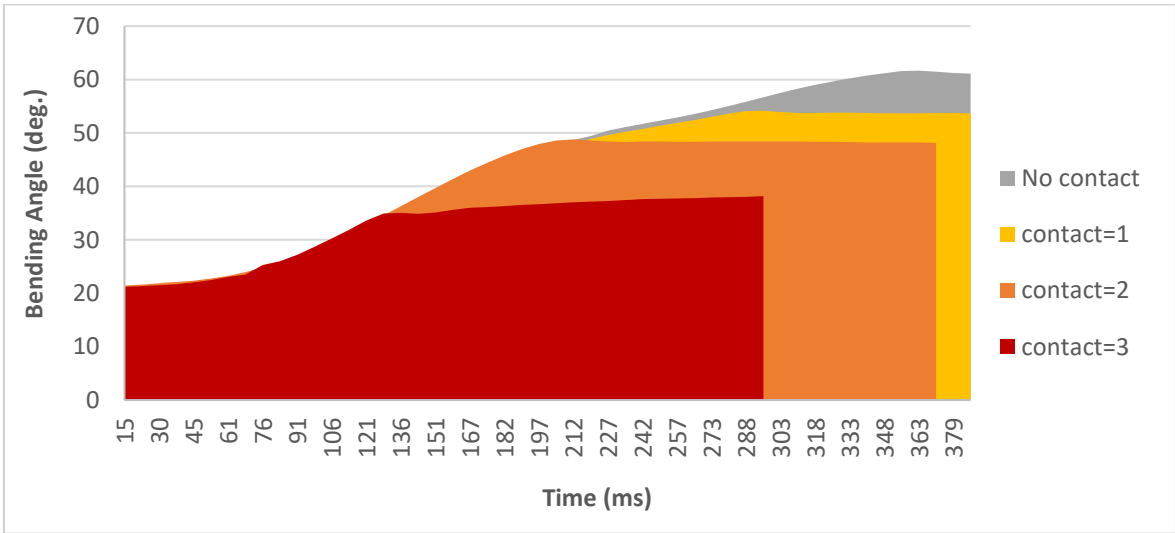


Figure 61: Bending angle response when making contact at different locations

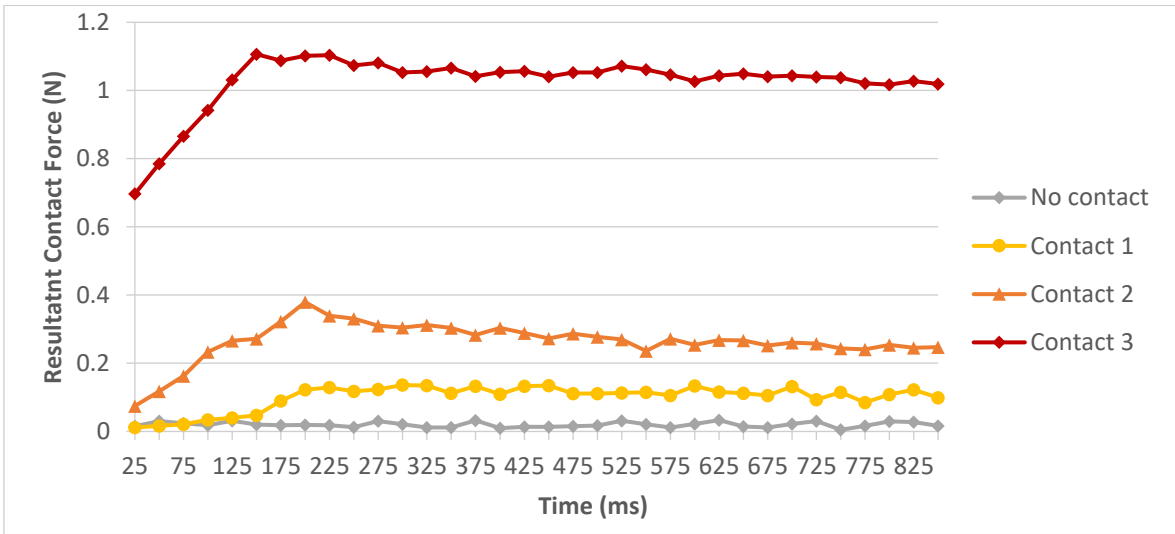


Figure 62: Maximum resultant force when making contact at different locations

4. 5. Conclusions and Perspective

1) Response Consistency:

The conducted tests showed that despite the simple structure of the soft fingers investigated here, their response was repeatable under variable actuation pressures and durations. During the first few tests, some material relaxation might occur as confirmed by previous research [16], yet the material behaviour remains consistent afterwards. Furthermore, supplying higher input pressures was observed to cause an oscillating trajectory path, as the dynamics of the non-linear material becomes more evident at higher accelerations. Thus, it is recommended to supply lower input pressures when actuating the fingers, in order to ensure a smooth trajectory that is easier to predict and control. The witnessed repeatability in the bending response and the mostly linear relationship between input pressure and maximum bending encouraged the proposed data-driven modelling approach. This also means that it should be possible to control the position of soft fingers by controlling the supplied pressure or actuation duration, to stop the fingertip at a point along its previously known free-bending trajectory path.

2) The effect of the number of chambers:

The conducted experiments also showed that for a fixed length of a soft finger, increasing the number of chambers within the internal channels generally enhanced their bending and force capabilities, particularly when $R=2$. This was achieved by minimising the dimensions of the individual pneumatic chambers, so that the total volume of the internal channels can be divided into a larger number of chambers. However, considering the limitations of the manual fabrication process used to create these soft fingers, it becomes challenging to create features that are less than 1 mm in length. The viscous nature of the silicone rubbers used to create the soft fingers makes it challenging to fill narrow features during the moulding process and increases the risk of air entrapment. Additionally, the 3D printed moulds used to imprint the features could be subject to dimensional inaccuracy if using basic extrusion-based 3D printers, which becomes more critical as the dimensions of the printed features become finer. Hence, understanding the effect of the ratio as a design parameter allows further enhancement to their performance when reaching the limit of the smallest practical chamber size.

3) Effect of the ratio between wall thickness and chamber width:

To the authors' knowledge, the ratio between the wall thickness and chamber width of soft fingers with ribbed morphology has not been previously investigated as a design parameter

that can be tuned to enhance their performance. The results of the experiments showed that designing the internal channels following an $R=2$, rather than the typical value of 1, can improve the maximum bending angle and contact forces achieved by a soft finger especially when combined with a larger number of chambers. Additionally, fingers 5 and 6 developed the maximum internal pressures for a given step pressure input of 10 Psi and exhibited the least deformation in cross-sectional area compared to the remaining finger designs tested under the same conditions. It is expected that having the $R=2$, was a key reason that leads to the almost identical responses in terms of the internal pressure, and reduced expansion in the cross-sectional area. However, when considering the bending angle response and the trajectory profile, finger 5 achieved a larger bending angle and longer trajectory path. This can be related to the fact that for finger 5, the same total volume of internal channels was divided into double the number of chambers in finger 6 with half the chamber width.

4) Best performing soft finger design

It can be concluded that for a given volume of internal channels inside a soft finger, the general approach towards enhancing the bending response and contact forces, is to divide this volume into the largest possible number of chambers while maintaining a ratio of two between the wall thickness and chamber length of internal channels. For a fixed finger size, this will consequently mean creating narrower individual pneumatic chambers, as much as the fabrication process would allow. The enhanced performance resulting from this design has been demonstrated by the superiority of finger 5 in all tests compared to the remaining finger samples. This conclusion provides a useful guideline for designing similar soft fingers, which would aid in creating more efficient soft fingers with ribbed channel morphology that can achieve more bending and higher contact forces with reduced lateral deformation.

5) A systematic procedure for vision-aided testing of soft actuators:

Finally, the experimental procedure followed here with the aid of the automated vision analysis program provides a systematic approach that can be utilised to analyse and compare the performance of different soft actuators. This experimental approach becomes particularly useful when accurate material models and coefficients for the nonlinear hyper-elastic materials are difficult to acquire. Additionally, the experimental data generated from such tests can be further utilised in deriving empirical models that implicitly account for uncontrollable variations in the fabricated soft finger samples. The main limitation, however, is the need for fabricating many samples that cover all the possible combinations of the

studied parameters, with several repetitions for each test to reduce sources of random errors. This could be a relatively time-consuming process when investigating many parameters.

In the next chapter, the conclusions drawn from the conducted experiments will lay the foundations for designing and fabricating simplified soft fingers that are able to exhibit stable and repeatable bending angle response. The design of internal channels for finger 5 will be adopted, which will be transformed into a more controllable soft finger, via the embedding of flexible sensors. The repeatability of the bending response encourages the proposed data-driven bending response, and the same experimental setup will be used to generate the required data.

CHAPTER 5:

Data-driven Modelling and Control of Soft Fingers

Addressed Research Question: *How accurate can the bending of soft fingers be modelled and controlled when following a purely data-driven approach using feedback from embedded flexible sensors?*

Chapter Objectives:

- Embed flex sensors in soft fingers based on the design from the previous chapter.
- Regulate the supply pressure smoothly using high-speed valve switching.
- Characterise the embedded flex sensor response under variable pressure and tilt.
- Model and compare bending accuracy using regression analysis and neural networks.
- Control bending based on derived model using a PID controller and evaluate accuracy.

Generated Publication: K. Elgeneidy, N. Lohse, and M. Jackson, “*Bending angle prediction and control of soft pneumatic actuators with embedded flex sensors – A data-driven approach*,” *Mechatronics*, vol. 50, pp. 234–247, Oct. 2018.

5. 1. Introduction

The primary aim of this research was to develop sensor-guided soft grippers to enable their utilisation in more complex applications that require both a delicate touch and a more controllable operation. Although soft grippers relying solely on the embodied intelligence of their morphology can passively comply with a range of delicate objects, the lack of feedback regarding the grasp quality and finger position is a limitation hindering their full exploitation. Conventional analytical modelling and finite element methods require accurate material models and their relevant material coefficients, in order to accurately model the nonlinear behaviour of the hyperelastic materials used in fabricating soft grippers. This becomes even more complicated when grippers are fabricated from combinations of different materials, or when equipped with external reinforcements and embedded components. Furthermore, the conventional manual fabrication process is likely to introduce variations in the geometry or material properties of the fabricated soft grippers due to human error, which would influence their expected grasping response. Therefore, the main contribution of this chapter is in the proposition of a purely data-driven modelling approach that utilises feedback from inexpensive commercially available sensors, to derive empirical models that can accurately predict and control the free bending response of soft gripper fingers. This novel data-driven approach not only lifts the need for deriving precise physical and material models that are difficult to achieve in some cases, but also the experimental data generated from real tests

implicitly accounts for variations arising in material preparation and the manual fabrication that are otherwise difficult to model mathematically. Also, the approach is not constrained to a specific actuator morphology or input conditions, since it is entirely based on the generated experimental data rather than physical models. The primary requirement of this approach, however, is to generate sufficient experimental data under similar operating conditions, so that the derived models can be further generalised to new untrained scenarios. Hence, equipping soft fingers with reliable sensing elements that do not hinder their compliance becomes essential to generate the required sensory feedback. Ultimately, the outcomes of this research can be adopted by soft robotics researchers to model and control other morphologies of soft grippers, by following the approach presented here.

5. 2. Embedding Flex sensors

The primary challenge in sensing is to directly measure the bending motion of soft fingers as they curve towards their base, without hindering their compliant behaviour. Hence, a flexible sensor is required that can be embedded at the inextensible layer of a soft finger, to provide a measurable change in a physical parameter that can be related to bending. This is one of several applications motivating research over the past few years into developing new concepts for flexible and stretchable sensors, which can be integrated with soft bodies in general [109]. The main flexible sensing methods that could be seamlessly integrated with soft gripper fingers for measuring and controlling their bending angle have been reviewed in the literature review chapter. The work presented here utilises a commercially available resistive flex sensor (Datasheet in Appendix (D) – Datasheets) for measuring the bending angle of a soft finger design. This is achieved by correlating the change in the sensor's resistance due to bending to the actual bending angle measured using a vision system. A soft finger based on a standard bending actuator design with ribbed channel morphology (shown in Figure 63), was fabricated from Ecoflex-50²⁰. The dimensions were based on the results of Chapter 4 identifying the best performing soft finger design in terms of the bending and force generation. Engineering drawing for the finger design is given in Appendix (E) – Soft Finger Design. The standard soft lithography approach is again followed here to create the soft finger samples, but with a modification to the strain limiting layer to embed the flex sensor. The soft finger body is composed of three sections:

- 1) The main body moulded from Ecoflex-50 with the imprinted fluidic channel pattern,

²⁰ EcoFlex-50, SmoothOn. http://www.smooth-on.com/Silicone-Rubber-an/c2_1115_1130/index.html

- 2) the bottom base also made from EcoFlex-50 or a stiffer elastomer if desired, which seals the internal channels,
- 3) and the strain limiting layer in the form of a sheet of paper between those two parts, to prevent the finger from extending allowing only a bending motion towards its base.

The flex sensor is glued to the strain limiting sheet of paper so that it changes in resistance as the soft finger bends. The sensor is thin and flexible, so it does not significantly hinder the bending response, but causes a small increase in the overall stiffness of the soft finger. Wires can be then soldered to the sensor terminals (Figure 63) to connect the sensor to a 5V supply from an Arduino board so that the voltage drop caused by any change in sensor's resistance can be measured.

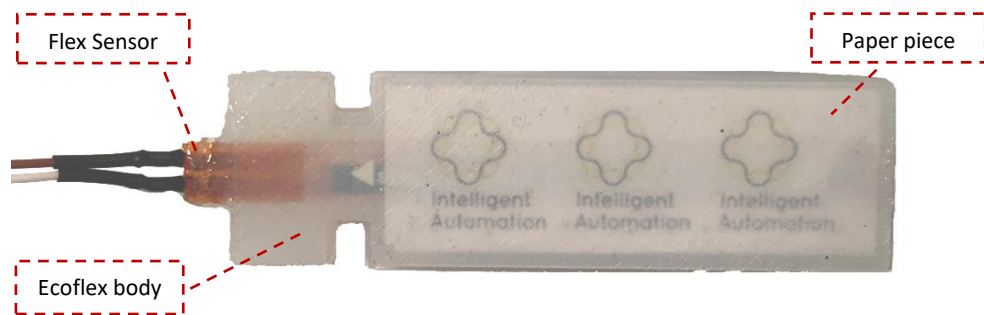


Figure 63: Soft Pneumatic actuator sample embedded with a flex sensor

The outlined fabrication process uses inexpensive materials and requires simple equipment to implement. However, the manual nature of the process could introduce variations during different stages of the fabrication process including; the material preparation, mould printing, sensor placement, and manual bonding. The uncertainty in the actuator dimensions and material properties is one of the factors limiting the accuracy of analytical models that are derived based on theoretical values, which are difficult to guarantee. Hence, the data-driven modelling approach considered here is encouraged, as variations arising during the manual fabrication process will be implicitly accounted for within the experimental data.

5. 3. Experimental Testing

The experimental setup outlined in Chapter 4 was again used here to systematically test fabricated soft finger samples, embedded with the flex sensor at variable operating conditions. This includes controlling the pressure and duration of the input pneumatic supply, as well as setting the initial orientation of the actuator. The pneumatic supply flows through a 1.6 mm diameter needle attached to the end of the supply tube. The needle passes through a locating hole inside the 3D printed fixture, which guides it to pierce the actuator at the base of its internal channels. This allows easy and fast switching between different soft finger

samples, without the need for bonding the pneumatic tubes directly to the actuator body. The initial orientation ' φ ' of the soft actuator can be varied by simply rotating a 3D printed fixture that securely holds the soft actuator to a fixed frame, and is measured from the positive x-axis as illustrated in Figure 64.

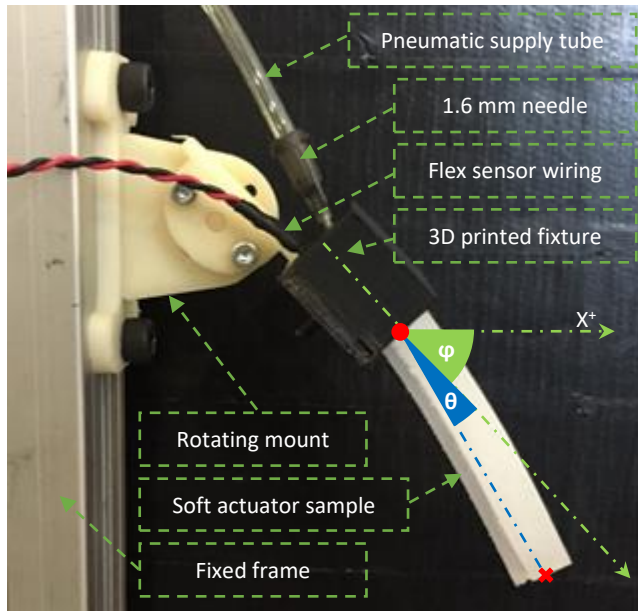


Figure 64: Experimental setup for testing soft actuators embedded with a flex sensor

5.3.1. Pressure Control Using High-Speed Valve Switching

As for varying the pressure of the pneumatic supply, this is achieved through high-speed valves on the pneumatic control board outlined in section 4.3.1. The board includes high-speed switching solenoid valves (SMC-VQ110U-5M) controlling the flow of pneumatic supply, pressure sensors (Honeywell-ASDXAVX100PGAA5) measuring the resulting internal pressure, and an Arduino Mega board that is programmed to control the timing of the actuation and the effective pressure supply. The onboard pressure sensors and the embedded flex sensors are also interfaced with the Arduino board to feedback the resulting sensory readings at 60 Hz for each actuation test conducted. The resulting sensory feedback from the embedded flex sensor and the measured internal pressure response is recorded and synchronised with measurements for the actual bending angle calculated using the image processing program described in section 4.3.2. The input pressure to the tested soft actuators can be effectively varied through high-speed valve switching, controlled by a pulse width modulated (PWM) signal at 60 Hz from the Arduino board. A fixed input regulated pressure line can be thus effectively reduced to a desired value according to the duty cycle of the generated PWM signal. This provides a simple and inexpensive method for controlling the pressure supply to the soft actuator. However, it has the drawback of introducing noise to the measured internal

pressure response because of the mechanical switching of the valves. Having noisy sensory feedback will limit the accuracy of any predictive models or controllers that rely on such data.

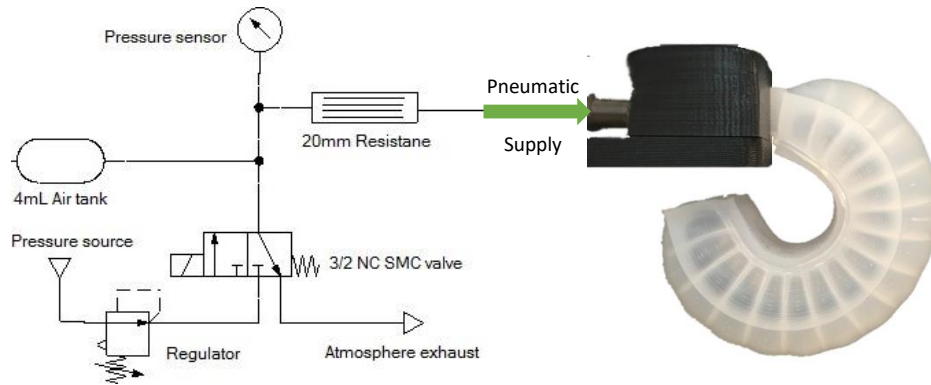


Figure 65: A schematic for the pneumatic circuit controlling the actuation

One way of overcoming this problem is the use of a pneumatic tank in the form of fixed volume syringe and a pneumatic resistance in the form of a porous plug [89]. shows a schematic diagram for the pneumatic circuit including a 4ml syringe and a 20mm pneumatic resistor between the valve and the pressure sensor, while Figure 66 shows how this results in significantly damping the oscillations in the pressure response measured at 50% duty cycle. It can be observed from Figure 66 that introducing the pneumatic tank and resistor have minimal effect on the maximum measured internal pressure, but in return results in a significant improvement in noise reduction. It is important however to avoid changing the size of the pneumatic tank and resistor after collecting the experimental data required for the data-driven modelling since this would affect the prediction accuracy of the derived models as the measured pressure changes slightly. Furthermore, a moving average can be applied to further smoothen remaining oscillations in the signal, yet this would come at the expense of an added delay to the response of the system depending on the window size. The final smoothed pressure response is shown in Figure 66 is the combined outcome of adding the pneumatic tank and resistor as well as applying a two-point moving average, which would introduce a delay of around 20 ms.

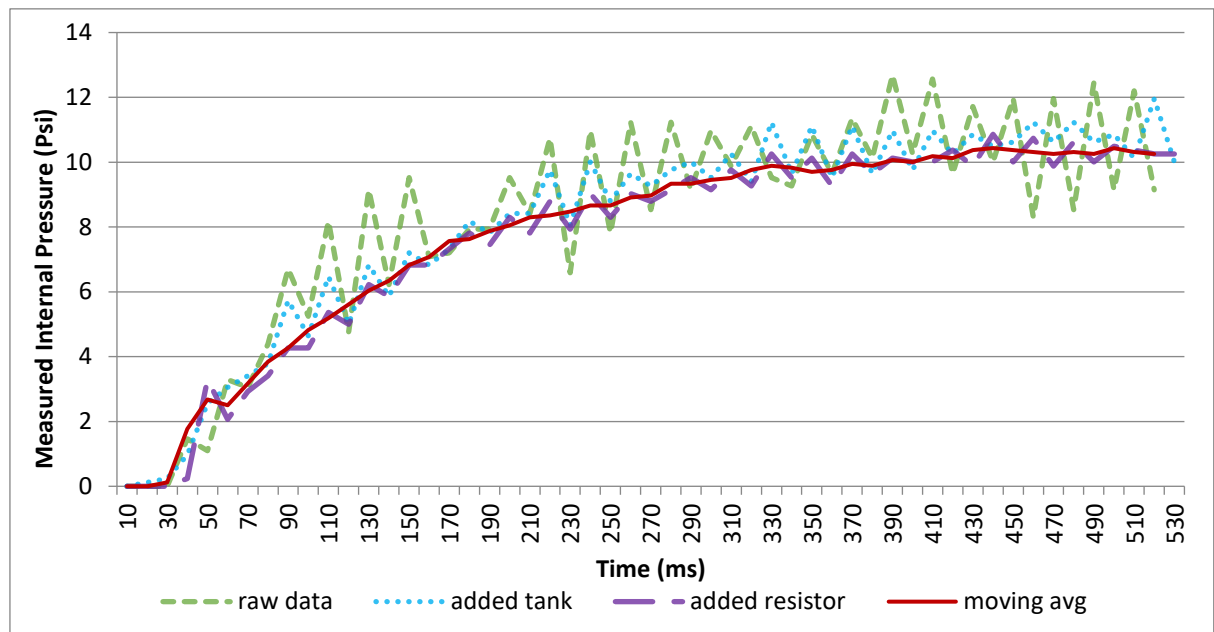


Figure 66: Damping of oscillations in internal pressure measurements using a pneumatic tank and resistance

5.3.2. Embedded Flex Sensor Characterisation

The primary sensory feedback of interest is the change in resistance of the embedded flex sensor due to the bending motion of the actuator, which is converted to voltage and measured through the analogue input port of the Arduino board. This provides a direct sensory measurement that can be correlated to the actual bending angle of the actuator, to enable accurate prediction and closed-loop control of such actuators. In order to evaluate the quality and repeatability of the feedback from the embedded flex sensors, a soft actuator sample was repeatedly actuated at different magnitudes and durations of the pneumatic supply. Figure 67 plots the internal pressure measured against the resulting flex sensor readings, when supplied with a step pressure input of 12 Psi (82.7 kPa) for different durations. The plotted flex sensor readings are the result of the analogue to digital conversion of the voltage received from the flex sensor, in which the 0V to the 5V range is converted to values between 0 to 1023. The plotted cycle shows the readings from the flex sensor decreasing upon actuation as the internal pressure builds up until the pneumatic supply stops and the soft finger retracts back to its original shape. The response was observed to be repeatable, with longer actuation duration causing a systematic extension to the witnessed response.

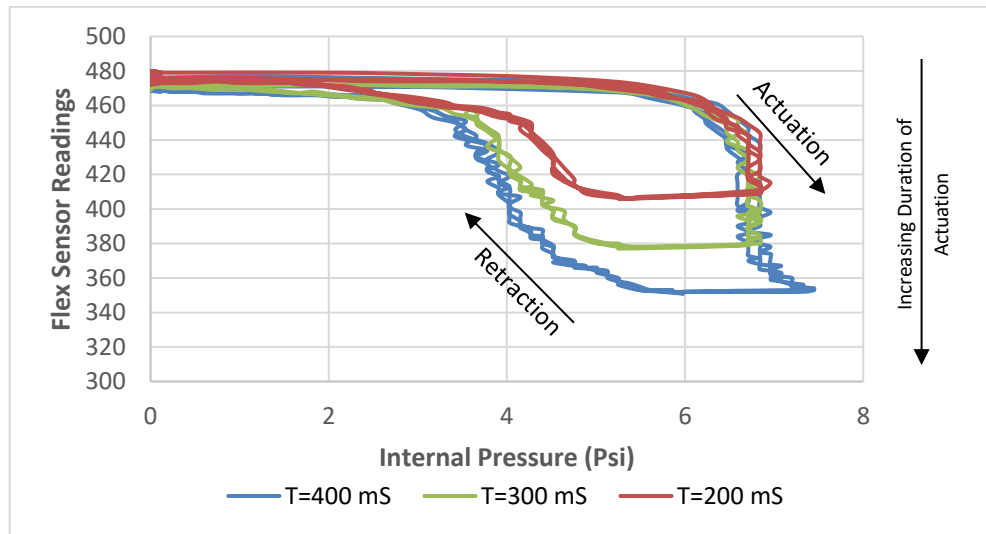


Figure 67: Flex sensor response against the internal pressure at variable durations.

Furthermore, the same test was repeated, yet this time the actuation duration was fixed at 500 ms, while the soft finger was actuated at pressure inputs of 10 Psi (68.9 kPa) and 12 Psi (82.7 kPa). Figure 68 shows that changing the input pressure had a more significant effect on the recorded sensory response, influencing not only the final reading from the flex sensor, but also the rate of change of the response. This highlights the need for incorporating the measured internal pressure response, if accurate models are to be derived for the estimation of the bending angle of soft actuators. The pressure term, in this case, will account for the rate of change of the flex sensory reading, allowing more generic models to be derived that are capable of estimating the bending angle at varying input pressures.

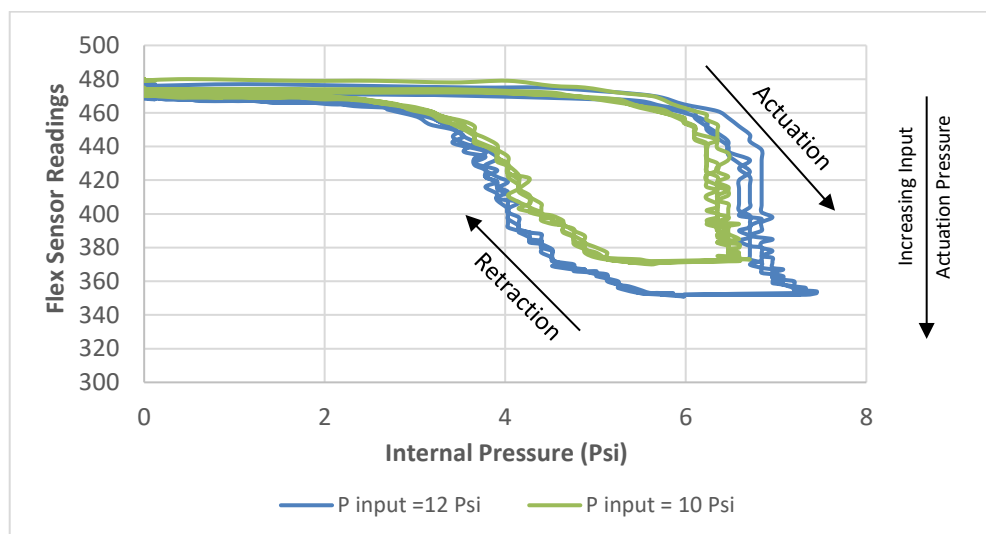


Figure 68: Flex sensor response against the internal pressure at variable pressures.

Finally, Figure 69 shows the relation between the measured internal pressure and the flex sensor readings at three different soft finger initial orientations of 45° , 0° , and -45° . A slight deviation in the response can be observed in each case, even though the input conditions were held constant. The deviation is more evident during the retraction of the soft finger to its initial position, since the pneumatic supply is stopped and gravity becomes the dominant force acting on the finger. This illustrates the benefit of taking the initial orientation of soft fingers into consideration when modelling their bending response to be able to compensate for the effect of gravity and generate more accurate models [164]. The orientation here is known for each test since the tested soft finger is fixed using the 3D printed mounts. However, in actual grasping applications, the orientation can be measured in real-time using an accelerometer sensor mounted at the gripper base or using the positional feedback from a robotic arm carrying the gripper. This would be an additional sensory input that can be interfaced to the Arduino board.

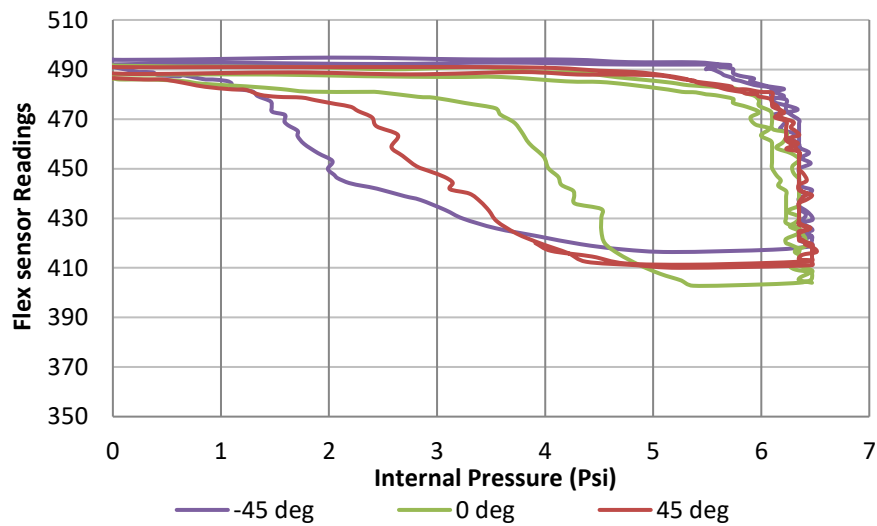


Figure 69: Flex sensor response against the internal pressure at variable orientations.

5. 4. Data-Driven Modelling of the Free Bending Response

In this section, the data acquired from experimental tests are utilised for deriving an empirical model that describes the bending response of the investigated soft actuator. The initial tests for the flex sensor identified the potential benefit of including the pressure input and finger orientation for more accurate and generic models to be driven. The available feedback from a typical actuation test comprises of (1) the measured voltage from the change in resistance due to bending of the embedded flex sensor “ F ”, (2) internal pressure “ P ” measured using onboard pressure sensors, (3) and the initial orientation of the soft finger within its bending plane “ φ ” set using the tilting fixture. A soft actuator sample with an embedded flex sensor

was tested at three different initial orientations of -45° , 0° , and 45° , with three step pressure inputs of 8, 10, and 12 Psi (55.2, 68.9, and 82.7 kPa). To determine the minimum amount of data required to derive an accurate model, two actuations were initially performed for each test, since relying on only one actuation risks including faulty data. If the accuracy of the resulting models needed improvement, then additional actuations can be added to increase the training and validation datasets. The resulting flex and pressure sensory feedback, as well as the actual bending angle measured from the captured image frames were recorded and synchronised. A sample of this data, which was acquired at a 0° orientation is shown in Figure 70 with labels showing the start and end of each actuation. It can be seen that as the actuator bends the readings from the flex sensor decreases in synchronisation with the increase in bending angle values. As the pressure supply is switched off to end an actuation, the measured internal pressure starts to drop as highlighted in the graph. In total, a data set of 1664 observations was generated at a unified sampling rate of 10 ms, with each observation being an array of four elements in the form of $[F, P, \varphi, \vartheta]$. The first three elements in the array are the input variables, while the fourth element is the target bending angle output for training and testing the derived empirical models. Regression analysis and neural networks are two data-driven modelling techniques that are implemented and compared here, in order to derive empirical models which will be better suited to predicting and controlling the bending angle of the tested soft actuators based on real-time sensory feedback.

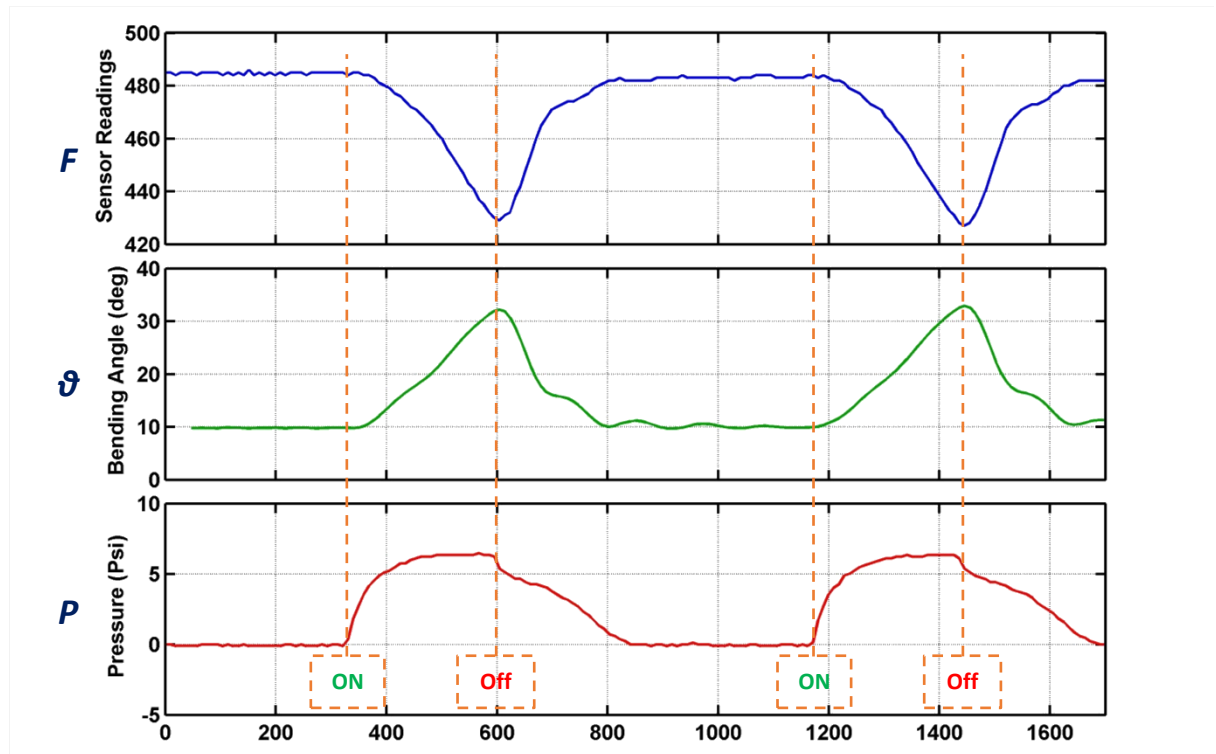


Figure 70: Sample of the feedback from the flex sensor, pressure sensor, and bending angle when bending the actuator twice at a 0° orientation

5.4.1. Regression Analysis

Linear regression is a common data-driven technique that can be used to derive an empirical model using the Least Square Method to compute the best fit relation between the target bending angle and the generated sensory feedback. For this analysis, the dataset generated from the experimental tests was split into two sets for training and testing purposes. The training dataset included a total of 1108 observations acquired at the three tested initial orientations when the actuator is supplied with an input pressure of 10 and 12 Psi (68.9 and 82.7 kPa) for a fixed duration of 300 ms. The remaining 556 observations, were the ones acquired at a different pressure input of 8 Psi at the three orientation values for testing the derived models at new input conditions. The primary variable of the regression model is the measured change in resistance (converted to voltage) from the embedded flex sensor as the soft actuator bends. Hence, the simplest form of the regression model will be a linear equation that directly relates the target bending angle to the voltage readings from the flex sensor. Equation 1 below shows the output model from the regression analysis, with an R^2 value of 0.88 and a standard error of 2.28°. The R^2 value reflects how much of the variance was successfully represented by the model, while the standard error is a measure of the accuracy of the predictions made by the regression model [166].

$$\text{Model 1: } \vartheta_{relative} = -206.87 + 0.422 * F \quad (1)$$

In order to improve the accuracy of the model in predicting the bending angle when actuated at variable input pressure values, the measured internal pressure was added to the model to account for the rate of change in the flex sensory readings. The regression analysis, in this case, results in equation 2 with an improved R^2 value of 0.943 and a reduced standard error of 1.576° . This is expected since the dataset used in deriving the model was acquired at different pressure input levels and hence including the P term should yield an improved fit.

$$\text{Model 2: } \vartheta_{relative} = -150.39 + 0.309 * F - 0.91 * P \quad (2)$$

Moreover, the models so far were derived using the relative bending angle measured from the initial orientation of the soft actuator. However, the vision system can measure the bending angle as an absolute value from the positive x-axis of a fixed reference frame (Figure 64). Hence, the initial orientation of the actuator needs to be added to the model to allow more meaningful predictions of the bending angle as an absolute value, regardless of how the actuator was oriented initially. This is achieved by labelling the training dataset with the initial orientation of the actuator and using this value as an additional variable in the regression model. Thus, the outcome of the regression analysis will now include three variables as shown in equation 3 and results in a further improvement in the model fit as the R^2 value increased to 0.949 and the standard error further decreased to 1.489° . The updated model, in this case, is not only able to cope with variable input pressure conditions, but also outputs the absolute value of the bending angle given a constant value for the initial orientation of the actuator. The coefficient of the ϕ term (0.973) is essentially adjusting the value of the initial orientation to account for the static bending of the actuator under gravity. This explains the additional improvement in the model fit since the training dataset was collected at three different orientations that are influenced differently by gravity.

$$\text{Model 3: } \vartheta_{abs} = -228.405 + 0.32 * F - 0.85 * P + 0.973 * \phi \quad (3)$$

A summary of the regression statistics for the derived models is given in Table 4. It shows how the model accuracy was improved gradually by the inclusion of the P and ϕ variables. It is clear that using the feedback from the flex sensor alone is not sufficient to derive a model that can accurately predict the actual bending angle under different operating conditions. The addition of the P term significantly improves the accuracy of fit since the change in the input pressure is reflected in the model, while adding the ϕ term allows the prediction of the absolute bending angle values while accounting for the static bending under gravity. In order to verify

the derived models, the testing dataset was fed to each model, and their predicted bending angle was compared to the actual values measured using the vision system. The dataset for testing was generated at input conditions that were not covered by the training dataset used in deriving those models. The results of testing the three models are in Table 4, showing the mean squared error (MSE) and standard deviation (SD) of the predicted bending angles.

Table 4: Comparison of the regression statistics for the three derived models

	<i>Model 1</i>	<i>Model 2</i>	<i>Model 3</i>
Number of variables	1	2	3
Adjusted R ²	0.880	0.943	0.998
Standard error (deg)	2.280	1.576	1.443
<i>MSE (deg²)</i>	4.13	1.54	1.36
<i>SD (deg)</i>	1.94	1.21	1.15

It becomes evident that the inclusion of the ***P*** and ***φ*** parameters contribute to a more accurate empirical model that can accurately reproduce the bending angle values under untrained input conditions, with an MSE of only 1.36 and a SD of 1.15° (Model 3). Figure 71 shows a sample of the test results comparing the predicted bending angle of each model to the target values measured using the vision system. It can be observed that even though models 1 and 2 result in almost the same final bending angle value, model 2 better follows the actual bending angle response since the ***P*** parameter is adjusting the output to the correct the rate of change. As expected, model 3 can be seen to provide the closest predictions compared to the actual target values, yet a small error of 1.54° in the final value still exists. The remaining deviation between the predicted and target values can be accounted to sources of non-linearity in the response that cannot be captured effectively by a linear regression model.



Figure 71: Sample of the test results comparing the prediction accuracy of the three regression models

5.4.2. Artificial Neural Networks

Another data-driven modelling technique investigated here is the use of a feed-forward artificial neural network (ANN) that is known to cope well with handling sources of uncertainty [167]. It is hence a good candidate for modelling the complex behaviour of continuum soft robots in general [168]. The same training dataset used in the regression analysis was used again here to train and validate a feed-forward neural network with one hidden layer and seven neurons using MATLAB. This network structure was found to reduce the MSE while avoiding overfitting. The inputs to the neural network are the same as model 3, which include the sensory feedback from the pressure and flex sensors, labelled with the initial orientation of the soft finger. The target output is again the measured bending angle of the soft finger recorded by the vision system. Training was conducted using the Levenberg-Marquardt algorithm [169], which would stop when the generalisation accuracy stops improving. The results of the training showed an excellent fit between the inputs and the target output with an R-value of almost 1, as shown in Figure 72.

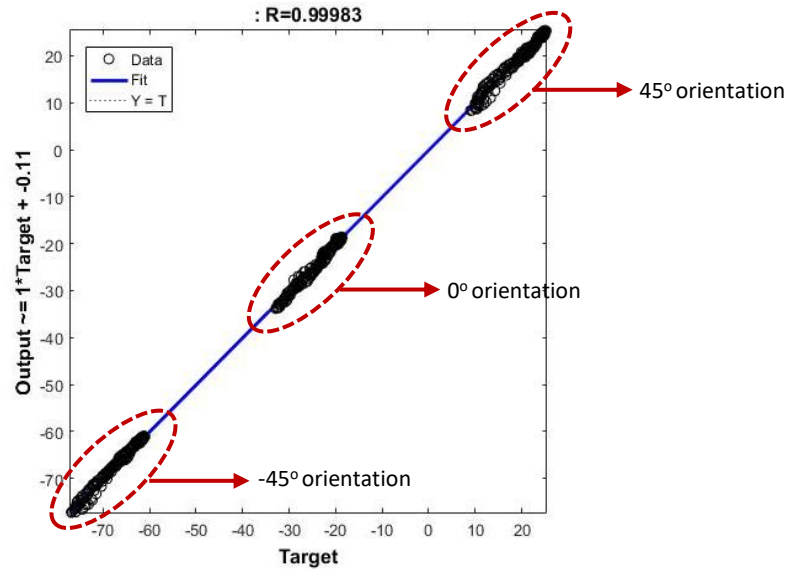


Figure 72: ANN training results

The trained ANN was tested with the same test dataset previously used for testing the regression models and achieved a much lower MSE of only 0.37 with a SD of 0.6 ° (Table 5) when compared to the best performing regression model. This means that the trained network is able to better capture the non-linearity in the response of the soft actuator, which the linear regression model was not able to fully account for. On the other hand, the neural network is more complicated in structure compared to a simple linear equation resulting from the regression analysis. Thus, depending on the application needs, the slightly less accurate regression model might still be favoured when deploying the model to a controller with limited processing power, so that a faster sampling rate for the required sensory feedback can be maintained. This is essential especially when operating at higher input pressure, during which the actuation would typically last for less than 500 ms.

Table 5: Error statistics for testing the trained ANN

	ANN	Regression		
		Model 1	Model 2	Model 3
MSE (deg ²)	0.37	4.13	1.54	1.36
SD (deg)	0.60	1.94	1.21	1.15
Max Error (deg)	2.29	4.97	3.12	3.06

Finally, Figure 73 shows the residual errors from testing the prediction accuracy of the derived regression model 3 and the trained neural network on untrained validation dataset. It is clear how the residual errors from the ANN estimates were less than the best performing regression

model at the tested finger orientations. Hence, it can be concluded that both techniques can be used to predict the bending angle response when given new data sets acquired at untrained operating conditions. Yet, the trained neural network provides more accurate bending estimates compared to the regression model, at the expense of requiring more computational power when deployed to a controller.

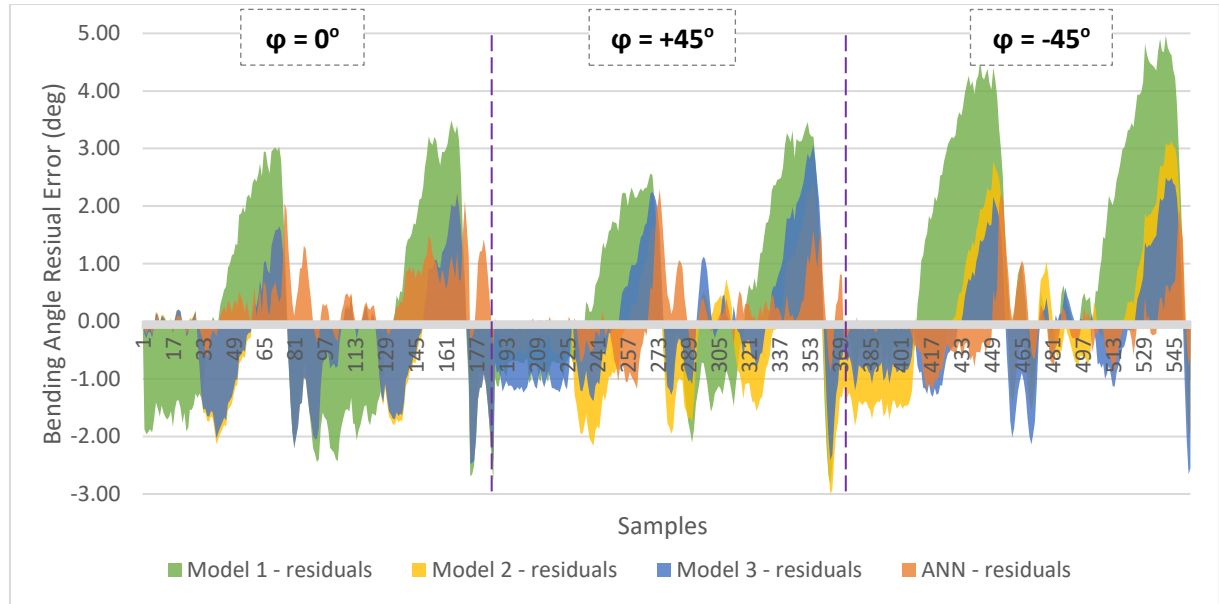


Figure 73: Comparing error residuals of regression models and trained ANN

5.5. Closed loop PID control of soft finger bending

After successfully deriving models that predict the bending angle of soft actuators based on the combined sensory feedback, the next step was to utilise those models in controlling the bending angle according to a set target value. A closed-loop PID controller was designed and tuned using Matlab Simulink, which:

- 1) Collects the real-time sensory feedback from the Arduino,
- 2) predicts the current bending angle using the derived regression model according to the sensory data,
- 3) calculates the duty cycle value of the PWM signal driving the valve switching, based on the difference between the current and target bending angles.
- 4) regulates the supply pressure by generating a PWM signal based on the new duty cycle value, which controls the high-speed valve switching.

Figure 73 shows a schematic diagram summarising the basic operation of the MATLAB control program communicating with the Arduino controller on the pneumatic control board. The PID controller gains were tuned and initiated online following the Ziegler–Nichols method [170] until the settling error and oscillations were minimised. This involved setting the controller's

integrator gain (K_i) and derivative gain (K_d) to zero while increasing the proportional gain (K_p) until the system reaches its stability boundary. The corresponding values of this gain and period of oscillations were recorded and used to calculate the initial values of the PID controller gains. Further tuning of the gain values was manually conducted online based on the monitored bending response when tested with different target values. The final values of the tuned PID gains were found to be: $K_p=26$, $K_i=11$, and $K_d=0.2$. This heuristic tuning approach is well suited for the data-driven modelling approach adopted here since the physical model of the system is not available for typical model-based tuning and stability analysis tests to be performed. Instead, the availability of the real-time response is utilised to tune the PID controller gains and confirm the controller stability within the required operating conditions as further demonstrated in the tests to follow.

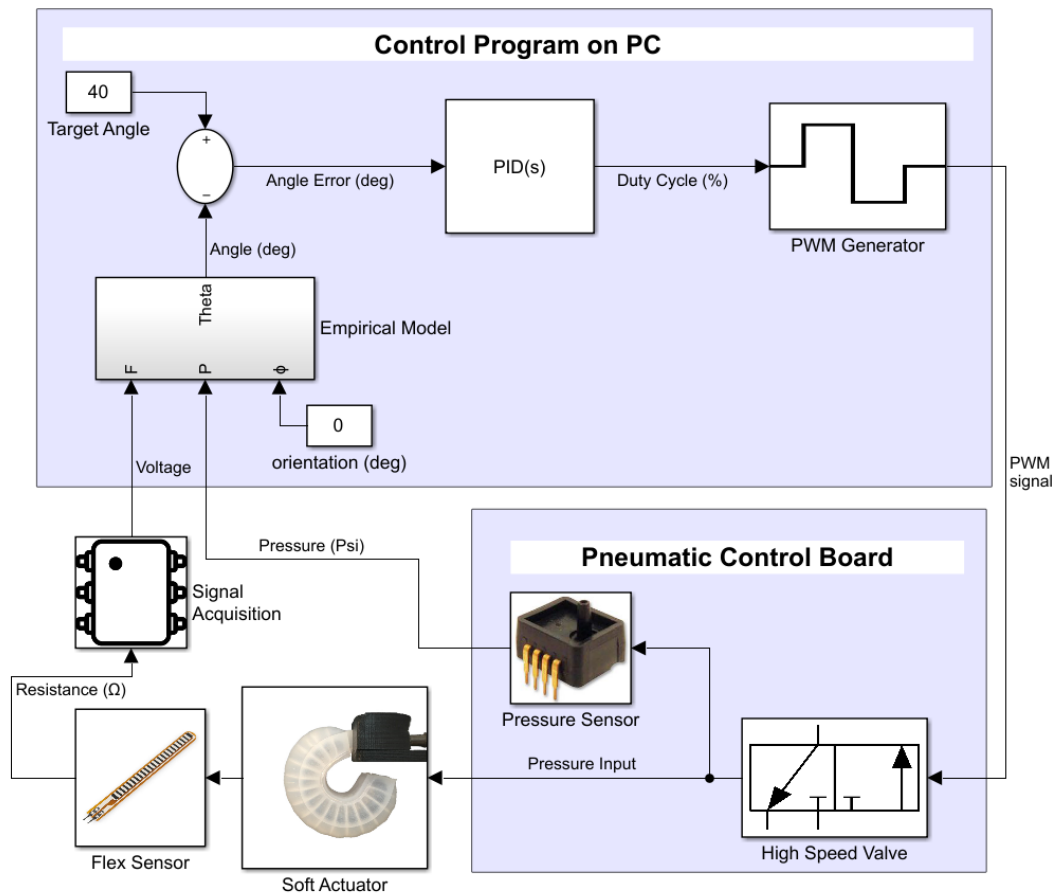


Figure 74: Schematic diagram of the controller architecture

In order to test the accuracy and stability of the controller in meeting a target bending angle value, a series of experiments were conducted in which a step, as well as sinusoidal reference signals, were supplied to the controller and compared to the measured bending angle. Once a switch on the pneumatic controller board is toggled (Figure 75 - labelled "ON"), the valve

opens to supply a constant pressure input to the tested soft actuator with an initial duty cycle value of 100%. The sensory feedback from the embedded flex sensor and the onboard pressure sensor is continuously fed to the derived regression model to convert it to the current bending angle value of the soft actuator. The difference between the target and current bending angles is fed to the PID controller as the error signal (Figure 73), which as it decreases causes the PID controller to reduce the duty cycle value of the PWM signal accordingly. Reducing the duty cycle below 100% initiates the high-speed valve switching, which in turn reduces the effective internal pressure supplied to the soft actuator as previously explained. Hence, the rate of increase in the bending of the soft actuator attenuates until settling at the target bending angle value, even though a fixed pressure input is being supplied. Figure 75 shows the measured bending angle response, the measured internal pressure, and the duty cycle output from the controller when testing an actuator at 8 Psi (55.2 kPa) pressure input and setting the target bending angle to a value of -35° (measured from the positive X-axis). It can be observed how the measured internal pressure response settled to a value of nearly 5.5 Psi (37.9 kPa), as the controller reduced the duty cycle value to values in the range of 60% to 80%. The fluctuations in the duty cycle value are due to the small residual oscillations in the internal pressure measurement, which is expected when using a high-speed valve switching to control the pressure. Once the actuation switch is toggled off (Figure 75 - labelled "Off"), the input pressure is stopped causing the soft actuator to retract to its original position. Since the exhaust of the pneumatic circuit was left at atmospheric pressure, the duty cycle output from the controller settles around the value required to achieve an internal pressure that is just enough for the actuator to maintain the target bending angle. Alternatively, if the exhaust was instead sealed to hold the pressure, then the output duty cycle will continue to drop until reaching zero, which closes the valve completely to stop any further pneumatic supply. However, in this case, the exhaust must be manually opened for the soft actuator to retract to its original position, which means that the bending can only be controlled during the forward actuation phase. Hence, the exhaust was left at atmospheric pressure.

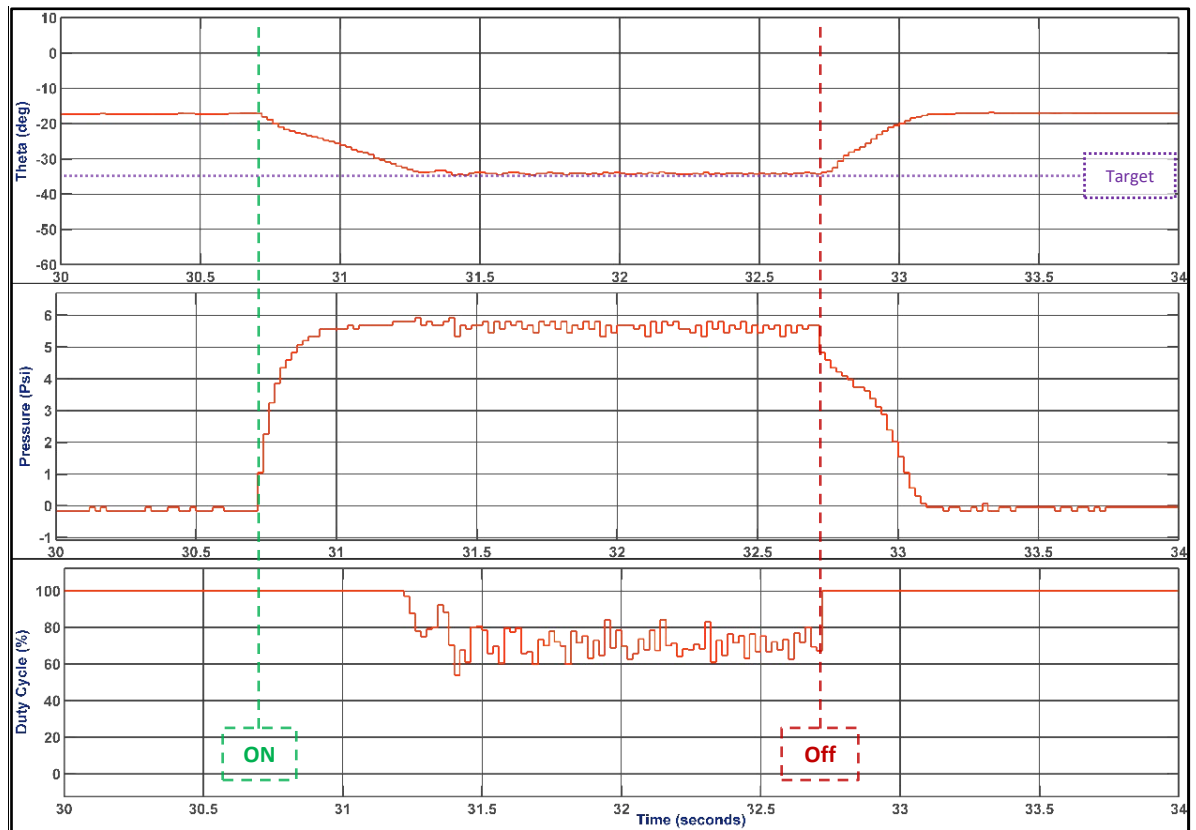


Figure 75: Sample data for the internal pressure response to the change in the duty cycle of the PWM signal

Moreover, further tests were conducted in which the target bending angle was supplied to the controller as stepped as well as a sinusoidal reference signal. For the step response experiment the reference signal increases from 30° to 40° and falls back with 5° increments, while the sinusoidal reference signal oscillated from 30° with an amplitude of 10° and a period of 3s. The measured bending angle response closely followed that of both the stepped and sinusoidal reference signals with a mean error of only 0.752° and a standard deviation of 2.09° as shown in Figure 76. The convergence time was around 150 ms on average, yet this largely depends on the input pressure value which for these tests was 8 Psi (55.2 kPa). The results of these tests confirmed that the soft actuator could be accurately controlled to follow a variable reference signal, based on the acquired real-time sensory feedback.

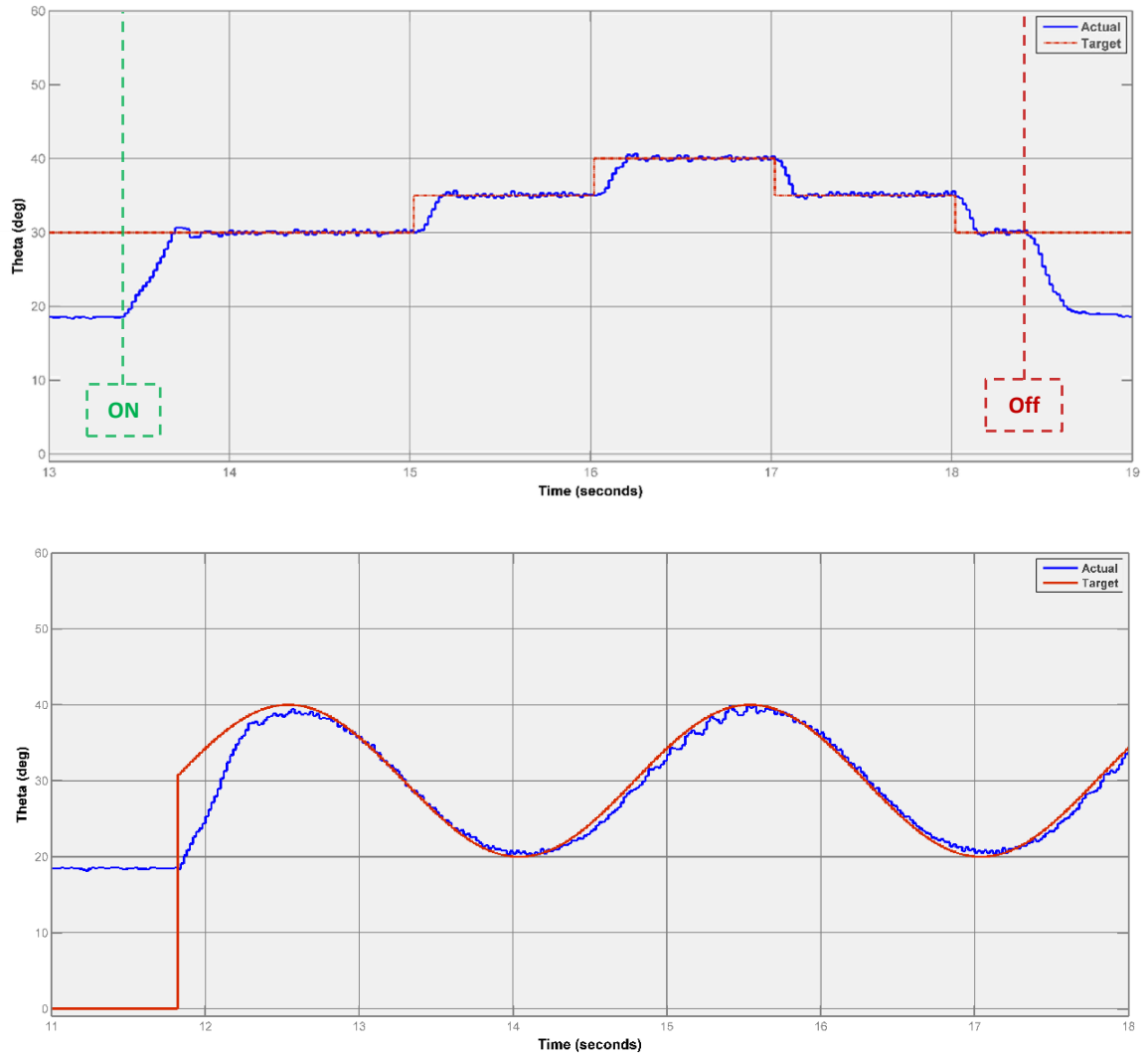


Figure 76: Bending angle response to a stepped and sinusoidal reference signals

Moreover, a key feature of this controller is the fact that it relies on feedback from both the embedded flex sensor as well as the internal pressure response to estimate the current bending angle. Thus, not only can the controller operate effectively at different pressure inputs, but also it can handle external disturbances in the form of pressure leaks. This was witnessed during the conducted tests when a leak from the inlet of the supply tubes to the base of the soft actuator caused an unexpected drop in the measured internal pressure. Consequently, the controller automatically increased the output duty cycle value to compensate for the witnessed pressure drop until meeting the target bending angle. The pressure leak, in this case, is no different from a change in the pressure, which the derived model was trained to accommodate. Thus, the inclusion of the filtered internal pressure measurements with the feedback from the embedded flex sensor in the derived models enhances the robustness of the controller to external disturbances. This also allows accurate

predictions of the bending angle during both the actuation and retraction of the actuator, which is important to measure and control the fluctuations around the target bending value in both directions. Finally, including the initial orientation of the soft actuator in the derived models allows the user to set meaningful target bending angle values that are measured as an absolute value from a known fixed reference.

5. 6. Conclusion

The work presented here demonstrated an alternative approach for predicting and controlling the bending angle of soft gripper fingers based on a common soft pneumatic actuator, using a purely data-driven approach that relies on generated datasets of sensory feedback without the need for analytically deriving complex physical and material models. A resistive flex sensor was embedded within the strain limiting layer of the soft actuator, while an onboard pressure sensor measures the internal pressures response during actuation. The soft actuator was tested at different operating conditions using a controlled pneumatic supply. The resulting bending response was recorded using a high-speed camera and processed using an image processing program, to track and measure the change in bending angle during each test. Regression analysis and neural networks were utilised to model the measured bending angle output based on the generated sensory feedback. This was achieved by correlating the change in the sensor's resistance due to bending in conjunction with the internal pressure readings from onboard pressure sensors to the actual bending angle measured using the vision system. Both techniques were successful in capturing the bending response of the soft actuator, with neural networks providing more accurate predictions. The trained models were successfully validated using a new dataset generated at untrained operating conditions. Furthermore, the derived regression model was integrated as part of a closed-loop PID controller, in order to control soft actuator bending based on real-time sensory feedback. The controller was tested using stepped and sinusoidal reference signals and was able to accurately maintain the desired target angle with a mean error of only 0.752° and a standard deviation of 2.09° .

The result of this work showed how simple empirical models and trained neural networks are able to accurately predict the bending angle of a soft finger at different operating conditions, using a relatively small dataset from inexpensive commercial sensors. Feeding the internal pressure to the model allows reliable predictions at varying input pressures during both the actuation and retraction phases, even if the system is disturbed with some pressure losses. In addition, the static bending due to gravitational forces is accounted for, by including the initial bending angle as an additional variable in the model. This allows for more accurate predictions

of the absolute bending angles at different orientations of the soft actuator, which would be necessary when used as part of a robotic gripper. The main benefit of this approach lies in elevating the need for exact physical models that require prior knowledge about the geometry and material properties of the tested soft actuators. Instead, inexpensive commercial sensors are used to generate experimental data required for deriving the empirical models, which implicitly accounts for any variations that could arise during the manual fabrication of such actuators. Thus, the approach can be potentially adopted for other soft actuator morphologies, as long as the required sensory feedback can be generated to derive the models.

CHAPTER 6:

A Modular Soft Gripper for Sensor-guided Grasp Feedback

Addressed Research Question: *Can the simple feedback from sensorised soft gripper fingers be further utilised to enable contact detection and additional grasp feedback?*

Chapter Objectives:

- Create a modular soft gripper prototype with sensorised soft fingers.
- Evaluate the relationship between the grasped object size and weight against the combined sensory feedback from opposing soft fingers.
- Investigate simple contact detection using knowledge of the free-bending response.
- Examine the rate of change of readings from flex sensor against internal pressure.

Generated Publication: K. Elgeneidy, G. Neumann, S. Pearson, M. Jackson, and N. Lohse, “*Contact Detection and Size Estimation Using a Modular Soft Gripper with Embedded Flex Sensors*”, 2018 IEEE/RSJ International Conference on Intelligent Robots and Systems, Accepted.

Introduction:

The passive compliance of soft grippers allows gentle adaptation to the geometry of grasped objects, which enables successful grasping of different objects without the need for sophisticated sensing or control. Initial tests presented in this chapter demonstrate how simple soft gripper prototypes were able to grasp delicate and complex objects by simply actuating the grippers with a fixed pneumatic supply. Despite being a desired trait for adaptation to variation, relying solely on passive compliance has its limitations. The absence of sensing means that not only feedback to confirm the grasp success is lacking, but also the grasped object remains unknown. Those limitations can hinder the utilisation of soft grippers as part of automation solutions since their grasping performance would be difficult to monitor. Hence, it would be interesting to develop soft grippers that combine the desired benefits of passive compliance with additional sensor-guided control for more robust performance. In this chapter, a simple modular soft gripper prototype was created using the sensorised soft finger modules presented in Chapter 5. The aim of was to investigate how the combined raw readings from the embedded flex sensors in the soft gripper fingers can be further utilised to detect contact with a grasped object and infer additional information about the grasp. The work in chapter 5 showed that individual soft finger modules could be calibrated to accurately estimate bending angle based on the feedback from flex and pressure sensors. However, this would require testing and calibrating each finger individually. The key

contribution is in proposing a simple relationship between the object size and combined raw readings from the flex sensors without the need for calibration, in addition to enabling simple contact detection utilising knowledge of the known free-bending response.

6. 1. Soft gripper porotype development

6.1.1. Entirely soft silicone rubber grippers

The first soft gripper porotype was created in the early stages of this work, which was a replication of the first soft gripper design proposed by Harvard Whiteside group [34]. Fabrication of this soft gripper provided a practical sense of the challenges with the manual moulding process, as well as the capabilities and limitations of a soft gripper made entirely from silicone rubber with fixed finger layout. The gripper was tested by manually positioning it close to target objects that differ in geometry and material, then activating a fixed pressure pneumatic supply to achieve grasping. Figure 77 shows examples of successful grasping attempts, in which the gripper was able to grasp a plastic cube and a 3D printed part with intricate details. It can be seen from this simple grasping demonstration that unlike traditional rigid grippers, this very simple soft gripper is able to comply with the different geometries without the need for any sensory feedback or control algorithms. The grasping behaviour is determined through the morphology of the air channels embedded in the gripper structure, allowing the soft fingers to passively comply with the geometry of the target object upon pneumatic actuation. On the other hand, the main observed weaknesses of this completely soft gripper were the limited payload it is able to lift (around 100g for this small gripper). Additionally, the size and layout of the gripper fingers should be suited for the size of target objects and the intended grasp type. In other words, this particular gripper design was well suited for grasping similarly sized objects using power grasps. However, attempting to grasp small nuts, for example, was unreliable, because the fingers are all laid flat (180° apart) and hence have to undergo significant bending to reach the small nut. This excessive bending hinders the stability of precision grasps. Additionally, anticipating the bending of the fingers becomes essential to choose the correct initial position of the gripper, so that the fingertips will reach the target location. In this case, a gripper with fingers that are closer together (45° apart) with shorter soft fingers would be better suited for picking up small nuts using a precision grasp. However, creating complete grippers with fingers that are 45° apart is not possible using the conventional soft lithography process. As for the grasping forces limitations, there are several ways to enhance the grasping forces for such a soft gripper to lift heavier payloads, including adding reinforcements or scaling up the gripper size. Yet, it remains limited

compared to conventional rigid grippers. Increasing the supplied pressures limited by how much the soft material used in making the gripper can tolerate. Hence, using stiffer material grades would be necessary if higher pressures are supplied. Scaling up the size of the gripper would be necessary to grasp larger and heavier objects, so that the gripper is able to maintain sufficient contact area with the grasped object. However, increasing the gripper size, changing the material, or even adding internal or external reinforcements are all modifications that would require fabricating a completely new gripper. Additionally, there will always be a trade-off between enhancing the gripper payload and maintain the desired compliance of the fingers.

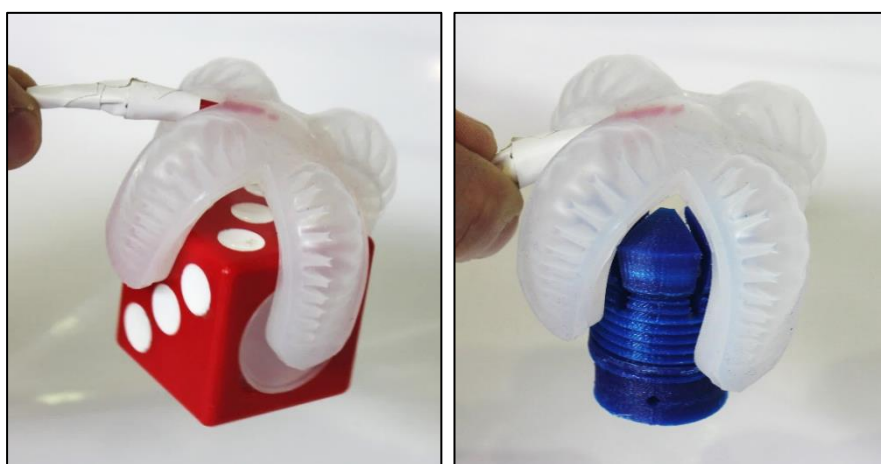


Figure 77: Grasping a cube and a complex 3D printed object using a simple soft gripper

All of those challenges with the initial soft gripper prototype have motivated the consideration of a modular soft gripper design where the individual gripper fingers can be easily replaced by others that are made from a different material or size. Hence, short soft fingers can be used when small objects are to be picked up using precision grasps, which would not require much bending. While longer soft fingers can be used when grasping larger objects that require a power grasp to completely encapsulate the target object within the fingers and maintain sufficient contact area. Similarly, stiffer soft fingers made from high Shore hardness silicone rubbers can be used when enhancing the contact forces is desired to lift denser objects. While softer fingers made from low Shore hardness silicone rubber can be favoured when softer gripper fingers are more preferred for handling a deformable object.

6.1.2. Modular two-fingered soft gripper

Based on the initial investigations with the entirely soft gripper, a second prototype was designed and fabricated to demonstrate the idea of using a modular soft gripper design, in which soft bending actuators are utilised as detachable soft fingers held using a stiffer 3D

printed gripper body. Using a modular soft gripper design, stiffer or larger fingers can be used when the higher payload is desired, while more flexible or smaller fingers can be used when lighter but more delicate objects will be grasped. Hence, the soft gripper can be easily customised according to the application needs. Another benefit of a modular design is the ease of replacement when a single finger is damaged, instead of having to replace the complete soft gripper. The 3D printed gripper base can be easily customised to hold different sized fingers and secures the pneumatic tubing. Additionally, the angle between opposing soft fingers can be adjusted using the 3D printed base, enabling new soft gripper layouts that were not possible if the entire gripper is made using the conventional moulding approach. Additionally, the design of this gripper body can provide additional degrees of freedom, which would be particularly useful to provide the initial positioning of the soft fingers close to the target object. In other words, the stroke of the gripper can be varied according to the target object size, by moving the soft fingers closer or further apart, using small servo motors attached to the gripper body. Once, the fingers are roughly in place and ready to grasp the target object; the pneumatic supply will be activated to actuate the soft fingers, creating the desired bending motion required to grasp the target object. The advantage of this grasping approach compared to traditional rigid grippers lies in the simple control required to grasp a given object without the need for its accurate location and pose with respect to the gripper. A rough estimation of the target object location and pose through a simple vision system would be sufficient to direct the manipulator carrying the soft gripper within close reach of the target object with the required stroke. The contact points required for a successful grasp are delegated to the soft finger morphology to be passively determined as the soft fingers interact with the target object.

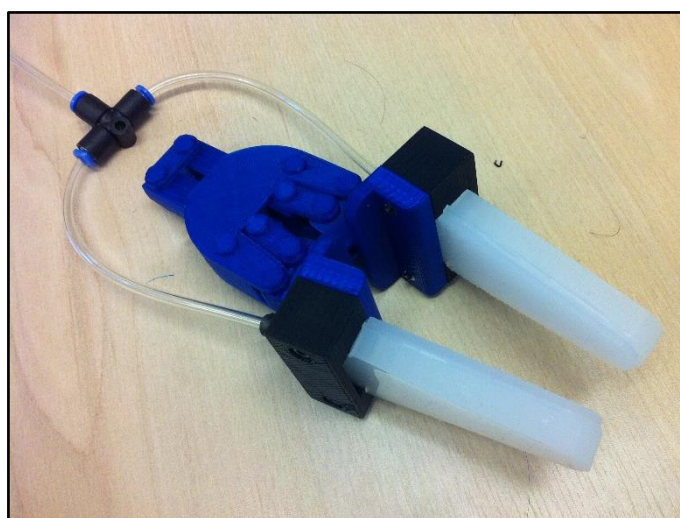


Figure 78: Soft gripper prototype with the 3D printed body and interchangeable fingers

Figure 79 shows sample images in which objects of different geometry and delicacy were successfully grasped. It was observed that this hybrid soft gripper prototype performed better than the entirely soft one, as the 3D printed gripper body enhanced its overall stiffness and hence grasp stability. The gripper successfully grasped and lifted heavier objects in the range of 500g, which is a reasonable payload considering the total weight of the gripper and the fact that only two small fingers were used.



Figure 79: Grasping tests of components with different weights and delicacy

6.1.3. Reconfigurable Multi-fingered soft gripper with embedded flex sensing

The final soft gripper prototype utilised individual soft bending actuators with embedded flex sensors to create a multi-fingered modular soft gripper that can be assembled with 2, 3 or 4 soft fingers. Having more than two fingers would be necessary when grasping complex shaped objects that require at least three contact areas to ensure a stable grasp. The base of each soft finger is held using a 3D printed casing, which guides the needle to puncture the base of the internal pneumatic channels, as well as securing the sensor wiring and pneumatic tubes as shown in Figure 80. Connecting the pneumatic tubes to the fingers through a needle allows easy switching between fingers, which is desired to maintain the desired modularity of the gripper. Reconfiguring the soft gripper is achieved using a 3D printed flange that carries the soft finger modules in different arrangements through the 3D printed casing. Hence, Individual fingers can be easily swapped or rearranged depending on the application needs.

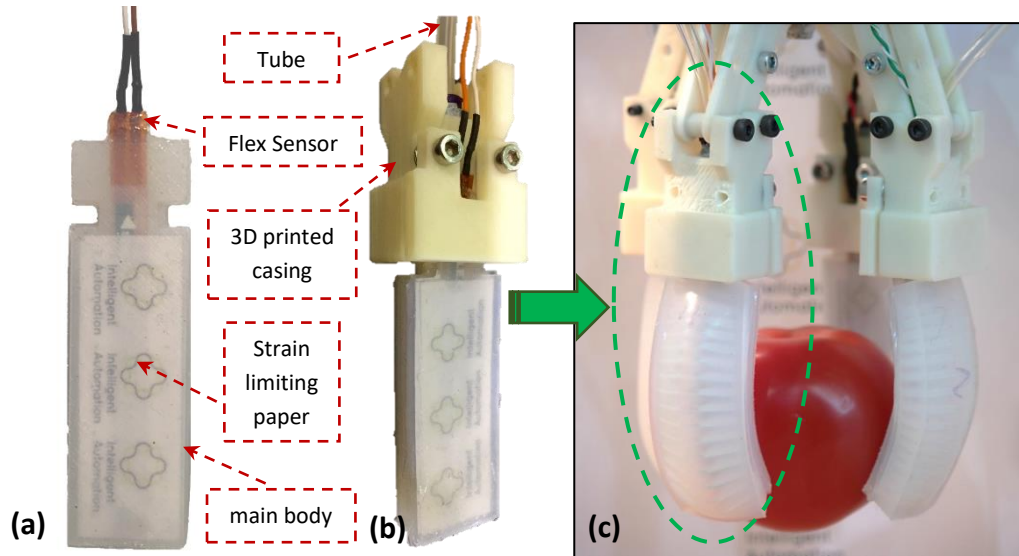


Figure 80: A reconfigurable soft gripper prototype consisting of four sensorised soft finger modules. (a) Individual soft finger is showing embedded flex sensor. (b) Printed casing added for routing wires and tube. (c) Four soft fingers assembled using 3D printed connectors to grasp a tomato gently

The advantages of this proposed soft gripper prototype can be summarised as follows:

- **Modular:** individual soft fingers can be easily changed when damaged or to meet different application criteria, such as size and stiffness.
- **Reconfigurable:** The gripper can be assembled using 2, 3 or 4 soft fingers based on the nature of the target object and the workspace limitations
- **Variable Stroke:** the initial spacing between the fingers can be increased to allow more space for grasping larger objects, or decreased to avoid excessive bending when grasping smaller ones using precision grasps.
- **Customisable interface:** The stiffer 3D printed base can be easily customised to allow the gripper to be securely mounted to an existing robotic arm.
- **Low-cost solution:** this adaptable soft gripper prototype is simple in structure and inexpensive to fabricate, compared to conventional rigid grippers with active compliance.

6. 2. Design of experiment

An experiment was designed to investigate the effect of the grasped object size and weight on the resulting sensory feedback from the embedded flex sensors and onboard pressure sensors. The aim was to investigate the potential of inferring the grasped object size and weight based on the measured change from the flex and pressure sensors. To achieve this, a set of objects of different sizes and weights were prepared for grasping tests. The set included seven spheres with diameters of 50.8 mm (2") and 25.4 mm (1"), which were machined with

high precision ($\pm 0.05\text{mm}$) from different materials, so that spheres of the same diameter can have different weights. Additional test objects with different geometries and weights were also included for validation purposes. The different combinations of sizes and weights of the grasped objects are shown in Table 6.

Table 6: Summary of the properties of the test objects

Object	geometry	Grasped size (mm)	Weight (g)	training	testing
Sphere 1	sphere	50.8	62	x	
Sphere 2	sphere	50.8	81	x	
Sphere 3	sphere	50.8	93	x	
Sphere 4	sphere	50.8	143	x	
Sphere 5	sphere	25.4	7	x	
Sphere 6	sphere	25.4	9	x	
Sphere 7	sphere	25.4	18	x	
Ping pong	sphere	37.5	3		x
Tennis ball	sphere	64.5	57		x
Bulb	Var curvature	~ 59	28		x
Block	Cuboid	20.5	9		x
Dice	cube	39	29		x

The procedure of the experiment involved grasping each of those objects twice at the same input pressure of 10 psi, using the 4-fingered sensorised soft gripper outlined in the previous section. The resulting readings from the each of the four embedded flex sensors (Flex1 to 4), as well as the two pressure sensors (P1 and P2), were recorded for each test and converted to digital values through the analogue inputs of the Arduino board. Each two opposing soft fingers were connected together through the same pressure input (Flex2 and Flex 3 connected to P1, while Flex1 and Flex4 connected to P2), to allow them to reach an equilibrium position. Figure 81 shows sample images for some of the grasping tests. The soft gripper was able to successfully grasp all the objects throughout the testing procedure.

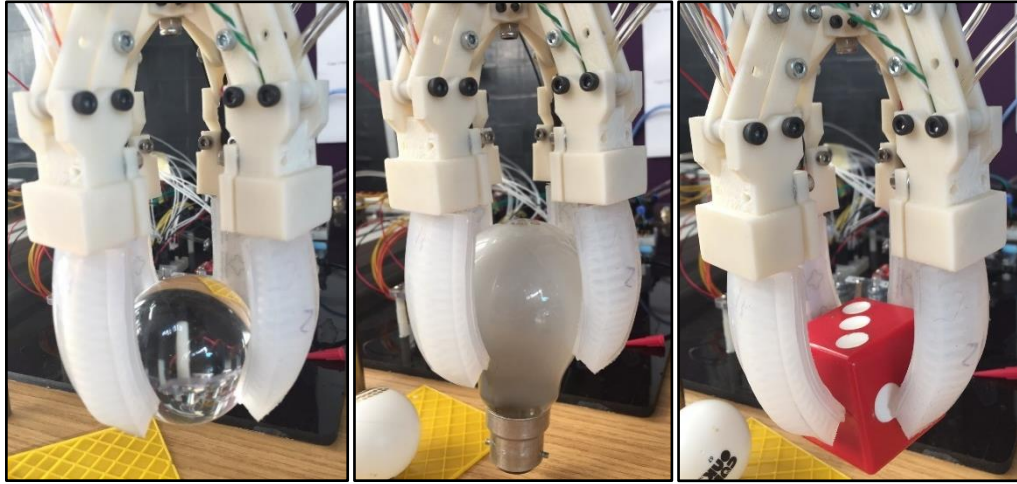


Figure 81: Sample images for grasping tests showing the soft gripper successfully grasping a 25.4mm sphere, light bulb, and a cuboid block

6. 3. Results

The following results from the experiment will focus on a pair of the soft gripper fingers (Flex2 and Flex3), which are pressurised with the same pressure input (P1).

6.3.1. Size estimation

The primary objective of this experiment was to investigate if an empirical relationship can be derived between the flex sensors' feedback and grasped object size. Figure 82 plots the final values from flex sensors 2 and 3, after analogue to digital conversion, against the grasped object size. In addition to the final average value from both sensors (Final_FLEX_{2,3}). Taking the average value from the opposing soft fingers reduces the effect of random variance, which is demonstrated by the improved R^2 value of 0.971 (compared to 0.957 and 0.915 for the individual sensors). A simple linear relationship is clear from the data acquired from grasping the 12 objects. It can also be observed that the response from each sensor is noticeably different since the sensor sensitivity is not identical for different samples. Yet, the relationship remains consistent for each individual sensor. Objects with the same size are closely clustered around the same value with some variance as to be expected from the difference in weight and contact type. The average standard deviation between the grasp repetitions for each object was 1.2. Also, test objects of different geometries still followed the same relationship, indicating that such a relationship can be used not only to distinguish between objects based on size, but also can be potentially generalised to estimate the sizes of new objects that were not tested before. However, a difference in size of at least 10 mm is required to cause a noticeable difference in the sensor readings due to its limited sensitivity.

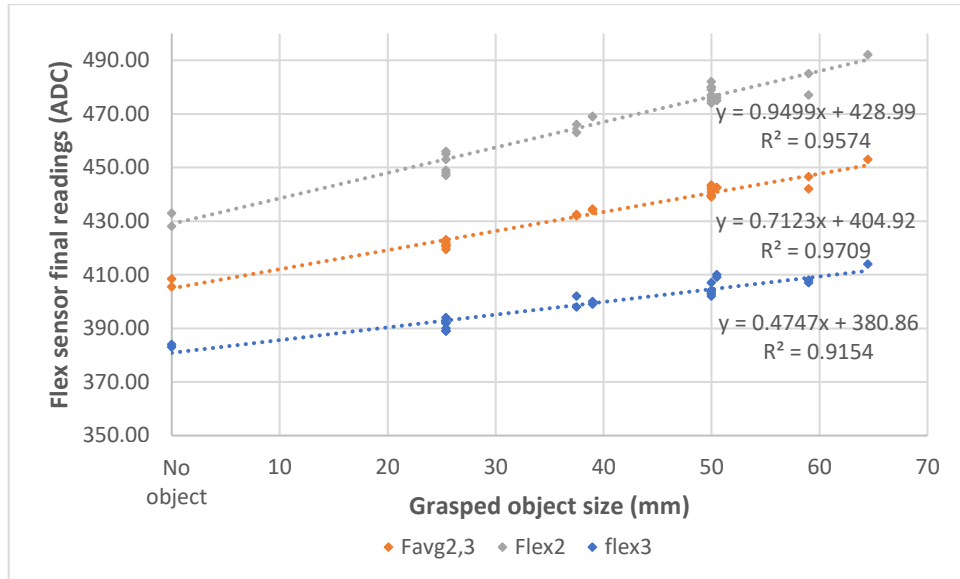


Figure 82: Final readings from embedded flex sensors against the grasped object size

6.3.2. Weight estimation

The second objective of this experiment was to investigate if a relationship exists between the grasped object weight and the generated sensory feedback. Similar to the previous section, the final readings from flex sensors 2 and 3 are plotted against the object weight in Figure 83, as well as the average of those two plots. The figure shows that it is difficult to interpret a clear generic relationship across the data from all grasp tests, as it was the case for object size estimation. If only the data from grasping the seven high-precision spherical objects are considered (circular dots) excluding the other non-spherical test objects (labelled with a cross), a clearer second order polynomial fit is possible with an R^2 value of more than 0.9 as shown. However, this means that the relationship is non-linear and hence would not aid in making reliable estimations. This observation means that the data acquired is not sufficient to infer a more generic relationship that can be valid across a range of different objects. It is expected that the nature of the contact with the grasped object has a strong influence that is contributing to the witnessed variation in the test objects. This effect was less evident when studying the object size since the influence of the object size on the flex sensor readings is significantly more than that caused by the object weight. On the other hand, the results still show that the object weight does influence the final readings from the embedded flex sensors, demonstrated by an overall small and non-linear increase in the flex sensor readings. The relationship was consistent with both tested sensors, following different response curves due to the difference in sensor sensitivity.

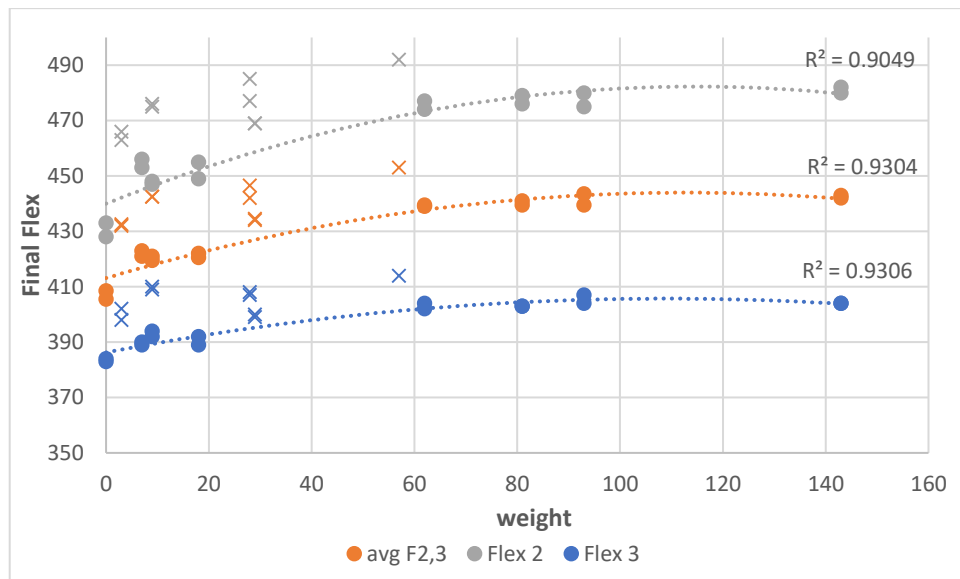


Figure 83: Final readings from embedded flex sensors against the grasped object weight

To further highlight the witnessed small effect of the object weight on the flex sensor readings, Figure 84 shows the flex sensor readings against the object weight for the 50.8 mm and 25.4 mm spheres separately. Fixing the object size better clarifies the influence of increasing the object weight on the flex sensor readings. It can be seen that the influence of the object weight is more apparent for the larger and heavier spheres, while for smaller spheres the relationship is not conclusive.

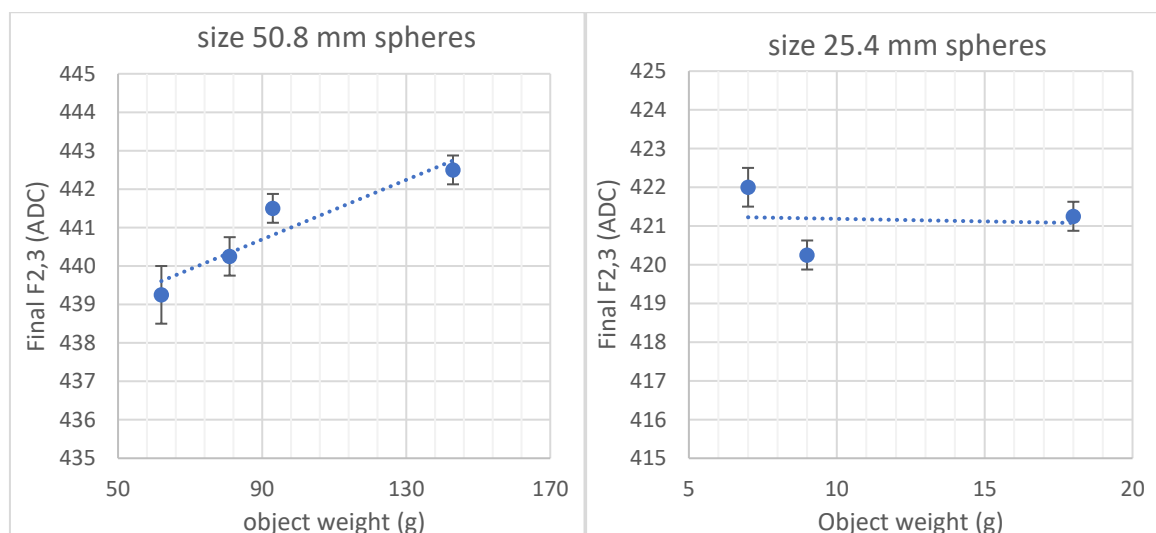


Figure 84: Comparing the effect of object weight on the final flex sensor reading for both the 50.8 and 25.4 mm spheres

6.3.3. Contact Detection

Figure 85 shows the average responses from the embedded flex sensors 2 and 3 when grasping the set of spheres (1 to 7) of sizes 50 and 25.4 mm, as well as the free bending response at the same input pressure. It is observed that the three distinct response curves are visible, for each of the 25.4 mm spheres, 55 mm spheres, and the free bending response. This not only confirms the repeatability of the results acquired for grasping an object of a specific size at a fixed input pressure, but also illustrates how the response from the flex sensor varies when conforming to different sized objects. For the free bending case, the response is the steepest, as no external contact is interfering with the soft gripper fingers. It is also observed that the other two responses for the 25.4 and 50 mm spheres start to deviate away from the free bending response at different points, with the 25.4 mm response deviating later with a steeper rate of change. This is due to the early contact that the soft fingers make with the larger 50 mm spheres along the fingers' length, limiting the bending response early on while continuing to deform to conform to the grasped object surface. The 25.4 mm response on the other hand initially follows the free bending response, since the fingers are indeed freely bending when the actuation first starts until they reach the smaller 25.4 mm spheres. Once the fingertip makes contact with the spheres, the response will be restrained causing the witnessed deviation from the free bending response. However, the response does not completely stop at this stage since the fingers are only constrained at the tip, so their bodies continue to deform until reaching a stable grasp.

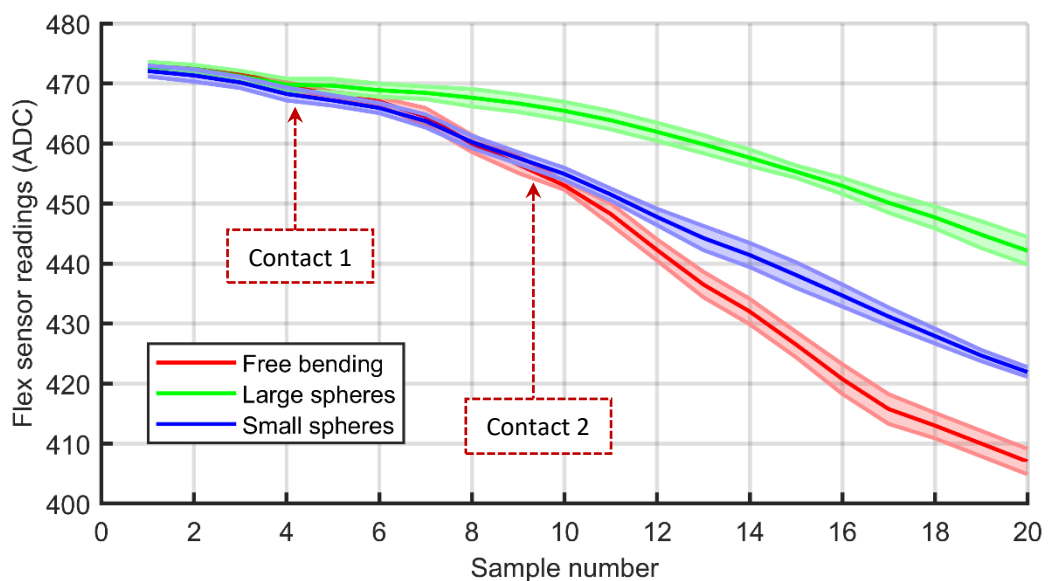


Figure 85: Comparing the flex sensor responses for contact and free-bending scenarios

Therefore, contact detection would be possible by monitoring the real-time response from the embedded flex sensors in individual fingers and comparing it to the known free-bending response at the same input pressure. In other words, by recording the free bending response before starting any grasping tests and storing this within the gripper controller, the contact with an external object can be detected once the calculated difference between the current and free bending response exceeds a set threshold. This would allow better control over the grasping performance, as the supplied pressure can be adjusted accordingly to avoid excessive bending that could risk the grasp stability or even damage a delicate target.

6.3.4. Grasp type Identification

Plotting the resulting sensory response from the flex sensors against the measured internal pressure from the onboard sensor allows visualising the grasping response. Figure 86 shows the average readings from flex 2 and flex 3 against the supplied pressure P_1 when grasping each of the seven spheres (balls 1 to 7) of sizes 25.4 and 50 mm twice. An interesting feature becomes clear, as the response is divided into two distinct response curves. The smaller spherical objects all follow the same response, which is steeper than the one followed by the larger spheres. This is expected to be due to the difference in nature of contact when grasping the two sized spheres. Smaller spheres are grasped at the fingertips of the gripper (precision grasp), while the larger spheres are encapsulated within the gripper fingers with a larger contact area with the inside surface of the fingers (power grasp). The free bending response followed the same response of the smaller spheres, since in both cases the fingers are free during most of the bending, with the latter stopping earlier when making contact with the object. This is also reflected in the response curves as the free bending response extends further than the response by the smaller spheres. Hence, as long as the monitored response follows the free bending response, then it can be assumed that no significant contact with the target object has been made yet. However, If the monitored response deviates from the free bending response, then this highlights that the object is being encapsulated inside the gripper with some contact happening with the inside surface of the fingers. Still, the soft fingers continue to deform to conform to the grasped object surface. Therefore, if the objects are intended to be grasped by the fingertips, then the monitored response should continue to follow the free bending response, only ending earlier depending on the object size. While if power grasps are desired then a different less steep response is to be expected early on. Hence, it is possible to identify the general grasp type corresponding to how much area is in contact with the grasped object, by monitoring the slope of this response.

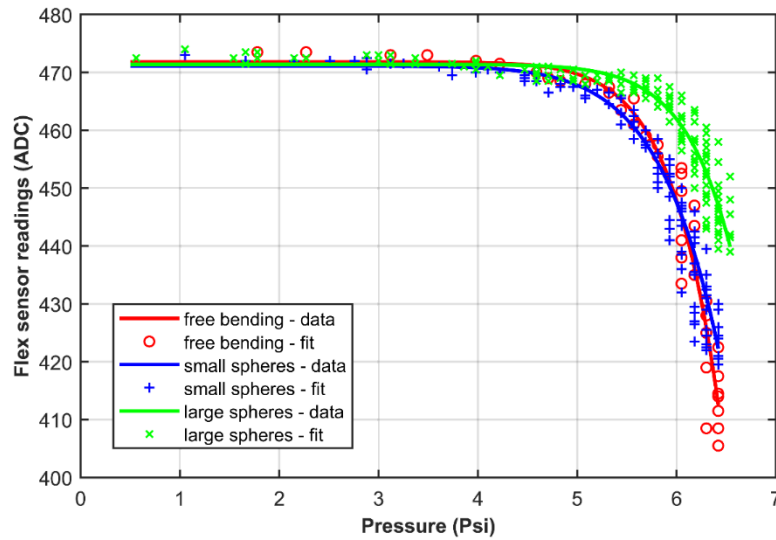


Figure 86: Flex sensor response against the measured internal pressure during actuation

To validate these observations, each of the test objects was also grasped twice while recording the sensory response to be compared to the original two responses identified as shown in Figure 87. The new responses fell within one of the previously identified response curves. It can be observed that the light bulb and tennis ball fell closely along the fitted response of the large spheres, which is expected since the diameters were in the same range and were grasped following a power grasp (Figure 81). On the other hand, the ping pong ball, dice, and block all fell closer to the fitted response from the small spheres. Again, the sizes of those objects were small and grasped following the precision grasp at the fingertip (Figure 81). Thus, the results highlighted the potential for monitoring the time series response from the soft gripper fingers to identify the general type of grasp.

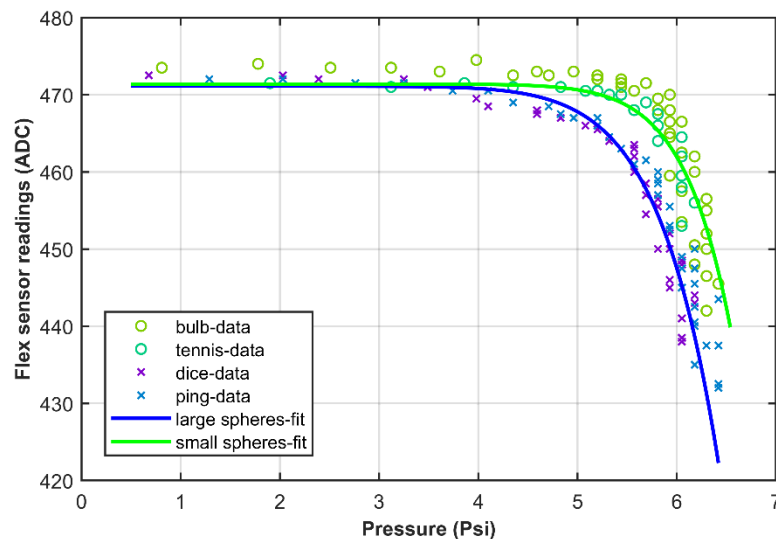


Figure 87: Flex sensor response against the measured internal pressure with responses from test objects

6. 4. Discussion

Coarse object size estimation using raw sensory data:

The results of this experiment showed that a linear relationship between the raw final values from the embedded flex sensors and the distance between opposing soft gripper fingers, corresponding to the grasped object size. The relationship was consistent for each flex sensor across all the grasped objects despite the variation in their shape and weight. Hence, such a relationship can be utilised to distinguish between objects of different sizes, which has the benefit of working on raw sensory data without additional processing. However, due to the limited sensitivity of the flex sensors, it would be difficult to differentiate between objects that are less than 10 mm different in size. Also, the sensitivity is not the same for different sensor samples, which is a limitation quoted in the datasheet of the commercial flex sensors.

Challenges with weight estimation:

As for the grasped object weight, no certain relationship could be generalised for all the tested objects with sufficient confidence. When limiting the results to the set of high precision spherical balls only, a more consistent relationship showing an increase in the final value from the embedded flex sensors as the weight of the grasped object increases. This can be explained by the fact that after reaching the equilibrium position when grasping an object, the denser it is, the more it will pull the soft finger downwards due to gravity, and hence causing an additional stretch to the fingers that will consequently affect the measured change in resistance. However, the results from the remaining test objects of different geometries deviated from the best fitting function. This means that the acquired experimental data was not sufficient to derive a more generic relationship across a wider range of object types, because the influence of the object weight on the flex sensory readings is currently minimal and be easily confused with random sources of variation between samples. Thus, more data will be required from a larger test objects set of variable geometries to generate a more generic relationship with better confidence. Additionally, using an ADC with finer resolution will allow smaller changes in the flex sensor readings to be detected, which would be particularly useful for capturing the effect of lighter objects. Nevertheless, the results do indicate that the grasped object weight does influence the final readings from the embedded flex sensors, but further investigations into this with a more sensitive flexible sensor and data acquisition would be required to fully characterise the effect. Accurately quantifying this effect will be of particular importance when the gripper operates at different orientations, as the

weight of the object will not be evenly distributed between fingers and hence should be compensated for to allow accurate bending and size estimations.

Simple contact detection based on modelled free-bending response:

Furthermore, examining the time-series response of the embedded flex sensor during grasp tests showed that the rate of change of the response curve is affected by how the soft fingers make contact with the grasped objects. More specifically, all the 25.4 mm spheres grasp tests followed the same response curve, which is steeper than that witnessed by all the larger 50.8 mm spheres. Comparing those to the free bending response shows that initially, all responses follow the same path, with the response from the 50.8 mm spheres deviating early on followed later by the deviation of the 25.4 mm response. Hence, three distinct responses can be clearly witnessed, which were consistent across all the repetitions of the grasp tests. This is expected to be due to the early contact that the soft fingers make with the larger objects as they get encapsulated within the gripper in a power grasp, causing the witnessed early deviation. The contact area, in this case, is much larger than the case when grasping smaller 25.4 mm spheres, which are grasped only by the tip of the soft fingers. This is why the response from the larger spheres is shallower due to the restriction from the grasped object making contact across a wider area of the base of the soft fingers. The importance of this observation lies in the fact that prior knowledge of the free bending response of a particular soft finger module can be utilised to detect contact with a target by merely monitoring the difference between the current response and the known free bending one at the same input pressure. Results from the previous chapters showed that the free bending response of the studied soft actuator is consistent and unique for a given input pressure, which can be modelled as previously discussed. Thus, once the difference between the current response and modelled free-bending one exceeds a set threshold, it can be assumed that contact occurred and the supplied pressure can be stopped. The ability to detect contact would also allow the controller to switch from free-bending angle estimation to potentially force and slippage estimation as the fingers come in contact with the target, avoiding excessive forces that can damage delicate objects or risk the grasp stability.

Differentiating between power and precision grasps

Moreover, another interesting finding from this experiment was demonstrated by plotting the response from the embedded flex sensors against the response from the measured internal pressure supplied to the corresponding fingers. The results demonstrated consistent cycles

representing the actuation and retraction of the soft fingers, which can be clearly divided into two distinct sets. The first included all the large objects, which were encapsulated within the gripper (power grasp). While the second set included all the smaller objects, which were grasped using the gripper fingertips (precision grasp) type. The free bending response was among the second set, which is to be expected as grasping smaller objects includes a free-bending phase initially, which is stopped when making contact with the object. Hence, small objects grasped using a precision grasp have limited effect on the bending profile of the soft finger, since they only make contact with the fingertip. The clear difference, however, is the fact that the free-bending response extends the furthest when compared to the responses from precision grasps, as it is completely unrestrained. In fact, the response from each grasped object ends at a different point depending on its size, which was already confirmed by the clear relationship between object size and the final flex sensor value. This interesting observation showed that combining the internal pressure response with the flex sensor response better illustrates the rate of actuation, which allows differentiating between the general grasp types. Currently, only precision and power grasps were implemented in the test considering the structure of the gripper, yet this shows the potential of combining multi-sensory feedback to infer additional grasp information that is not easy to achieve for a soft gripper.

6. 5. Conclusions

In this chapter, a reconfigurable soft gripper prototype was presented which is composed of soft finger modules that are embedded with flex sensors. The soft finger modules are combined using a 3D printed base, which allows different assembly configurations to create a two, three, or four-fingered soft gripper. The individual soft finger modules were tested and characterised in the previous chapter to model and control their free-bending response under different pressure inputs. It was demonstrated how a purely data-driven approach could be adopted to utilise the relatively limited sensory feedback resulting from the experiments, to derive empirical models that accurately estimate the bending angle for individual fingers. The next step presented in this chapter was to investigate how important grasp information can be inferred using the limited sensory information available when the soft finger modules are combined as a soft gripper. An experiment was designed which involved repeated grasp tests for a set of objects including seven high-precision spheres with combinations of different sizes and weights, in addition to additional test objects with variable geometries for validation. Processing the resulting sensory feedback showed that clear linear relationship exists between

the final value from a flex sensor and the grasped object size. Hence, it may not be necessary to model each soft finger module individually, instead of grasping a small set of objects of known sizes can be sufficient to derive an empirical relationship that estimates the size of grasped objects. This would be particularly useful when continuous measurement of individual finger bending is not required, but only the final position of the fingers defined by the grasped object size is of interest. Furthermore, the results showed that the object weight causes a limited and inconsistent increase in the final readings from the flex sensor. However, a more generic relation could not be concluded with sufficient confidence. A larger set of objects with more variations in geometry would be required to achieve that. As well as a finer resolution for the ADC, since the effect of the object weight on the flex sensor readings is minor and can be easily confused with random sources of variations between samples.

Furthermore, the second objective of this experiment was to investigate the feasibility of contact detection using the free bending response from the flex sensor as a reference. The results showed that objects of the same size consistently followed the same response as previously demonstrated in the previous chapter. More importantly, the responses acquired during grasping deviated from the free bending response at different points depending on the object size. Thus, it is possible to detect contact with the grasped object, by simply actuating the soft gripper a few times without an object to record the free bending response from each finger. Afterwards, this response can be embedded within the controller and subtracted from the measurements made during the grasping test. By setting a threshold for this difference, contact with the target object can be detected as the current response deviates from the known bending response at the same input pressure. It is even possible to rely on the raw data from the sensor without calibrating to real bending angle value (as done in the previous chapter), if only contact detection is required rather than accurate positioning the fingers at a specific bending angle. The later would require the novel data-driven modelling procedure presented in the previous chapter. Moreover, the experiment uncovered another interesting observation when plotting the flex sensor response against the measured internal pressure. A clear distinction can be made from the data between objects that were grasped using a precision grasp and those grasped using a power grasp. This shows how combining simple sensory information has the potential of providing additional useful grasp information, such as the general grasp type, which is demonstrated for the first time in this work.

An extension to the current work would be to repeat the experiment using a larger set of test objects with more variation in their size, weight and geometry. This will also benefit from a

more sensitive flex sensor combined with a higher resolution ADC to capture small deviations more accurately. Furthermore, flex sensors with variable sensitivity along their length would be an interesting extension to this work, so that the measured overall resistance of the sensor would depend on its profile, not just the absolute bending. This is expected to result in more accurate results, as the effect of object profile can be potentially decoupled from the change due to object size or weight. One way of achieving this could be through 3D printing to allow customisation of the flex sensor's conductive tracks to achieve multi-model sensing. The potential of 3D printing in fabricating soft actuators and flex sensors is hence investigated in the next chapter.

CHAPTER 7:

Direct Printing of Soft Fingers with Integrated Strain Sensing

Addressed Research Question: *Can 3D printing technology be utilised to aid the automation of the manual fabrication process of soft grippers for a faster and more consistent output?*

Chapter Objectives:

- Investigate direct 3D printing of air-tight soft actuators and flexible strain sensors.
- Test the fatigue and repeatability of 3D printed actuators at different input conditions.
- Investigate the potential for direct 3D printing a complete sensorised soft actuator.
- Implement the proposed data-driven approach to model the free-bending response.
- Analyse force generation and investigate the potential for simple contact detection.

Generated Publication: K. Elgeneidy, G. Neumann, M. Jackson, and N. Lohse, “Directly Printable Flexible Strain Sensors for Bending and Contact Feedback of Soft Actuators,” *Front. Robot. AI*, vol. 5, no. February, pp. 1–14, 2018.

Introduction:

In this chapter, the well-established material extrusion printing technology is investigated as an alternative fabrication method for soft actuators that would be faster and more consistent than the conventional manual moulding process. Although advanced polyjet 3D printers enable more flexibility in creating complex multi-material bodies, the choices for elastic and soft materials often suffer from tearing and degrading under long UV light exposure and repeated use [96]. Hence, NinjaFlex material (datasheet in Appendix (F)) is considered here, which at the time of conducting this work, was the softest commercially available material filament (85A Shore hardness and 660% elongation at break) that can be 3D printed using low-cost FFF printers. The material is not as elastic as commonly used silicone rubbers, but offers higher tensile strength as compared in Section 2.4.2. Hence, successfully 3D printed actuators can operate at a higher pressure range to enable higher contact forces for lifting heavier objects, which has been confirmed for the first time in a recent publication while conducting this work [37]. The work presented here goes further beyond state of the art, by optimising the printing processes for dual-extrusion of flexible and conductive filaments to create soft actuators with integrated flexible strain sensors for positional feedback. The soft actuators are printed with a finger shell thickness for enhanced flexibility. The key contribution of this chapter is in the characterisation of a fully 3D printable soft bending actuator with integrated bend sensing following the purely data-driven modelling approach proposed in Chapter 50.

7. 1. Fused Filament Fabrication of soft fingers

7.1.1. FFF Printing Hardware

Extrusion based 3D printing of flexible material filaments has special hardware requirements, in order to ensure smooth deposition of the flexible material without filament buckling or nozzle jamming. There is a wide range of FFF printers that can print different material filaments, yet printing flexible materials requires a printer that meets the following criteria:

- 1) Due to the soft nature of the flexible filaments a direct extruder is essential, since with a Bowden setup the filament tends to buckle due to friction with the tube.
- 2) Minimal gap between the drive gear and the hot end to avoid filament bending.
- 3) Minimum nozzle diameters of around 0.5 mm is recommended, since it is more difficult to maintain smooth disposition of flexible filaments when using finer nozzles.
- 4) An all-metal hot end with good thermal distribution is also important to be able to operate at a stable higher extrusion temperature in the range of 220 – 240°C.

Any FFF printer with tool heads meeting those specifications should be capable of printing flexible materials as long as it is calibrated and recommended printing settings are followed, which will be discussed later. Here we used a Lulzbot TAZ 5²³ printer with a Flexytruder tool-head²⁴ that was designed specifically to meet specifications for printing flexible materials (Figure 88). More details about hardware in Appendix (F) – Materials . This is a direct extruder that has a customised drive gear featuring a spring-loaded feed mechanism with a roller bearing, and no gap between the hot end and the extruder to minimise filament buckling

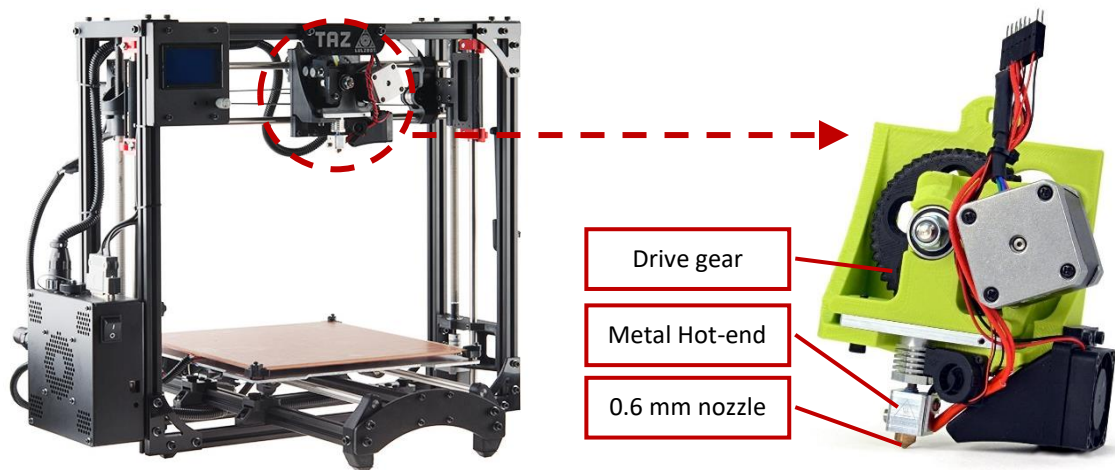


Figure 88: TAZ 5 3D printer and the Flexytruder unit

²³ <https://www.lulzbot.com/store/printers/lulzbot-taz-5>

²⁴ <https://www.lulzbot.com/store/tool-heads/lulzbot-taz-flexystruder-tool-head-v2>

7.1.2. Design Guidelines

The design concept of the 3D printable soft finger is based on the same principals of soft bending actuators in general, in which chambers are pressurised to expand while the base is constrained to generate a bending motion. However, the key difference here is the fact that the flexible extruded materials in general cannot elongate as much as the silicone rubber materials do. At the time of writing this thesis, the most flexible commercial material that can be 3D printed using material extrusion is NinjaFlex, which can only elongate up to a 65% before yielding (Appendix (F) – Materials). This is significantly lower than most silicone rubber alternatives, which are able to stretch several times their original length without yielding. Hence, the design of a printable bending actuator must take this difference into consideration, so that a full bend can be achieved at reasonable input pressures. Consequently, the ribbed actuator morphology, previously followed in designing silicone rubber based fingers, can no longer be used since it exhibits excessive stretching that the flexible, printable material cannot tolerate. Hence, the pleated morphology, in which chambers are individually separated by gaps (Figure 89), is adopted here to minimise the material stretching. Additionally, the higher stiffness of the NinjaFlex material is better suited to overcome the limitation associated with actuators following the pleated morphology, which suffers from static bending under gravity, since soft silicone rubbers are unable to hold their weight when chambers are separated.

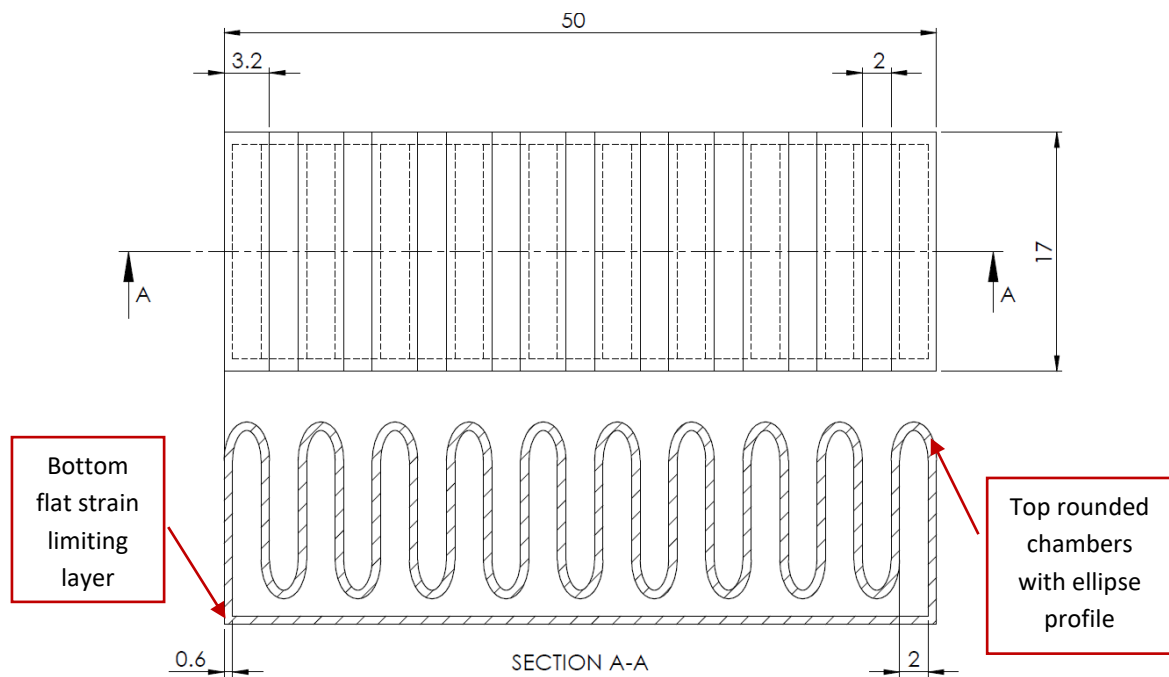


Figure 89: A cross-sectional view of the pleated morphology of the printed soft finger

Furthermore, the chambers were rounded as shown in Figure 89 to remove any sharp corners that may result in a localised increase in strain, which can restrain the bending motion as the material reaches its elongation limit. A curved profile was chosen for sealing the chambers to maximise the overall circumference of the actuator's top profile, allowing enhanced bending without having to stretch the material excessively. This overcomes the limited material elongation in comparison to silicone rubbers. On the other hand, the strain limiting layer at the bottom of the actuator, in this case, can be simply achieved through a thicker straight base. Hence, there is no need to embed an external strain limiting layer as is the case when using highly flexible silicone rubbers. For an individual chamber, the bottom layer is a straight profile of length = $2a$, while the top is a rounded profile with a larger length than its straight base. This difference in lengths allows the actuator to bend when pressurised since the top curved profile stretches while the bottom remains constrained. Hence, the larger the circumference of the curved profile, the more flexible the actuator becomes. Figure 90 compares three chambers with a flat, circular, and ellipse top profiles, which are all feasible geometries to print. The arc length of the circular profile is 57% more than the straight base, while arc length of the ellipse profile depends on its height " b ". Using a height of length = $2a$, the ellipse profile yields a 92.3% increase in the top profile length compared to the straight base and hence results in the most flexible chamber for bending.

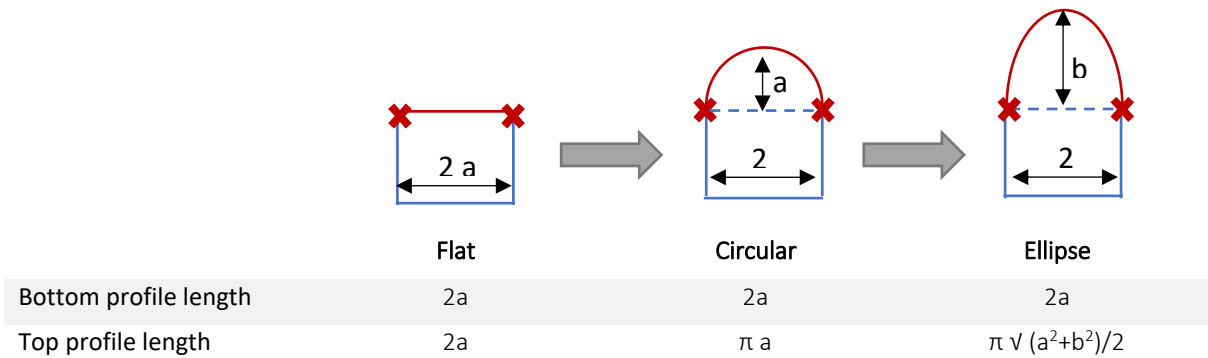


Figure 90: Comparing the increase in the length of the chambers' top profile using different geometries

The first step in ensuring successful printing of airtight soft gripper fingers is to design the actuator geometry in a way that simplifies the printing process and minimises the chance of issues that could result in cavities leaking pressure. A summary of the key design guidelines are given below, which are in line with the guidelines in recent work [37] published during this documentation:

- 1) **Designing Internal geometry:** the actuator can be designed with its internal geometry for the fluidic channels entirely using CAD packages, or only the outer geometry of the actuator is designed on CAD while the internal geometry is decided based on the setting used with a slicing software such as the popular open-sourced CURA software²⁵. The first method allows better control over the geometry of the actuator, but requires careful attention for the geometry to match with the settings used in printing. The second method is easier and quicker especially when different printing settings need to be tested. However, the internal geometry will be defined as a constant offset from the outer geometry of the model with no further modifications possible.
- 2) **Defining actuator thickness:** thicker walls are more likely to result in air-tight actuators, but will consequently reduce the flexibility of the actuator and require higher input pressure to bend. Hence, the thinnest possible wall thickness that still results in airtight actuator is desired. Care must be taken in designing the wall thickness to be increments of the nozzle diameter, which for the Lulzbot printer used here was 0.6 mm. In this work, functional actuators with a wall thickness of only ~0.6mm were successfully printed, which is less than the reported minimum thickness of 1.2 mm in the recent relevant work [37].
- 3) **Minimising bridging distance:** designing the internal geometry of the actuator must take into consideration that unsupported areas will result in bridging, which means dispensing material as a bridge between two edges with no supporting material underneath. Generally bridging results in areas that are likely not airtight, since the layers are not being pushed against each other due to the absence of material underneath resulting in poor bonding. Thus, it is generally desired to reduce the bridging distance to less than 5mm to avoid excessive sagging, and ensure multiple layers of at least 1 mm thickness are deposited on top to make the bridged area airtight. This, however, limits the versatility of the print since the actuator has to be printed sideways in this case, so that bridging happens only for small distances within the cross-section. It is later demonstrated that printing in an upright position with a bridging distance of nearly 10 mm is possible while relying on further coating to seal any developing leaks in bridged areas.

²⁵ <https://ultimaker.com/en/products/cura-software>

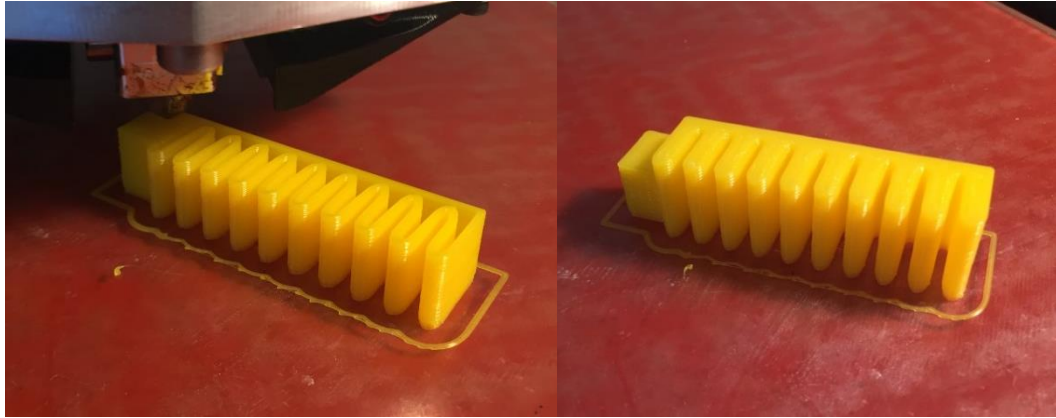


Figure 91: Printing of a soft gripper finger sample in sideways configuration

7.1.3. Flexible filament printing settings

- 1) **Over/under extrusion:** a key factor in successfully printing airtight actuators is getting exactly the right amount of extrusion, which is mostly controlled by the nozzle temperature and can be further adjusted using the flow percentage. Under-extrusion happens when the nozzle is not depositing enough material during printing, which results in small cavities that leak pressure during actuation. While over-extrusion happens when excessive material is being deposited during printing, which could again result in some cavities as the following layer is deposited on top of an uneven surface. Here, the optimum temperature was found to be 218°C with a 100% flow, yet this largely depends on the choice of printer hardware and material used.
- 2) **Retraction settings:** optimising the retraction setting would be necessary to minimise any oozing of material after setting the right nozzle temperature. This reduces the chance of depositing undesired blobs that might create cavities. Unfortunately, retraction speed for the flexible material is usually limited to the range of 10 mm/s, in order to avoid buckling. Hence, the retraction distance is the main controllable parameter here, which was gradually increased until the heated nozzle is not oozing material while idle. A retraction distance of 4 mm was found to be the minimum value that would achieve this for the work presented here.
- 3) **Minimising layer height:** thinner layer height results in a smoother surface with better adhesion between layers. Hence, resulting in more air-tight soft grippers. However, this is usually limited by the printer capabilities. The minimum layer height tested here was 0.3 mm.

- 4) **Minimising crossing:** when the nozzle is crossing overprinted areas without printing, the flexible material still tends to deposit some material. This extra deposited blobs might cause gaps when printing the following layer. Hence, it is important to ensure printing the perimeter as one continuous contour, minimising any crossing if possible. The clever design of the part with smooth consistent cross-section aids in minimising crossing as demonstrated in the slicing results shown in Figure 92 for an actuator sample.

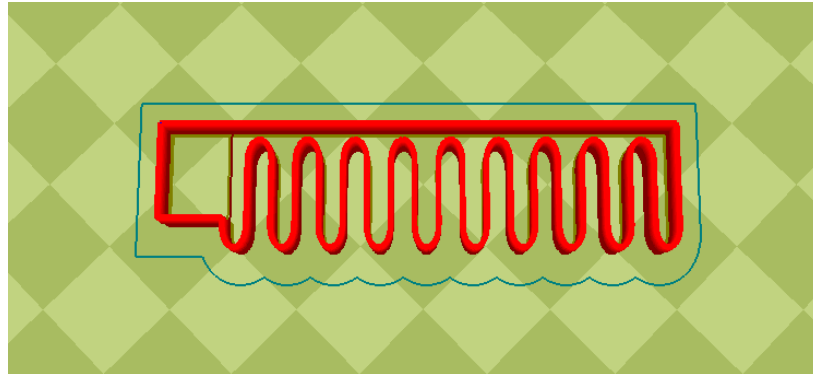


Figure 92: slicing results from Cura software showing one continuous contour for the printer to follow

- 5) **Slow printing speeds:** slower printing speeds are generally desired when printing with flexible materials. It is advised not to go beyond a printing speed of 20 mm/s to meet the sensitive quality requirements here.
- 6) **Bed adhesion:** the Ninjaflex material bonds too well to Polyetherimide (PEI) print surfaces, and hence it is recommended to print on a cold print bed coated with a thin layer of PVA glue stick to ease the removal of the printed piece.
- 7) **No supports:** it is difficult to remove supports made from Ninjaflex filaments, so it is recommended to rely on bridging for creating internal features if needed.
- 8) **Clean nozzle:** it is important to keep the nozzle clean when printing since impurities sticking to the nozzle can stick to the print causing a gap, and generally tend to make the nozzle prone to collecting more globs while printing.

Table 7 summarises for the print settings used to print the soft finger from NinjaFlex when oriented sideways, using the calibrated Lulzbot TAZ5 printer with the Flexydually tool head.

Table 7: Summary of print settings for sideways configuration

Printing Parameters	Value
<i>Layer height</i>	0.3 mm
<i>Shell thickness</i>	0.6 mm
<i>Bottom/top thickness</i>	1.2 mm
<i>Nozzle temperature</i>	218°C
<i>Bed temperature</i>	Off
<i>Print speed</i>	17 mm/s
<i>Fill density</i>	100%
<i>Retraction distance</i>	10 mm/s
<i>Retraction speed</i>	4 mm
<i>Diameter 1</i>	2.8 mm

7.1.4. Repeatability Analysis

Soft actuator samples were tested following systematic experimentation, in order to evaluate the effectiveness of the tuned printing setting in consistently creating air-tight soft actuators. Two experiments were implemented to evaluate the repeatability and fatigue of the printed soft actuators. In the first experiment, five soft actuator samples were printed and tested three times using a fixed input pressure of 20 Psi that would be expected during typical grasping scenarios. All five samples were found to be air-tight and can be tested right after printing without additional repairs. The mean absolute trajectory of the three repetitions for one of the samples is shown in Figure 93 with 95% confidence bounds. It is clear that the trajectory response of a printed actuator is highly consistent for a fixed pressure input, with the standard deviation from the mean response of each sample in the range of 0.1 to 0.25 mm. This confirms the repeatability of the response of a single printed actuator under short testing.

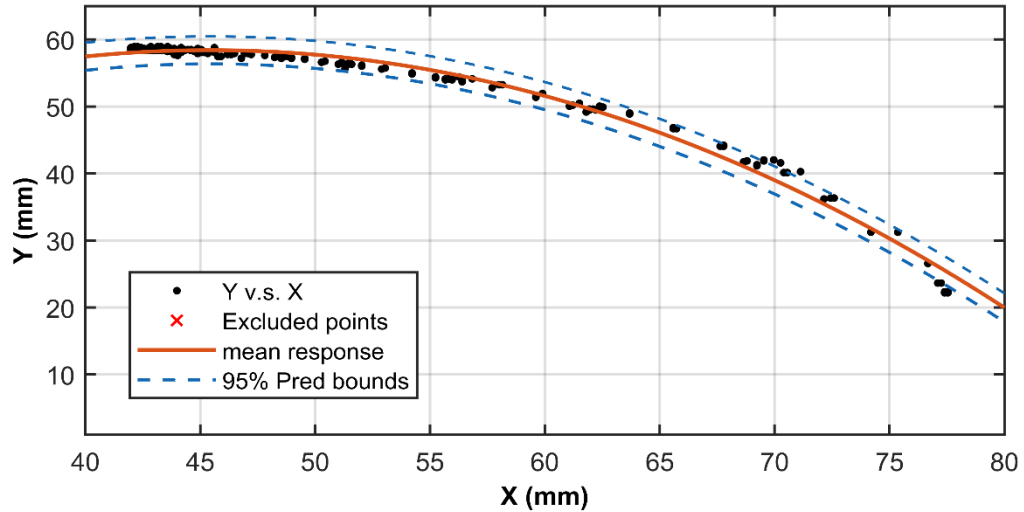


Figure 93: The variation in the absolute trajectory response between repetitions for one sample

Furthermore, the mean trajectories for all five tested samples when actuated with an input pressure of 20 Psi is shown in Figure 94. The coordinates of the tip are measured relative to its initial position, in order to negate the variation in the initial position that might occur while mounting the actuator into place. Hence, any variation in the tracked trajectory can be only due to the variation in bending from one sample to another. It can be observed that all the five tested samples followed the almost the same response within 95% confidence bounds from the mean response, with a mean error of only 0.83 mm. Thus, it can be concluded that the printed actuator response is highly repeatable with negligible variation during short-term repetitions and minimal variation across different samples. It is important to highlight that this is assuming all samples were printed using the same settings and orientation, which was the case for the tests conducted here.

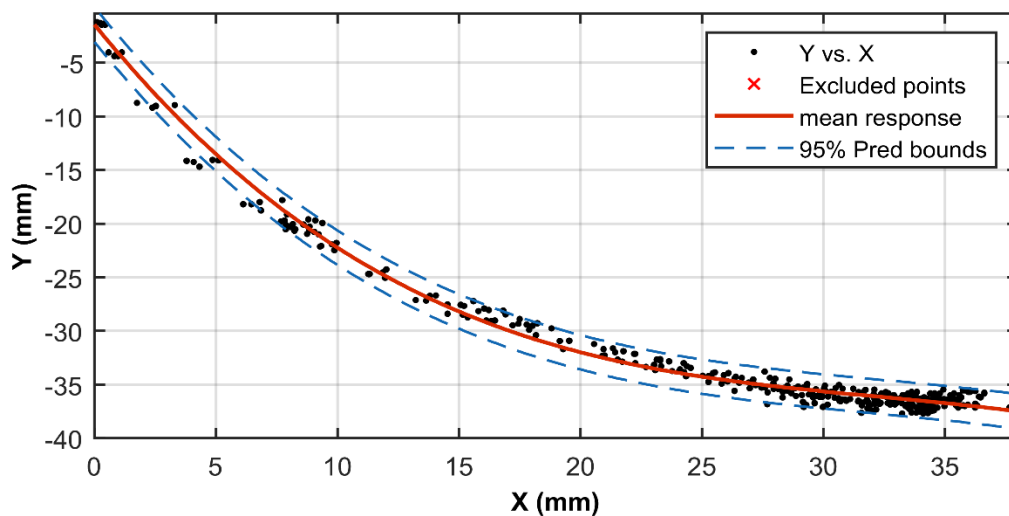


Figure 94: The variation in the relative trajectory response between five tested samples

7.1.5. Fatigue Analysis

For the next stage of the analysis, two of the previously tested samples were actuated 1000 times each at the same input pressure of 20 Psi. This test aims to evaluate the fatigue exhibited by those printed actuators upon prolonged use, using a median pressure input value that is expected during typical grasping applications. The test is controlled using the pneumatic control board, which was programmed to actuate the desired number of repetitions, while triggering the calibrated high-speed camera to record the retracted and actuated positions of each repetition. Each time the actuator is pressurised for 500 ms, and then the pressure is released for another 1000 ms. Upon completion of the test, the 2000 image frames generated are automatically processed using the developed image processing program to measure the coordinates of the actuator tip at the retracted and actuated positions throughout the experiment. Figure 95 highlights the witnessed deviation in the trajectory by overlaying two image frames representing the initial and final positions of the actuator tip for the first and last actuation. It can be observed that by the end of the fatigue test that some deviation occurs in the final actuated and retracted positions.

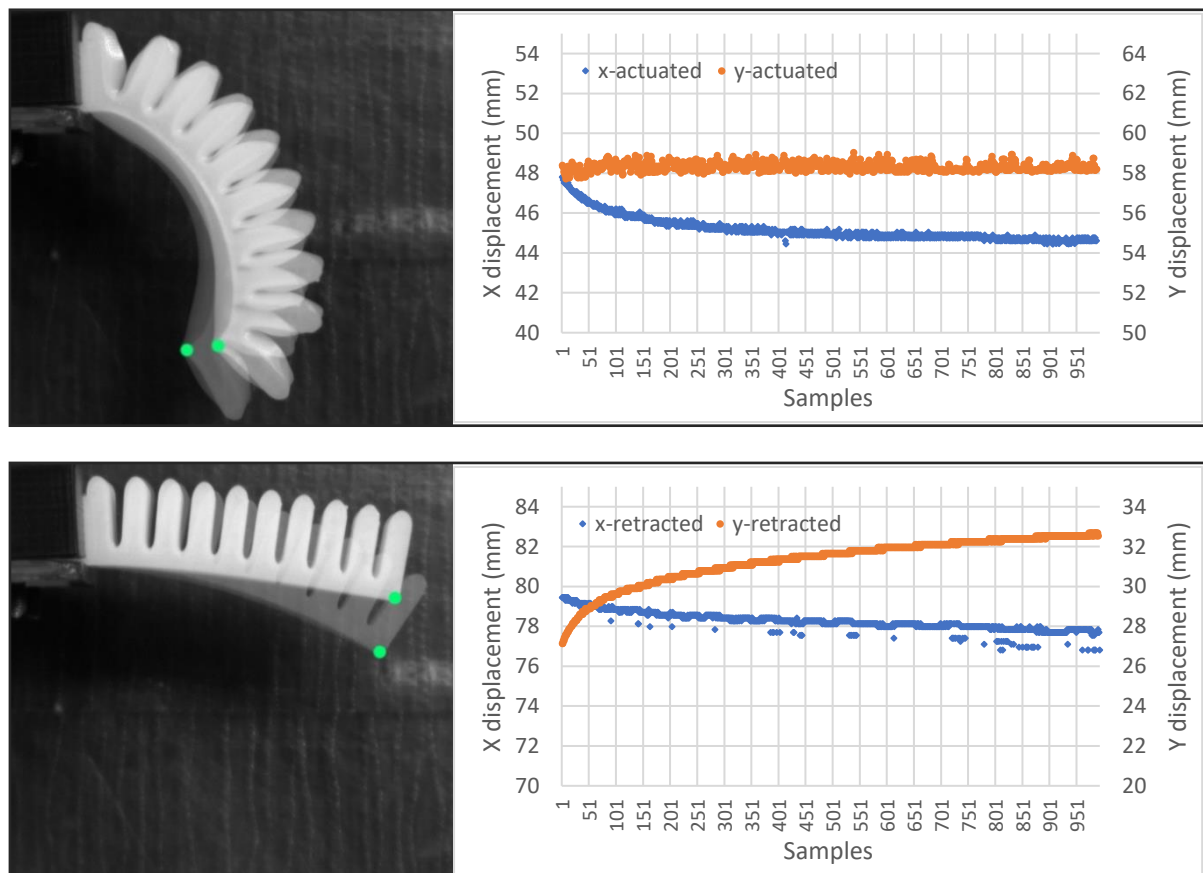


Figure 95: Comparing the deviation in the retracted and actuated positions after 1000 actuations

The exact deviation is illustrated in the trajectory plots in Figure 95, showing the coordinates of the tracked actuator tip for both the actuated and retracted positions throughout the 1000 actuation tests. For the actuated position, the tip has deviated 5.39 mm in the X-axis direction and only 1.75 mm in the Y-axis direction. The deviation is caused by a reduction in the bending curvature of the actuator as it goes through some material relaxation. As for the retracted position, a slightly larger deviation is witnessed with a total of 2.47 mm in the X-axis direction and 9.34 mm in the Y-axis direction. This time the deviation was mostly in the Y-axis direction, as the chambers do not fully retract to its original position during the allowed retraction time of 1 second. The deviation could have been possibly reduced if the actuator was allowed more time to retract. However, for applications that require fast grasping and releasing, the better solution for a quick and full retraction is to apply negative pressure during retraction, instead of leaving the vent at atmospheric pressure. Moreover, looking at the bending angle response of the actuator, Figure 96 highlights the witnessed deviation in the final bending angle throughout the 1000 actuation tests. The maximum deviation at the end of the fatigue test was only 3.4°, half of which occurred during the first 100 actuations. Using MATLAB curve fitting functions, the data was used to derive the best fit model representing the trend in the bending angle deviation. The red curve represents a first order power function in the form $\theta = a \cdot x^b$, with coefficients $a = 47.37$ and $b = -0.011$. The model has a good R^2 value of 0.71 and a mean error of only 0.3°. Such fatigue model can be combined with the actuator's bending angle model, to correct the estimated bending angle of the actuator when more accurate predictions are desired. Still, for the small deviation of only 1.7° occurring between the 100th and the 1000th actuations, this can be accommodated by the soft and compliant nature of a soft gripper.

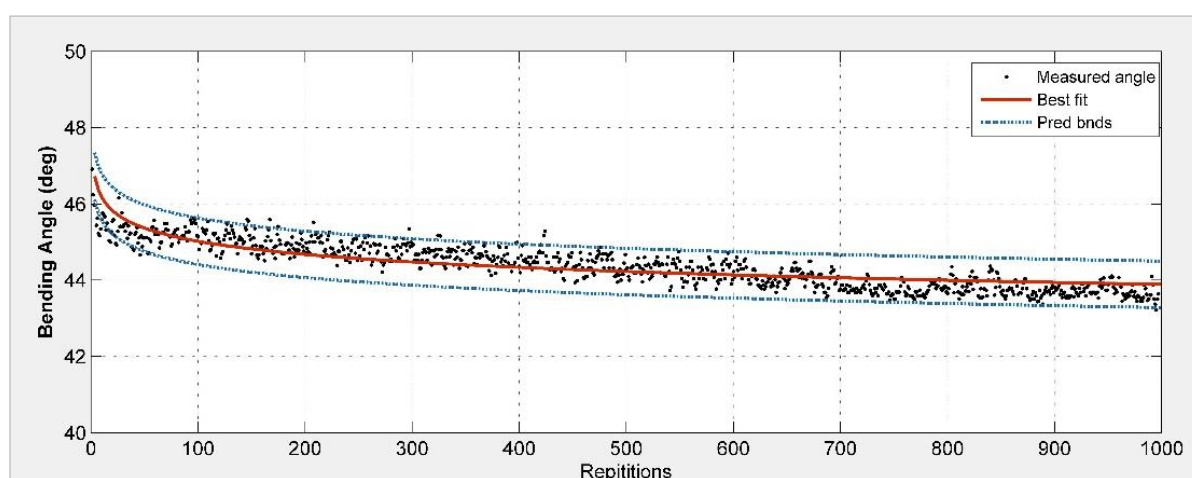


Figure 96: The bending angle measurements

Another fatigue test was performed this time at twice the previous input pressure (40 Psi) for 250 actuations. This pressure value would significantly deform the soft actuator to achieve a full bend towards the fixed base (Figure 97), which is actually beyond the required bending for typical grasping scenarios. Yet, the aim was to test not only if the actuator can handle such a large input pressure, but also if it can continue to operate consistently under this pressure. Figure 97 shows the output of the image processing program measuring the tip coordinates for the image frames captured throughout the test. Similar to the previous test, it was observed at the end of the experiment that a limited deviation (1.01 mm horizontally and 3.79 vertically) occurred for the actuated position even at such a large input pressure, while a larger deviation (6.6 mm horizontally and 7.88 vertically) was evident for the retracted position. This again shows that the printed soft actuators do not fully retract to their original position when vented at atmospheric pressure. A negative pressure needs to be applied to return the actuator completely to its original state if required. Nevertheless, the actuated position does not seem to be affected by this deviation in the retracted position, as it undergoes a limited deviation even when achieving full bends at 40 Psi.

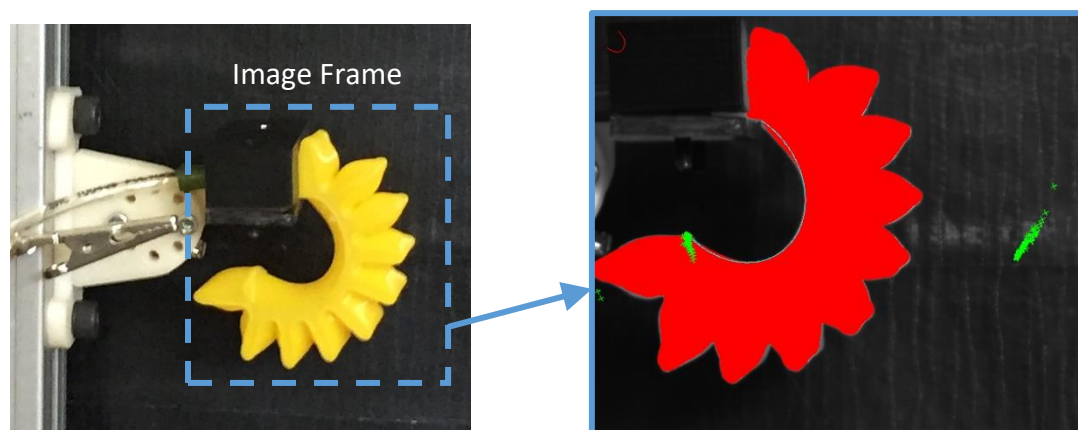


Figure 97: The image processing output for tracking the tip trajectory after 500 cycles

The results of those experiments showed that the printed soft actuators tested here exhibit limited deviation after repeated actuations, even when operating at the maximum pressure input. The deviation in the actuated position is due to some material relaxation that is similar to that witnessed with silicone rubber actuators. However, it takes longer for the printed actuators' bending response to settle (~100 actuations). This material relaxation causes a deviation that is mostly in the horizontal direction due to the decrease in bending curvature. On the other hand, the retracted position was shown to undergo a larger deviation after repeated actuations, which can be reduced if the waiting time increased beyond the 1-second allowance given here. Yet, it would be more effective to apply a negative pressure, if a full

retraction back to the actuator's original position is desired. Moreover, the 3.4° deviation in the bending response after 1000 actuations would be an acceptable error for soft grippers based on those printed actuators, since their soft nature can adapt to this small variation. Thus, it can be concluded that the printed actuators presented here provide a consistent bending response under a wide operating range, with small deviations that are to be expected from actuators fabricated using a layer-based printing process.

7. 2. Dual-extrusion 3D Printing of Flexible Strain Sensors

A key contribution here to the recent attempts in printing soft grippers is the integration of sensory elements that can also be directly 3D printed using the same FFF printer setup. This not only offers highly customisable sensors that can be matched to the geometry of the gripper fingers, but also enables a low cost and repeatable fabrication solution that can be implemented using the well-established FFF printing technology. This was achieved via the utilisation of what is referred to as “dual-extrusion” FFF process, in which two different material filaments that can bond to each other are simultaneously printed to create more complex prints with varying material properties. In the context of soft gripper printing, this means that localised stiffness variation can be achieved at the strain limiting layer by the inclusion of a thin layer of more rigid material such as PLA. More interestingly, combining a conductive material filament with the flexible material used for the body of the soft actuator would result in flexible strain sensors that can be easily integrated while printing the soft gripper body. This provides a faster and more consistent method for embedding low-cost strain sensors within the soft gripper fingers, without hindering much of their desired flexibility. In addition, the ability to directly print the sensor means that they can be customised to fit the desired actuator size, which is a key advantage when compared to commercially available flex sensors that come in fixed sizes. This idea has been investigated here using a dual extrusion tool head with two nozzles to print flexible strain sensors from both NinjaFlex and conductive PLA from Protopasta²⁷ in order to be integrated with the printed soft fingers. The main challenges were first to confirm if both materials can bond well together when printed simultaneously, while the other challenge was to optimise the sensor design and print settings so that the thinnest functional sensor can be successfully printed. Increasing the cross-sectional area of the conductive tracks will ensure that they remain functional as a sensor when bent, but will consequently downgrade the flexibility of the sensor, since the

²⁷ <https://www.proto-pasta.com/pages/conductive-pla>

conductive material is far less flexible than NinjaFlex material. Thus, initially the sensor was designed with thick conductive tracks to confirm the validity of the proposed idea, then the track width and height were incrementally reduced and printed following the design guidelines and print settings later discussed, until the thinnest functional sensor is consistently printed with success.

7.2.1. Design Concept

The design of the printed sensor follows that of standard strain gauge sensors, in which conductive tracks follow the pattern shown in Figure 98. When the sensor is subjected to strain, a change in the resistivity of the conductive tracks will be witnessed, which can be measured and related to the strain. For the soft gripper application, the interest is primarily in measuring the bending of the soft gripper fingers. Hence such a strain sensor should be placed so that the channels are parallel to the direction of bending. Since the sensor body is made from flexible material that allows significant bending, the thin conductive channels embedded inside will also be bent, causing a change in resistance due to the deformation of the channels' dimensions. Hence, the bending angle can be measured by relating it to this change in resistance. Furthermore, since the conductive PLA material is not naturally flexible, it must be printed with a very fine thickness to maintain the flexibility of the sensor. The thinnest possible thickness would be equivalent to a single layer thickness set in the print settings, which was 0.3 mm here. However, it is recommended to add another layer on top in case any cavities arising during printing of the first layer can be sealed by the following layer, resulting in more resilient conductive tracks. In order to maximise the adhesion between the Ninjaflex and conductive PLA materials, the conductive tracks are sandwiched inside the flexible sensor body. Again to avoid an excessive increase in the overall thickness of the sensor, only one layer of Ninjaflex is added on top as well as below the conductive tracks layer. Additionally, the areas in between the conductive tracks are filled with Ninjaflex material, not only to enhance the adhesion between the layer, but also to ensure proper all-around insulation for the conductive tracks.

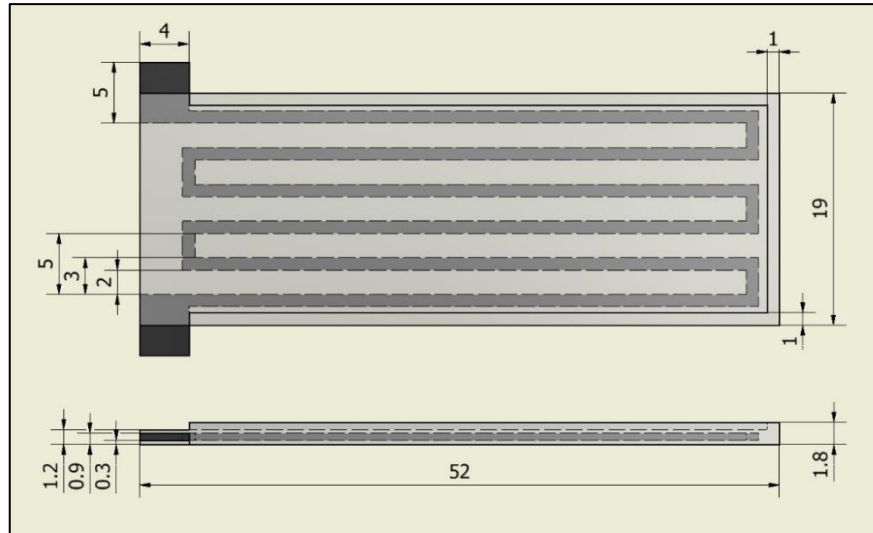


Figure 98: The design of the printed strain sensor (dimensions in mm) with the flexible NinjaFlex body (grey) and embedded conductive PLA tracks (black).

7.2.2. Dual-extrusion printing settings

To enable direct 3D printing of the complete sensor in a single stage, a standard FFF printer (Lulzbut TAZ 5) fitted with a dual-extruder print head (FlexyDually²⁸) was used. Having an extruder with two nozzles allows printing of the two filaments (flexible and conductive) simultaneously. The primary target was to optimise the sensor design and print settings such that the thinnest possible sensor can be printed. Increasing the cross-sectional area of the conductive tracks will ensure they remain intact when bent, but the flexibility of the sensor will be downgraded as the conductive material is stiffer than the NinjaFlex material. Additionally, the dimensions of the sensing tracks must account for the printer specifications, such as nozzle diameter, so that the tracks can be printed successfully without over or under extrusion problems. The following guidelines were followed to ensure successful and consistent printing of highly flexible and functional strain sensors.

- **Printing orientation:** the preferred sideways orientation for printing the soft gripper body minimises bridging distance and enhances the bonding between layers. However, this complicates the printing of the embedded conductive tracks and limits the geometry that can be printed effectively. Hence, upright printing is considered in this case to have full control over the geometry of the conductive tracks and ensure they remain functional.

²⁸ <https://www.lulzbot.com/store/tool-heads/lulzbot-taz-flexydually-tool-head-v2>

- Design considerations:** This consequently means that the design of the gripper geometry needs to be updated to ensure all planer dimensions are a function of the nozzle diameter, while all vertical dimensions are a function of the layer height, following the previously discussed design considerations. Furthermore, in order to ensure connectivity for the printed sensors, the width of the tracks needs to be at least twice as thick as the nozzle size, while limiting the vertical height to less than 0.5 mm, to avoid hindering the desired actuator flexibility. The spacing between the tracks needs to be at least three times larger than the nozzle diameter to ensure that no short-circuiting will occur at any point along the length of the tracks, due to extra deposited blobs. Maintaining a consistent spacing between the tracks is also encouraged to minimise crossing.
- Extruder switching settings:** switching between nozzles is a critical source of discontinuity in the print that could negatively affect the connectivity of the conductive tracks and encourage the formation of voids between layers that leak pressure during actuation. Careful tuning of the retraction settings for both materials becomes essential to not only prevent the deposition of extra lumps that accumulate when the nozzle is idle, but also to avoid excessive retraction that can delay the deposition of material when the nozzle becomes active again. The optimum retraction distance and speeds for conductive PLA were found to be 10 mm/s and 4 mm at a nozzle temperature of 218°C. This is the minimum nozzle temperature that allows smooth printing, as any further increase tends to cause uncontrollable oozing of material.

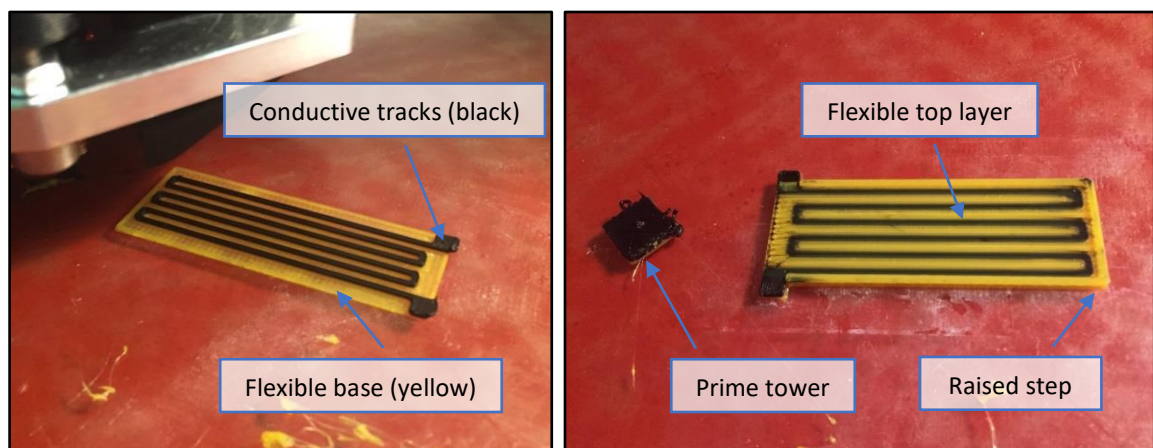


Figure 99: Printing the flexible strain sensor with embedded conductive tracks.

- Prime and wipe tower:** Additionally, the activation of the prime and wipe tower in the Cura settings, forces the printer to print an additional wall around the part to wipe off any excess material sticking to the nozzle during switching, as well as starting the printing away

from the part initially until the flow becomes more consistent (Figure 99). This option can be activated if oozing from the nozzle is still evident, although it adds to the print time since more switching would be necessary. Here, it was also possible to print a clean sensor without the use of a prime and wipe towers after tuning the print settings as summarised in Table 8.

Table 8: Summary of print settings for upright configuration in dual-extrusion mode

Printing Parameters	Value
<i>Layer height</i>	0.3 mm
<i>Shell thickness</i>	0.6 mm
<i>Bottom/top thickness</i>	0.9 mm
<i>Nozzle temperature</i>	218°C
<i>Bed temperature</i>	Off
<i>Print speed</i>	17 mm/s
<i>Fill density</i>	30%
<i>Retraction distance</i>	10 mm/s
<i>Retraction speed</i>	4 mm
<i>Dual-extrusion</i>	On
<i>Wipe and prime tower</i>	On, 25 mm ³
<i>Diameter 1</i>	3.2
<i>Diameter 2</i>	2.7

Following those print settings, functional samples of the flexible strain sensor were successfully printed each time. Figure 100 shows one of the samples being tested right after printing by bending the sensor while measuring the resistance. It can be observed that a significant change in resistance is evident upon bending the sensor, which can be related to the bending angle as demonstrated in the following sections. The base resistance for the sensor and the overall change in resistance depends on the dimensions of the conductive tracks as to be expected. Using the same dimensions for printing different sensor samples results in nearly the same base value with a tolerance of around 0.5 KΩ.

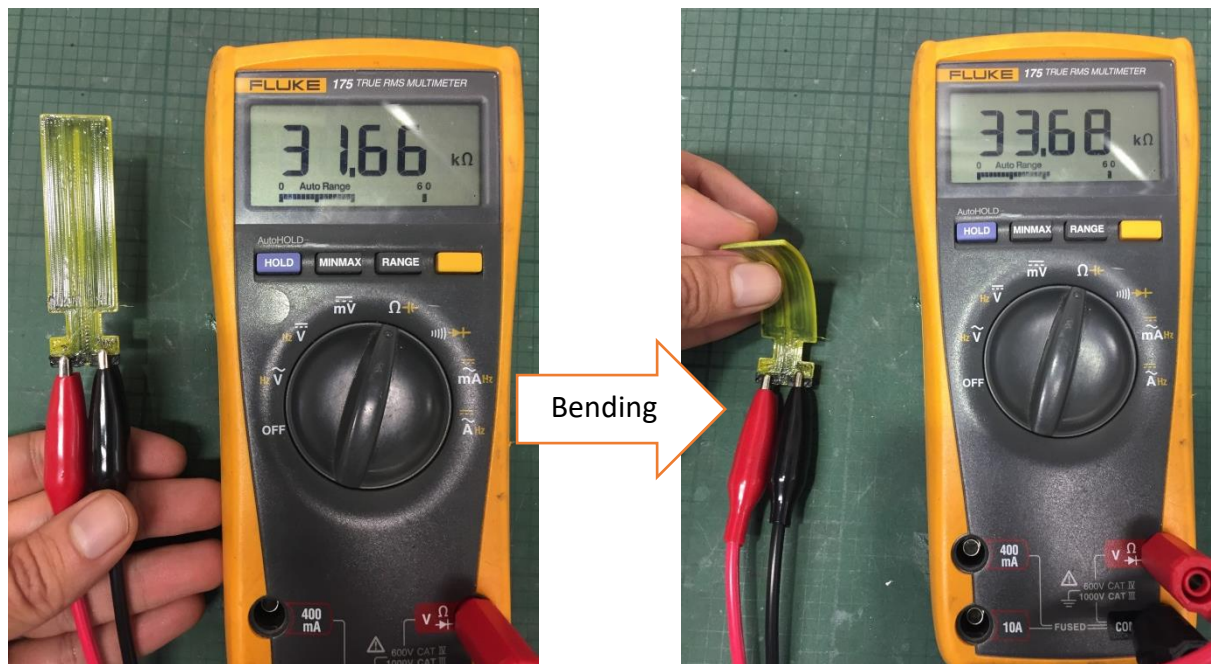


Figure 100: Initial tests showing a change in sensor's resistance upon bending

7.3. Integrated Strain Sensing in Printed Actuators

The next step after the successful printing and characterisation of the printed flexible strain sensors would be to integrate this with the printed soft gripper fingers, to create a fully printable soft gripper with integrated sensing capability. Again dual-extrusion FFF printing is used to enable printing of the flexible soft finger body and the conductive sensor tracks.

7.4.1. Direct printing in a sideways configuration

Initially, sideways printing was considered since it is the desired printing orientation to minimise bridging and ensure air-tightness. However, printing the sensor in this orientation was challenging with limited control over the sensor geometry, since the printing happens along the cross-section of the sensor as shown in Figure 101. Printing in sideways orientation ensured air-tight actuators, yet the embedded sensor was not always functional. The main reason for this was due to the occasional occurrence of a short-circuit at one point between the sensor tracks, which prevents any useful measurements to be made in this case. In addition, the sensor thickness in this orientation would be multiple of the nozzle diameter (0.5 mm), which results in thicker conductive tracks compared to printing in an upright configuration. These challenges have encouraged the consideration of printing the soft gripper finger with embedded sensing in an upright orientation.



Figure 101: Printing a complete sensorised gripper finger in sideways orientation

7.4.2. Direct printing in an upright configuration

Printing in upright orientation offers better control over the sensor geometry and allows for printing thinner sensor tracks to maintain flexibility. However, it is not the ideal orientation for printing the actuator since excessive bridging will be required, which is a major threat to the air-tightness of the gripper. Bridging for up to 10 mm was possible, but still results in micro-cavities in bridged areas that leak pressure, since layers do not stick well to each other due to the absence of a support beneath. This can be resolved by coating these layers with flexible glue to seal the cavities, but it goes against the interest of automating the fabrication process as it introduces an additional manual coating step with the risk of inconsistencies. Thus, this approach results in functional embedded sensors, but with limited consistency in the airtightness of the actuator that needs further coating. Figure 103 shows the measured change in resistance of the embedded strain sensor when the printed soft finger is manually bent. It can be seen that a change of around $2.5 \text{ K } \Omega$ can be measured, which is significant considering that this is a raw measurement with no additional amplification used.

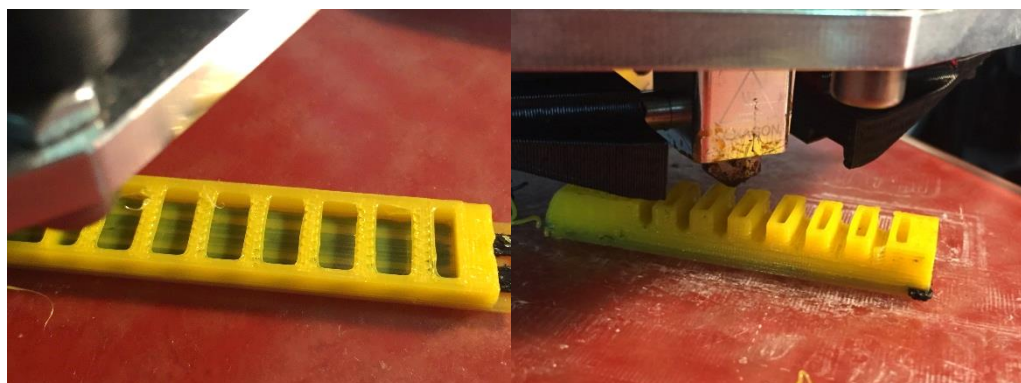


Figure 102: Printing a complete sensorised soft finger in an upright orientation



Figure 103: comparing the measured resistance of the conductive tracks in flat and bent orientations

7.4.3. Two-stage printing and welding

Moreover, the more effective solution to this was to actually print each of the soft finger and the sensor separately using the printing configuration that best suits each. The soft finger body is printed sideways to minimise bridging and ensure airtight actuators, while the sensor is printed upright to have better control over the geometry of the conductive tracks and ensure they are thin enough to maintain flexibility. Merging the two together is then achieved by merely welding along the edges using a soldering iron to locally melt the Ninjaflex material and bond the two parts together. A small step around the perimeter of the sensor facilitates placing the soft actuator on top in the right location. This additional step although manual is straightforward and quick to achieve while allowing each part to be printed following its optimised printing settings. Hence, the two-stage printing and welding approach was the one adopted in the remainder of the work in this chapter, in order to ensure air-tight actuators and functional sensors with consistent output.

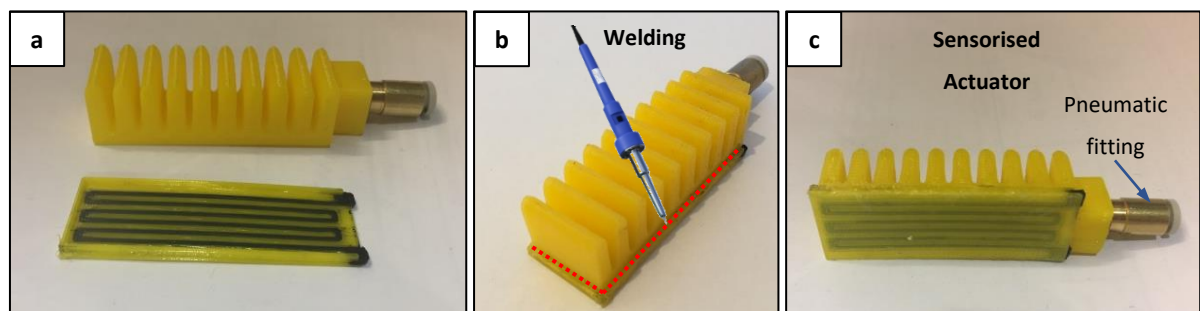


Figure 104: Welding the printed bending actuator and strain sensor together to create a sensorised actuator. (a) Individual actuator and sensor after printing, (b) soldering iron used to weld along the raised step of the sensor, (c) sensorised actuator after welding.

7. 4. Printed Sensor Acquisition and Characterisation

The first challenge faced when attempting to characterise the printed strain sensor, was to create a stable interface for wiring the sensor. The conductive PLA material used in printing the conductive tracks cannot be soldered directly to wires, and hence wires need to be clamped or tied to the sensor terminals to measure the sensor resistance. However, when connecting wires with crocodile clips for example to the sensor terminals, the measured resistance of the sensor was very unstable and kept changing whenever the wire moves. This was because the conductive tracks were printed with a very fine thickness (~ 0.5 mm), so the wires clamped to the terminals are much heavier than the tracks. Hence, any small movement introduces oscillations to the printed tracks that affect the acquired readings. In fact, the metal crocodile clips are much harder than this flexible sensor, so they can easily damage the sensor terminals after repeated use. In order to resolve this problem, an innovative wiring approach is proposed that use low-cost conductive threads³⁰ as wires. The thread is simply wound around the sensor terminals, and hot glue is applied to fix the conductive thread in place (Figure 105). At the other end, the conductive thread is again wound around a metal pin and fixed using hot glue, to facilitate connecting the sensor to circuit boards (Figure 105). This results in a very light and flexible wiring option that can be fixed securely to the sensor terminals without damaging them or influencing the sensor reading by the wires own weights. Using this alternative wiring approach, the measured sensor resistance does not fluctuate significantly by movement of the wires, and hence more stable readings can be recorded.

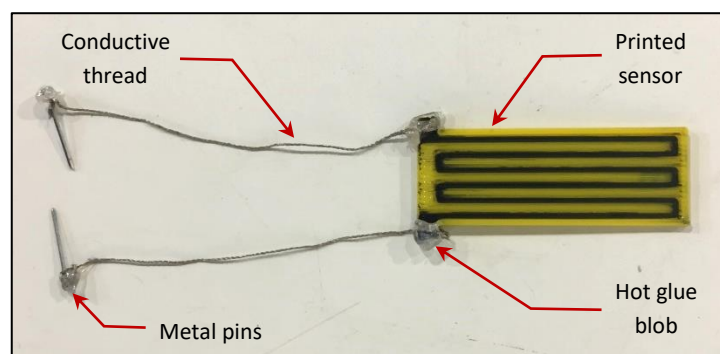


Figure 105: Wiring of the printed strain sensor using conductive threads glued to the exposed terminals.

A signal acquisition circuit was designed and implemented to: (1) convert the sensor's change in resistance into voltage, (2) amplify the output voltage to utilise the full 0 to 5v range, (3) convert the voltage to a digital value through the analogue input of the Arduino board, and (3) add a bias function to reset readings to zero when required. Figure 106 shows the

³⁰ <https://www.proto-pic.co.uk/conductive-thread-bobbin-60ft.html>

schematic design of the circuit which comprises of a Wheatstone bridge circuit that outputs a voltage corresponding to the change in the sensor's resistance. The value of R_1 was set to be close to the base resistance value of the printed sensor, which was 24 k Ω . The bridge is initially balanced by setting the same resistance value for resistors R_2 and using a potentiometer (POT) to zero the final voltage output due to any errors in the resistance values when the sensor is laid flat. This bridge circuit is then followed by an instrumentation amplifier integrated circuit ($INA122$, Texas Instruments) that converts the change in resistance due to the sensor's bending to voltage and amplifies it based on the R_{gain} value. The gain function and internal structure of the instrumentation amplifier's circuit are shown in Appendix (D) – Datasheets. Finally, the output voltage is then fed to an analogue input pin on the Arduino board to convert it to a digital value reading (from 0 to 1023) for upcoming processing steps.

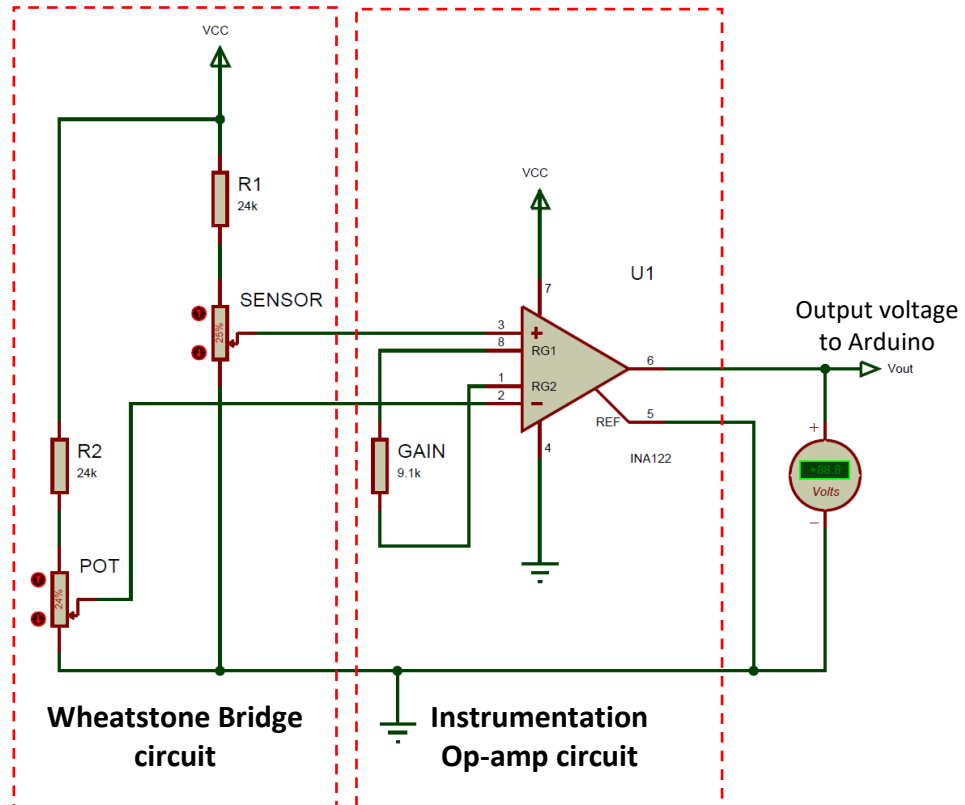


Figure 106: Schematic design of the printed sensor acquisition circuit

The acquisition circuit was simulated to decide the required gain value that will fully utilise the 0 to 5v output voltage range for a better measurement resolution. Figure 107 compares the simulated voltage output against the simulated change in printed sensor resistance for gain values of 34.4, 26.9, and 20, which were set using standard resistance values of 6.8 k Ω , 9.1 k Ω , and 13.3 k Ω respectively . It can be observed that using R_{gain} of 9.1 k Ω results in the

most linear voltage response across the change in sensor's resistance without output saturation, and hence was the gain used for the circuit. The corresponding voltage output from the circuit in this case varied from 0.4 to 4.8 V, which effectively utilises the 5V range for enhanced resolution.

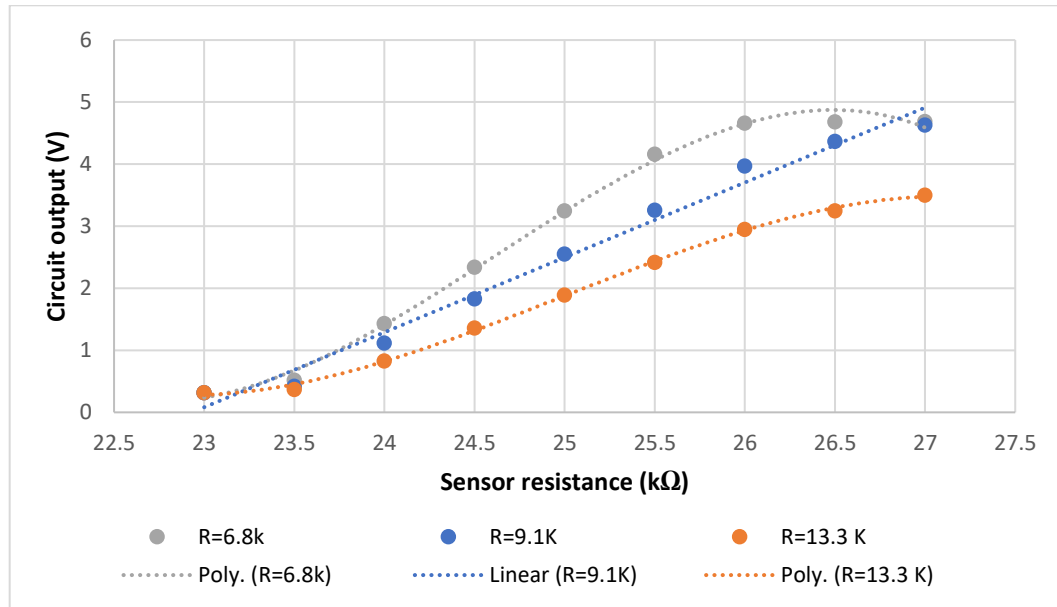


Figure 107: Acquisition circuit simulation at different amplification gains

The printed sensor was tested when connected to the accusation circuit with the chosen gain value to evaluate the quality of its response. Figure 108 shows the voltage measured from the circuit using an Arduino board when bending the sensor repeatedly. It can be observed that the variation in the final was limited. Any remaining noise in the signal can be further reduced by using a three-point moving average as shown in the same graph, to achieve a response that is almost as clean as the commercial flex sensor used before. Adding de-bouncing capacitors to the circuit also yields a similar result in smoothing the signal, yet introduces some delay in the response which is undesired for short actuation durations. Hence, it is preferred to acquire the readings at the highest possible sampling rate without delays, and then deciding the desired moving average window, if any, depending on the application needs.

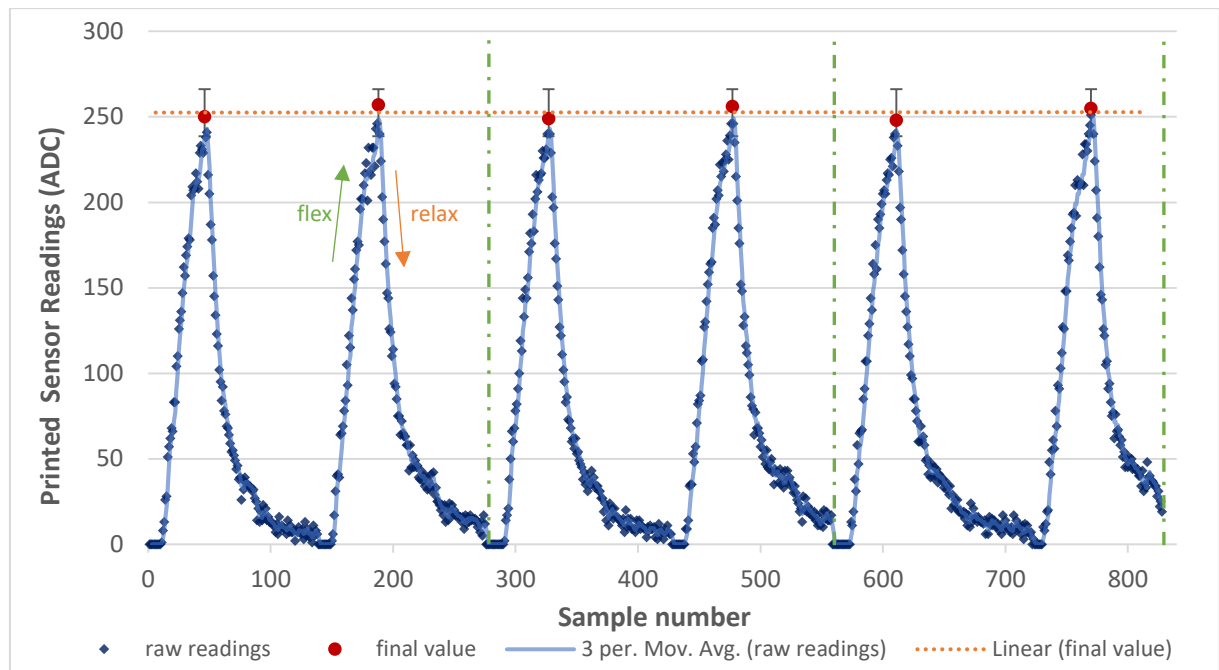


Figure 108: Sample voltage output (after analogue to digital conversion) from the acquisition circuit when repeatedly bending the printed sensor

7. 5. Characterisation of Bending Response

In order to evaluate the consistency of the feedback from the printed strain sensor, the sensorised soft finger module was tested at varying input pressures while recording the resulting readings from the strain sensor changing with the actuator bending and onboard pressure sensor measuring internal pressure. Figure 109 shows the response from the printed strain sensor against the measured internal pressure when the soft finger is actuated repeatedly at pressure inputs from 12 to 20 Psi at 2 Psi increments. Five distinct cycles can be seen in the graph, each representing the response for given pressure input. The response is increasing (actuation stage) following a consistent parabolic response for each input pressure value, then starts to fall back (retraction stage) after the input pressure is switched off. The gradient of the response increases as the input pressure increases, while the retraction phase for all input pressure tends to join towards the same curve since gravity mainly governs retraction. Plotting a curve through the top point of each cycle representing the final position of the actuated finger yields a parabolic function that describes the relationship between the input pressure and maximum bending. The cycle from the pressure input of 20 Psi was used to validate the relationship and be seen to follow the same trend. The results from this experiment confirmed the following:

- The bending response of the printed actuator, as well as the readings from the printed sensor, are repeatable and consistent for fixed actuation conditions.

- The rate of change in the sensor's response increases consistently with increased input actuation pressure and can be described by a simple parabolic function for each input pressure.

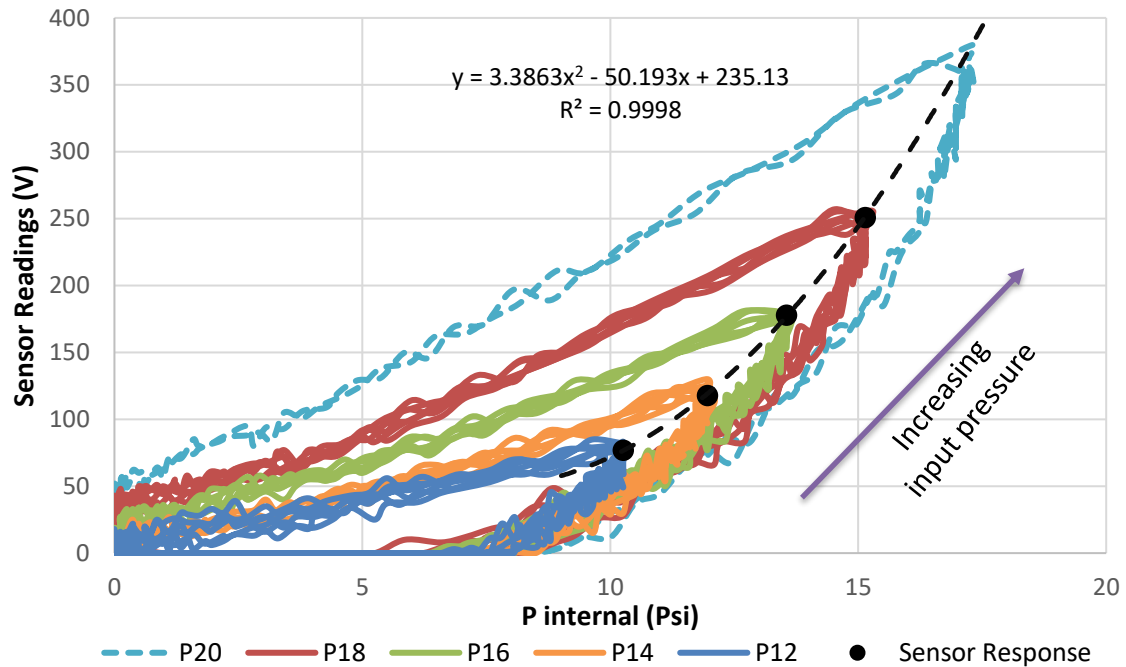


Figure 109: Printed strain sensor response against the internal pressure

7.5.1. Empirical modelling

Following the same procedure of data-driven modelling explained in Chapter 5, an empirical model for the bending response of the printed actuator was derived, but this time using the feedback from the printed strain sensor rather than the commercial flex sensor previously used. The measured input pressure was again incorporated into the model so that it can be used with varying input conditions. The procedure for generating the experimental data and deriving the empirical model can be summarised as follows:

- The desired input pressure supply to the actuator is set.
- The actuator is fixed to the setup and repeatedly actuated while recording the image frames and sensory feedback.
- The output voltage from the pressure and bending sensors are converted to digital values via the analogue inputs of the Arduino board and recorded as a time series.
- The captured image frames are stored on the PC and processed using the image processing program to track the tip trajectory and calculate the corresponding bending angle value for each image frame.

- v. The bending angle values are synchronised with the processed readings from the strain sensor and onboard pressure sensor.

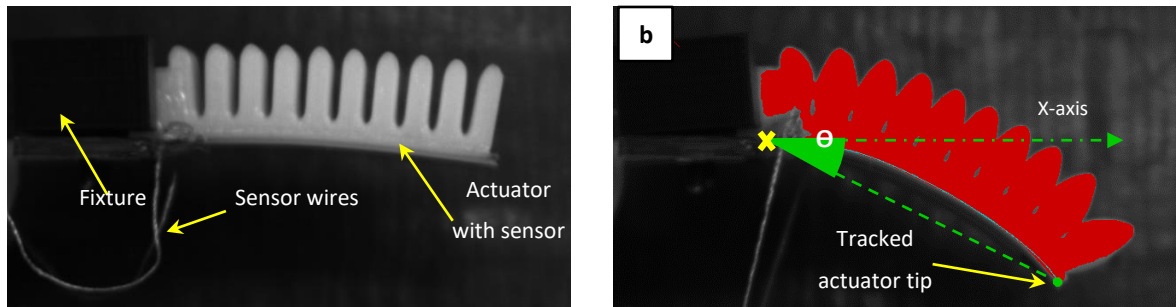


Figure 110: Image processing program tracking the bending trajectory of a tested printed soft finger sample

The training data is shown in Figure 111 resulting from actuating the soft finger module three times at an input pressure of 18 Psi for a fixed duration of 3000 ms. A total of 500 samples were collected at a sampling rate of 3 ms; each sample is an array containing a reading from each of the printed sensor and the pressure sensor, as well as the corresponding synchronised measurement for the actual bending angle using the vision system. It can be noticed that compared to the commercial flex sensor, the printed sensor results in a slightly more noisy signal, which is minimised by taking a moving average of 2 or 3 samples. on the other hand, the printed sensor offers a wide range of customisation in the functionality and dimensions of the sensor at a low cost, which is not possible using the commercial alternative.

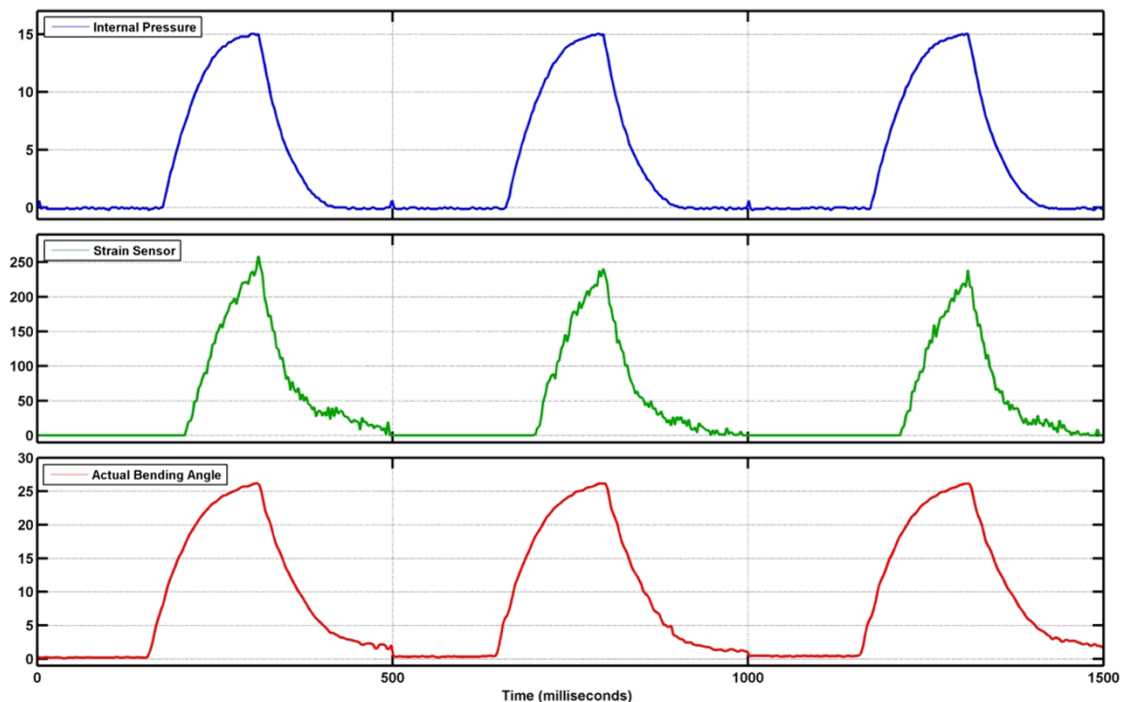


Figure 111: Sensory readings for deriving the empirical model

Using linear regression, an empirical model can be derived that relates the measured bending angle of printed soft fingers to the sensory feedback from the embedded strain sensor and the onboard pressure sensor. The outcome of the regression analysis is a polynomial function with coefficients derived based on the experimental data used. Table 9 below tabulates the derived first order and second order polynomial functions relating the bending angle to the sensory inputs. Figure 112 compares the predicted bending angle values in comparison to the actual values measured using the vision system, for the derived first and second order models. It can be seen that both models are able to reproduce the bending angle values used in training the models, with the second order model providing excellent prediction accuracy with a mean error of only 0.899° and STD of 1.16.

Table 9: Goodness of fit for the derived empirical model

	Derived Model	Adj. R ²	RMSE
First order	$\theta = a + b \cdot P + c \cdot V_s$	0.9659	1.784
Second order	$\theta = a + b \cdot P + c \cdot V_s + d \cdot P^2 + e \cdot V_s^2 + f \cdot P \cdot V_s$	0.993	0.78

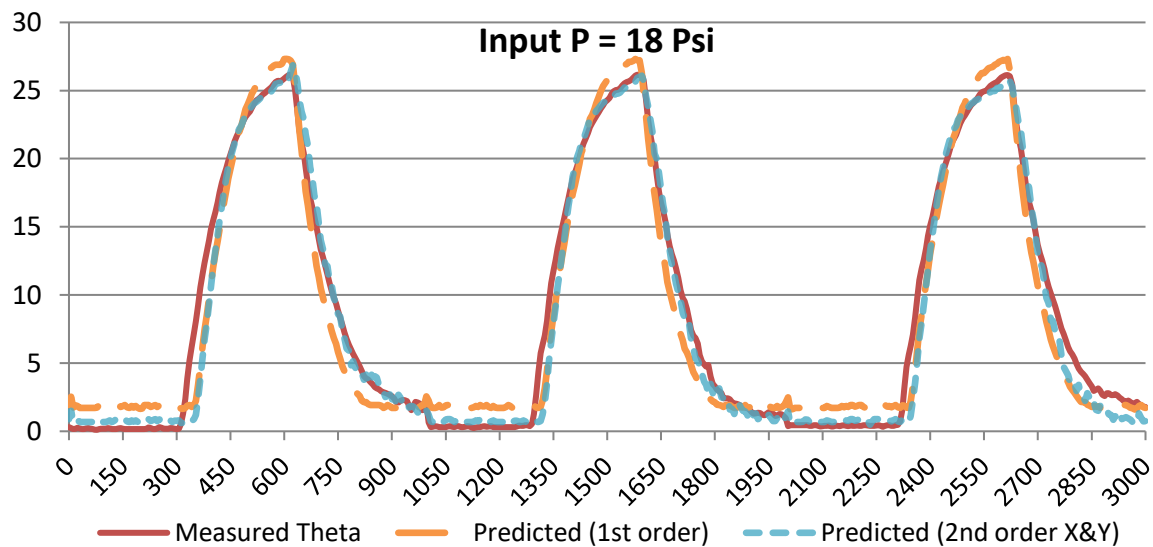


Figure 112: Comparing the prediction accuracy of derived empirical models

7.5.2. Validation Tests

Moreover, in order to validate the derived models, their prediction accuracy has to be tested using new experimental data that was not used in deriving the models. Hence, two additional experiments were performed in which the soft finger was tested at a higher input pressure of 20 Psi and a lower input pressure of 16 Psi. The generated sensory data of 550 samples in total was fed to each model to calculate the predicted bending angle and compare that to the actual

bending angle measured using the vision system. The actual and predicted bending angles for each experiment are plotted in Figure 113. The results confirmed the ability of such simple empirical models to predict the bending angle values using the acquired sensory feedback, with the second order model providing better prediction accuracy with a mean error of only 0.977° and STD of 0.61.

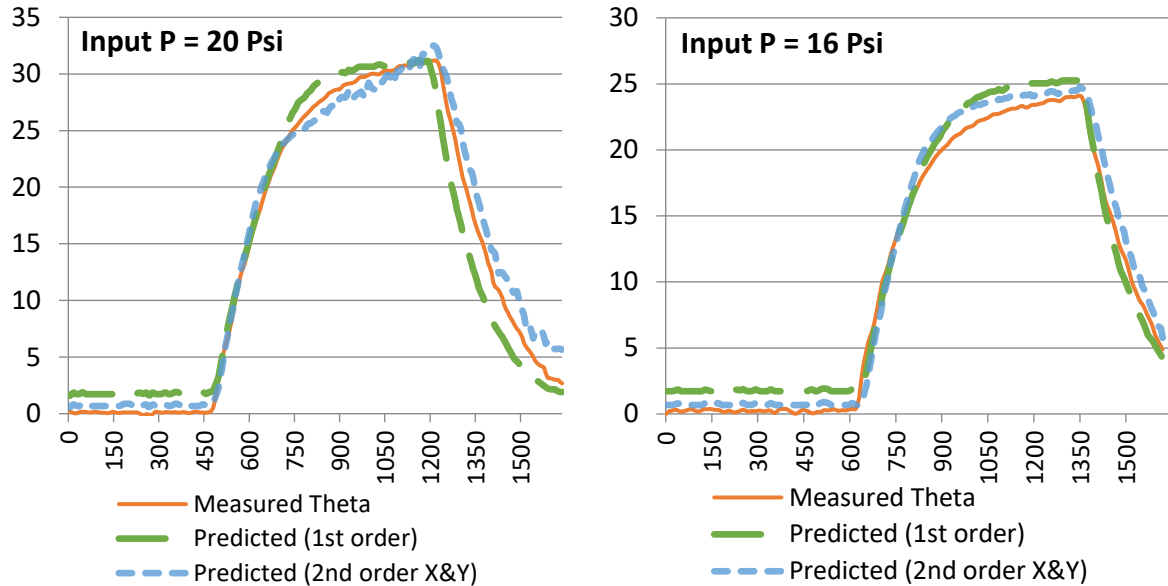


Figure 113: Results of the validation tests

7. 6. Contact Force Analysis

The last experiment conducted with the soft printed actuators with integrated sensor presented here investigates the generated forces upon making contact with a target object. The same setup used for controlled testing of the actuators was used again here, but this time a force/torque sensor with a force post on top was placed beneath the actuator tip to measure the forces generated upon actuation. The samples tested here were for the soft actuator were integrated with the flexible strain sensor presented in the previous sections. The test was repeated twice for input pressures ranging from 12 to 20 Psi in 2 Psi increments. Figure 114 plots the measured resultant contact force response for each test. A consistent increase in the force response is observed when raising the input pressure from 10 to 20 Psi, with both repetitions for each test closely following the same response.

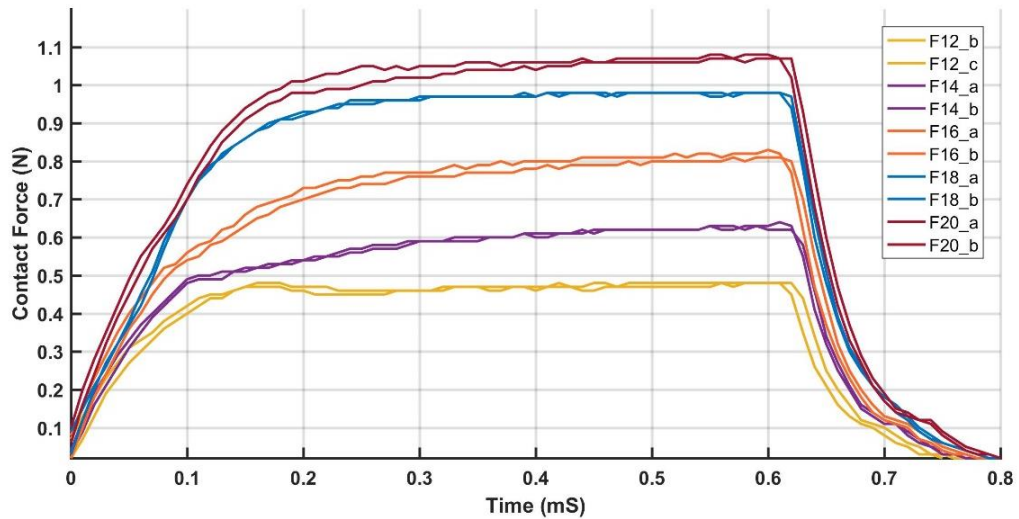


Figure 114: Resultant contact force response for varying input pressure values

Moreover, Figure 115 plots the resulting voltage measurements from the integrated flexible strain sensor during those contact force tests. It is observed that the readings from the sensor continue to increase even though the actuator has been physically stopped when making contact with the force post. This is because the sensor is pushed against the force post causing compressive forces that brings the printed layers of the conductive tracks closer together, which in turn increases the overall resistivity of the sensor causing a further increase in the measured output voltage. Hence, the sensor can be potentially used for simple contact detection as well, which is briefly illustrated in the following test.

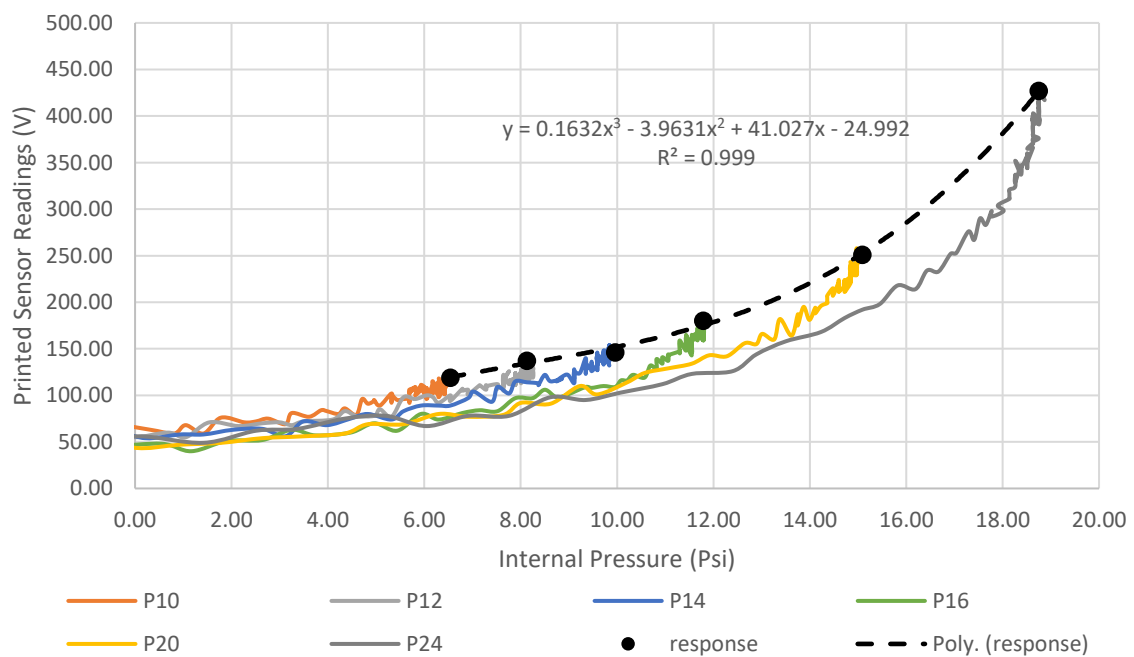


Figure 115: Embedded flex sensor response against input pressures during contact state

In order to highlight the potential for using the integrated strain sensor for contact detection, its response when the actuator is in a contact state is compared to that when in the free bending state at three different input pressure values. Figure 116 highlights the noticeable difference in response for the contact and free states when tested at pressures of 14, 16 and 20 Psi. This means that even though the readings do continue to increase upon making contact, the readings acquired for the free bending state at the same operating condition actually increases with a much higher rate as seen in the graphs. Hence, it is possible to distinguish when contact is made by comparing the real-time sensor response to that of the free bending response at the same input pressure. This provides a simple means of detecting contact during typical grasping applications without the need for integrating additional sensors. Furthermore, Figure 116 also plots the difference in sensor's reading between the free and contact states, against the corresponding measured resultant contact force. The graph shows a linear relationship between the difference in the sensor's readings to the measured resultant contact forces for the tested input pressure values. Clearly, this relation also depends on the contact location and nature of the target object, but those were the same for this test just to facilitate the comparison. Nevertheless, this test highlights the potential for relating this difference in the sensor's readings to make an inference about the strength of the contact forces, which would be useful when grasping delicate objects. Acquiring an exact value for the contact forces will be quite challenging due to the complex nature of this contact, but will still provide useful insight into the magnitude of the forces.

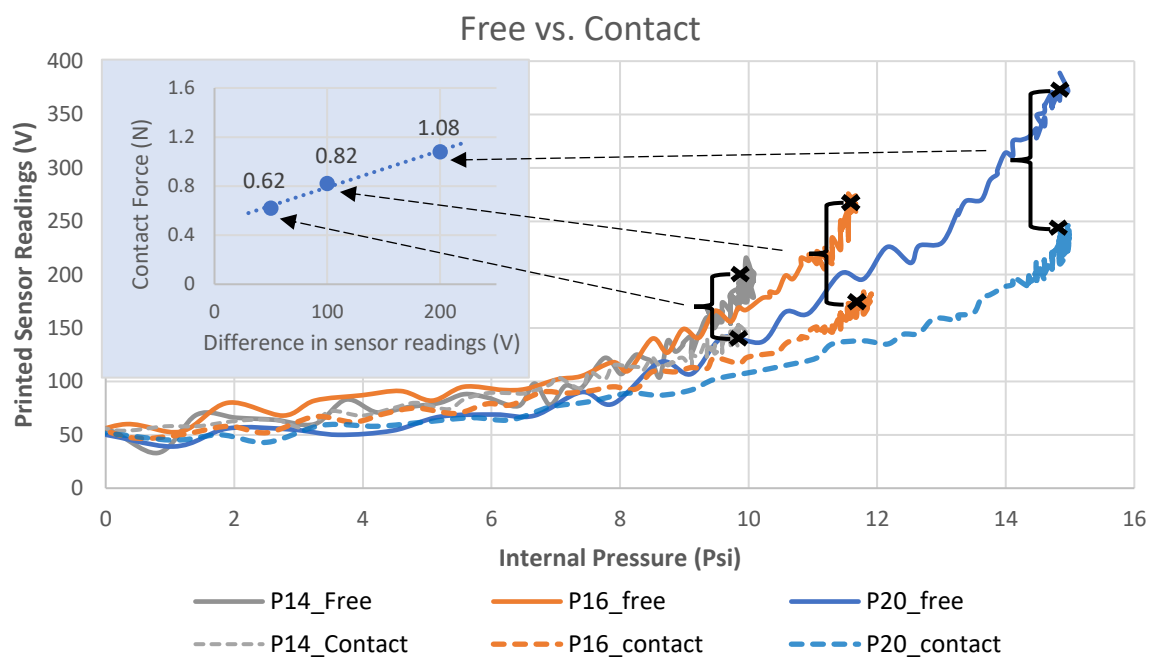


Figure 116: Comparing the free bending response of the embedded sensor to that when making contact

7. 7. Discussion and conclusion

It can be concluded that FFF printing provides an alternative more automated fabrication process for soft grippers that is faster, more repeatable and accurate than the conventional multi-stage manual moulding process. In the same time, FFF printing requires easily accessible hardware and relatively inexpensive materials, when compared to more advanced powder and resin-based 3D printers. Regarding material properties, the flexible material filaments printed using FFF printers have better mechanical properties in terms of tear strength and durability when compared to those produced by polyjet printers, but are not as flexible as the highly stretchable silicone rubbers used with manual moulding. This reduced flexibility, on the other hand, allows printed soft actuators to operate at a higher pressure input range, which can be utilised for enhanced contact force generation. The conventional moulding process that uses flexible silicone rubbers remains a favourable choice for applications where safe interactions with delicate targets is the key challenge, since soft fingers made using this approach are highly compliant and provide a remarkably soft grasp. Yet, for applications requiring a more stable grasp and more accurate positioning, the printed actuators provide a better alternative due to its ability to operate at higher input pressures, while being more dynamically stable as seen in their bending response.

Through systematic experimental analysis, it was shown that the bending response of the printed soft actuators presented here is highly repeatable for a given sample and well consistent across different samples (mean error = 0.83 mm), as long as the morphology and printing parameters remain the same. It was also shown through fatigue tests that after prolonged use the printed actuators exhibit some material relaxation similar to that witnessed by silicone rubbers, but it takes more time to stabilise. Nevertheless, the deviation in the actuator's bending response was measured to be 3.4°, half of which occurs during the first 100 actuations, while the remaining deviation is spread across the remaining 900 actuation cycles. Such a small deviation should not be a major concern for grippers based on those printed actuators since their soft nature can passively adapt to small errors. Furthermore, all the tested actuators were able to withstand input pressures of up to 40 Psi, which is sufficient to excessively deform the actuator to achieve a full bend. Those series of tests confirmed the repeatability and resilience of the soft printed actuators presented here, despite their remarkable flexibility encouraged through minimal shell thickness of 0.6 mm.

Moreover, the integration of flexible printed sensors to the body of the soft gripper fingers is a novel contribution presented in this chapter that offers reliable strain sensing capability,

which soft grippers usually lack. The main advantage here is the fact that low-cost sensors can be easily customised to the actuator dimensions, rather than being limited to the commercially available flex sensors. A dual-extrusion FFF process was tuned to successfully print the sensor body from the flexible NinjaFlex material while simultaneously printing thin conductive tracks using conductive PLA. After signal acquisition, it was shown that the printed sensor provides a consistent output with limited noise, which is comparable to that of the commercially available alternatives, yet enables higher degree of customisation. However, a limitation in this sensor, which is often associated with resistive based sensors, is the drift in readings that becomes evident as it is used for a longer duration. A dummy printed sensor can be connected at the opposing side of the active sensor in the Wheatstone bridge, in order to negate the undesired change in resistance due to drift. Future work should consider modelling the drift response for the conductive PLA material. However, since most actuations lasted for less than 2 seconds, this was not necessary, and the acquisition circuit output was sufficient.

Furthermore, it was also demonstrated that the complete soft actuator with an embedded strain sensor could be directly printed as one piece, though it is difficult to maintain a consistently air-tight actuator and a functional strain sensor. Hence, the proposed two-stage printing and welding offers a more reliable fabrication approach, while requiring only one additional simple welding step to join the actuator and sensor. The printed actuator with integrated strain sensor was tested at varying input pressure to record the sensory feedback and model its free-bending response, following the novel data-driven approach presented in the previous chapter. The derived model was validated using new datasets and successfully provided accurate bending angle estimations with a mean error of 0.977° and STD of 0.61° .

In summary, the outcomes of the work presented here demonstrated the potential of the well established FFF printing process in reliably producing highly flexible soft bending actuators that are consistently air-tight when following the tuned printing parameters documented here. The work goes further beyond the state of the art in this direction, by designing, printing and calibrating flexible strain sensors, and integrating those into the printed actuators for bending feedback. Systematic experimental analysis showed that the bending actuators exhibit a consistent free-bending response, which was successfully modelled empirically following a purely data-driven approach to estimate the bending angle based on the feedback from the integrated printed sensors. Combining printable soft actuators together results in an entirely printable soft gripper with integrated sensing capability, which is inexpensive and fast to fabricate, for applications requiring safe handling of delicate and complex shaped objects.

CHAPTER 8

Conclusions

8. 1. Research Overview

This research was motivated by the need for low-cost adaptable grippers than can gently grasp delicate objects and adapt to variation in their geometries. Conventional rigid gripper would require the integration of sophisticated force and tactile sensing to accurately sense and control the grasping forces. This approach has resulted in complex and bulky grippers with expensive hardware and software requirements. The conducted literature review showed a shift from complex anthropomorphic grippers that are actively compliant, to simpler passively compliant grippers that utilise underactuation to achieve the desired adaptation. The emergence of the soft robotics area provided novel concepts for soft bending actuators that can be utilised as soft gripper fingers to gently interact with delicate objects and passively adapt to their shapes. The grasping mechanism is in a sense delegated to the morphology, relaxing the requirements for precise sensing and control. However, relying solely on the passive compliance has the drawback of lacking any grasp feedback and limited control over the grasp operation. This has motivated research into modelling and controlling the response of different soft actuators so that their bending behaviour can be predicted and potentially controlled. The primary approach towards achieving this, as highlighted in the literature review, was through analytical modelling and finite element methods. This requires characterising the soft materials used in fabrication in order to derive accurate hyperelastic material models that accurately capture their non-linear behaviour. Such approach not only results in computationally expensive analytical models that are not favoured for real-time control applications, but also the accurate models become even more difficult to achieve when reinforcing with embedded or external components, or combining different materials.

Those challenges have motivated the consideration of a purely data-driven modelling approach in this research that elevates the need for complex analytical modelling and material characterisation, providing a more generic modelling approach that is not limited to a specific morphology as long as sufficient experimental data can be generated. This also means that sources of variation arising during the fabrication process can be implicitly reflected in the derived models since it is based on data from real tests of that particular actuator sample. However, being heavily reliant on experimental data means that having larger datasets at broader operating conditions will always aid in developing more accurate and more generic

models. Nevertheless, the derived models proved to be accurate in predicting and controlling the bending response with less than 1° mean bending error even at untrained conditions and despite the reasonably small dataset used in training. Such control accuracy is very difficult to achieve with existing approaches that attempt to model the exact physical deformation. Especially as the complexity of the geometry is increased and combinations of different materials are used. Furthermore, the data-driven approach essentially provides a mapping between inputs and outputs, which does not describe the actual physical deformation captured by analytical or finite element models. Hence, to optimise the morphology according to specific performance objectives, the resulting empirical models will not be as effective as analytical and finite element models. Combining both approaches is an interesting area for further exploration. In this case, a finite element model, even if limited in accuracy, can guide initial experimentation to realise the optimum morphology for a given task. Afterwards, the proposed data-driven approach can be followed to derive simpler and more computationally efficient models for accurate control purposes.

The outcomes of this research provided a simple purely data-driven approach for modelling and controlling soft gripper fingers, as well as an alternative automated fabrication process that allows for better consistency and a higher degree of customisation. The approach was tested at different operating conditions on soft silicone rubber actuators following the ribbed morphology with variable internal channel dimensions, as well as soft 3D printed actuators following the pleated morphology. This showed that the approach is not limited to specific morphology or material, which is a key advantage compared to analytical approaches. The results of this research also showed that limited datasets of sensory feedback acquired during systematic experimentation were sufficient to derive simple empirical models that can be efficiently computed as part of a controller for online position control. Thus, the proposed approach combines the desired traits of passive compliance of soft actuators to gently adapt to various geometries, with the addition of sensory feedback for a more predictable and controllable response. Having sensor-guided soft grippers brings soft grippers closer to real industrial applications as they performance becomes more reliable and controllable.

8. 2. Research Contributions

At the beginning of this research, it was hypothesised that a more controllable soft gripper could be realised following a purely data-driven modelling approach that utilises simple sensory feedback from embedded flexible sensors. Accordingly, four key research questions were identified to tackle the proposed hypothesis. Each research question was successfully addressed in a separate contribution chapter in this thesis. The key achievements identified limitations, and suggested extensions are summarised in the following subsections:

8.2.1. *Vision-aided experimental characterisation of soft bending actuators*

The first step in this research was to experimentally analyse the free-bending response of soft gripper fingers based on the ribbed morphology so that the potential of a purely data-driven approach can be evaluated. The aim was to evaluate the consistency of the response at different actuation pressures and durations for soft fingers of different morphologies. To achieve this an experiment was designed to systematically test soft finger samples made from the same material and with same outer dimensions, but variable internal channel dimensions, at controlled operating conditions. Six different designs for the soft fingers were generated based on variations in the key design parameters defining the internal channel geometry while maintaining the outer dimensions. Additionally, an image processing program was developed to automatically segment the tested sample from the background, track its tip trajectory, calculate the bending angle and cross-sectional area for each image frame. The availability of such experimental data is essential not only to enable systematic performance comparisons between different soft finger designs, but also to be utilised in the next steps for data-driven modelling and control.

Findings and Contributions:

- The free-bending response of an individual soft finger with a given morphology was repeatable for fixed operating conditions. A clear relationship between the input pressure and maximum bending angle can be defined that is unique for each actuator morphology. This relationship can be used for offline control, as the final bending angle can be predicted based on the supplied pressure and actuation duration. In other words, the minimum pressure supply can be identified to ensure that the soft gripper fingers can achieve the desired bending during actuation.
- Increasing the input pressure consistently extends the free-bending response and generates higher forces during contact. However, higher pressures cause a more unstable

response evident as oscillations in the trajectory as the dynamics of the non-linear flexible material becomes more evident at higher accelerations.

- Increasing the number of chambers within a given actuator length increases the maximum bending angle and force generation during contact. Additionally, it was discovered that maintaining a ratio of two between the wall thickness and chamber width, further enhances the bending and contact generation, while minimising undesired radial deformation. This allowed identifying the best performing soft finger design which was adopted in the following modelling and control work.
- The experimental procedure followed here with the aid of the developed vision system provides a simple systematic approach for characterising and comparing different soft actuators. The experimental approach becomes particularly useful when accurate material models and coefficients for the nonlinear hyper-elastic materials are not available.

Limitations and perspective:

- As it is the case with any experimental work, more data and averaged repetitions are always encouraged to minimise random errors and allow further generalisation of the results. Hence, six different morphologies that were repeatedly tested at five different input pressure values covering the practical operating range. Yet, any significant changes in the morphology outside the tested range could introduce other effects that were not captured in the conducted experiment. Hence, additional tests are still required to further generalise the results with better confidence. Alternatively, if many design parameters need to be studied, then an approach combining FEA and experimental tests would be recommended. Although the accuracy of FEA results is difficult to guarantee for soft actuators made from hyperplastic materials and complex geometries, it can still be used to provide general trends on the expected effects of different design parameters, which can then be verified experimentally on selected cases to minimise the number of samples that need to be fabricated and tested.
- Additionally, the setup used in this research allowed controlled operating conditions and facilitated quick repetitions using the automatic image processing program, yet variations arising during fabrication are still difficult to control due to their manual nature. Experience in fabricating soft actuators is required to ensure consistently functional samples that do not suffer from problems such as trapped air bubbles or poor bonding between actuator layers. Thus, three samples per design had to be created to ensure that they all follow the same response. Samples that suffered from fabrication problems

exhibited significantly different response and were hence discarded from the experiment. This limitation has motivated the consideration of 3D printing as an alternative automated fabrication process that can provide more consistent output.

8.2.2. *Accurate data-driven modelling and control for sensorised soft fingers*

The next stage of this research investigated the feasibility of the proposed purely data-driven approach for accurately modelling and controlling the bending response of soft gripper fingers. After surveying the emerging concepts in soft flexible sensors, commercial flex sensors were chosen as a simple and inexpensive solution that can be seamlessly embedded within the soft actuators while maintaining their desired compliance. The next step was to generate sufficient experimental data from testing the soft sensorised finger samples at varying input pressures for the data-driven modelling. Linear regression and Artificial Neural Networks were used to derive an empirical model relating the actual bending angle to the combined sensory feedback. The derived regression model was used as part of a tuned PID controller to estimate the current bending angle based on the combined sensory feedback and regulate supplied pressure using valve switching to meet a target bending angle. The supply pressure is initially set based on the desired maximum bending angle according to the known free-bending models deduced in chapter 4. At that input pressure, the actuator is expected to reach the known final bending angle at the end of the actuation duration, yet the controller regulates the internal pressure to gradually end the actuation and achieve a target reference signal. This way an adequate supply pressure can be pre-set based on the known pressure-bending relationship for that actuator, while on-line control is used to accurately control the bending.

Findings and Contributions:

- Resistive flex sensors were successfully embedded inside soft fingers and their response evaluated through systematic experimentation under different input pressures, durations, and orientations. The tests showed that the sensor's response is well repeatable for fixed operating conditions.
- The results also showed the importance of incorporating the actuator's internal pressure to realise a more generic model that can be valid for variable input pressures. Additionally, the orientation of the actuator during bending has a less significant effect on the response due to gravity, which was incorporated for improved accuracy.
- The prediction accuracy of the ANNs (0.37 MSE) was better than the linear regression model (1.36 MSE) since ANNs are better in handling non-linearity. However, this comes at

the expense of higher computation requirements, which would be harder to deploy on hardware with limited processing power.

- The developed PID controller was able to follow a sinusoidal and stepped reference signals accurately as demonstrated by the tests. The advantage in this controller lies in the fact that the current bending angle is estimated based on the instantaneous measured internal pressure, which means that losses or pressure drops do not affect the prediction accuracy and hence the controller is more robust.
- The results confirmed the feasibility of the proposed data-driven modelling approach in accurately modelling and controlling the bending of soft fingers, without any physical or material models that are difficult to model accurately. The only requirement is to have simple sensory feedback across different operating conditions.

Limitations and perspective:

- Although the developed data-driven models were shown to provide accurate estimations that were validated at untrained operating conditions, the quoted accuracy of the models cannot be guaranteed if tested at levels that are significantly outside the tested range. Hence, it is crucial when collecting the training data to spread the tested levels to cover the expected operating range so that the prediction accuracy can be maintained. Nevertheless, the work presented in this chapter showed how accurate estimations were achieved despite the relatively small datasets used.
- The derived models were concerned with the accurate positioning of a soft finger within its bending plane. However, once contact occurs, the models can no longer be used to estimate bending as the soft fingers become suppressed. In this case, the last bending angle value is where the target object is expected to be, while any further deviation from this value is due to radial bending of the actuator rather than additional bending. This deviation can be potentially utilised for contact detection, and as a qualitative measure of the estimated grasp strength, which was studied in the following chapters.

8.2.3. *Contact detection and size estimation for a modular soft gripper*

The work so far considered the modelling and control of the free bending response of soft gripper fingers. However, once the soft fingers are in contact with an external object, the derived free-bending models are no longer valid. Hence, it is essential to have the ability to identify when contact is made so that the controller can switch from using the free-bending models for bending estimation to provide other grasp quality feedback. In order to study the

response of the sensorised soft fingers during contact state, a soft gripper prototype was created to conduct controlled grasp tests for objects of varying weights and sizes. The potential for utilising the integrated sensing capability of the studied soft fingers for contact detection and providing additional grasp feedback was investigated. The combined flex and pressure sensory feedback from all grasp tests was studied and compared to the free bending case when the gripper is actuated with no object to grasp. The aim of the experiment was to investigate the potential for contact detection, as well as studying the effect of grasped object size and weight on the recorded sensory feedback. Simple contact detection and size estimation were successfully demonstrated using multi-sensory feedback from opposing sensorised soft fingers connected to same pressure supply.

Findings and Contributions:

- Developing a modular, low-cost soft gripper, which is composed of the sensorised soft fingers studied in the previous chapters that can be assembled using 3D printed mounts in different configurations (two, three, or four fingers). This not only facilitates easy swapping between the soft finger of different sizes or stiffness, but also means that replacing damaged fingers can be done with more ease.
- The conducted experiment illustrated a significant difference in the flex sensory response between free and contact states. Hence, contact detection can be simply achieved by monitoring the difference between the known free bending response and the current response during grasping operation. Once the difference exceeds a set threshold, then contact has occurred, and the final bending angle can be recorded. Any deviations in the flex sensory readings beyond this point are due to radial deformation rather than bending.
- The results of the grasping experiments also showed a clear relationship between the object size and final flex sensor readings from opposing soft fingers. However, for object weight, no conclusive relationships could be identified.
- An interesting finding was uncovered during this experiment when plotting the flex sensor response against the measured internal pressure. Two distinct responses can be observed, which depend on the grasping mode. The first response was for all objects grasped at the fingertips in what resembles a precision grasp, while the second was for all objects encapsulated within the gripper in what resembles a power grasp. The deviation from both responses occurs early on, which can provide additional grasp feedback to identify how the target object is being grasped.

- The results were achieved using raw flex sensory feedback, which means that the calibration of individual soft fingers was not required. Instead, conducting few grasp tests with the complete gripper assembly is sufficient. This would be useful for simple pick and place tasks when the exact positioning of each soft finger is not needed, but instead, additional grasp feedback would be desired to detect when contact occurs and confirm if the grasped object is within the expected size range.

Limitations and perspective:

- To be able to further generalise the results from this experiment, more data from grasping a more extensive range of objects would be required. Additionally, the experiment was focused on studying the effects of object size and weight only. Hence, objects of the same profile (spherical) were used for the training dataset and grasped with a fixed gripper orientation, to avoid introducing other sources of variation that could influence the results. Thus, an extension of this work would be to also study the effect of different object profile as well as the gripper orientation, on the acquired sensory feedback. With larger datasets from diverse grasp tests, the use of more advanced machine learning algorithms would be of interest, by which more generic relationships can be deduced based on labelled data.
- The flex sensor was not sensitive enough to distinguish between small differences in object sizes that are less than 10 mm. This is also expected to be the reason why the effect of the change in object weight was not conclusive. The change due to the range of weight change could be minimal that it is difficult to distinguish it from noise. The results are expected to improve when using a higher resolution analogue to digital converter (ADC) so that finer changes in sensor resistance can be measured. Yet, ultimately a more sensitive flex sensor is desired that can be customised according to the application needs.

8.2.4. *Automated fabrication of soft actuators and sensors via FFF printing*

Recognising the limitations of the manual fabrication process of soft actuators and the need for customisable flex sensors, the research continued by investigating the potential of utilising the well-established Fused Filament Fabrication (FFF) processes to directly 3D print sensorised soft fingers. Hence, providing an automated fabrication process that is faster and more consistent, without the influence of human error. A commercially available flexible material filament (NinjaFlex) was tested in printing the soft actuators. The first step was to tune the print parameters and design dimensions so that airtight actuators can be directly printed. The

repeatability of the bending response and fatigue after 1000 cycles were evaluated experimentally. Furthermore, a dual-extruder tool-head printing flexible and conductive filaments simultaneously were utilised to directly printing a customisable flex sensor. The printed sensor was welded to the soft actuator to create a completely printable soft finger module, which was characterised at variable input pressures. Additional tests were also conducted when making contact with an object to evaluate the force capability of the actuator and the effect this has on the sensory feedback. Finally, the proposed data-driven modelling approach was again implemented on the printed soft finger module, as an additional validation of its applicability to different actuator morphologies.

Findings and Contributions:

- Demonstrated successful direct 3D printing of airtight soft fingers as well as flexible strain sensors without the need of additional processing using standard FFF printers. The outcomes of this work provide detailed design guidelines and recommended print setting to ensure successful printing results.
- Systematic characterisation of the printed soft actuators integrated with the printed sensors confirmed the repeatability of the bending response. It was observed that the printed soft finger requires higher input pressures to achieve full bend, which is expected since the material has a higher Shore hardness compared to silicone rubbers. Yet, this also means that larger contact forces can be generated as demonstrated in the force tests.
- The force analysis tests illustrated how the response from the printed flex sensor differs when comparing the free-bending and contact scenarios. Again, this can be utilised for simple contact detection, as proposed with the commercial flex sensor in chapter 5.
- The proposed data-driven approach was successful in accurately modelling the bending response of the printed actuator, in line with the results from chapter 5.

Limitations and perspective:

- Printing highly flexible and air-tight actuators rely on minimising the shell thickness and avoiding printing on unsupported areas. This, in turn, limits the actuator geometry to one that has a constant cross-section printed in sideways. If soft fingers with more complex geometries are desired, then further research in additive manufacturing technologies is required to realise this. Currently, multi-material PolyJet printers are indeed capable of printing very complex geometries. However, the durability of the flexible material choices is poor and tend to fail quickly even while extracting the support materials.

- The conducted fatigue test highlighted that some material relaxation occurs after repeated actuation, which causes the actuator not to retract completely to its original position while having a negligible effect on its final position. Although this does not affect the functionality of the actuator, it can be still minimised easily by retracting the actuator using vacuum instead of passive retraction that is driven solely by the material elasticity.
- An observed limitation with the printed sensor, which is often associated with resistive based sensors, is the drift in measurements after prolonged use. Further work on modelling the sensor's drift can enable automatic drift compensation, which would be important for applications requiring continuous long measurements.
- An interesting observation from this work was the relationship between the contact forces and the deviation in the printed sensor's readings between the free and contact states. However, it is accepted that this simple relationship cannot be generalised since it depends on many other parameters such as the contact location and object type, which were held constant for that test to facilitate comparison. Yet, the results showed how qualitative feedback about the grasping strength can be still inferred as additional grasp quality feedback using the same sensor. This can be even improved by customising the conductive track design for multi-modal sensing capability.
- With the ongoing development of new 3D printing technologies, alternative solutions are expected to enable direct 3D printing of silicone rubbers, as well as the development of better flexible polyjet materials with enhanced mechanical properties. Such developments can open up new possibilities in the automatic fabrication of complex, reliable, and highly flexible soft robotic components.

Future work and applications

An aspect of this research that would benefit from the extension is the work presented in chapter 6, which demonstrated simple contact detection and size estimation. It is envisioned that with a larger dataset from grasping a wide range of objects that vary in size, weight, and profile, more generic relationships can be deduced for enhanced grasp feedback. Yet, the sensitivity of the flex sensor was a limiting factor that needs to be addressed in future work. The 3D printed flex sensor presented in this work could provide an opportunity for further customisation the sensor design for multimodal sensing and enhanced sensitivity with the additional help of higher resolution ADC. A combination of tactile feedback at the tip and bend sensing for the rest of the actuator body can aid in better contact detection that does not require prior knowledge of the free-bending state. Additionally, by introducing variable

conductive track sensitivity, the change in the profile of the actuator can be decoupled from constant curvature bending due to actuation. This not only means that the grasped object profile can be potentially inferred, but also would enable continuous bend sensing even in contact state.

The research scope focused on the grasping process, yet the next step after implementing a successful grasp is to be able to maintain a stable grasp until moving the target safely to its destination. For industrial applications, this needs to be achieved as fast possible to cut down cycle times, which means that a soft gripper mounted on a robot arm could be accelerated quickly between the robot's start and goal positions. The dynamics of the soft finger will be more prominent in this case and will need further investigations to understand how the grasp stability can be affected by accelerating soft grippers of different morphologies. Controlled stiffening would be an interesting research direction to tackle this challenge, so that the desired softness of the fingers can be maintained while grasping, while stiffening the fingers after grasping to maintain a stable grasp. This would be another opportunity demonstrating the benefit of utilising sensorised soft fingers, in this case, to potentially detect slippage and dynamically control the robot acceleration accordingly. Furthermore, combining an additional grasping mode to the pneumatic bending actuators, namely adhesion-based grasping, can combine the benefits of both methods and result in a stable grasp that is less influenced by acceleration. The added adhesion capability, whether static or active, can increase the grasp forces after being successfully picked by the pneumatic soft fingers, which are better in adapting to targets of varying shapes and sizes. The author has already contributed to a paper in this direction combining soft pneumatic gripper with flexible electroadhesion pads [80].

Moreover, in-hand manipulation is another interesting extension to this work that can be investigated based on the results achieved here. Having the ability to control individual soft fingers accurately and receive continuous bending and contact feedback, can facilitate some level of grasp dexterity that is currently difficult to achieve with soft grippers. A more dextrous soft gripper would be desired for field applications that involve manipulation tasks in a cluttered environment, such as harvesting in farms or search and rescue operations in damaged areas. The gripper softness will not only enable passive adaptation to variation in those unstructured environments, but also with added dexterity active grasping can be achieved as the soft gripper gently interacts with the scene to make a grasp more feasible. This would require soft actuators with additional degrees of freedom, which can be another opportunity for utilising 3D printing fabrication to reliably achieve the desired complexity.

Finally, many applications would benefit from more controllable, low cost and customisable soft grippers that combine the traits of passive compliance as well as sensor-guided grasping. A notable application domain is the handling of delicate crops and food products within the agri-food sector. The ability to safely and reliably manipulate delicate food products and crops using affordable and customisable solutions is a bottleneck for automating various tasks from harvesting to packaging. With controllable soft grippers that can be easily customised, modelled and 3D printed this can become more feasible especially for SMEs that cannot afford to invest in expensive robotic grippers, as well as for tasks involving seasonal demands.

REFERENCES

- [1] G. Fantoni *et al.*, “Grasping devices and methods in automated production processes,” *CIRP Ann. - Manuf. Technol.*, vol. 63, pp. 679–701, Jul. 2014.
- [2] E. Mattar, “A survey of bio-inspired robotics hands implementation: New directions in dexterous manipulation,” *Rob. Auton. Syst.*, vol. 61, no. 5, pp. 517–544, May 2013.
- [3] L. Birglen, T. Laliberté, and C. M. Gosselin, “Underactuated Robotic Hands,” *Springer Tracts Adv. Robot.*, vol. 40, p. 244, 2008.
- [4] D. T. Pham Heginbotham, Wilfred B., and D. T. Pham Heginbotham, Wilfred B., *Robot grippers*. Wiley, 1986.
- [5] R. Bogue, “Artificial muscles and soft gripping: a review of technologies and applications,” *Ind. Robot An Int. J.*, vol. 39, no. 6, pp. 535–540, 2012.
- [6] L. U. Odhner *et al.*, “A compliant, underactuated hand for robust manipulation,” *Int. J. Rob. Res.*, vol. 33, pp. 736–752, 2014.
- [7] P. Liljebäck, K. Y. Pettersen, Ø. Stavdahl, and J. T. Gravdahl, “A review on modelling, implementation, and control of snake robots,” *Rob. Auton. Syst.*, vol. 60, no. 1, pp. 29–40, Jan. 2012.
- [8] G. Bao *et al.*, “Soft Robotics: Academic Insights and Perspectives Through Bibliometric Analysis,” *Soft Robot.*, vol. 5, no. 3, pp. 229–241, Jun. 2018.
- [9] D. Trivedi, C. D. Rahn, W. M. Kier, and I. D. Walker, “Soft robotics: Biological inspiration, state of the art, and future research,” *Appl. Bionics Biomech.*, vol. 5, no. 3, pp. 99–117, Dec. 2008.
- [10] J. Rossiter, J. Winfield, and I. Ieropoulos, “Eating, drinking, living, dying and decaying soft robots,” in *Biosystems and Biorobotics*, vol. 17, Springer, 2017, pp. 95–101.
- [11] C. Majidi, “Soft Robotics: A Perspective—Current Trends and Prospects for the Future,” *Soft Robot.*, vol. 1, no. 1, pp. 5–11, Mar. 2014.
- [12] P. Polygerinos, Z. Wang, K. C. Galloway, R. J. Wood, and C. J. Walsh, “Soft robotic glove for combined assistance and at-home rehabilitation,” *Rob. Auton. Syst.*, vol. 73, pp. 135–143, 2015.
- [13] K. C. Galloway *et al.*, “Soft Robotic Grippers for Biological Sampling on Deep Reefs,” *Soft Robot.*, vol. 3, no. 1, pp. 23–33, 2016.
- [14] M. T. Tolley *et al.*, “A Resilient, Untethered Soft Robot,” *Soft Robot.*, vol. 1, no. 3, pp. 213–223, Sep. 2014.
- [15] M. Wehner *et al.*, “An integrated design and fabrication strategy for entirely soft, autonomous robots,” *Nature*, vol. 536, no. 7617, pp. 451–455, 2016.
- [16] A. D. Marchese, C. D. Onal, and D. Rus, “Autonomous Soft Robotic Fish Capable of Escape Maneuvers Using Fluidic Elastomer Actuators,” *Soft Robot.*, vol. 1, no. 1, pp. 75–87, Mar. 2014.

- [17] R. Deimel and O. Brock, "A novel type of compliant and underactuated robotic hand for dexterous grasping," *Int. J. Rob. Res.*, vol. 35, no. 1–3, pp. 161–185, 2016.
- [18] M. Cianchetti *et al.*, "Soft Robotics Technologies to Address Shortcomings in Today's Minimally Invasive Surgery: The STIFF-FLOP Approach," *Soft Robot.*, vol. 1, no. 2, pp. 122–131, 2014.
- [19] M. Cianchetti, M. Calisti, L. Margheri, M. Kuba, and C. Laschi, "Bioinspired locomotion and grasping in water: The soft eight-arm OCTOPUS robot," *Bioinspiration and Biomimetics*, vol. 10, no. 3, pp. 1–19, 2015.
- [20] S. Bauer, S. Bauer-Gogonea, I. Graz, M. Kaltenbrunner, C. Keplinger, and R. Schwödiauer, "25th anniversary article: A soft future: From robots and sensor skin to energy harvesters," *Adv. Mater.*, vol. 26, no. 1, pp. 149–162, Jan. 2014.
- [21] A. D. Marchese, R. K. Katzschmann, and D. Rus, "A Recipe for Soft Fluidic Elastomer Robots," *Soft Robot.*, vol. 2, no. 1, pp. 7–25, 2015.
- [22] F. Ilievski, A. D. Mazzeo, R. F. Shepherd, X. Chen, and G. M. Whitesides, "Soft robotics for chemists," *Angew. Chemie - Int. Ed.*, vol. 50, no. 8, pp. 1890–1895, Feb. 2011.
- [23] J. Hughes, U. Culha, F. Giardina, F. Günther, and A. Rosendo, "Soft Manipulators and Grippers: A Review," *Front. Robot. AI*, vol. 3, no. November, pp. 1–12, 2016.
- [24] J. Shintake, V. Cacucciolo, D. Floreano, and H. Shea, "Soft Robotic Grippers," *Adv. Mater.*, vol. 30, no. 29, 2018.
- [25] B. Mosadegh *et al.*, "Pneumatic networks for soft robotics that actuate rapidly," *Adv. Funct. Mater.*, vol. 24, no. 15, pp. 2163–2170, Apr. 2014.
- [26] F. Daerden and D. Lefeber, "Pneumatic artificial muscles: actuators for robotics and automation," *Eur. J. Mech. Environ. Eng.*, vol. 47, pp. 11–21, 2002.
- [27] Z. Zhang and M. Philen, "Pressurized artificial muscles," *J. Intell. Mater. Syst. Struct.*, vol. 23, no. 3, pp. 255–268, Sep. 2012.
- [28] Y. Sugimoto, K. Naniwa, K. Osuka, and Y. Sankai, "Static and dynamic properties of McKibben pneumatic actuator for self-stability of legged-robot motion," *Adv. Robot.*, vol. 27, no. 6, pp. 469–480, Apr. 2013.
- [29] M. E. Giannaccini, C. Xiang, A. Atyabi, T. Theodoridis, S. Nefti-Meziani, and S. Davis, "Novel Design of a Soft Lightweight Pneumatic Continuum Robot Arm with Decoupled Variable Stiffness and Positioning," *Soft Robot.*, vol. 00, no. 00, p. soro.2016.0066, 2017.
- [30] F. Daerden, D. Lefeber, B. Verrelst, and R. Van Ham, "Pleated pneumatic artificial muscles: actuators for automation and robotics," *2001 IEEE/ASME Int. Conf. Adv. Intell. Mechatronics. Proc. (Cat. No.01TH8556)*, vol. 2, no. July, pp. 738–743, 2001.
- [31] H. Hauser, A. Ijspeert, R. Fuchslin, R. Pfeiffer, and W. Maass, "Towards a theoretical foundation for morphological computation with compliant bodies," *Biol. Cybern.*, no. 2011, pp. 355–370, Jan. 2012.
- [32] Y. Sun, Y. S. Song, and J. Paik, "Characterization of silicone rubber based soft pneumatic actuators," *IEEE Int. Conf. Intell. Robot. Syst.*, pp. 4446–4453, Nov. 2013.

- [33] Y. Xia and G. M. Whitesides, "Soft Lithography," *Annu. Rev. Mater. Sci.*, vol. 28, no. 1, pp. 153–184, 1998.
- [34] R. F. Shepherd *et al.*, "Multigait soft robot.," *Proc. Natl. Acad. Sci. U. S. A.*, vol. 108, no. 51, pp. 20400–3, Dec. 2011.
- [35] P. Polygerinos *et al.*, "Towards a soft pneumatic glove for hand rehabilitation," *IEEE Int. Conf. Intell. Robot. Syst.*, pp. 1512–1517, Nov. 2013.
- [36] S. Wakimoto, K. Suzumori, and K. Ogura, "Miniature Pneumatic Curling Rubber Actuator Generating Bidirectional Motion with One Air-Supply Tube," *Adv. Robot.*, vol. 25, no. 9–10, pp. 1311–1330, 2011.
- [37] H. K. Yap, H. Y. Ng, and C.-H. Yeow, "High-Force Soft Printable Pneumatics for Soft Robotic Applications," *Soft Robot.*, vol. 3, no. 3, pp. 144–158, 2016.
- [38] T. Laliberté, L. Birglen, and M. C. Gosselin, "Underactuation in robotic grasping hands," *Mach. Intell. Robot. Control*, vol. 4, pp. 1–11, 2003.
- [39] M. G. Catalano, G. Grioli, E. Farnioli, a. Serio, C. Piazza, and a. Bicchi, "Adaptive synergies for the design and control of the Pisa/IIT SoftHand," *Int. J. Robot. Res.*, vol. 33, no. 5, pp. 768–782, Apr. 2014.
- [40] M. G. Catalano, G. Grioli, a. Serio, E. Farnioli, C. Piazza, and a. Bicchi, "Adaptive synergies for a humanoid robot hand," *IEEE-RAS Int. Conf. Humanoid Robot.*, pp. 7–14, Nov. 2012.
- [41] M. Ciocarlie *et al.*, "The Velo gripper: A versatile single-actuator design for enveloping, parallel and fingertip grasps," *Int. J. Rob. Res.*, vol. 33, no. 5, pp. 753–767, Feb. 2014.
- [42] M. Grebenstein, *The Functionality-Driven Awiwi Robot Hand*, vol. 98. 2014.
- [43] A. Zisimatos, "Open-source, affordable, modular, light-weight, underactuated robot hands," *2014 IEEE/RSJ Int. Conf. Intell. Robot. Syst. (IROS 2014)*, vol. 14, 2014.
- [44] R. R. Ma, L. U. Odhner, and A. M. Dollar, "A modular, open-source 3D printed underactuated hand," *Proc. - IEEE Int. Conf. Robot. Autom.*, pp. 2737–2743, 2013.
- [45] a. M. Dollar and R. D. Howe, "The Highly Adaptive SDM Hand: Design and Performance Evaluation," *Int. J. Rob. Res.*, vol. 29, no. 5, pp. 585–597, Feb. 2010.
- [46] J. Gafford *et al.*, "Shape Deposition Manufacturing of a Soft, Atraumatic, Deployable Surgical Grasper1," *J. Med. Device.*, vol. 8, no. 3, p. 030927, Jul. 2014.
- [47] S. Shirafuji, S. Ikemoto, and K. Hosoda, "Development of a tendon-driven robotic finger for an anthropomorphic robotic hand," *Int. J. Rob. Res.*, vol. 33, no. 5, pp. 677–693, Feb. 2014.
- [48] Z. Xu and E. Todorov, "Design of a highly biomimetic anthropomorphic robotic hand towards artificial limb regeneration," 2016.
- [49] A. Grzesiak, R. Becker, and A. Verl, "The Bionic Handling Assistant: a success story of additive manufacturing," *Assem. Autom.*, vol. 31, no. 4, pp. 329–333, 2011.
- [50] E. Brown *et al.*, "Universal robotic gripper based on the jamming of granular material," *Proc. Natl. Acad. Sci.*, vol. 107, no. 44, pp. 18809–18814, Oct. 2010.

- [51] J. R. Amend, E. Brown, N. Rodenberg, H. M. Jaeger, and H. Lipson, "A positive pressure universal gripper based on the jamming of granular material," *IEEE Trans. Robot.*, vol. 28, no. 2, pp. 341–350, 2012.
- [52] Y. Wei *et al.*, "A Novel, Variable Stiffness Robotic Gripper Based on Integrated Soft Actuating and Particle Jamming," *Soft Robot.*, vol. 3, no. 3, pp. 134–143, 2016.
- [53] J. Amend and H. Lipson, "The JamHand: Dexterous Manipulation with Minimal Actuation," *Soft Robot.*, vol. 4, no. 1, p. soro.2016.0037, 2017.
- [54] W. Huang, "On the selection of shape memory alloys for actuators," *Mater. Des.*, vol. 23, no. June 2000, pp. 11–19, 2002.
- [55] M. Sreekumar, T. Nagarajan, M. Singaperumal, M. Zoppi, and R. Molfino, "Critical review of current trends in shape memory alloy actuators for intelligent robots," *Ind. Robot An Int. J.*, vol. 34, no. 4, pp. 285–294, 2007.
- [56] M. Follador, M. Cianchetti, a Arienti, and C. Laschi, "A general method for the design and fabrication of shape memory alloy active spring actuators," *Smart Mater. Struct.*, vol. 21, no. 11, p. 115029, Nov. 2012.
- [57] S. Seok, C. D. Onal, K. J. Cho, R. J. Wood, D. Rus, and S. Kim, "Meshworm: A peristaltic soft robot with antagonistic nickel titanium coil actuators," *IEEE/ASME Trans. Mechatronics*, vol. 18, pp. 1485–1497, 2013.
- [58] C. Laschi, M. Cianchetti, B. Mazzolai, L. Margheri, M. Follador, and P. Dario, "Soft robot arm inspired by the octopus," *Adv. Robot.*, vol. 26, no. 7, pp. 709–727, Jan. 2012.
- [59] M. Calisti *et al.*, "An octopus-bioinspired solution to movement and manipulation for soft robots," *Bioinspir. Biomim.*, vol. 6, no. 3, p. 036002, Sep. 2011.
- [60] J. Rossiter, K. Takashima, F. Scarpa, P. Walters, and T. Mukai, "Shape memory polymer hexachiral auxetic structures with tunable stiffness," *Smart Mater. Struct.*, vol. 23, no. 4, p. 045007, Apr. 2014.
- [61] S. Mao *et al.*, "Gait Study and Pattern Generation of a Starfish-Like Soft Robot with Flexible Rays Actuated by SMAs," *J. Bionic Eng.*, vol. 11, no. 3, pp. 400–411, Jul. 2014.
- [62] a. Villoslada, A. Flores, D. Copaci, D. Blanco, and L. Moreno, "High-displacement flexible Shape Memory Alloy actuator for soft wearable robots," *Rob. Auton. Syst.*, Oct. 2014.
- [63] Y. Bar-Cohen, "Electroactive polymers as artificial muscles-capabilities, potentials and challenges," *Handb. biomimetics*, vol. c, pp. 1–9, 2000.
- [64] R. Pelrine, R. Kornbluh, and G. Kofod, "High-Strain Actuator Materials Based on Dielectric Elastomers," *Adv. Mater.*, vol. 12, no. 16, pp. 1223–1225, Aug. 2000.
- [65] Y. Bahramzadeh and M. Shahinpoor, "A Review of Ionic Polymeric Soft Actuators and Sensors," *Soft Robot.*, vol. 1, no. 1, pp. 38–52, Mar. 2014.
- [66] R. K. Jain, S. Datta, and S. Majumder, "Design and control of an IPMC artificial muscle finger for micro gripper using EMG signal," *Mechatronics*, vol. 23, no. 3, pp. 381–394, Apr. 2013.
- [67] S. Sareh, J. Rossiter, A. Conn, K. Drescher, and R. E. Goldstein, "Swimming like algae:

- Biomimetic soft artificial cilia," *J. R. Soc. Interface*, 2013.
- [68] J. Rossiter, K. Takashima, and T. Mukai, "Shape memory properties of ionic polymer-metal composites," *Smart Mater. Struct.*, vol. 21, no. 11, p. 112002, Nov. 2012.
 - [69] G. Kofod, M. Paajanen, and S. Bauer, "Self-organized minimum-energy structures for dielectric elastomer actuators," *Appl. Phys. A*, vol. 85, no. 2, pp. 141–143, Nov. 2006.
 - [70] G. Kofod, W. Wirges, M. Paajanen, and S. Bauer, "Energy minimization for self-organized structure formation and actuation," *Appl. Phys. Lett.*, vol. 90, no. 8, p. 081916, Feb. 2007.
 - [71] G. K. Lau, K. R. Heng, A. S. Ahmed, and M. Shrestha, "Dielectric elastomer fingers for versatile grasping and nimble pinching," *Appl. Phys. Lett.*, vol. 110, no. 18, p. 182906, May 2017.
 - [72] J. Shintake, S. Rosset, B. Schubert, S. Mintchev, D. Floreano, and H. R. Shea, "DEA for soft robotics: 1-gram actuator picks up a 60-gram egg," *Electroact. Polym. Actuators Devices*, vol. 9430, p. 94301S(6pp), 2015.
 - [73] J. Shintake, H. Shea, and D. Floreano, "Biomimetic underwater robots based on dielectric elastomer actuators," *IEEE Int. Conf. Intell. Robot. Syst.*, vol. 2016-Novem, pp. 4957–4962, 2016.
 - [74] A. O'Halloran, F. O'Malley, and P. McHugh, "A review on dielectric elastomer actuators, technology, applications, and challenges," *J. Appl. Phys.*, vol. 104, no. 7, p. 071101, 2008.
 - [75] D. Ruffatto, A. Parness, M. Spenko, and M. Spenko, "Improving controllable adhesion on both rough and smooth surfaces with a hybrid electrostatic/gecko-like adhesive," *J. R. Soc. Interface*, vol. 11, no. 93, p. 20131089, Apr. 2014.
 - [76] K. Asano, F. Hatakeyama, and K. Yatsuzuka, "Fundamental study of an electrostatic chuck for silicon wafer handling," *IEEE Trans. Ind. Appl.*, vol. 38, no. 3, pp. 840–845, May 2002.
 - [77] P. M. Taylor, G. J. Monkman, and G. J. F. Farnworth, "Principles of electroadhesion in clothing robotics," *Int. J. Cloth. Sci. Technol.*, vol. 1, no. 3, pp. 14–20, Mar. 1989.
 - [78] J. Guo, T. Bamber, J. Petzing, L. Justham, and M. Jackson, "Experimental study of relationship between interfacial electroadhesive force and applied voltage for different substrate materials," *Appl. Phys. Lett.*, vol. 110, no. 5, p. 051602, Jan. 2017.
 - [79] J. Shintake, S. Rosset, B. Schubert, D. Floreano, and H. Shea, "Versatile soft grippers with intrinsic electroadhesion based on multifunctional polymer actuators," *Adv. Funct. Mater.*, pp. 1–28, 2015.
 - [80] J. Guo, K. Elgeneidy, C. Xiang, N. Lohse, L. Justham, and J. Rossiter, "Soft pneumatic grippers embedded with stretchable electroadhesion," *Smart Mater. Struct.*, vol. 27, no. 5, p. 055006, 2018.
 - [81] "Bioinspired Dry Adhesive Materials and Their Application in Robotics: A Review," *J. Bionic Eng.*, vol. 13, no. 2, pp. 181–199, Apr. 2016.
 - [82] K. Autumn and A. M. Peattie, "Mechanisms of Adhesion in Geckos," *Integr. Comp. Biol.*, vol. 42, no. 6, pp. 1081–1090, Dec. 2002.
 - [83] Sangbae Kim, M. Spenko, S. Trujillo, B. Heyneman, D. Santos, and M. R. Cutkosky,

- "Smooth Vertical Surface Climbing With Directional Adhesion," *IEEE Trans. Robot.*, vol. 24, no. 1, pp. 65–74, Feb. 2008.
- [84] L. Daler, A. Klaptocz, A. Briod, M. Sitti, and D. Floreano, "A perching mechanism for flying robots using a fibre-based adhesive," 2013.
 - [85] E. W. Hawkes, D. L. Christensen, A. K. Han, H. Jiang, and M. R. Cutkosky, "Grasping without squeezing: Shear adhesion gripper with fibrillar thin film," *Proc. - IEEE Int. Conf. Robot. Autom.*, vol. 2015-June, no. June, pp. 2305–2312, 2015.
 - [86] E. W. Hawkes, H. Jiang, and M. R. Cutkosky, "Three-dimensional dynamic surface grasping with dry adhesion," *Int. J. Rob. Res.*, vol. 35, no. 8, pp. 943–958, Jul. 2016.
 - [87] S. Song, C. Majidi, and M. Sitti, "GeckoGripper: A soft, inflatable robotic gripper using gecko-inspired elastomer micro-fiber adhesives," *IEEE Int. Conf. Intell. Robot. Syst.*, no. Iros, pp. 4624–4629, 2014.
 - [88] H. Shahsavan, S. M. Salili, A. Jákli, and B. Zhao, "Thermally Active Liquid Crystal Network Gripper Mimicking the Self-Peeling of Gecko Toe Pads," *Adv. Mater.*, vol. 29, no. 3, p. 1604021, Jan. 2017.
 - [89] M. Memarian, R. Gorbet, and D. Kulic, "Control of soft pneumatic finger-like actuators for affective motion generation," *IEEE Int. Conf. Intell. Robot. Syst.*, vol. 2015-Decem, pp. 1691–1697, 2015.
 - [90] A. D. Marchese, K. Komorowski, C. D. Onal, and D. Rus, "Design and Control of a Soft and Continuously Deformable 2D Robotic Manipulation System," *Proc. IEEE Int. Conf. Robot. Autom. 2014*, pp. 2189–2196, May 2014.
 - [91] S. Kim, C. Laschi, and B. Trimmer, "Soft robotics: A bioinspired evolution in robotics," *Trends Biotechnol.*, vol. 31, no. 5, pp. 287–294, May 2013.
 - [92] R. Deimel and O. Brock, "A Novel Type of Compliant , Underactuated Robotic Hand for Dexterous Grasping," *Proc. Robot. Sci. Syst.*, p. p18, 2014.
 - [93] A. Zolfagharian, A. Z. Kouzani, S. Y. Khoo, A. A. A. Moghadam, I. Gibson, and A. Kaynak, "Evolution of 3D printed soft actuators," *Sensors Actuators, A Phys.*, vol. 250, pp. 258–272, 2016.
 - [94] R. L. Truby and J. A. Lewis, "Printing soft matter in three dimensions," *Nature*, vol. 540, no. 7633, pp. 371–378, 2016.
 - [95] J. Z. Gul *et al.*, "3D printing for soft robotics—a review," *Sci. Technol. Adv. Mater.*, vol. 19, no. 1, pp. 243–262, 2018.
 - [96] N. W. Bartlett *et al.*, "A 3D-printed, functionally graded soft robot powered by combustion," 2015.
 - [97] B. N. Peele, T. J. Wallin, H. Zhao, and R. F. Shepherd, "3D printing antagonistic systems of artificial muscle using projection stereolithography," *Bioinspir. Biomim.*, vol. 10, no. 5, p. 055003, 2015.
 - [98] R. MacCurdy, R. Katschmann, Y. Kim, and D. Rus, "Printable Hydraulics: A Method for Fabricating Robots by 3D Co-Printing Solids and Liquids," *arXiv Prepr. arXiv1512.03744*,

2015.

- [99] Z. Wang and S. Hirai, "A 3D printed soft gripper integrated with curvature sensor for studying soft grasping," in *SII 2016 - 2016 IEEE/SICE International Symposium on System Integration*, 2017, pp. 629–633.
- [100] B. Ward-Cherrier *et al.*, "The TacTip Family: Soft Optical Tactile Sensors with 3D-Printed Biomimetic Morphologies," *Soft Robot.*, vol. 00, no. 00, p. soro.2017.0052, 2018.
- [101] R. Niiyama, X. Sun, C. Sung, B. An, D. Rus, and S. Kim, "Pouch Motors: Printable Soft Actuators Integrated with Computational Design," *Soft Robot.*, vol. 2, no. 2, pp. 59–70, 2015.
- [102] D. K. Patel, A. H. Sakhaei, M. Layani, B. Zhang, Q. Ge, and S. Magdassi, "Highly Stretchable and UV Curable Elastomers for Digital Light Processing Based 3D Printing," *Adv. Mater.*, vol. 29, no. 15, p. 1606000, 2017.
- [103] J. H. Low *et al.*, "Hybrid Tele-Manipulation System Using a Sensorized 3-D-Printed Soft Robotic Gripper and a Soft Fabric-Based Haptic Glove," *IEEE Robot. Autom. Lett.*, vol. 2, no. 2, pp. 880–887, 2017.
- [104] A. Dijkshoorn *et al.*, "Embedded sensing: Integrating sensors in 3-D printed structures," *J. Sensors Sens. Syst.*, vol. 7, no. 1, pp. 169–181, 2018.
- [105] R. L. Truby *et al.*, "Soft Somatosensitive Actuators via Embedded 3D Printing," *Adv. Mater.*, vol. 30, no. 15, pp. 1–8, 2018.
- [106] J. P. Moore and C. B. Williams, "Fatigue properties of parts printed by PolyJet material jetting," *Rapid Prototyp. J.*, vol. 21, no. 6, pp. 675–685, 2015.
- [107] C. Tröger, A. T. Bens, G. Bermes, R. Klemmer, J. Lenz, and S. Irsen, "Ageing of acrylate-based resins for stereolithography: Thermal and humidity ageing behaviour studies," *Rapid Prototyp. J.*, vol. 14, no. 5, pp. 305–317, 2008.
- [108] T. Sekitani and T. Someya, "Stretchable, large-area organic electronics," *Adv. Mater.*, vol. 22, no. 20, pp. 2228–2246, May 2010.
- [109] N. Lu and D.-H. Kim, "Flexible and Stretchable Electronics Paving the Way for Soft Robotics," *Soft Robot.*, vol. 1, no. 1, pp. 53–62, Mar. 2014.
- [110] M. Amjadi, K. U. Kyung, I. Park, and M. Sitti, "Stretchable, Skin-Mountable, and Wearable Strain Sensors and Their Potential Applications: A Review," *Adv. Funct. Mater.*, vol. 26, no. 11, pp. 1678–1698, 2016.
- [111] Y. Menguc *et al.*, "Soft wearable motion sensing suit for lower limb biomechanics measurements," in *Proceedings - IEEE International Conference on Robotics and Automation*, 2013, pp. 5309–5316.
- [112] J. Chossat, Y. Tao, V. Duchaine, and Y. Park, "Wearable Soft Artificial Skin for Hand Motion Detection with Embedded Microfluidic Strain Sensing," *2015 IEEE Int. Conf. Robot. Autom.*, pp. 2568–2573, 2015.
- [113] R. Matsuzaki and K. Tabayashi, "Highly Stretchable, Global, and Distributed Local Strain Sensing Line Using GaInSn Electrodes for Wearable Electronics," *Adv. Funct. Mater.*, vol.

- 25, no. 25, pp. 3806–3813, 2015.
- [114] R. K. Kramer, C. Majidi, R. Sahai, and R. J. Wood, “Soft curvature sensors for joint angle proprioception,” *IEEE Int. Conf. Intell. Robot. Syst.*, pp. 1919–1926, Sep. 2011.
 - [115] J. B. H. Tok and Z. Bao, “Recent advances in flexible and stretchable electronics, sensors and power sources,” *Sci. China Chem.*, vol. 55, no. 5, pp. 718–725, Feb. 2012.
 - [116] P. Polygerinos *et al.*, “Soft Robotics: Review of Fluid-Driven Intrinsically Soft Devices; Manufacturing, Sensing, Control, and Applications in Human-Robot Interaction,” *Adv. Eng. Mater.*, pp. 1–22, 2017.
 - [117] U. Culha, S. G. Nurzaman, F. Clemens, and F. Iida, “SVAS3: Strain vector aided sensorization of soft structures,” *Sensors*, vol. 14, no. 7, pp. 12748–12770, Jan. 2014.
 - [118] S. Zhu, Y. Huang, and T. Li, “Extremely compliant and highly stretchable patterned graphene,” *Appl. Phys. Lett.*, vol. 104, no. 17, p. 173103, Apr. 2014.
 - [119] M. A. Lacasse, V. Duchaine, and C. Gosselin, “Characterization of the electrical resistance of carbon-black-filled silicone: Application to a flexible and stretchable robot skin,” *Proc. - IEEE Int. Conf. Robot. Autom.*, pp. 4842–4848, May 2010.
 - [120] J. T. Muth *et al.*, “Embedded 3D printing of strain sensors within highly stretchable elastomers,” *Adv. Mater.*, vol. 26, no. 36, pp. 6307–6312, Jun. 2014.
 - [121] M. Issa, D. Petkovic, N. D. Pavlovic, and L. Zentner, “Sensor elements made of conductive silicone rubber for passively compliant gripper,” *Int. J. Adv. Manuf. Technol.*, vol. 69, no. 5–8, pp. 1527–1536, Jun. 2013.
 - [122] D. Petković, M. Issa, N. D. Pavlović, L. Zentner, and Ž. Čojbašić, “Adaptive neuro fuzzy controller for adaptive compliant robotic gripper,” *Expert Syst. Appl.*, vol. 39, no. 18, pp. 13295–13304, Dec. 2012.
 - [123] M. D. Dickey, R. C. Chiechi, R. J. Larsen, E. a. Weiss, D. a. Weitz, and G. M. Whitesides, “Eutectic gallium-indium (EGaIn): A liquid metal alloy for the formation of stable structures in microchannels at room temperature,” *Adv. Funct. Mater.*, vol. 18, no. 7, pp. 1097–1104, Apr. 2008.
 - [124] D. M. Vogt, Y.-L. Park, and R. J. Wood, “Design and Characterization of a Soft Multi-Axis Force Sensor Using Embedded Microfluidic Channels,” *IEEE Sens. J.*, vol. 13, no. 10, pp. 4056–4064, Oct. 2013.
 - [125] Y. L. Park, B. R. Chen, and R. J. Wood, “Design and fabrication of soft artificial skin using embedded microchannels and liquid conductors,” *IEEE Sens. J.*, vol. 12, no. 8, pp. 2711–2718, Aug. 2012.
 - [126] Y. L. Park and R. J. Wood, “Smart pneumatic artificial muscle actuator with embedded microfluidic sensing,” *IEEE SENSORS 2013 - Proc.*, pp. 1–4, Nov. 2013.
 - [127] C. Majidi, R. Kramer, and R. J. Wood, “A non-differential elastomer curvature sensor for softer-than-skin electronics,” *Smart Mater. Struct.*, vol. 20, no. 10, p. 105017, Oct. 2011.
 - [128] Y.-L. Park, C. Majidi, R. Kramer, P. Bérard, and R. J. Wood, “Hyperelastic pressure sensing with a liquid-embedded elastomer,” *J. Micromechanics Microengineering*, vol. 20, no.

12, p. 125029, Dec. 2010.

- [129] E. L. White, J. C. Case, and R. K. Kramer, "Multi-mode strain and curvature sensors for soft robotic applications," *Sensors Actuators, A Phys.*, vol. 253, pp. 188–197, 2017.
- [130] J. Morrow *et al.*, "Improving Soft Pneumatic Actuator fingers through integration of soft sensors, position and force control, and rigid fingernails," in *Proceedings - IEEE International Conference on Robotics and Automation*, 2016, vol. 2016-June, pp. 5024–5031.
- [131] J. C. Case, E. L. White, and R. K. Kramer, "Sensor enabled closed-loop bending control of soft beams," *Smart Mater. Struct.*, vol. 25, no. 4, p. 045018, 2016.
- [132] R. Adam Bilodeau, E. L. White, and R. K. Kramer, "Monolithic fabrication of sensors and actuators in a soft robotic gripper," in *IEEE International Conference on Intelligent Robots and Systems*, 2015, vol. 2015-Decem, pp. 2324–2329.
- [133] V. Wall, G. Zoller, and O. Brock, "A method for sensorizing soft actuators and its application to the RBO hand 2," in *Proceedings - IEEE International Conference on Robotics and Automation*, 2017, pp. 4965–4970.
- [134] M. G. Mohammed and R. Kramer, "All-Printed Flexible and Stretchable Electronics," *Adv. Mater.*, vol. 29, no. 19, 2017.
- [135] M. Cianchetti, F. Renda, A. Licofonte, and C. Laschi, "Sensorization of continuum soft robots for reconstructing their spatial configuration," in *Proceedings of the IEEE RAS and EMBS International Conference on Biomedical Robotics and Biomechatronics*, 2012, pp. 634–639.
- [136] J. Hou, R. H. C. Bonser, and G. Jeronimidis, "Developing tactile sensors for a soft-bodied robot," *2012 IEEE Int. Conf. Robot. Biomimetics, ROBIO 2012 - Conf. Dig.*, pp. 1979–1984, Dec. 2012.
- [137] H. A. Wurdemann *et al.*, "Embedded electro-conductive yarn for shape sensing of soft robotic manipulators," *Proc. Annu. Int. Conf. IEEE Eng. Med. Biol. Soc. EMBS*, vol. 2015-Novem, pp. 8026–8029, 2015.
- [138] S. Sareh, Y. Noh, M. Li, T. Ranzani, H. Liu, and K. Althoefer, "Macrobend optical sensing for pose measurement in soft robot arms," *Smart Mater. Struct.*, vol. 24, no. 12, p. 125024, 2015.
- [139] G. Saggio, F. Riillo, L. Sbernini, and L. R. Quitadamo, "Resistive flex sensors: a survey," *Smart Mater. Struct.*, vol. 25, no. 1, p. 013001, 2016.
- [140] B. S. Homberg, R. K. Katzschmann, M. R. Dogar, and D. Rus, "Haptic identification of objects using a modular soft robotic gripper," in *IEEE International Conference on Intelligent Robots and Systems*, 2015, vol. 2015-Decem, pp. 1698–1705.
- [141] Y. She, C. Li, J. Cleary, and H.-J. Su, "Design and Fabrication of a Soft Robotic Hand With Embedded Actuators and Sensors," *J. Mech. Robot.*, vol. 7, no. May, p. 021007, 2015.
- [142] G. Gerboni, A. Diodato, G. Ciuti, M. Cianchetti, and A. Menciassi, "Feedback control of soft robot actuators via commercial flex bend sensors," *IEEE/ASME Trans. Mechatronics*, vol. 22, no. 4, pp. 1–1, 2017.

- [143] H. M. Jaeger, "Celebrating Soft Matter's 10th Anniversary: Toward jamming by design.," *Soft Matter*, vol. 11, no. 1, pp. 12–27, Dec. 2014.
- [144] M. Manti, V. Cacucciolo, and M. Cianchetti, "Stiffening in Soft Robotics: A Review of the State of the Art," *IEEE Robot. Autom. Mag.*, vol. 23, no. 3, pp. 93–106, 2016.
- [145] P. a L. S. Martins, R. M. N. Jorge, and a. J. M. Ferreira, "A comparative study of several material models for prediction of hyperelastic properties: Application to silicone-rubber and soft tissues," *Strain*, vol. 42, no. 3, pp. 135–147, Aug. 2006.
- [146] H. Lipson, "Challenges and Opportunities for Design, Simulation, and Fabrication of Soft Robots," *Soft Robot.*, vol. 1, no. 1, pp. 21–27, Mar. 2014.
- [147] T. Lu, L. Finkenauer, J. Wissman, and C. Majidi, "Rapid prototyping for soft-matter electronics," *Adv. Funct. Mater.*, vol. 24, no. 22, pp. 3351–3356, Jun. 2014.
- [148] R. Deimel and O. Brock, "A compliant hand based on a novel pneumatic actuator," *Proc. - IEEE Int. Conf. Robot. Autom.*, pp. 2047–2053, 2013.
- [149] F. Iida and C. Laschi, "Soft robotics: Challenges and perspectives," *Procedia Comput. Sci.*, vol. 7, pp. 99–102, Jan. 2011.
- [150] V. Tincani, M. G. Catalano, E. Farnioli, and M. Garabini, "Velvet Fingers : A Dexterous Gripper with Active Surfaces," *2012 IEEE/RSJ Int. Conf. Intell. Robot. Syst.*, pp. 1257–1263, Oct. 2012.
- [151] S. El-Khoury, M. Li, and A. Billard, "On the generation of a variety of grasps," *Rob. Auton. Syst.*, vol. 61, no. 12, pp. 1335–1349, Dec. 2013.
- [152] R. K. Katzschmann, A. D. Marchese, and D. Rus, "Autonomous Object Manipulation Using a Soft Planar Grasping Manipulator," *Soft Robot.*, vol. 2, no. 4, pp. 155–164, 2015.
- [153] R. J. Webster and B. A. Jones, "Design and Kinematic Modeling of Constant Curvature Continuum Robots: A Review," *Int. J. Rob. Res.*, vol. 29, no. 13, pp. 1661–1683, 2010.
- [154] Y. Matia and A. D. Gat, "Dynamics of Elastic Beams with Embedded Fluid-Filled Parallel-Channel Networks," *Soft Robot.*, vol. 2, no. 1, pp. 42–47, 2015.
- [155] F. G. Serchi, A. Arienti, and C. Laschi, "A biomimetic, swimming soft robot inspired by the Octopus vulgaris," in *Lecture Notes in Computer Science (including subseries Lecture Notes in Artificial Intelligence and Lecture Notes in Bioinformatics)*, vol. 7375 LNAI, Springer, Berlin, Heidelberg, 2012, pp. 349–351.
- [156] T. George Thuruthel, Y. Ansari, E. Falotico, and C. Laschi, "Control Strategies for Soft Robotic Manipulators: A Survey," *Soft Robot.*, no. January, p. soro.2017.0007, 2018.
- [157] I. S. Godage, R. Wirz, I. D. Walker, and R. J. Webster, "Accurate and Efficient Dynamics for Variable-Length Continuum Arms: A Center of Gravity Approach," *Soft Robot.*, vol. 2, no. 3, pp. 96–106, 2015.
- [158] M. Luo, M. Agheli, and C. D. Onal, "Theoretical Modeling and Experimental Analysis of a Pressure-Operated Soft Robotic Snake," *Soft Robot.*, vol. 1, no. 2, pp. 136–146, Jun. 2014.
- [159] M. Giorelli, F. Renda, M. Calisti, A. Arienti, G. Ferri, and C. Laschi, "Learning the inverse kinetics of an octopus-like manipulator in three-dimensional space," *Bioinspir. Biomim.*,

- vol. 10, no. 3, p. 035006, 2015.
- [160] Y. Elsayed *et al.*, "Finite Element Analysis and Design Optimization of a Pneumatically Actuating Silicone Module for Robotic Surgery Applications," *Soft Robot.*, vol. 2, no. 00, p. 141031124711007, Oct. 2014.
 - [161] P. Moseley, J. M. Florez, H. A. Sonar, G. Agarwal, W. Curtin, and J. Paik, "Modeling, Design, and Development of Soft Pneumatic Actuators with Finite Element Method," *Adv. Eng. Mater.*, vol. 18, no. 6, pp. 978–988, 2016.
 - [162] A. Sedal, D. Bruder, J. Bishop-Moser, R. Vasudevan, and S. Kota, "A Continuum Model for Fiber-Reinforced Soft Robot Actuators," *J. Mech. Robot.*, vol. 10, no. 2, p. 024501, 2018.
 - [163] X. Wang, T. Geng, Y. Elsayed, C. Saaj, and C. Lekakou, "A unified system identification approach for a class of pneumatically-driven soft actuators," *Rob. Auton. Syst.*, vol. 63, pp. 136–149, 2015.
 - [164] P. Polygerinos *et al.*, "Modeling of Soft Fiber-Reinforced Bending Actuators," *IEEE Trans. Robot.*, vol. 31, no. 3, pp. 778–789, 2015.
 - [165] J. C. Case, E. L. White, and R. K. Kramer, "Soft Material Characterization for Robotic Applications," *Soft Robot.*, vol. 2, no. 2, pp. 80–87, 2015.
 - [166] D. C. Montgomery, E. A. . Peck, and G. Geoffrey Vinning, *Introduction To Linear Regression Analysis*. 2006.
 - [167] M. Giorelli, F. Renda, M. Calisti, A. Arienti, G. Ferri, and C. Laschi, "Neural Network and Jacobian Method for Solving the Inverse Statics of a Cable-Driven Soft Arm with Nonconstant Curvature," *IEEE Trans. Robot.*, vol. 31, no. 4, pp. 823–834, 2015.
 - [168] D. Braganza, D. M. Dawson, I. D. Walker, and N. Nath, "A neural network controller for continuum robots," *IEEE Trans. Robot.*, vol. 23, no. 6, pp. 1270–1277, 2007.
 - [169] J. J. More, "Levenberg. Marquardt Algorithm: Implementation and Theory," in *Numerical analysis*, vol. 630, no. Lecture notes in mathematics, 1977, pp. 105–116.
 - [170] J. G. Ziegler and N. B. Nichols, "Optimum settings for automatic controllers," *ASME Trans.*, vol. 64, no. 6, pp. 759–768, 1942.

APPENDICES

Appendix (A) – Arduino Code for Pneumatic Control Board

```
/* Code was originally based on the code provided on Soft Robotics Toolkit31*/

int prescaler = 256; // set this to match whatever prescaler value you set in CS
registers below

// initialize values for the PWM duty cycle set by pots
float potDC1 = 0;
float potDC2 = 0;
float potDC3 = 0;
float potDC4 = 0;

long previousMillis = 0;          // will store last  actuation time
unsigned long currentMillis = 0;
long actuating_duration = 2300;    // duration at which to actuate
(millisecons) >> now set by POTs
int Max_duration = 4000;           // maximum duration for actuation when POT is
set at max value
long serial_print_interval = 20;   // interval at which to print pressure
readings (millisecons)
long Last_reading_time = 0;

#define Flex_sensor1_pin A15
#define Flex_sensor2_pin A14
#define Flex_sensor3_pin A13
#define Flex_sensor4_pin A12

#define Pressure_sensor1_pin A8
#define Pressure_sensor2_pin A9
#define Pressure_sensor3_pin A10
#define Pressure_sensor4_pin A11

volatile int interrupt_flag = LOW;

int potPWMfq = 50;                // manually setting the freq  until POT is connected to
A7
int Duty_cycle = 100;
int incomingByte = 0;
int target_reps = 1000;
int current_reps = 0;
int x=0;
unsigned int once = 0;

void setup() {

    Serial.begin(9600);

    //  input pins for valve switches
    // pinMode(50, INPUT);
    // pinMode(51, INPUT);
    //pinMode(52, INPUT);
    //pinMode(53, INPUT);

    //  pinMode(21, OUTPUT);    // interrupt pin 21 (for interrupt 2 on arduino Mega)
```

³¹ **Fluidic Control Board:** <https://softroboticstoolkit.com/book/control-board>

```

// attachInterrupt(digitalPinToInterrupt(21), ISR_func_1, RISING); // call
interrupt func when pin 21 is HIGH

// pinMode(20, OUTPUT); // interrupt pin 20 (for interrupt 3 on arduino Mega
// attachInterrupt(digitalPinToInterrupt(20), ISR_func_2, RISING); // call
interrupt func when pin 20 is HIGH

pinMode(19, OUTPUT); // interrupt pin 20 (for interrupt on arduino Mega
attachInterrupt(digitalPinToInterrupt(19), ISR_func_3, RISING); // call interrupt
func when pin 19 is HIGH

pinMode(18, OUTPUT); // interrupt pin 20 (for interrupt on arduino Mega
// attachInterrupt(digitalPinToInterrupt(18), ISR_func_4, RISING); // call
interrupt func when pin 18 is HIGH

// output pins for valve PWM
pinMode(5, OUTPUT); digitalWrite (5, LOW); // initialise output pin for valve
selonoid to be low
pinMode(6, OUTPUT); digitalWrite (6, LOW); // initialise output pin for valve
selonoid to be low
pinMode(7, OUTPUT); digitalWrite (7, LOW); // initialise output pin for valve
selonoid to be low
pinMode(8, OUTPUT); digitalWrite (8, LOW); // initialise output pin for valve
selonoid to be low

pinMode(4, OUTPUT); // for 5th port on MOSFET circuit (powering up step down
volt reg)
digitalWrite (4, HIGH); // keep 5th port on MOSFET circuit on to maintain 24V
supply to breadboard

pinMode(10, OUTPUT); // camera external trigger pin
digitalWrite (10, LOW); // initially LOW

int eightOnes = 255; // this is 11111111 in binary
TCCR3A &= ~eightOnes; // this operation (AND plus NOT), set the eight bits in
TCCR registers to 0
TCCR3B &= ~eightOnes;
TCCR4A &= ~eightOnes;
TCCR4B &= ~eightOnes;

// set waveform generation to frequency and phase correct, non-inverting PWM
output
TCCR3A = _BV(COM3A1);
TCCR3B = _BV(WGM33) | _BV(CS32);

TCCR4A = _BV(COM4A1) | _BV(COM4B1) | _BV(COM4C1);
TCCR4B = _BV(WGM43) | _BV(CS42);
}

void pPWM(float pwmfreq, float pwmDC1, float pwmDC2, float pwmDC3, float pwmDC4) {

// set PWM frequency by adjusting ICR (top of triangle waveform)
ICR3 = F_CPU / (prescaler * pwmfreq * 2);
ICR4 = F_CPU / (prescaler * pwmfreq * 2);

// set duty cycles
OCR3A = (ICR4) * (pwmDC1 * 0.01);
OCR4A = (ICR4) * (pwmDC2 * 0.01);
OCR4B = (ICR4) * (pwmDC3 * 0.01);
OCR4C = (ICR4) * (pwmDC4 * 0.01);
}

```

```

void loop()
{
    if (interrupt_flag == HIGH)
    {
        currentMillis = millis();
        potDC1 = 0; potDC2 = 0; potDC3 = 0; potDC4 = 0; // reset duty cycles to zero
        for all
            // pPWM(potPWMfq,potDC1,potDC2,potDC3,potDC4); // sends freq and duty
            cycle to func

        if (once == 0)
        {
            previousMillis = millis();
            once=1; // dont enter this function again
        }

        while (current_reps < target_reps) // cycle through this until
        reaching target repitions
        {
            digitalWrite (10, HIGH); // enable camera trigger >> take
            photo (initial pos)
            delay (10); // wait to ensure photo is taken
            at initial position
            digitalWrite (10, LOW); // disable camera trigger

            potDC3 = Duty_cycle; // open valve 3 full to start
            actuation
            pPWM(potPWMfq,potDC1,potDC2,potDC3,potDC4); // sends freq and duty
            cycle to func

            currentMillis = millis();

            while (currentMillis - previousMillis <= actuating_duration)
            {
                currentMillis = millis();
            }

            digitalWrite (10, LOW); // disable camera trigger
            delay (5); // wait to ensure photo is taken
            digitalWrite (10, HIGH); // enable camera trigger >> take
            photo (final pos)
            delay (10); // wait to ensure photo is taken
            digitalWrite (10, LOW); // disable camera trigger

            potDC3 = 0; // close valve 3 to stop
            actuation
            pPWM(potPWMfq,potDC1,potDC2,potDC3,potDC4); // sends freq and duty
            cycle to func

            delay (700); // wait to ensure full retraction

            float P = (analogRead(Pressure_sensor2_pin)/1024.0 - 0.1)*100.0/0.8; //
            read pressure sensor and convert to PSI
            int Flex = analogRead(Flex_sensor1_pin); // read voltage from flex
            sensor in finger 1

            Serial.print(P); Serial.print("\t");
            Serial.print(Flex); Serial.print("\n"); // print all readings

            current_reps ++; // increment current repetition
            value

            previousMillis = millis();
        }
        interrupt_flag=0; // reset interrupt flag
        once=0; // reset once before leaving
    }
}

```

```

else
{
    once=0;
}
}

void ISR_func_1() // interrupt func for MODE1: actuate first set of opposing
fingers
{
    interrupt_flag = HIGH;
    actuating_duration = actuating_duration;
    digitalWrite (10, HIGH); // enable camera trigger
    digitalWrite (5, HIGH); // activate port 1 for valve selonoid (start actuation)
    potDC1 = Duty_cycle; // manually setting duty cycles
    pPWM(potPWMfq,potDC1,potDC2,potDC3,potDC4); // sends freq and duty cycle to
func
}

void ISR_func_2() // interrupt func for MODE2: actuate second set of opposing
fingers
{
    interrupt_flag = HIGH;
    actuating_duration = actuating_duration;
    digitalWrite (10, HIGH); // enable camera trigger
    digitalWrite (6, HIGH); // activate port 2 for valve selonoid (start actuation)
    potDC2 = Duty_cycle; // manually setting duty cycles
    pPWM(potPWMfq,potDC1,potDC2,potDC3,potDC4); // sends freq and duty cycle to
func
}

void ISR_func_3() // interrupt func for MODE4: actuate ALL four fingers
{
    interrupt_flag = HIGH;
    digitalWrite (10, HIGH); // enable camera trigger
    digitalWrite (5, HIGH); // activate port 1 for valve selonoid (start actuation)
    digitalWrite (6, HIGH); // activate port 2 for valve selonoid (start actuation)
    pPWM(potPWMfq,potDC1,potDC2,potDC3,potDC4); / use pot values for pwm activation
of vales
}

```


Appendix (B) – Halcon Image Processing Code

```
** ----- Inputs:
number_of_images := 240
Finger_no := 'Finger 5 embed'
Pressure := '10 Psi'
Time := '2000 ms'
orient_angle := '0 deg'

** ----- Tuning parameters:
* Maximum angle between 2 contour tangents to union them (0.55)
Max_contour_angle := 0.55
* min length of contour to preserve after splitting (125)
Min_contour_length := 120
* smoothing edges (was 2.5)
opening_value := 3
* no of columns of output matrix
matrix_columns := 11
* run program on steps or continuously (if =0)
enable_stop := 0
* offset threshold value to remove noise (12-24)
threshold_offset := 20

** ----- load calibration parameters:
*CameraParameters := [0.0171191, 148.823, 5.6006e-006, 5.6e-006, 318.812, 270.551,
655, 490]
*CameraPose := [-0.0252656, -0.0176713, 0.449446, 357.332, 1.40636, 269.326, 0]
read_cam_par ('C:/Users/mmkame/Dropbox/PhD/Experiments/Controlling_Bending/Camera
callib/cam_param.cal', CameraParameters)
read_pose ('C:/Users/mmkame/Dropbox/PhD/Experiments/Controlling_Bending/Camera
callib/cam_pose.dat', CameraPose)

** ----- load images:
read_image (background, 'C:/Users/mmkame/Desktop/Controlling_Bending/orient=-
45/background.tiff')
*rgb1_to_gray (background, Gray_background)
dev_resize_window_fit_image (background, 0, 0, -1, -1)
*mean_image (background, background, 9, 9)
create_matrix (number_of_images, matrix_columns, 0, results)

for i := 1 to number_of_images by 1
read_image (Image, 'C:/Users/mmkame/Desktop/Controlling_Bending/orient=-
45/P=8/Frame ('+i+')')
if (i=1)
draw_point (3600, org_Row, org_Column)
endif

** ----- Segmentation:
*sub_image (Image, background, ImageSub1, 1, 128)
smooth_image (Image, Image, 'gauss', 0.2)
*threshold (Image, RegionDynThresh, 135, 200)
dyn_threshold (Image, background, RegionDynThresh, threshold_offset, 'light')
opening_circle (RegionDynThresh, RegionOpening, opening_value)
* opening_rectangle1 (RegionDynThresh, RegionOpening, 12, 12)
* set_system ('max_connection', '4')
connection (RegionOpening, ConnectedRegions)
*area_center (ConnectedRegions, Area, Row1, Column1)
select_shape (ConnectedRegions, SelectedRegions, 'area', 'and', 10000, 100000)
*get_region_polygon (SelectedRegions, 5, Rows3, Columns3)
*dev_clear_window ()
*disp_polygon (3600, Rows3, Columns3)
*gen_struct_elements (StructElements, 'noise', 10, 10)
*fitting (SelectedRegions, StructElements, RegionFitted)
*points_lepetit (Image, 3, 1, 15, 30, 'interpolation', Row2, Column2)
*disp_polygon (3600, Row2, Column2)

** ----- Region properties:
region_features (SelectedRegions, 'area', blob_area)
```

```

*Row index of upper left corner (ref)
region_features (SelectedRegions, 'row1', upper_left_Y)
*Column index of upper left corner (ref)
region_features (SelectedRegions, 'column1', upper_left_X)
*Row index of lower right corner (tip)
region_features (SelectedRegions, 'row2', lower_right_Y)
*Column index of lower right corner (tip)
region_features (SelectedRegions, 'column2', lower_right_X)
*draw_point (3600, Row, Column)

** ----- generating contour and splitting:
get_region_polygon (SelectedRegions, 2, Rows, Columns)
*dev_clear_window ()
*disp_polygon (3600, Rows, Columns)
*get_region_points (SelectedRegions, Rows1, Columns1)
*tuple_min (Rows1, minY)
*sub_image (Image, background, ImageSub1, 1, 128)
*edges_sub_pix (ImageSub1, Edges, 'canny', 1, 20, 40)
gen_contour_polygon_xld (Contour, Rows, Columns)
*intersection_closed_contours_xld (Contour, Contour, ContoursIntersection1)
*select_contours_xld (ContoursIntersection1, SelectedContours3, 'contour_length',
1000, 3000, -0.5, 0.5)
gen_polygons_xld (Contour, Polygons1, 'ramer', 1)
*segment_contours_xld (SelectedContours3, ContoursSplit4, 'lines_circles', 2, 4, 2)
split_contours_xld (Polygons1, Contours1, 'polygon', 10, 20)
smooth_contours_xld (Contours1, Contours1, 5)

** ----- processing generated contours to select only 2 (upper & lower)
*get_contour_attrib_xld (Contours1, 'regr_norm_row', lengths)
count_obj (Contours1, Number_contours)
if (Number_contours > 2)
    if (Number_contours > 4)
        union_cotangential_contours_xld (Contours1, UnionContours1, 0, 20,
Max_contour_angle, 5, 10, 2, 'attr_forget')

        else
            UnionContours1 := Contours1
        endif
        select_contours_xld (UnionContours1, SelectedContours4, 'contour_length',
Min_contour_length, 2000, -0.5, 0.5)

        count_obj (SelectedContours4, Number_contours_2)

        if (Number_contours_2>2)
            *union_cotangential_contours_xld (SelectedContours4, SelectedContours5,
0, 20, 1, 5, 10, 2, 'attr_forget')
            union_adjacent_contours_xld (SelectedContours4, UnionContours5, 10,
0.8, 'attr_keep')

            SelectedContours4 := UnionContours5
        endif
    else
        SelectedContours4 := Contours1
    endif
*union_cocircular_contours_xld (Contours1, UnionContours2, 0.5, 0.2, 0.2, 30, 30,
20, 'true', 1)

* get_contour_attrib_xld (ContoursIntersection1, 'edge_direction', Attrib)
*segment_contour_attrib_xld (ContoursSplit4, ContourPart, 'distance', 'and', 150,
99999)
*clip_end_points_contours_xld (SelectedContours4, ClippedContours, 'num_points', 1)
*count_obj (UnionContours1, Number_contours)

** ----- fitting ellipse to each of the 2 contours selected
select_obj (SelectedContours4, upper_contour, 1)
*fit_circle_contour_xld (upper_contour, 'atukey', -1, 0, 0, 3, 2, Row6, Column6,
upp_Radius, StartPhi2, EndPhi2, PointOrder2)

```

```

fit_ellipse_contour_xld (upper_contour, 'ftukey', -1, 0, 0, 200, 3, 2, Row7,
Column7, Phi1, Radius1_upper, Radius2_upper, StartPhi4, EndPhi4, PointOrder4)
select_obj (SelectedContours4, lower_contour, 2)
*fit_circle_contour_xld (lower_contour, 'atukey', -1, 0, 0, 3, 2, Row5, Column5,
lower_Radius, StartPhi1, EndPhi1, PointOrder1)
fit_ellipse_contour_xld (lower_contour, 'ftukey', -1, 0, 0, 200, 3, 2, Row8,
Column8, Phi2, Radius1_low, Radius2_low, StartPhi5, EndPhi5, PointOrder5)
length_xld (upper_contour, Length_upper_contour)
length_xld (lower_contour, Length_lower_contour)

** ----- define upper & lower based on their length (assuming upper is always
longer)
tuple_greater (Length_upper_contour, Length_lower_contour, Greater)
if (Greater)
    first_contour := upper_contour
    second_contour := lower_contour
else
    first_contour := lower_contour
    second_contour := upper_contour
endif

** ----- get end point of upper & lower contours

get_contour_xld (first_contour, upper_cont_row, upper_cont_col)
get_contour_xld (second_contour, lower_cont_row, lower_cont_col)

tuple_length (lower_cont_col, no_Xs_lower)
tuple_length (lower_cont_row, no_Ys_lower)

tuple_length (upper_cont_col, no_Xs_upper)
tuple_length (upper_cont_row, no_Ys_upper)

** ----- selects last point as tip point considering idx writing direction
(useless)
if (PointOrder5 = 'positive')
    idx_y := 0
    idx_x := 0
elseif (PointOrder5 = 'negative')
    idx_y := 0
    idx_x := 0
endif

lower_tip_Y := lower_cont_row[idx_y]
lower_tip_X := lower_cont_col[idx_x]

*****
if (PointOrder4 = 'positive')
    idx_y := no_Ys_upper - 1
    idx_x := no_Xs_upper - 1
elseif (PointOrder4 = 'negative')
    idx_y := no_Ys_upper - 1
    idx_x := no_Xs_upper - 1
endif

upper_tip_Y := upper_cont_row[idx_y]
upper_tip_X := upper_cont_col[idx_x]

** ----- calculate Final coordinates for midpoint between 2 tip points
Tip_X := (upper_tip_X+lower_tip_X)/2
Tip_Y := (upper_tip_Y+lower_tip_Y)/2

*Org_X := (upper_org_X+lower_org_X)/2
*Org_Y := (upper_org_Y+lower_org_Y)/2

*dev_clear_window ()
dev_display (Image)
dev_display (SelectedRegions)

```

```

dev_set_color ('green')
gen_circle (Circle, Tip_Y, Tip_X, 5.5)
dev_display (Circle)

*draw_point (3600, Row4, Column4)

dev_set_color ('cyan')
*dev_display (upper_contour)
*gen_circle_contour_xld (ContCircle1, Row6, Column6, upp_Radius, StartPhi2,
EndPhi2, 'negative', 1)
gen_ellipse_contour_xld (ContEllipse_upp, Row7, Column7, Phi1, Radius1_upp,
Radius2_upp, StartPhi4, EndPhi4, PointOrder4, 1)
length_xld (ContEllipse_upp, upper_Length)

dev_set_color ('yellow')
*dev_display (lower_contour)
*gen_circle_contour_xld (ContCircle, Row5, Column5, lower_Radius, StartPhi1,
EndPhi1, 'positive', 1)
gen_ellipse_contour_xld (ContEllipse_low, Row8, Column8, Phi2, Radius1_low,
Radius2_low, StartPhi5, EndPhi5, PointOrder5, 1)
length_xld (ContEllipse_low, lower_Length)
dev_set_color ('red')
* fit_circle_contour_xld (SelectedContours4, 'algebraic', -1, 0, 0, 3, 2, Row3,
Column3, Radius, StartPhi, EndPhi, PointOrder)
*disp_circle (3600, Row3, Column3, Radius)
*disp_arc (3600, Row3, Column3, 3.14159, Row3, Column3)
*fit_line_contour_xld (UnionContours, 'tukey', -1, 0, 5, 2, RowBegin1, ColBegin1,
RowEnd1, ColEnd1, Nr1, Nc1, Dist1)
*disp_line (3600, RowBegin1, ColBegin1, RowEnd1, ColEnd1)
*detect_edge_segments (Image, 5, 32, 3, 20, BeginRow1, BeginCol1, EndRow1, EndCol1)

** ----- convert to world coordinates using camera calibration file
*read_cam_par ('C:/Users/mmkame/Dropbox/PhD/Soft Finger Analysis (9-12-15)/Camera
Callib/Basler_acA640-120gm.dat', CameraParameters)
*read_pose ('C:/Users/mmkame/Dropbox/PhD/Soft Finger Analysis (9-12-15)/Camera
Callib/CameraPose.dat', CameraPose)

    image_points_to_world_plane (CameraParameters, CameraPose, Tip_Y, Tip_X, 'mm',
Tip_X_mm, Tip_Y_mm)
    *image_points_to_world_plane (CameraParameters, CameraPose, upper_left_Y,
upper_left_X, 'mm', upper_left_X_mm, upper_left_Y_mm)
    image_points_to_world_plane (CameraParameters, CameraPose, org_Row, org_Column,
'mm', org_X_mm, org_Y_mm)

    contour_to_world_plane_xld (lower_contour, lower_contour_mm, CameraParameters,
CameraPose, 'mm')
    length_xld (lower_contour_mm, Length_lower_contour_mm)

    contour_to_world_plane_xld (upper_contour, upper_contour_mm, CameraParameters,
CameraPose, 'mm')
    length_xld (upper_contour_mm, Length_upper_contour_mm)

** ----- converting remaining parameters using pixel/mm ratio
blob_area_mm2 := blob_area/46.376
Radius1_upp_mm := Radius1_upp/6.81
Radius2_upp_mm := Radius2_upp/6.81
Radius1_low_mm := Radius1_low/6.81
Radius2_low_mm := Radius2_low/6.81

** writing output to matrix
set_value_matrix (results, i-1, 0, org_X_mm)
set_value_matrix (results, i-1, 1, org_Y_mm)
set_value_matrix (results, i-1, 2, Tip_X_mm)
set_value_matrix (results, i-1, 3, Tip_Y_mm)
set_value_matrix (results, i-1, 4, blob_area_mm2)
set_value_matrix (results, i-1, 5, Length_upper_contour_mm)
set_value_matrix (results, i-1, 6, Length_lower_contour_mm)

```

```

set_value_matrix (results, i-1, 7, Radius1_upp_mm)
set_value_matrix (results, i-1, 8, Radius2_upp_mm)
set_value_matrix (results, i-1, 9, Radius1_low_mm)
set_value_matrix (results, i-1, 10, Radius2_low_mm)
* save the matrix automatically in the corresponding folder & name it accordingly
write_matrix (results, 'ascii',
'C:/Users/mmkame/Desktop/Controlling_Bending/orient=-45/P=8/RESULTS.mtx')

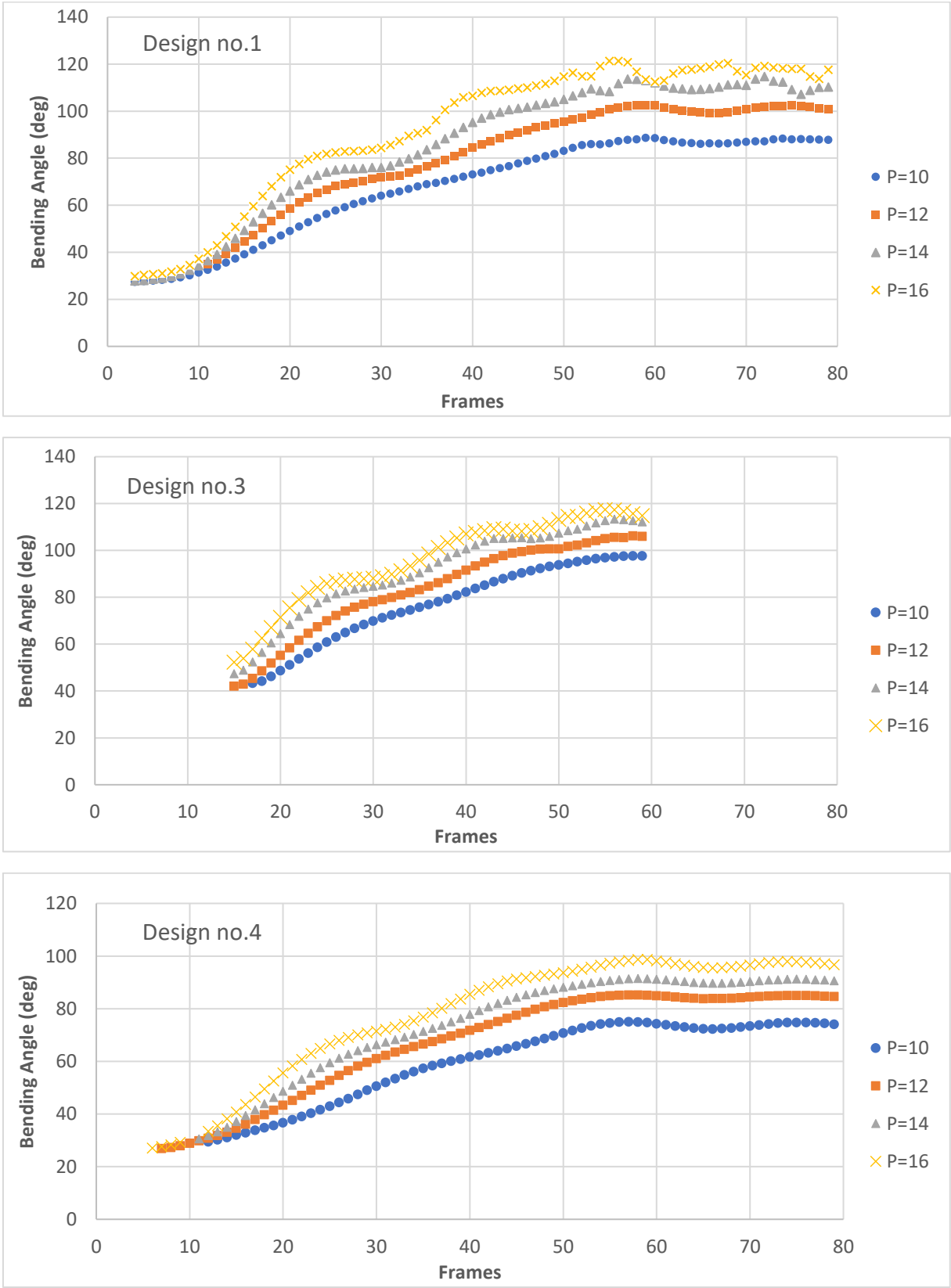
** ----- create an array for all points to use later in plotting trajectory
Tip_X_array[i-1] := Tip_X
Tip_Y_array[i-1] := Tip_Y
*create_funct_ld_array (blob_area, Finger_area)
*create_funct_ld_pairs (upper_left_X, upper_left_Y, ref_coordinates)
*create_funct_ld_pairs (lower_right_X, lower_right_Y, tip_coordinates)
*write_funct_ld (tip_coordinates, 'C:/Users/mmkame/Desktop/tip_coordinates')
if (enable_stop =1)
    stop ()
endif
endfor

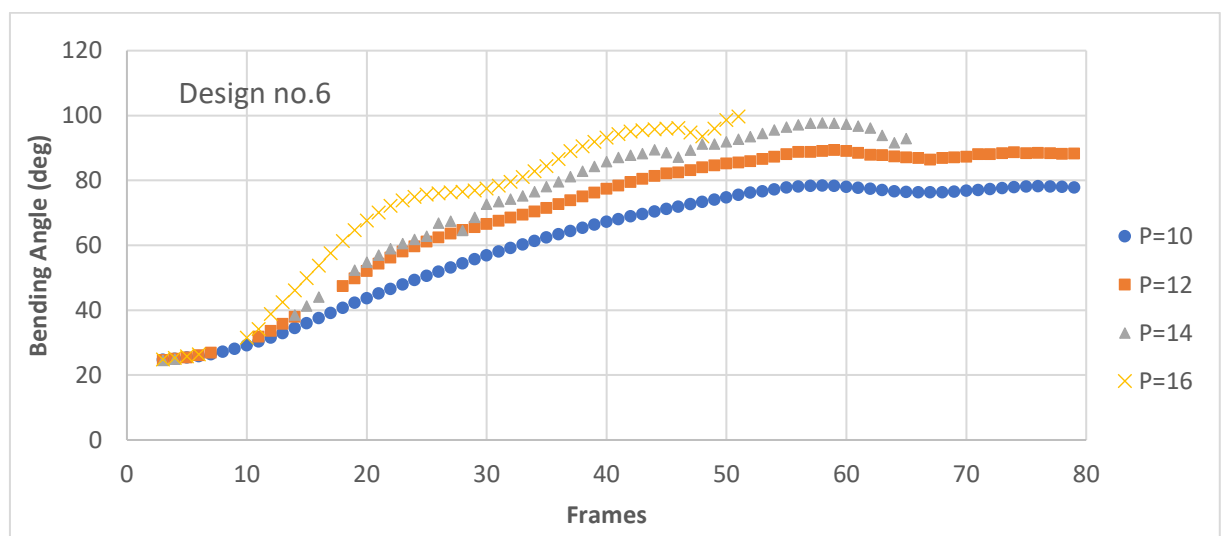
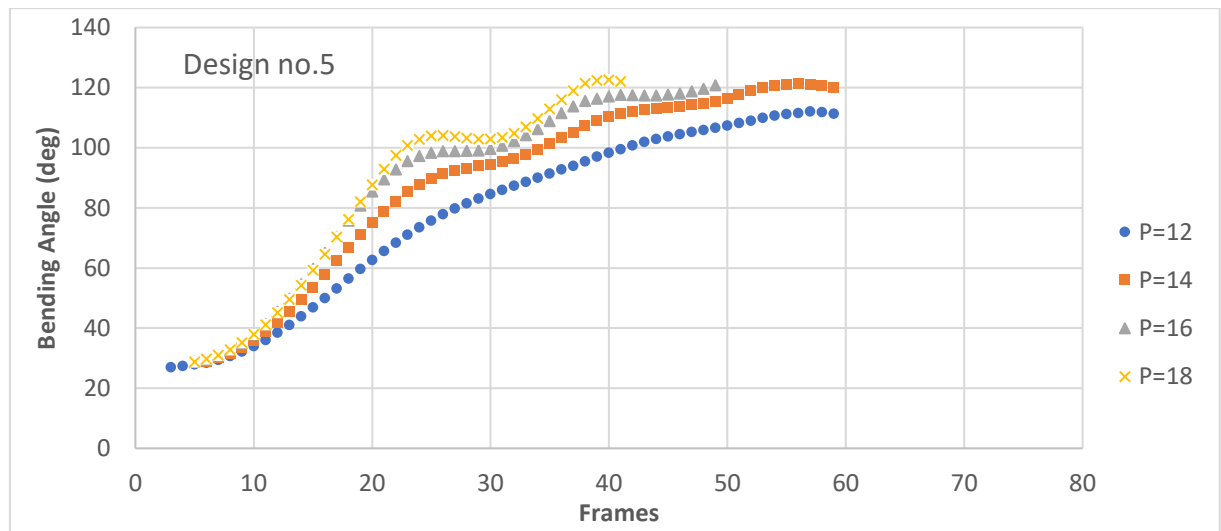
** ----- plot all tip points using the array to create trajectory
dev_set_color ('green')
for j := 1 to number_of_images by 1
    gen_circle (Circle, Tip_Y_array[j-1], Tip_X_array[j-1], 5.5)
    dev_display (Circle)
endfor

```

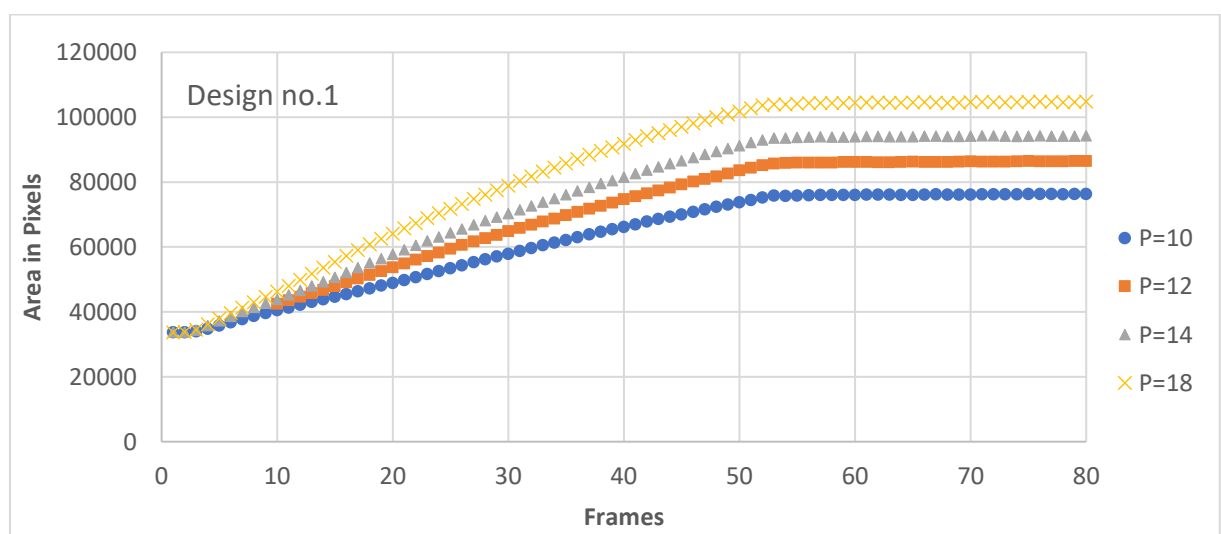
Appendix (C) – Additional Experimental Results

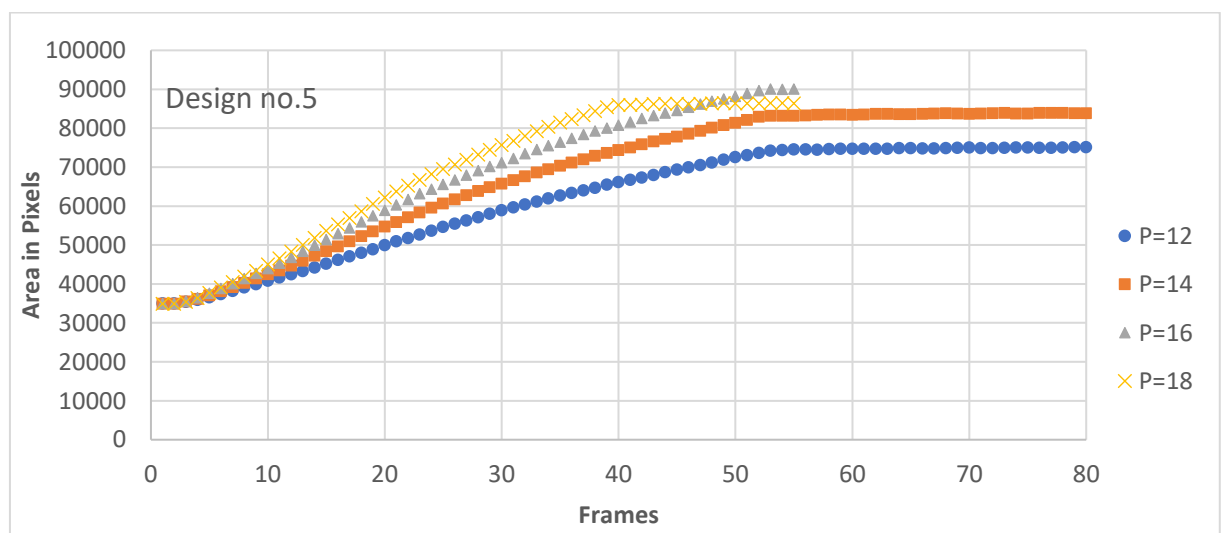
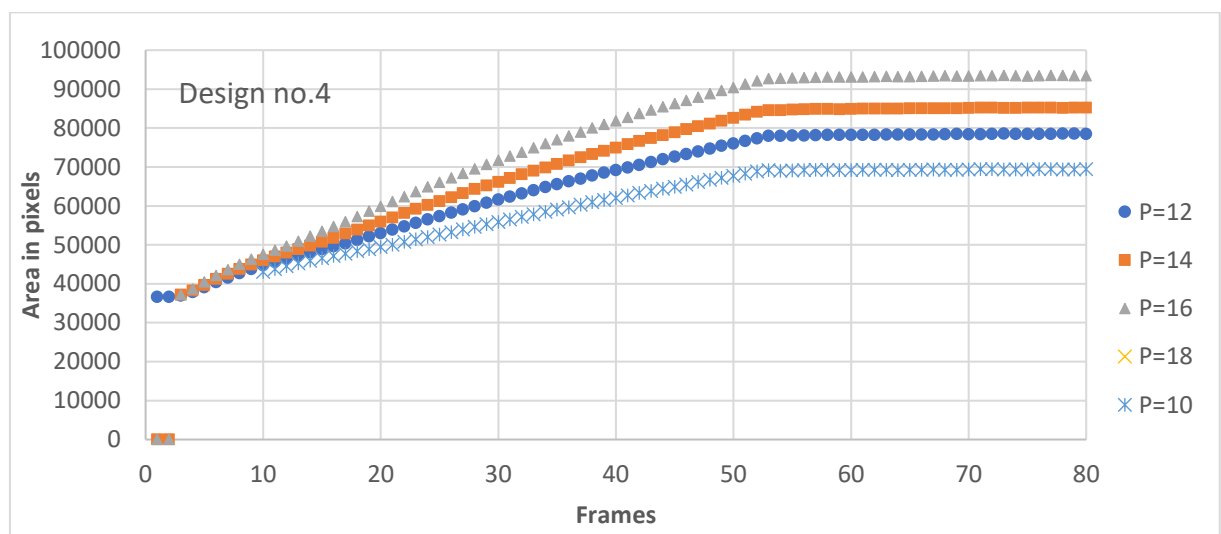
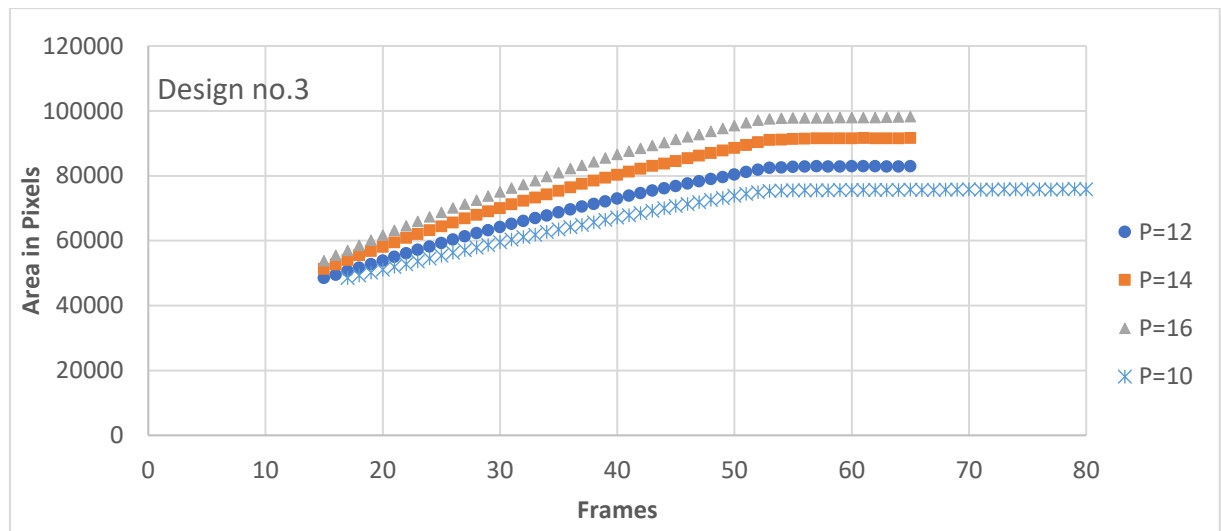
Bending angle response for remaining finger designs at variable input pressures:

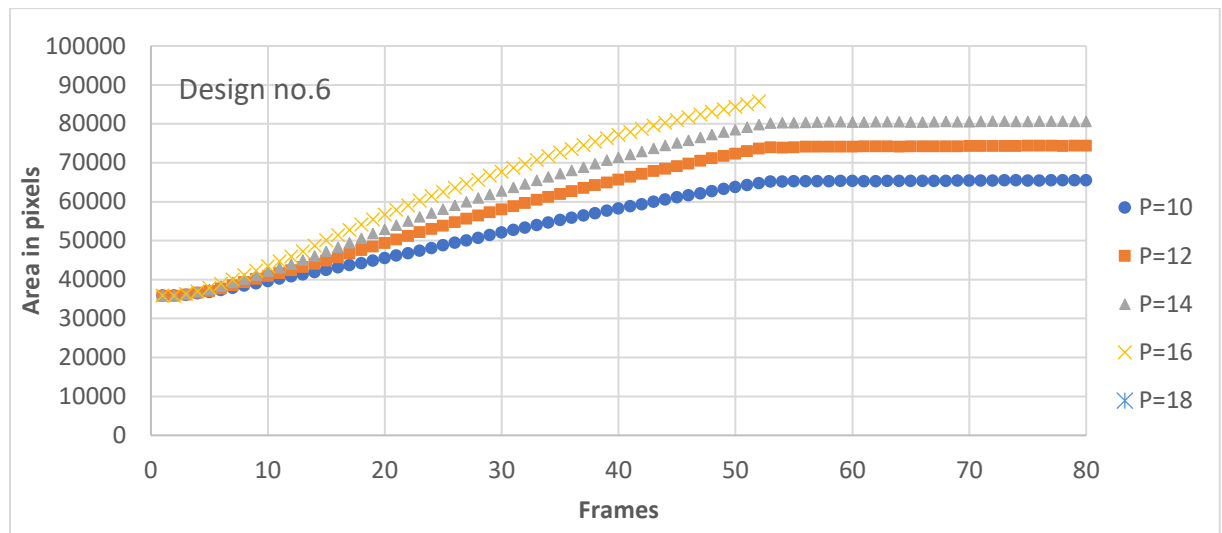




Cross-sectional area response for remaining designs at variable input pressures:

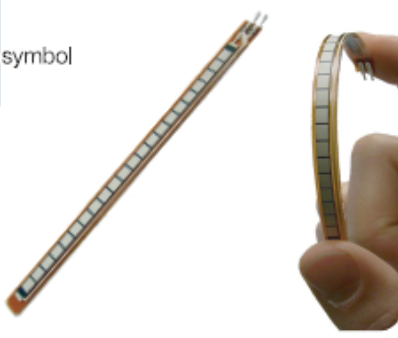






Appendix (D) – Datasheets for Sensors and Components

I. Flex sensor's datasheet:



FLEX SENSOR FS

Features

- Angle Displacement Measurement
- Bends and Flexes physically with motion device
- Possible Uses
 - Robotics
 - Gaming (Virtual Motion)
 - Medical Devices
 - Computer Peripherals
 - Musical Instruments
 - Physical Therapy
- Simple Construction
- Low Profile

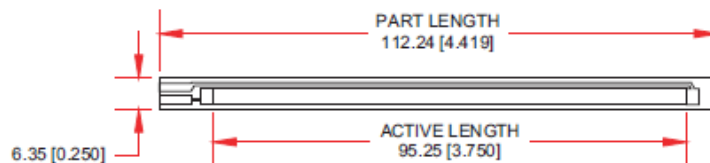
Mechanical Specifications

- Life Cycle: >1 million
- Height: $\leq 0.43\text{mm}$ (0.017")
- Temperature Range: -35°C to $+80^{\circ}\text{C}$

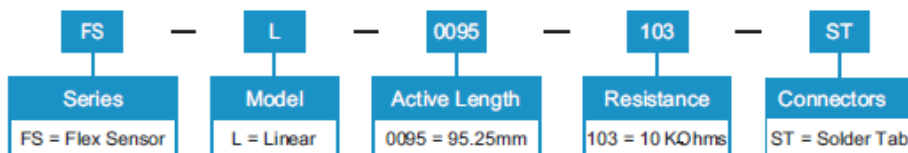
Electrical Specifications

- Flat Resistance: $10\text{K Ohms} \pm 30\%$
- Bend Resistance: minimum 2 times greater than the flat resistance at 180° pinch bend (see "How it Works" below)
- Power Rating : 0.5 Watts continuous; 1 Watt Peak

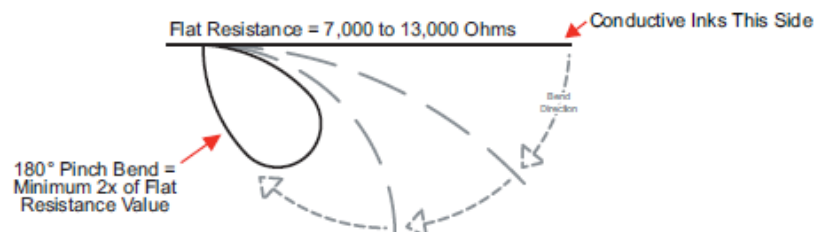
Dimensional Diagram - Stock Flex Sensor



How to Order - Stock Flex Sensor



How It Works



II. Honeywell-ASDXAVX100PGAA5 pressure sensor³²:

ASDX Series Silicon Pressure Sensors

Low Pressure and Ultra-Low Pressure Digital Output,
±2% Total Error Band,
10 Inches H₂O to 100 psi



DESCRIPTION

The ASDX Series is a Silicon Pressure Sensor offering either an I²C or SPI digital interface for reading pressure over the specified full scale pressure span and temperature range.

The ASDX is fully calibrated and temperature compensated for sensor offset, sensitivity, temperature effects and non-linearity using an on-board Application Specific Integrated Circuit (ASIC). Calibrated output values for pressure are updated at approximately 1 kHz.

The standard ASDX is calibrated over the temperature range of 0 °C to 85 °C [32 °F to 185 °F]. The sensor is characterized for operation from a single power supply of either 3.3 Vdc or 5.0 Vdc.

FEATURES

- Output options: I²C- or SPI-compatible 12-bit digital
- Precision ASIC conditioning and temperature compensated over 0 °C to 85 °C [32 °F to 185 °F] temperature range
- Low operating voltage
- Absolute, differential and gage types
- Pressure ranges from 10 inches H₂O to 100 psi
- Standard calibrations in inches H₂O, cm H₂O, psi, mbar, bar, kPa
- Total error band of ±2.0% of full scale span maximum
- RoHS compliant

These sensors are available to measure absolute, differential and gage pressures. The absolute versions have an internal vacuum reference and an output value proportional to absolute pressure. Differential versions allow application of pressure to either side of the sensing diaphragm. Gage versions are referenced to atmospheric pressure and provide an output proportional to pressure variations from atmosphere.

The ASDX Series sensors are intended for use with non-corrosive, non-ionic working fluids such as air and dry gases. They are designed and manufactured according to standards in ISO 9001.

POTENTIAL APPLICATIONS

- Flow calibrators
- Ventilation and air flow monitors
- Gas flow instrumentation
- Sleep apnea monitoring and therapy equipment
- Barometry
- Pneumatic controls
- HVAC

Table 1. Absolute Maximum Ratings¹

Parameter	Min	Max	Unit
Supply voltage (V _{supply})	-0.3	6.0	Vdc
Voltage to any pin	-0.3	V _{supply} + 0.3	Vdc
Digital clock frequency:			
I ² C	100	400	kHz
SPI	50	800	
ESD susceptibility (human body model)	3	-	kV
Storage temperature	-50 [-58]	125 [257]	°C [°F]
Lead temperature (2 s to 4 s)	-	250 [482]	°C [°F]
External capacitance between V _{supply} and ground ²	100	470	nF

³² Pressure sensor's full datasheet: <https://www.mouser.co.uk/datasheet/2/187/honeywell-sensing-asdx-series-digital-pressure-sen-1224345.pdf>

Pressure calibration function provided as follows:

Table 5. Sensor Types

Type	Description
Absolute	Output is proportional to difference between applied pressure and built-in reference to vacuum (zero pressure).
Gage	Output is proportional to difference between applied pressure and atmospheric (ambient) pressure.
Differential	Output is proportional to difference between pressure applied to each of the pressure ports (Port 1 – Port 2).

Figure 2. Transfer Functions and Limits

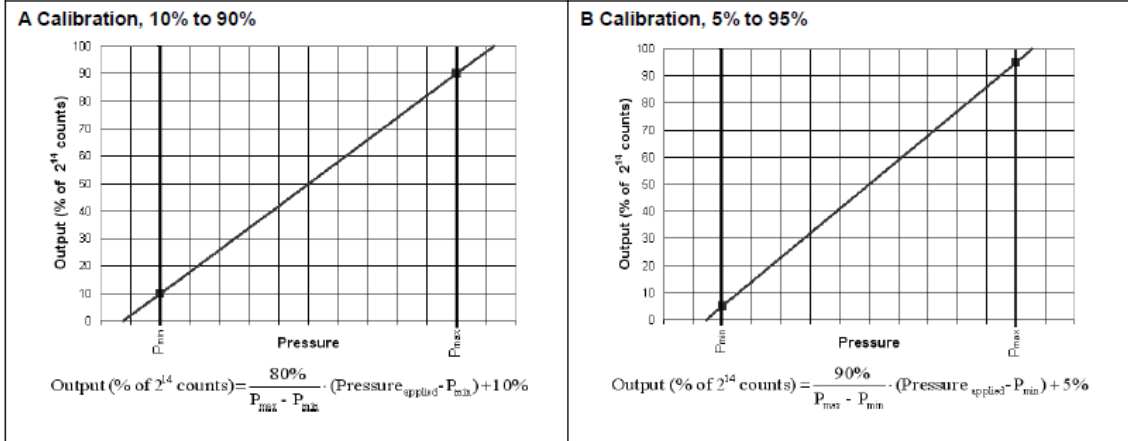
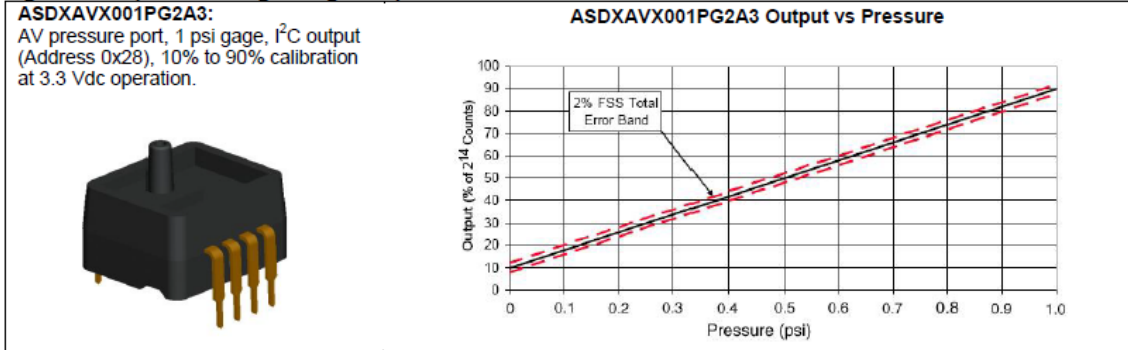


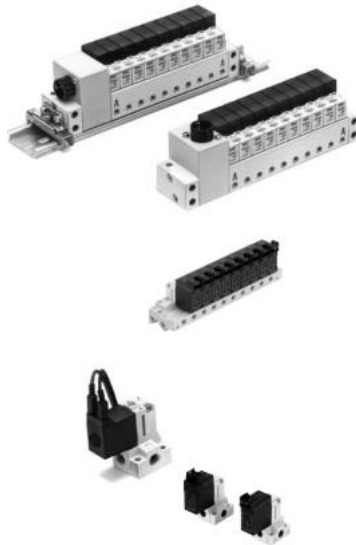
Table 6. Sensor Output at Significant Percentages

% Output	Digital Counts (dec)	Digital Counts (hex)
0%	0	0x0000
5%	819	0x0333
10%	1638	0x0666
50%	8192	0x2000
90%	14746	0x399A
95%	15565	0x3CCD
100%	16383	0x3FFF

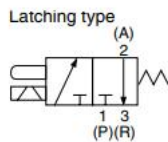
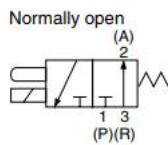
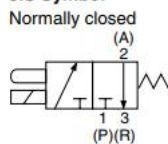
Figure 3. Completed Catalog Listing Example



SMC VQ110U-5M solenoid valves³³



JIS Symbol



Standard Specifications

Item			Type	Standard type (1 W)	High pressure type (1.5W)	Low wattage type (0.5 W)
Valve specifications	Valve construction			3 port direct operated poppet (NC)		
	Fluid			Air/Inert gas		
	Maximum operating pressure			0.7 MPa	0.8 MPa	0.7 MPa
	Minimum operating pressure			0 MPa (−0.1 MPa ⁽⁵⁾)		
	Flow characteristics	1 → 2	C[dm ³ /(s·bar)]	0.055		0.042
			b	0.22		0.27
			Cv	0.014		0.011
		2 → 3	C[dm ³ /(s·bar)]	0.083		0.045
			b	0.28		0.28
			Cv	0.021		0.012
	Response time ⁽¹⁾			ON: 3.5 ms, OFF: 2 ms		ON: 3.5 ms, OFF: 2.5 ms
	Ambient and fluid temperature			−10 to 50°C ⁽²⁾		
	Lubrication			Not required		
	Manual override			Non-locking push type/Locking type (Tool required) ⁽³⁾		
	Mounting orientation			Unrestricted		
Shock/Vibration resistance ⁽⁴⁾			150/30 m/s ²			
Enclosure			Dustproof			
Weight			12.6 g (L/M plug connector, Without sub-plate)			
Electricity specifications	Coil rated voltage		DC	24 V, 12 V		
	Allowable voltage fluctuation			±10% of rated voltage		
	Coil insulation type			Class B or equivalent		
	Power consumption (Current)		DC	1 W (42 mA)	1.5 W (63 mA)	0.5 W (21 mA)
	Electrical entry			Grommet Plug-in, L plug connector, M plug connector (With light/surge voltage suppressor)		

Option

Item		Type	Latching type	AC type	Large flow type	Normally open type
Valve specifications	Model		VQ110L-□	VQ110-□	VQ110U-□	VQ120-□
	Maximum operating pressure		0.7 MPa		0.6 MPa	0.5 MPa
	Ambient and fluid temperature		0 MPa(—100 MPa ⁽⁴⁾⁽⁵⁾)			
	Flow characteristics	1 → 2 ⁽⁶⁾ (3 → 2)	C[dm ³ /(s·bar)]	0.042	0.14	0.04
			b	0.27	0.26	0.11
			Cv	0.011	0.036	0.009
		2 → 3 ⁽⁶⁾ (2 → 1)	C[dm ³ /(s·bar)]	0.045	0.14	0.044
			b	0.28	0.25	0.3
Cv			0.012	0.036	0.011	
Response time ⁽²⁾		5 ms or less	15 ms or less	5 ms or less	5 ms or less	
Electricity specifications	Power consumption (Current)	24 VDC	1 W (42 mA)	—	0.7 W (29 mA) ⁽³⁾	1 W (42 mA)
		12 VDC	1 W (83 mA)	—	0.7 W (58 mA) ⁽³⁾	1 W (83 mA)
		100 VAC	0.6 VA (6 mA)	0.5 VA (5 mA)	—	
		110 VAC	0.65 VA (5.9 mA)	0.55 VA (5 mA)	—	
		200 VAC	1.2 VA (6 mA)	1.0 VA (5 mA)	—	
		220 VAC	1.3 VA (5.9 mA)	1.1 VA (5 mA)	—	
	Electrical entry ⁽¹⁾		Plug-in, L plug connector, M plug connector (With light/surge voltage suppressor)			

³³ Full valve catalogue: <https://www.smc-pneumatics.com/pdfs/vq100.pdf>

APPLICATION INFORMATION

Figure 1 shows the basic connections required for operation of the INA122. Applications with noisy or high impedance power supplies may require decoupling capacitors close to the device pins.

The output is referred to the output reference (Ref) terminal which is normally grounded. This must be a low-impedance connection to ensure good common-mode rejection. A resistance of 10Ω in series with the Ref pin will cause a typical device to degrade to approximately 80dB CMR.

SETTING THE GAIN

Gain of the INA122 is set by connecting a single external resistor, R_G , as shown:

$$G = 5 + \frac{200k\Omega}{R_G} \quad (1)$$

Commonly used gains and R_G resistor values are shown in Figure 1.

The 200kΩ term in equation 1 comes from the internal metal film resistors which are laser trimmed to accurate absolute values. The accuracy and temperature coefficient of these resistors are included in the gain accuracy and drift specifications of the INA122.

The stability and temperature drift of the external gain setting resistor, R_G , also affects gain. R_G 's contribution to gain accuracy and drift can be directly inferred from the gain equation (1).

OFFSET TRIMMING

The INA122 is laser trimmed for low offset voltage and offset voltage drift. Most applications require no external

offset adjustment. Figure 2 shows an optional circuit for trimming the output offset voltage. The voltage applied to the Ref terminal is added to the output signal. An op amp buffer is used to provide low impedance at the Ref terminal to preserve good common-mode rejection.

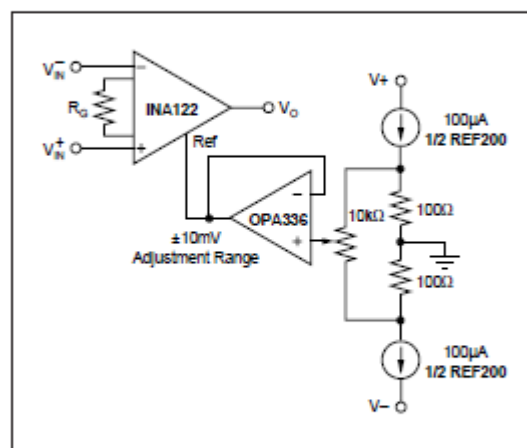


FIGURE 2. Optional Trimming of Output Offset Voltage.

INPUT BIAS CURRENT RETURN PATH

The input impedance of the INA122 is extremely high—approximately $10^{10}\Omega$. However, a path must be provided for the input bias current of both inputs. This input bias current is approximately -10nA (current flows out of the input terminals). High input impedance means that this input bias current changes very little with varying input voltage.

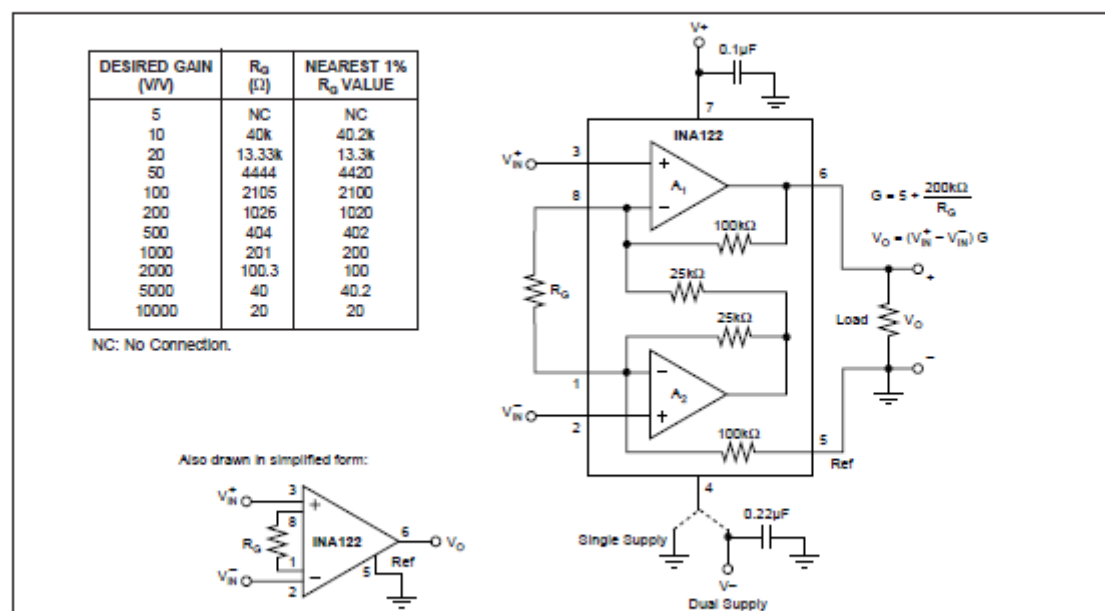
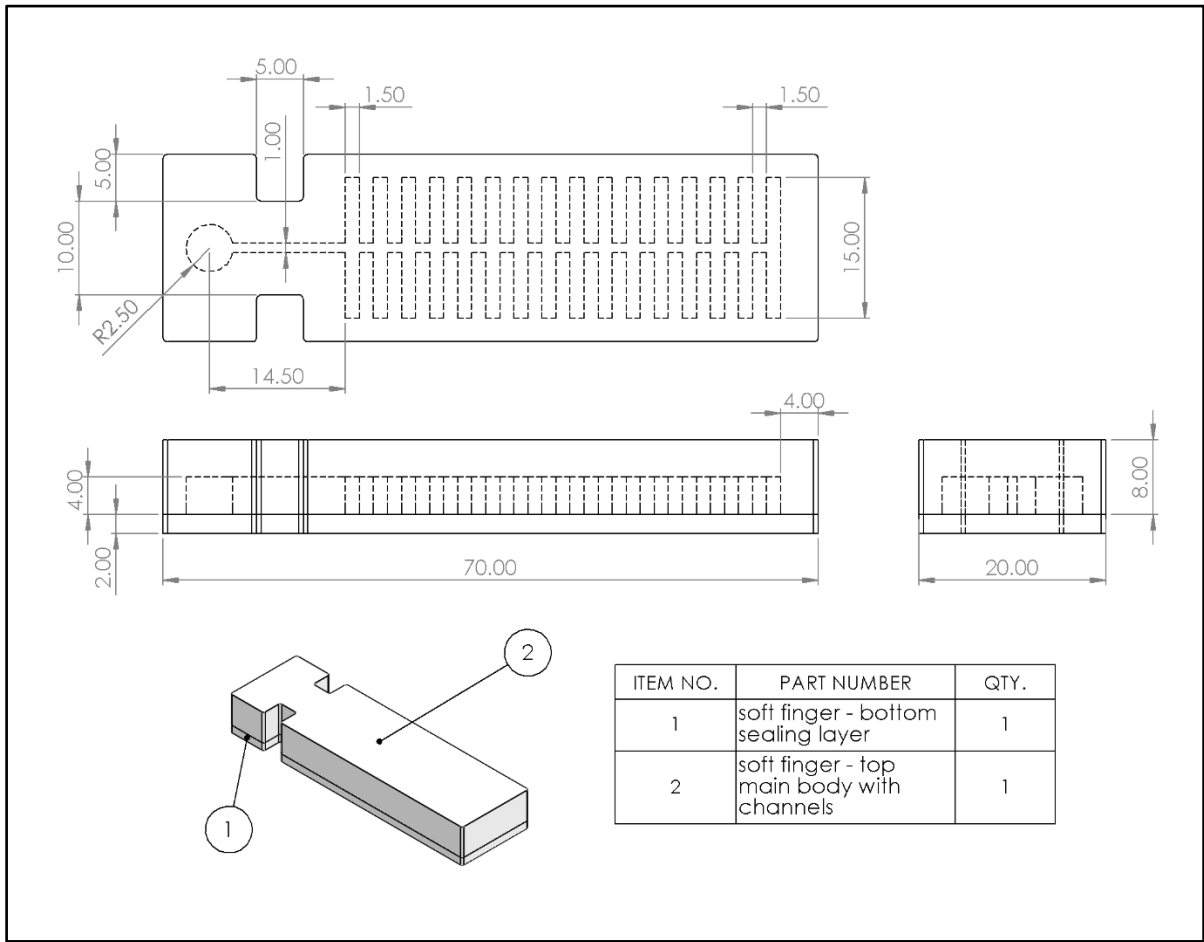


FIGURE 1. Basic Connections.

³⁴ Instrumentation amplifier's full datasheet: <http://www.ti.com/lit/ds/symlink/ina122.pdf>

Appendix (E) – Soft Finger Design

The following engineering drawings details the design of the ribbed soft finger studied in this thesis. The dimensions are based on design number 5 from Chapter 4, which was adopted in the later chapters after embedding the flex sensor. A CAD model for the mould design used to fabricate the 6 design variations tested in Chapter 4 is also available on the Loughborough University’s repository as a Solidworks file. The design variations can be selected from a list under the configuration menu. Additionally, new design variations can be generated using the embedded design table, by typing the desired values for the key design parameters and a new model will be automatically generated.



Appendix (F) – Materials Specifications for FFF

Ninjabflex flexible filament from Ninjatek³⁵:



NinjaFlex® 3D Printing Filament

Flexible Polyurethane Material for FDM Printers

NinjaFlex flexible filament leads the industry with superior flexibility and longevity compared to non-polyurethane materials. Its consistency in diameter and ovality (roundness) outpaces other polyurethane materials. Made from a specially formulated thermoplastic polyurethane (TPU) material, this patented technology contains a low-tack, easy-to-feed texture. The result is uniquely flexible, strong prints ideal for direct-drive extruders.

General Properties	Test Method	Imperial	Metric
Specific Gravity	ASTM D792	1.19 g/cc	1.19 g/cc
Moisture Absorption - 24 hours	ASTM D570	0.22 %	0.22 %

Mechanical Properties	Test Method	Imperial	Metric
Tensile Strength, Yield	ASTM D638	580 psi	4 Mpa
Tensile Strength, Ultimate	ASTM D638	3,700 psi	26 Mpa
Tensile Modulus	ASTM D638	1,800 psi	12 Mpa
Elongation at Yield	ASTM D638	65%	65%
Elongation at Break	ASTM D638	660%	660%
Toughness (integrated stress-strain curve; calculated stress x strain)	ASTM D638	12,000 in·lbF/in ³	82.7 m ³ N/m ³ x10 ⁶
Hardness	ASTM D2240	85 Shore A	85 Shore A
Impact Strength (notched Izod, 23C)	ASTM D256	2.0 ft.lbf/in ²	4.2 kJ/m ²
Abrasion Resistance (mass loss, 10,000 cycles)	ASTM D4060	0.08 g	0.08 g

Thermal Properties	Test Method	Imperial	Metric
Melting Point (via Differential Scanning Calorimeter)	DSC	420° F	216° C
Glass Transition (Tg)	DSC	-31° F	-35° C
Heat Deflection Temperature (HDT) @ 10.75psi/ 0.07 MPa	ASTM D648	140° F	60° C
Heat Deflection Temperature (HDT) @ 66psi/ 0.45 MPa	ASTM D648	111° F	44° C

NinjaTek filament is capable of being printed by a variety of printers in a variety of configurations. This specification sheet gives results as they pertain to the defined test standard and specimen details. Different slicing and/or printing configurations, test conditions, ambient environments, etc. may result in different results.

Impact Strength and Heat Deflection Temperature results were both provided by an accredited university testing laboratory. Specific Gravity and Hardness are innate characteristics of the material. Moisture Absorption, values associated with the Tensile Strength tests, Melting Point and Glass Transition data were prepared by Fenner Drives, Inc.

NinjaTek makes no warranties of any type, express or implied, including, but no limited to, the warranties of fitness for a particular application.

Test Specimen Details (by ASTM Test Number)

All printed specimens were created using the TA25 printer 0.75mm nozzle. For ASTM D638 tests, the extrusion multiplier is 1.05.

Specific Gravity (D792): Results determined by nature of material.

Moisture (D570): 30g of filament tested in moisture analyzer evaluated at 125°C until the mass change is < 0.005% over 1 minute.

Tensile (D638): Dogbone Style IV, 100% fill, diagonal line fill. Dimensions: 5mm thick. See drawing for other dimensions.



Hardness (D2240): Solid testing block.

Dimensions:
2" L x 2" H x 0.75" W

Impact (D256): Un-notched test specimen, notch added post print by testing facility.

Dimensions:
2.5" L x 0.55" H x 0.5" W

Abrasion (D4060): Rectangular block sized to fit labor abrader.

Dimensions:
5" L x 0.5" H x 0.5" W

HDT (D648): Bar shape.

Dimensions:
7.5" L x 0.125" H x 0.5" W

³⁵ Ninjabflex: <https://ninjatek.fppsites.com/wp-content/uploads/2018/10/NinjaFlex-TDS.pdf>

Conductive PLA from Proto-Pasta³⁶:

Proto-pasta Conductive PLA is a compound of Natureworks 4043D PLA, a dispersant and conductive carbon black. In filament form, it is quite flexible, and is compatible with any PLA printing printer.

Strength and Performance

We have not done substantial mechanical testing on this product but have some subjective parameters that should be useful in comparing this material with others:

- Strength: Fair strength. More flexible than PLA, but less layer adhesion
- Stiffness: Low, semi-flexible
- Heat Resistance: Similar to PLA, use below 50C
- Layer Adhesion: Fair layer adhesion. Not as good as normal PLA
- Flexibility: Filament is quite flexible but will break if bent repeatedly (particularly 2.85mm). Printed parts are rigid if more than a mm or two thick. Thin sections are somewhat flexible but fail along layer lines if flexed more than a few times.
- Failure Mode: If flexed to breakage, failure will be along layer lines.
- Warping: Very low warping
- Dual-Head compatibility: Compatible with (sticks to) PLA in dual material prints

Density:

1.15 g/cm³ (1500 kg/m³)

Parameters:

Bed Temp (if available, is not required): 50° C

Hot End Temp: 215 – 230° C (we run it on the hotter side to encourage layer adhesion)

How Conductive Is It?

The measure normally used to characterize a conductor is “volume resistivity” with the units of Ohm-cm. This can be confusing because it is not obvious what it means like “miles per hour.” It is simply the resistance through a 1cm X 1cm X 1cm cube of material, with full sheet contact at 2 opposing surfaces. It is often misprinted as ohm/cm which is not a common unit of measure.

We measured the conductivity using a fixture we machined that clamps a sample between 2 sheet conductors and 1cm cubes printed on a Printbot Simple Metal and machined from solid resin. Here are the results:

- Volume resistivity of molded resin (not 3D Printed): 15 ohm-cm
- Volume resistivity of 3D printed parts perpendicular to layers: 30 ohm-cm
- Volume resistivity of 3D printed parts through layers (along Z axis): 115 ohm-cm
- Resistance of a 10cm length of 1.75mm filament: 2-3kohm
- Resistance of a 10cm length of 2.85mm filament: 800-1200ohm

³⁶ **Conductive PLA:** <https://www.proto-pasta.com/pages/conductive-pla>

Specification of the Lulzbot TAZ 5 FFF printer³⁷:

Print Surface: Heated borosilicate glass bed covered with PEI print surface.

Print Area: 290mm x 275mm x 250mm (11.4in x 10.8in x 9.8in)

Print Volume: 199375 cm³ (1206 in³) of usable space

Top Print Speed: 200mm/sec (7.9in/sec)

Layer Thickness with 0.5mm nozzle: 0.075mm to 0.5mm (0.003in - 0.0196in)

Capable Materials: ABS, PLA, HIPS, PVA, wood filled filaments, Polyester (Tritan), PETT, bronze and copper filled filaments, Polycarbonate, Nylon, PETG, conductive PLA and ABS, UV luminescent filaments, PCTPE, PC-ABS, Alloy 910, and more every day.

Discouraged Materials: 3D printing with carbon fiber filaments is not recommended at this time because carbon fiber filaments can degrade both the nozzle and hot end of the LulzBot TAZ 5 Tool Head.

Filament Sizes: standard 3mm (0.1in)

Maximum Tool Head Temperature: 300°C (572°F)

Maximum Heated Bed Temperature: 120°C (248°F)

Specification of the Flexytruder tool-head³⁸:

Required filament diameter: 3mm

Hot end temperature range: 120°C - 300°C

Nozzle diameter: 0.6mm

Using stiff, non-flexible filament with the green flexystruder is not advised as it can lead to premature extruder body wear and purging difficulty when switching between materials.

³⁷ **Lulzbot TAZ 5:** <https://www.lulzbot.com/support/lulzbot-taz-flexystruder-tool-head-v2>

³⁸ **Flexytruder tool-head:** <https://www.lulzbot.com/store/printers/lulzbot-taz-5>